AN INVESTIGATION OF LIQUID NOBLE METAL ALLOYS

USING NUCLEAR MAGNETIC RESONANCE

by

Ian P. Host, M.Sc.

A thesis submitted for the degree of

Doctor of Philosophy of the

University of Warwick.

School of Physics,

University of Warwick.

November, 1971.

Memorandum

This dissertation is submitted to the University of Warwick in support of my application for admission to the degree of Doctor of Philosophy. It contains an account of my own work performed at the School of Physics of the University of Warwick in the period September 1967 to December 1970 under the supervision of Dr. Graham Styles. No part of it has been used previously in a degree thesis submitted to this or any other University. The work described in this thesis is the result of my own independent research except where specifically acknowledged in the text. The preparation of specimens described in chapter two has been published in J. Phys. (E), 3, (1970), 391 and the cesium-oxygen results published in J. Nuc. Mat., 35, (1970), 55. The results for the noble metal-tin systems are to be published shortly in the Journal of Nuclear Resonance and it is anticipated that the noble metal-indium data will presently appear in print.

Ian Host

Ian Host

November, 1971.

Acknowledgements

I am indebted to my supervisor Dr. Graham Styles for his guidance, patience and interest which has been a continual source of inspiration during the course of this work and in the preparation of this thesis; further I would like to thank him for the friendship he has extended to me. Also I would like to acknowledge the help and advice of Professor E. F. W. Seymour in all aspects of NMR and liquid metals. My thanks are due also to Mr. Chris Ford for his assistance with the susceptibility measurements, to Mr. Barry Sheffield for his technical assistance and to Dr. David Brown and Mr. David Moore for their help with and discussion of relaxation measurements. It is a pleasure to acknowledge the advice and assistance of Dr. Rod Devine in connection with the phase shift calculations and of Professor John Perdew with the pseudopotential calculations. Further, I thank Professor A. J. Forty for allowing me to use the facilities of the School of Physics.

I would like to acknowledge the generous support of A.E.R.E., Harwell who provided both a personal grant and equipment grant and in particular to thank Mr. B. W. Mott for his continual interest and encouragement. Finally I thank Mrs. Elizabeth Emes for her careful and rapid preparation of this manuscript.

ABSTRACT

Nuclear magnetic resonance (NMR) Knight shift and spin-lattice relaxation time measurements of ^{63}Cu, ^{115}In and ^{119}Sn in some liquid noble metal-indium alloys and noble metal-tin alloys are presented together with magnetic susceptibility measurements in the liquid noble metal-indium systems and gold-tin system. The problems associated with the preparation of suitable powder samples for NMR studies are discussed together with some original methods of solving them. The measured properties are first examined in the light of the information they yield regarding atomic distributions in liquid alloys. In contrast to some earlier X-ray and neutron diffraction data the NMR results do not indicate that any short range atomic ordering is taking place in any of these systems. Assuming that the alloy systems are random mixtures of the two components, an attempt is then made to reproduce the observed Knight-shift data by using spin susceptibilities deduced from the total susceptibility data together with a calculation of the conduction electron contact density at the nucleus using firstly a partial wave analysis of the electron-scattering and secondly a pseudopotential approach. Both calculations give semi-quantitative agreement with experiment. The relaxation rate data for these systems are then considered. For the noble metal-tin systems the relaxation rate of ^{119}Sn is wholly accounted for by the magnetic contribution predicted from the observed Knight shift through the Korringa relation. However in the noble metal-indium alloys the relaxation rates for ^{115}In, and to a lesser extent ^{63}Cu, can only be wholly described by both magnetic and quadrupolar contributions. The latter can be understood qualitatively in terms of a theory due to Sholl. Finally an NMR investigation of the solvent ^{133}Cs

resonance in the liquid cesium-oxygen system is presented. The results strongly favour a model in which the oxygen exists in doubly ionized form in the metal matrix.

CONTENTS

CHAPTER ONE

INTRODUCTION

1.1 Liquid Metals

The most fruitful approach to any field of science is a mutual, complementary combination of experimental observation and theory. This is being successfully achieved in the field of, say, solid state physics but not as yet in the physics of liquid metals. The approach to this subject is one which combines the physics of crystalline metals and the physics of liquids, which has been concerned mainly with non-metallic systems. The picture of a crystalline metal is now a familiar one to solid state physicists. The long range lattice periodicity produces electron energy bands whose separation is determined essentially by the perturbing lattice potential on the electron states. Basically, the electronic properties are different aspects of a dense electron gas which interacts with a system of positive ions. This interaction is partly responsible for the ion-ion interaction which determines the atomic distributions in liquid metals. Thus the experimental study of liquid metals has this interaction at its focus, from which two rather distinct fields have grown, namely the study of electronic properties, such as the Knight shift, Hall effect and resistivity and the study of the ionic distributions, using X-ray and neutron diffraction. Measurements of electronic properties, however, may relate directly to structure data in that they test a structural model postulated for a particular metal or alloy.

In the experimental study of simple (non-transition) liquid metals, the observations are invariably tested by seeing whether they fit one or more aspects of the free electron model. According to the free electron model the

conduction electrons form a dense electron gas with Z electrons per atom (Z = valency), the conduction electron states are plane waves and the electron energy E is related to the wave vector $\underline{k}$ by $E = \hbar^2 k^2/2m$, from which follows a sharp spherical Fermi surface, an isotropic relaxation time and a density of states $N(E_F) \propto E^{\frac{1}{2}}$. However it must be stressed that a particular property, though exhibiting one feature of the free electron model, does not necessarily exhibit the other features as well.

The physics of liquid metals has been comprehensively reviewed up to 1963 by Cusack[1]. The article by Wilson[2] interprets the properties of liquid metals and alloys, especially thermodynamic data, in terms of possible ordering and Mott (1965)[3] gives a short review of transport properties. Recently the whole field of liquid metals and alloys has been covered by the proceedings of the Brookhaven conference[4]. "Liquid metals" is the title of a recent book by March[5] which briefly but concisely considers the theoretical aspects of the subject. Consequently this introduction will be brief.

The experimental observations are divided into three groups. The first, transport properties, tells us whether a particular liquid metal has a spherical Fermi surface and if the relaxation time of the electron scattering is isotropic. The second includes density of states properties and gives information on the sharpness of the Fermi surface and on the magnitude of $N(E_F)$. Finally the atomic structure of liquid metals and alloys is considered.

1.1.2 Transport Properties

a) Hall Effect In nearly all metals the Hall coefficient R_H changes on melting and has a negative value for the liquid state. Except for Tl, Pb and Sb this value is accounted for by the free electron expression $R_H = -1/n|e|$, where n is the total number of carriers per unit volume and

e is the electronic charge. The weak temperature dependence observed in R_H is accounted for by the temperature dependence of the atomic volume. Though the data predict that the Fermi surface is spherical and relaxation time isotropic it does not necessarily mean that $N(E_F)$ is free electron like, since a free electron value of R_H is obtained for any E-$\underline{k}$ relationship having spherical symmetry. The deviations of Tl, Pb and Sb from the free electron model probably arise because the electronic mean free path is shorter than the range of order that exists, which causes a breakdown of the model.

The behaviour of R_H in alloys is less well understood. In the In-Hg[6] system for example the variation of R_H shows marked deviation from free electron behaviour even though both In and Hg give free electron values. In the Cu-Sn[7] system the behaviour of R_H, which also disagrees with free electron predictions, has been interpreted by postulating the existence of bound states which form at the expense of the Sn conduction electrons. The situation is far from clear at the moment and awaits a sounder theoretical basis.

b) Optical Properties Measurements of optical properties confirm the Hall effect data for most of the pure metals, the results being interpreted by the free electron Drude theory which assumes that the effective mass m * and relaxation times are given by the free electron model. Departure from free electron behaviour was found in Cd, Pb, Bi and Hg by Smith[8]. The values of N/m^* (N=no. of valence electrons/atom) are higher than predicted by the model and were accounted for semi-quantitatively by considering the coupling of the core states with the conduction electrons. Again the situation in alloys is less well documented. Measurements of Smith on the Hg-Bi system and Schulz[9] on Hg-In revealed that neither system is free electron like, even though the pure components are. The anomalous Hg-In results are consistent with those of R_H.

c) Resistivity and Thermopower Both of these properties change abruptly on melting. The resistivity ρ_L approximately doubles and in the liquid rises slowly with temperature in an approximately linear fashion (except for di-valent metals where ρ_L may fall slightly and pass through a minimum). The thermopower is roughly a linear function of temperature in the liquid and is often proportional to the absolute temperature. Much of the experimental data of both properties has been described by the Ziman[10] formalism which has successfully described both the magnitude and temperature dependence of ρ_L and thermopower in liquid metals. Essentially the model assumes that the conduction electrons form a degenerate free-electron gas having a spherical Fermi surface and are scattered by the random arrangement of the ions. The ion positions are represented by the structure factor $I(K)$ (where $K=4\pi\sin\theta/\lambda$, with θ=angle and λ=wavelength of incident beam) and their presence by a weak pseudopotential whose Fourier transform is $U(\underline{K})$. Considering the uncertainties in $I(K)$ and $U(\underline{K})$, good agreement with experiment is obtained and is improved further when corrections for spin-orbit coupling and non-local screening are incorporated. In fact Ziman's model seems to be standing the test of time as very recently Ashcroft and Schaich[11] have used an approximation for n-body ionic correlation which has lead to a generalization of Ziman's expression. Their work includes higher order terms which are only negligible because they tend to cancel each other.

Alloy measurements of these properties are legion; however the results are fairly well understood for most binary systems where an extension of Ziman's expression to alloys has reproduced much of the data. The Faber-Ziman[12] theory accounts for both ion positions in the alloy by the three partial structure factors $I_{ij}(K)$ and the ions are represented by the two ion pseudopotentials $U_i(\underline{K})$ and $U_j(\underline{K})$. The extent to which the theory reproduces the observed data must be considered however in the light of possible

ordering taking place in the liquid. The reasonable agreement obtained for most metals and alloys must be taken as supporting the free electron model.

The properties considered up to this point give support to two aspects of this model, namely that the Fermi surface is spherical and the relaxation time isotropic. Even though the Ziman formalism gives good agreement with experiment his resistivity expression does not give an indication of what $N(E_F)$ is really like because it remains valid if $N(E_F)$ does depart, though not too much, from the free electron value; also his treatment does not tell us anything about the sharpness of the Fermi surface. These aspects will now be considered more fully.

1.1.3 Density of States properties The resistivity ρ_L is a single number somewhat remote from the dynamics of the conduction electrons and points to the need for experimental and theoretical probes into the electron dynamical behaviour. The techniques of solid state physics, such as measurements of the de Haas-van Alphen effect, require low temperatures and long mean free paths and are thus ruled out in probing similar properties in liquid metals.

A real liquid metal, having an irregular wave function and constantly changing ionic positions, may be more usefully characterised by the probability, averaged over all allowable structures, that a wave function of energy E contains a Fourier component with wave vector $\underline{k}$. This quantity is defined as $\rho(\underline{k},E)$ which may be related to $N(E_F)$ by [13]

$$N(E_F) = \frac{1}{4\pi^3} \int \rho(\underline{k},E).d\underline{k} \qquad 1.01$$

and to the distribution of $\underline{k}$ values by

$$n(\underline{k}) = \int_{-\infty}^{+\infty} f(E,T).\rho(\underline{k},E).dE \qquad 1.02$$

where $f(E,T)$ is the Fermi function. For free electrons, where $E=\hbar^2k^2/2m$,

$\rho(\underline{k},E)$ is the δ-function $\delta(E-\hbar^2k^2/2m)$, and equation 1.1 then gives the usual free electron $N(E_F)$. In general, $\rho(\underline{k},E)$ represents the averaged Fourier spectrum of the conduction electron wave functions. For example, if the scattering in the liquid metal is large, the wave functions will depart from single plane waves, requiring a spread in $\underline{k}$ in their composition. This gives a blurred $\underline{k}$-space Fermi surface, though the Fermi energy is still well defined and $\underline{k}$ can no longer define an eigenstate as it can in the free electron model. $\rho(\underline{k},E)$ represents this by being smeared out in $\underline{k}$ for large scattering and well defined in $\underline{k}$ if the scattering is small. $\rho(\underline{k},E)$ may also be smeared out in E for a given $\underline{k}$ since this $\underline{k}$ may feature in wave functions of various energies. A calculation using Green functions by Edwards[14] and Ballentine[15] has yielded values of $\rho(\underline{k},E)$ and $N(E_F)$, where the electronic energy states are calculated from I(K) and a single-centre scattering potential of a screened ion. Ballentine obtained $\rho(\underline{k},E)$ and $N(E_F)$ curves for Sn,Al and Bi. In liquid Bi the shape of $\rho(\underline{k},E)$, which depends only on $|\underline{k}|$ in a liquid, indicates a width in k of about 24 per cent of k_F at energies near to E_F. The Fermi surface is therefore blurred in k-space and this is a consequence of the disorder. It is encouraging that Ballentine's first principles calculation of $\rho(\underline{k},E)$ was in fair agreement with the curve obtained experimentally from positron annihilation measurements. The corresponding $N(E_F)$ curve for liquid Bi also shows a departure from the free electron prediction. The results for Zn and Al however give results which are close to the free electron theory. Though these are essentially perturbation theory calculations and therefore not exact, they nevertheless represent a calculation of the energy spectrum which enables a limited comparison with experiment. For a detailed account of the theory the reader is referred to the papers of Edwards. The following properties will be considered in the light

of the information they yield regarding $N(E_F)$ and $n(\underline{k})$ and where applicable a comparison of the experimental data with the theoretical $\rho(\underline{k},E)$

a) Positron Annihilation and Soft X-ray emission Measurements in both these fields, relative to other properties of liquid metals, are fairly sparse. The angular correlation of two gamma-rays emitted when a positron annihilates in a liquid metal is a measure of the momentum distribution, $n(\underline{k})$. Kusmiss and Stewart[16] have measured positron annihilation in 15 liquid metals. Their results may be divided into three groups; 1) in which a change in angular correlation results on melting, 2) where the change occurs below the melting point and 3) no change at all takes place. The results for Bi are interesting, for $n(\underline{k})$ in the solid is parabolic and free-electron like, showing a sharp cut-off at k_F. However in the liquid this cut-off at k_F is smeared out which reflects the smeared nature of $\rho(\underline{k},E)$. This is comparable with the mean free path which is expected to be small in the liquid and long in the solid. The results for Na on the other hand show sharp cut-offs both in the solid and liquid, showing that the mean free path is long and that little smearing of $\rho(\underline{k},E)$ is present. Other metals show this smearing effect in the liquid as well as differences between solid and liquid phases. Though this technique appears promising in the information it yields regarding $n(\underline{k})$ and less directly $\rho(\underline{k},E)$ it is unfortunately subject to difficulties in the data interpretation as discussed by Kusmiss and Stewart.

Soft x-ray emission measures $N(E_F)$ multiplied by the transition probability for an electron to drop from the conduction band to an inner shell. Unfortunately the latter quantity is almost inaccessible to calculation though Edwards[17] has said that it might be the same for both solid and liquid so that a measurement in the change in $N(E_F)$ on melting may be

made. The results of Catterall and Trotter[18] on Al indicates that in this metal $N(E_F)$ changes little on melting. Certainly there is a need for more measurements of these properties together with a sounder theoretical interpretation.

b) Magnetic susceptibility If liquid metals are to be completely described by a free electron picture then on melting $N(E_F)$ ought to conform to the free electron model, as should the conduction electron spin susceptibility, $\chi_p = \mu_B^2 N(E_F)$, where μ_B = Bohr magneton. Direct measurements of χ_p are possible using conduction electron spin resonance (CESR) but in practice this has been limited to the alkali metals. However the results for Li, Na and K show that the change in χ_p on melting is at the most ten per cent. That Na and K remain free-electron like in the transition from solid to liquid is no surprise however, their near spherical Fermi surfaces in the solid being well known.

Recently Dupree and Seymour[19] have shown that consistent values of χ_p in pure liquid metals may be obtained from measurements of the total magnetic susceptibility. Previously the chief problem was obtaining values for the ion core contribution χ_i which do not leave a spurious, systematic atomic number dependence of the total electronic susceptibility χ_e. Using values of χ_i taken from Angus[20], they obtained a set of values for χ_p for 18 liquid metals. Their values are in good agreement with those obtained directly using CESR when available. Though their results, which are derived on the basis of a free electron model, point to $N(E_F)$ being approximately free-electron like for most of the liquid metals, the values of χ_e, and obviously χ_p are strongly influenced by electron-electron interactions. Dupree and Seymour took these into account but the χ_e values are consistently larger than those predicted by the then available models suggesting that these effects may be underestimated. Although a recent

estimate of electron-electron interactions by Dupree and Geldart[21] seems to improve the agreement it is clear that $N(E_F)$ deduced in this way is only approximate.

Since no direct measurements of χ_p in alloys have been made using CESR, values may be deduced only from total susceptibility measurements. However some of the assumptions made for the pure metals may become less valid, for example χ_i for both components will depend on the changing conduction electron density across the concentration range. Though a number of alloy systems have been investigated using magnetic susceptibility there has been no serious attempt at extracting values of χ_p from the data.

1.1.4 Atomic Structure The most direct method of investigating the atomic structure in a liquid is by the diffraction of neutrons or X-rays. Both methods yield the total structure factor I(K) whose Fourier transform gives the pair distribution function g(r) which represents the probability of finding an atom at a distance r from an atom at the origin. The structure of An alloy is fully characterised by its three partial structure factors $I_{ij}(K)$ and from their Fourier transforms $g_{ij}(r)$ the mean interatomic distances i-i, j-j and i-j can be determined as well as the number of nearest neighbours around one particular atom. Neutron diffraction data give more reliable values of I(K) though for an alloy three experiments are required to give the $I_{ij}(K)$ values. This limits the use of neutrons to those alloy systems where at least one of the components has two magnetic isotopes which can be obtained in enriched form. Enderby etal.[22] have investigated the liquid Cu-Sn system where the three specimens contained natural copper, copper enriched with ^{63}Cu and copper enriched with ^{65}Cu. Where an alloy system has been investigated using both neutrons and X-rays, the I(K) values obtained by both methods agree fairly well.

By postulating a liquid metal to be a random assembly of hard spheres, Ashcroft and Lekner[23] have successfully reproduced experimental values of I(K) for many liquid metals up to and including the principal diffraction peak. Ashcroft and Langreth[24] have extended this model to liquid binary alloy systems. Based on the solution of the Percus-Yevick integral equation for hard spheres, their model is now widely used to interpret structure in liquid metals and alloys.

1.2 Nuclear Magnetic Resonance

First discovered in 1945[25,26], the field of NMR has been well documented and is the subject of a number of text books[27,28,29]. Consequently only a brief description of the subject is given here, emphasis being placed on those aspects of NMR particularly relevant to liquid metals.

1.2.1 Basic Theory A nucleus with spin $\underline{I}$ and magnetic moment $\underline{\mu}$ located in a steady magnetic field $\underline{H}_0$ experiences an interaction energy $-\underline{\mu}\cdot\underline{H}_0$. If $\underline{H}_0$ is acting in the Z-direction the Hamiltonian takes the simple form

$$H = -\gamma_n \hbar H_0 I_z \ , \qquad 1.03$$

where I_z is the Z-component of the nuclear spin operator and γ_n the gyromagnetic ratio. Transitions between the (2I + 1) Zeeman levels, separated in energy by $\gamma_n \hbar H_0$, may be induced by applying electromagnetic radiation of angular frequency ω_0 given by $\hbar\omega_0 = \gamma_n \hbar H_0$, or $\omega_0 = \gamma_n H_0$ which is the resonance condition. Although the probability for upward and downward transitions to occur is the same, a net absorption of energy takes place if the spins are in thermal equilibrium because a lower energy level is more highly populated than the one above it by the Boltzmann factor $\exp(\gamma_n \hbar H_0/kT)$. Thus there are more upward transitions than down resulting in an absorption of energy from the exciting field. The spins achieve thermal equilibrium among themselves and with the lattice through various interactions which exist

between them. After absorbing energy from the radiating field the nuclear-spins distribute it among themselves by spin-spin relaxation and transfer it to the lattice via spin-lattice relaxation. The spin-lattice relation time T_1 characterises the exponential return of the nuclear-spin Z-magnetisation to its equilibrium condition. The mutual exchange of energy between the lattice thermal reservoir and the spin system is achieved by local magnetic fields (or sometimes inhomogeneous electric fields) that have a component fluctuating at the resonance frequency. There are a number of mechanisms that can produce such fields though in metals the dominant T_1 process is nearly always the contact interaction with the conduction electrons.

Spin-spin relaxation is due to various interactions between the spins themselves. At resonance the coherence of the precession of individual spins gives the component of magnetisation in the x-y plane. This coherence tends to be destroyed by the spin-spin interactions where the approach to equilibrium is characterised by the spin-spin relaxation time T_2. There are two 'static' local field effects which result in spin-dephasing and secular broadening of the line. Firstly the spread in local z-fields due to neighbouring spins causes a spread in precession rates and thus spin-dephasing and secondly the precession of neighbouring spins causes mutual spin-flipping between identical spins. This latter process limits the life-time of the state and broadens the energy level through the uncertainty principle. T_2 is related to the line shape by

$$T_2 = \frac{1}{2} g(\nu)_{max} , \qquad 1.04$$

where $g(\nu)_{max}$ is the lineshape function. A non-secular contribution to the line broadening arises from spin-lattice relaxation which limits the life-time of the nuclear energy level and broadens it through the uncertainty

principle. In the presence of thermal motion where the average value of the local field may be small, the line narrows and the contributions to T_2 may be summed up by

$$\frac{1}{T_2} = \frac{1}{T_2'} + \frac{1}{T_2''} = \frac{1}{T_2'} + \frac{1}{2T_1}, \qquad 1.05$$

where $1/T_2'$ arises from secular (static) broadening and $1/T_2''$ arises from non-secular (life-time) broadening. For very rapid motion $1/T_2' = 1/2T_1$ and thus for any relaxation mechanism $1/T_1 = 1/T_2$, so that the relaxation is determined solely by life-time limiting processes. Given these conditions the lineshape is Lorentzian and the width $\Delta\nu$, between the absorption derivative peaks, is given by

$$\Delta\nu = \frac{1}{\sqrt{3}\pi T_2} \qquad 1.06$$

There may be more than one contribution to the T_1 and T_2 processes in liquid metals and these will add to give the total relaxation rate.

1.2.2 NMR in Metals In metals the phenomenon of nuclear resonance is different from that in non-metals because of the interaction of the nuclei with the conduction electrons. This interaction is important in three respects. Firstly it produces a shift in the frequency of resonance absorption, secondly it is the dominant spin-lattice relaxation mechanism and finally it may produce marked changes in the line width and shape. These closely linked effects are now discussed.

a) Knight shift Over 20 years ago, W.D. Knight[30] found that the NMR of ^{63}Cu in metallic Cu was shifted to a higher frequency than in the salt CuCl. The Knight shift, which has been the subject of a number of reviews [31,32,33] is due predominantly to the contact hyperfine interaction of the nucleus with the conduction electrons. The applied field H_0 polarises the conduction electrons through their spin susceptibility χ_p which then interact

with the nuclei to produce a static non-zero average local field $\Delta\underline{H}$ at the nuclear site, which must be added to the main field $\underline{H}_O$. The Zeeman interaction is then modified to become $-\underline{\mu}.(\underline{H}_O + \Delta\underline{H})$ instead of $-\underline{\mu}.\underline{H}_O$, which produces the NMR shift. The contact interaction contribution to the Knight shift, K_S, has been shown to be given by[28]

$$K_S \equiv \frac{\Delta H_O}{H_O} = \frac{8\pi}{3}\chi_P \Omega \langle|\psi_K(0)|^2\rangle_F , \qquad 1.07$$

where Ω is the atomic volume and $\langle|\psi_K(0)|^2\rangle_F \equiv P_F$ is the probability density at the nucleus averaged over the Fermi surface electrons. A typical value of the Knight shift is 1%. As mentioned previously reasonable values of χ_P in the above equation may be determined for non-transition metals from total susceptibility measurements. Calculations of P_F have been made in pure metals by various authors [34,43,44] using a pseudopotential representation of the ions. The latter method has given P_F values for liquid non-transition metals which combined with χ_P values give good agreement with measured K_S values. Though K_S is the dominant contribution to the Knight shift, other terms are present which require consideration.

The polarised Fermi surface electrons also interact indirectly with the nucleus giving another contribution to the Knight shift. The spin density has associated with it a spin dependent exchange interaction which may polarise the closed shells of an ion core and the paired electrons in the conduction band below E_F. The exchange polarisation of s-electrons then interacts with the nucleus via the contact interaction and can result in either positive or negative contributions to the shift. Bennett, Watson and Carter[33] have summarised the hyperfine fields due to the exchange core polarisation response to a single unpaired open valence shell electron. Mahanti and Das[35] have recently calculated exchange core polarisation

contributions in all of the alkali metals. Their results when combined with direct contributions agree well with experimental Knight shifts and show that the core polarisation contribution varies between 10 and 25% of the direct contribution for alkali metals.

Another contribution to the shift arises from the dipole interaction of the conduction electrons with the nucleus. In general this interaction is anisotropic and gives an orientation dependent term in the shift, K_{aniso}, for nuclei at non-cubic sites. However in liquids, because they are isotropic, this contribution averages to zero and is not considered further.

A final contribution to the Knight shift, K_{orb}, comes from the orbital magnetic moment of the conduction electrons. This is usually only important in transition metals and therefore is not of interest here. In general it is not possible to separate the core polarisation and orbital contributions and these are often lumped together as

$$K_{other} = K_{cp} + K_{orb}$$

b) Linewidth, Relaxation and the Korringa Product As mentioned earlier, in a liquid metal the relaxation rate $R_1 \equiv 1/T_1$ is directly proportional to the linewidth. Because of the rapid thermal motion in a liquid metal the direct dipolar interaction between nuclei averages to zero and therefore makes no contribution to the line width. There are however two contributions which may arise due to the indirect interaction of the nuclear magnetic moments with each other via the conduction electrons, giving rise to pseudo-exchange and pseudo-dipolar broadening. The hyperfine interaction is responsible for pseudo-exchange whereas the pseudo-dipolar broadening arises because of the existence of a non-s part of the conduction electron wave function. For interactions between identical nuclei the pseudo-exchange term has no

effect on the second moment of the line but increases the fourth moment. If the nuclei are not identical then the second moment increases. In liquid metals both the pseudo-dipolar and pseudo-exchange terms average to zero. A full account and derivation of these interactions is given in Slichter[28].

The main contribution to the line width in liquid metals is usually produced by spin-lattice relaxation time broadening which arises from the contact interaction with the conduction electrons. In this T_1 process the nucleus and electron exchange energy via a mutual spin-flip scattering process where the hyperfine potential scatters the conduction electron from an initial state $\underline{k}$ to a final state $\underline{k}'$. The relaxation rate may be straightforwardly calculated for non-interacting electrons to be[28]

$$\frac{1}{T_1} = \frac{64\pi^3\hbar^3\gamma_e^2\gamma_n^2\{\langle|\psi_k(0)|^2\rangle_F N(E_F)\}^2 kT}{9}, \qquad 1.08$$

where the term $\langle|\psi_k(0)|^2\rangle_F$ is that which appears in the expression for K_s. A correction factor for electron-electron enhancement may be added. A relation between K and T_1 follows at once and is given by

$$T_1T(K_s)^2 = \left\{\frac{\chi_p}{N(E_F)}\right\}^2 \frac{1}{\pi k\hbar} \cdot \frac{1}{\gamma_n^2\gamma_e^2\hbar^3} \qquad 1.09$$

the above was first given by Korringa[36]. For a Fermi gas of non-interacting spins, 1.09 reduces to:

$$T_1T(K_s)^2 = \frac{\hbar}{4\pi k}\left\{\frac{\gamma_e^2}{\gamma_n^2}\right\} \qquad 1.10.$$

K_s and T_1 are those values which arise only from the contact interaction and as this usually dominates in metals it was expected that equation 1.10 would give reasonable agreement with experiment. However in practice the Korringa relation is seldom satisfied. In the alkali metals for example where the requirements of a dominant s-contact interaction should be satisfied, experi-

mental values of $T_1T(K_s)^2$ are considerably larger than predicted. This discrepancy has been attributed for some metals to electron-electron interactions which enhance χ_p relative to its free particle value which therefore gives rise to an enhanced Korringa product. An early attempt to take these effects into account by Pines[37] was not wholly successful because he only considered the effect on the Knight shift. The Knight shift depends on the static susceptibility $\chi_p(0,0)$ and in the presence of electron-electron interactions is enhanced relative to its independent particle value by the Stoner factor $(1-\alpha)^{-1}$ which gives

$$K = K_0/(1-\alpha)$$

where α is related to the strength of the effective electron interaction potential $V(\underline{q})$ and $N_0(E_F)$ by: $\alpha = V(0)N_0(E_F)$. Moriya[38] pointed out that R_1 is enhanced however by the wave number and frequency dependent susceptibility $\chi_p(\underline{q},\omega)$. Both effects can be taken into account by re-expressing equation 1.09 as

$$T_1T(K_s)^2 = \frac{\hbar}{4\pi K}\left\{\frac{\gamma_e}{\gamma_n}^2\right\} \cdot \frac{1}{K(\alpha)}\ , \qquad 1.11$$

where $K(\alpha)$ is a complicated function of α. A number of determinations of $K(\alpha)$ have been made,[39,40], the treatments differing essentially in the choice of the effective interaction potential $V(\underline{q})$. There are also contributions to the relaxation rate from core polarisation and orbital effects, though for most metals they are negligibly small. In a number of pure liquid metals a marked discrepancy still remained between the experimental and theoretical magnetic relaxation rates, even though electron-electron effects had been taken into account. The metals in question have nuclei which possess a nuclear quadrupole moment Q and it is well established that the extra relaxation mechanism is a quadrupolar one arising from the time

varying electric field gradients produced by the diffusing ions.

1.2.3 Present situation in Liquid Metals The factors χ_P and P_F in the Knight shift expression are sensitive to local atomic and electronic structure and K may therefore be expected to change significantly on melting. However, in contrast to R_H and ρ_L, K changes by only approximately 5% for most metals, the exceptions being Cd, Bi, Sb and Ga. Unfortunately there is no consistent correlation between changes in K and R_H on melting; for example in Cd though R_H changes very little, K in fact increases by 33% of itself. Ziman [41] suggested that the constancy in K through the melting point is due to the fact that P_F and χ_P hardly change. Indeed the alternative suggestion that there are compensating changes in χ_P and P_F is not very likely. Harrison [42] has in fact shown that under certain restrictions $N(E_F)$ for a band structure based on the nearly free electron model did not deviate far from the free electron value. Ziman's proposition tends to be corraborated by the fact that both χ_P and P_F depend mainly on atomic volume, which often stays very constant on melting. It therefore seems that the anomalous metals are those in which K does change on melting. In Cd Ziman asserted that this was due to an abrupt change in $N(E_F)$ and this has been quantitatively confirmed by a non-local pseudopotential calculation of Kasowski and Falicov [43], who obtained agreement with experiment by assuming that $N(E_F)$ was free-electron like in liquid Cd. Now that χ_P values for liquid metals are more accessible using the method of Dupree and Seymour [19], a more detailed comparison of the changes in χ_P and K can be made.

The estimation of the Knight shift in pure liquid metals by Heighway and Seymour [44] appears to give good agreement with experiment for a wide range of metals using only a zero-order pseudopotential calculation. The investigation of the change in K as a function of temperature has been less successful. Heighway [45] failed to reproduce his experimental $\delta K/\delta T$ data in solid

and liquid Pb using an expression due to Watabe and Tanaka[46]. More recently Das et al.[47] have predicted the observed temperature independence of the Knight shift in liquid Cd using a non-local pseudopotential calculation of the spin density. They conclude that any temperature dependence of the Knight shift arises through the change in the interference function I(K) as a function of temperature. The calculations of Perdew[55] reveal that the hyperfine contact densities in liquid alkali metals are strongly dependent on k_F. Clearly measurements of density as a function of temperature, which would allow k_F to be calculated using the free electron model, would show how much the change in Knight shift as a function of temperature is accounted for by a changing k_F value. Thus even for pure metals the theoretical situation is complicated though the theory and observations generally support the idea that liquid metals have a free-electron like $N(E_F)$.

The situation in alloys however is even more complex. Alloying the pure metal with a dilute amount of another metallic solute nearly always produces fractional changes in the solvent and solute shifts which are often linear in the concentration and the same for both solute and solvent. This change is due to the electron re-distribution which screens out the charge on the solute ion. Blandin etal.[48] using a nearly free electron approximation and a square well potential representation of the solute and solvent ions predicted with reasonable success the change in solvent and solute Knight shift for some dilute alkali alloys. However when the same model was applied to polyvalent alloys no agreement with experiment was obtained[49]. Using reasonable physical arguments Flynn[50] has shown that a set of semi-empirical phase shifts may be derived for an alloy system and these have been used to predict fairly well the observed change in solvent Knight shift for a number of alloy systems. A more fundamental advance in the calculation of phase shifts has been made by Young etal.[51] and by Asik etal.[52]. Both methods use a more realistic screened free atom potential representation of the solvent

and solute ions. Applied to some dilute alkali alloys the phase shifts calculated in this way give better agreement with experiment than the model of Blandin etal. The single centre scattering approach used to calculate solvent shifts is clearly inadequate for large solute concentrations. Consequently a pseudopotential method has been developed by Faber[53] and his theory applied to a number of alloy systems in the hope of predicting the solvent shift. Though reasonably successful for some dilute alkali alloys, when applied by Moulson[54] to some polyvalent alloys at high solute concentrations, the theory was unable to predict even the correct sign in the change of the ^{115}In Knight shift in the In-Sn or In-Pb systems. Perdew and Wilkins[55] have recently extended the Faber theory and calculated contact densities in some liquid alkali alloys across the complete range of concentration. Their data, when combined with measured Knight shifts, lead to reasonable values of χ_p for these alloys. However up to the present neither the phase shift theory of Young etal. and Asik etal. or the pseudopotential theory of Perdew and Wilkins has been applied to any polyvalent alloy systems. There have been a number of recent attempts to calculate absolute exchange core polarisation contributions to the Knight shift in metals. In particular those of Mahanti and Das[35] for the alkalis and Halder and Jena[56] for liquid magnesium have been fairly successful in predicting magnitudes of K_{cp} which are consistent with calculations of K_s and experimental Knight shifts.

The versatility of the Knight shift is apparent by its use as a probe for atomic as well as electronic structure in both solid and liquid metals and alloys. Drain[57] for example has investigated the phase changes in the Ag-Cd system by observing the variation in the ^{113}Cd and ^{109}Ag Knight shifts across the concentration range and more recently Styles[58] has interpreted his Knight shift and line width data in the liquid In-Bi system in terms of non-random atomic associations. However there has been no attempt

to correlate Knight shift data with x-ray or neutron diffraction data which suggests that ordering is taking place at particular compositions in an alloy system[59].

In many liquid metal and alloy systems where one of the nuclei concerned has $I>\frac{1}{2}$ there may be a quadrupolar contribution R_{1Q} to the relaxation rate as well as a magnetic contribution R_{1M}. In particular this has been found to be the case for ^{115}In and ^{209}Bi in the liquid Pb-Bi and In-Bi systems. Estimates of R_{1M} may be made with reasonable accuracy providing account is taken of K_{other} and an estimate is made of $K(\alpha)$. On the other hand the evaluation of R_{1Q} is difficult and at present it is not possible to calculate its value absolutely in a liquid metal or alloy without making some approximations to the theory[60].

1.3 Present Investigation

This work was initiated with the aim of continuing the investigation of electronic properties of liquid alloys and examining these properties in the light of the information they yield regarding liquid alloy structure.

Measurements have been made of the Knight shift, spin-lattice relaxation time and magnetic susceptibility in the liquid noble metal-tin and noble metal-indium systems. Chapter 2 contains an account of the experimental techniques used to measure these properties together with a description of the preparation of the specimens used. In chapter 3 the data obtained are presented in graphical form. In chapter 4 the NMR and susceptibility data are considered in the light of the information they yield regarding structure in these systems, in particular some x-ray and neutron diffraction data have pointed to the existence of structure for some of the liquid noble metal-tin systems. Chapter 5 considers the changes in the Knight shift arising from

changes in either or both factors χ_p and P_F and the first part contains an extraction of χ_p from the total susceptibility measurements. Following this is a calculation of the changes in the solvent P_F for these systems using a partial wave analysis of the impurity scattering for dilute concentrations of solute. Two model potentials are used to represent the solute, a square well and screened free atom potential, the latter being based on the work of Asik etal. The final part of chapter 5 contains an extension of Perdew and Wilkins' pseudopotential theory to polyvalent alloy systems where P_F is calculated at both solvent and solute nuclei across the complete range of concentration for the present alloy systems. In chapter 6 the relaxation rates of ^{119}Sn, ^{115}In and ^{63}Cu are considered. Reasonable estimates are made of the magnetic contributions R_{1M} by taking account of K_{other} and $K(\alpha)$. The significant quadrupolar contribution R_{1Q} to the relaxation of ^{115}In in the noble metal-indium alloys is considered in the light of existing theories. Finally chapter 7 illustrates that the above considerations can be applied also to cases where the solute is non-metallic. It contains an account of an NMR investigation of ^{133}Cs in the liquid cesium-oxygen system and the results are discussed with particular reference to the state of the oxygen atoms in liquid cesium.

REFERENCES

(1) Cusack N.E., Rep. Progr.Phys., 36, (1963), 361.

(2) Wilson J.R., Met. Rev., 10, (1965), 381.

(3) Mott N.F., Liquids: Structure, Properties and solid interactions, (ed. Hughel 1965), Elsevier, 152.

(4) The Properties of Liquid Metals, Proc. Int. Conf. at Brookhaven, Adv. Phys., 16, (1967), (ed. Adams, Davies and Epstein), Taylor and Francis Ltd., London.

(5) March N. H., Liquid Metals, (1968), Pergamon Press.

(6) Cusack N. E. and Kendall P. W., Phil. Mag., 8, (1963), 157.

(7) Enderby J. E., Hasan S. B. and Simmons C. J., Adv. Phys., 16, (1967), 667.

(8) Smith N. V., Adv. Phys., 16, (1967), 629.

(9) Schultz L. G., Adv. Phys., 6, (1957), 102.

(10) Ziman J. M., Phil. Mag., 6, (1961), 1013.

(11) Ashcroft N. W. and Schaich W., Phys. Rev. B, 1, (1970), 1370.

(12) Bradley C. C., Faber T. E., Wilson E. G. and Ziman J. M., Phil.Mag., 7, (1962), 865.

Faber T. E. and Ziman J. M., Phil. Mag., 11, (1965), 153.

(13) Cusack N. E., Contemp. Phys., 8, (1067), 61.

(14) Edwards S. F., Phil. Mag., 3, (1958), 1020, Ibid., 6, (1961), 617; Proc. Roy. Soc., A267, (1962), 518; Proc. Phys. Soc., 85, (1965), 1.

(15) Ballantine L. E., Can. J. Phys., 44, (1966), 2533.

(16) Kusmiss J. H. and Stewart A. T., Adv. Phys., 16, (1967), 471.

(17) Edwards S. F. Adv. Phys., 16, (1967), 359.

(18) Catterall J. A. and Trotter J., Phil. Mag., 8, (1963), 897.

(19) Dupree R. and Seymour E. F. W., Phys. Kondens,Materie, 12, (1970), 97.

(20) Angus W. R., Prod. Roy. Soc., A136, (1932), 569.

(21) Dupree R. and Geldart D. J. W., Sol. State Comm., 9, (1971), 145.

(22) Enderby J. E., North D. M. and Egelstaff P. A., Adv. Phys., 16, (1966), 171.

(23) Ashcroft N. W. and Lekner J., Phys. Rev., 145, (1966), 83.

(24) Ashcroft N. W. and Langreth D. C., Phys. Rev. 156, (1967), 685. Ibid., 159, (1967), 500.

(25) Purcell E. M., Torrey H. C. and Pound R. V., Phys. Rev., 69, (1946), 37.

(26) Bloch F., Hansen W. W. and Packard M. E., Phys. Rev., 69, (1946), 127.

(27) Andrew E. R., Nuclear Magnetic Resonance, (C.U.P. 1958).

(28) Slichter C. P., Principles of Magnetic Resonance., (Harper and Row, New York 1963).

(29) Abragam A., The Principles of Nuclear Magnetism, (Oxford 1961).

(30) Knight W. D., Phys. Rev., 76, (1949), 1259.

Townes C. H., Herring C. and Knight W. D., Phys. Rev., 77 (1950), 852.

(31) Rowland T. J., Prog. Mat. Sci., 9, (1961), 1.

(32) Drain L. E., Metall. Rev., 119, (1967), 195.

(33) Bennett L. A., Watson R. E. and Carter G. C., Jnl. Res. Nat. Bur. Stds., 74A, (1970), 569.

(34) Kasowski R. V., Phys. Rev., 187, (1969), 891.

(35) Mahanti S. D. and Das T. P., Phys. Rev. B, 3, (1971), 1599.

(36) Korringa J., Physica, 16, (1950), 601.

(37) Pines D., Solid State Physics, 1, (N.Y. Academic Press, 1955), 367.

(38) Moriya T., J. Phys. Soc. Japan, 18, (1963), 516.

(39) Narath A. and Weaver H. T., Phys. Rev., 175, (1968), 373.

(40) Shaw R. W. and Warren W. W., Phys. Rev. B, 3, (1971), 1562.

(41) Ziman J. M., Adv. Phys., 16, (1967), 421.

(42) Harrison W. A., Pseudopotentials in the Theory of Metals, (1966), New York, Benjamin, 117.

(43) Kasowski R. V. and Falicov L. M., Phys. Rev. Lett., 22, (1969), 1001.

(44) Heighway, J. and Seymour E. F. W., Phys. Kondens. Materie, 13, (1971), 1.

(45) Heighway J., Ph.D. Thesis, University of Warwick, 1969.

(46) Watabe M. and Tanaka W., Phil. Mag., 12, (1965), 347.

(47) Jena P., Das T. P., Gaspari G. D. and Halder N. C., Phys. Rev. B, 3, (1971), 2158.

(48) Blandin A., Daniel E. and Friedel J., Phil. Mag., 4, (1959), 180.

Blandin A. and Daniel E., J. Phys. Chem. Sol., 10, (1959), 126.

(49) Styles G. A., Ph. D. Thesis, University of Leeds, 1964.

(50) Flynn C. D. and Rigney D. A., Phil. Mag., 15, (1967), 1213.

Flynn C. P. and Odle R. L., Phil. Mag., 13, (1966), 699.

(51) Meyer A., Nestor C. W. and Young W. H., Proc. Phys. Soc., 92, (1967), 446.

(52) Asik J. R., Ball M. A. and Slichter C. P., Phys. Rev., 181, (1969), 645; Ibid; Phys. Rev., 181, (1969), 662.

(53) Faber T. E., Adv. Phys., 16, (1967), 637.

(54) Moulson D. J.,Ph.D., Thesis, University of Leeds, 1966.

(55) Perdew J. P. and Wilkins J. W., Sol. State Comm., 8, (1970), 2041.

(56) Halder N. C. and Jena P., Phys. Rev. B, 4, (1971), 2385.

(57) Drain L. E., Phil. Mag., 4, (1959), 484.

(58) Styles G. A., Adv. Phys., 16, (1967), 275.

(59) Wagner C. N. J., Halder N. C. and North D. M., Z. Naturforsch., 24a, (1969), 432.

(60) Sholl C. A., Private Communication.

CHAPTER TWO

EXPERIMENTAL METHODS

2.1 Introduction

Experimental observations have been made of steady state NMR, pulsed NMR and magnetic susceptibility. The apparatus and techniques required to make these measurements are well documented however, and will not therefore be described in detail here. Each experimental arrangement and method of measurement will be simply outlined, emphasis being given to those aspects of the work which are either original or, for one reason or another, demand particular attention.

It is essential that one has reliable specimens on which to perform the above measurements and the final section is therefore devoted to a detailed discussion of the methods used for specimen preparation, and the shortcomings of previously used techniques.

2.2 Steady State NMR Apparatus

The Spectrometer A Varian V.F.16 wide-line spectrometer was employed in the measurements. This has a frequency range of 2 - 16 MHz and uses the nuclear induction method of detecting resonance [1]. Used in conjunction with the spectrometer is a Varian 12" electromagnet, capable of maintaining fields up to 15 kgauss with homogeneity of 1 part in 10^5. The field can be swept in times varying from 0·5 - 100 minutes, with apparatus response times of 0·1 - 100 seconds. In use, the frequency is kept constant while the audio-modulated magnetic field is swept through the resonance value. The detected signal is amplified and de-modulated,

being fed either to the oscilloscope or phase sensitive detector and pen recorder. A block diagram of the apparatus is shown in fig. 2.01. The maximum sweep time, in conjunction with the corresponding response time, imposes a limitation on sensitivity and consequently a noise averager or Computer of Average Transients (C.A.T.) was used for weaker signals. The instrument employed was a Northern NS-544 Digital Memory Oscilloscope. As the field H_0 is swept through resonance, the output from the spectrometer is fed to 1,024 storage channels in the C.A.T. An address advance pulse generator opens each channel in synchronism with the field sweep, so that for one completed sweep all of the storage channels have been opened, each channel storing information relating to a small section of the sweep. On sweeping through the resonance N times, the r.m.s. random noise voltage stored is proportional to $\sqrt{N}$ while the signal is proportional to N, thus providing an improvement in signal to noise of $\sqrt{N}$. **For a typical ^{119}Sn measurement 30 half minute sweeps were made giving a signal to noise ratio of 5:1.**

A gas flow furnace was used in conjunction with the Varian spectrometer similar to that described by Schreiber[2]. The specimen temperature was measured using a Pt/Pt - 13% Rh thermocouple located immediately below the specimen tube. Experiment showed that the temperature gradient across the sample did not exceed 5K. A chromel-alumel thermocouple monitored the probe body temperature, the permissible maximum being 338K which subsequently limited the specimen temperatures to a maximum of 800K.

Frequency and Field Calibration To determine the resonance position and width exact values of frequency and magnetic field are required. The frequency was measured using a Venner TSA 3436 counter and the magnetic field calibration performed in the following manner. The signal of interest was first accumulated in the C.A.T. and then read out on an X-Y plotter. Using a subsidiary Watkins-Pound spectrometer the ^{2}D resonance in a sample of heavy water in the magnet gap was detected, and the frequency of the spectrometer

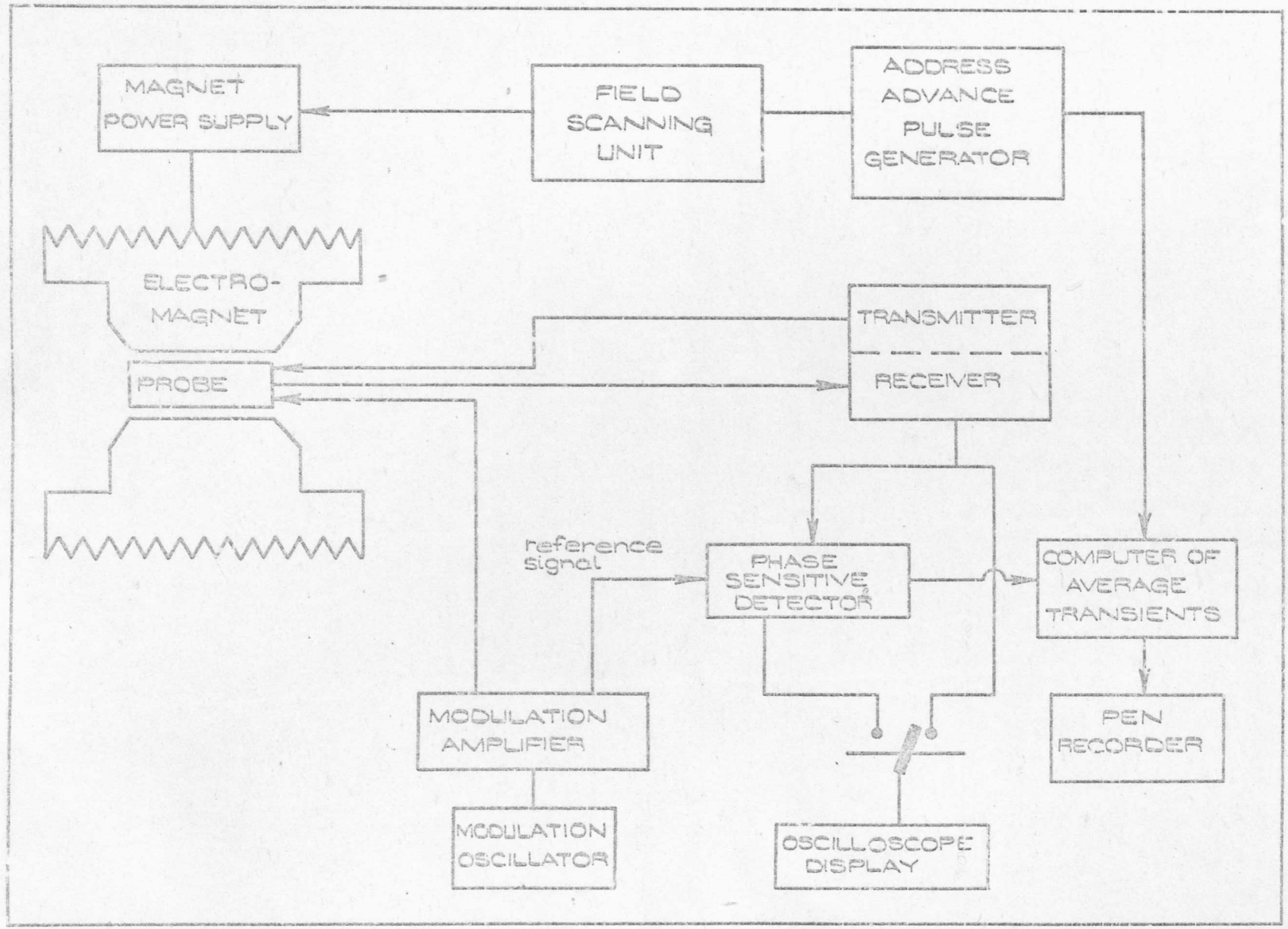

FIGURE 2·01.

BLOCK DIAGRAM OF STEADY STATE N.M.R. APPARATUS.

adjusted so that the resonance occurred near the beginning of the field sweep used in the main experiment. This signal was recorded on the C.A.T. using a single sweep of the magnetic field. Subsequently the frequency was changed so that the ^2D resonance occurred near the end of a sweep and the signal again recorded. These two field marker signals were then read out on the X-Y plotter below the signal previously recorded. From the measured frequencies of the two ^2D resonances and using the known ^2D gyromagnetic ratio the field at two points on the sweep used in the main experiment was thus precisely determined and by interpolation the position and width of the signal of interest can be readily measured.

High Temperature Apparatus NMR measurements at temperatures up to 1400 K were made possible by the construction of a high temperature furnace, shown schematically in fig. 2.02, which is used in conjunction with a Watkins-Pound Spectrometer. This experimental arrangement overcame the temperature maximum of 800 K to which the Varian spectrometer was limited. The sample is contained in a silica tube around which is wound the r.f. coil. These are in turn surrounded by the heater coil assembly which is a push fit in a silvered silica dewar. Located by an O-ring clamping arrangement at either end, the dewar is finally contained in a water jacket made from stainless steel tubing.

Initially the r.f. coil was constructed from copper wire, however use at temperatures in excess of 1100 K caused rapid deterioration in the coil due to oxidation and a subsequent reduction in signal-to-noise ratio. Thus a gold coil was used, which showed no signs of deterioration, after prolonged use at temperatures in excess of 1100 K. The heating coil assembly consists of a hollow Fibrefrax former onto which a non-inductive nichrome coil is wound. The coil is covered with layers of Fibrefrax until the whole is a push fit in the dewar. The inner diameter of the Fibrefrax

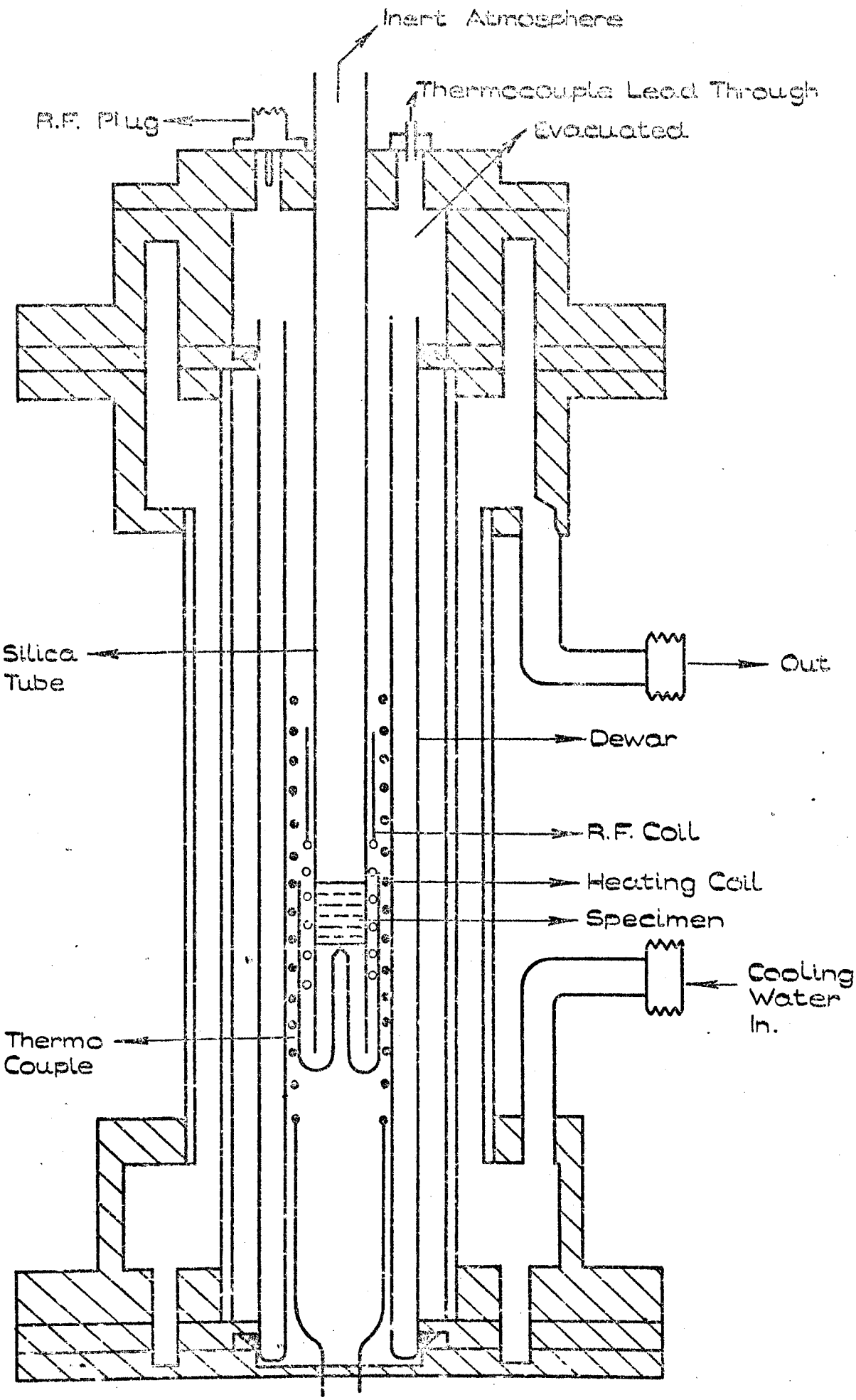

FIGURE 2.02.

HIGH TEMPERATURE FURNACE.

former had to be sufficient to take the r.f. coil assembly. The heater coil is matched to the power supply, which supplies 10 amps at 50 volts. The coil when supplied with 5 amps at 25 volts gave a temperature of 1100 K. The top and bottom ends of the furnace, (the shaded portion of fig. 2.02.) are made of brass and connected by the water jacket which kept the temperature of the outer tube, in places touching the magnet pole faces, below the ambient temperature. Since the temperature measuring thermocouple is not in exactly the same position as the specimen, it was necessary to check that the thermocouple reading was a true indication of the specimen temperature. This was done by observing the thermocouple reading at which the ^{115}In resonance signal first appeared on heating up the specimens. This should occur at the melting points of pure indium (429 K) and the compound $Ag\ In_2$ (693 K) since the resonance is more easily observable in the liquid. It was found that the thermocouple and specimen temperatures were within 5 K and 7 K at 429 K and 693 K respectively. This agreement was considered to be satisfactory.

2.3 Pulse Apparatus

This is shown in block diagram form in fig. 2.03, and is based on a design by Clarke[4]. The sample is placed in a coil assembly containing a transmitter and receiver coil, which are mounted orthogonally to each other and to H_0. A non-inductively wound heater coil, insulated with Fibrefrax, surrounds both coils. A Varian 9" electro-magnet produces the steady magnetic field H_0. A sequence of high power r.f. pulses at the Larmor frequency may be applied to the transmitter coil, the pulses being produced at a fixed rate by a pulse sequence generator. The pulses are continuously variable in length from 1 μs - 2 ms and are modulated at the radio-frequency by a free running crystal controlled oscillator. The output of the receiver is fed into a phase sensitive detector along with a reference signal derived from the free-running oscillator. The detected signal is then fed into a Boxcar

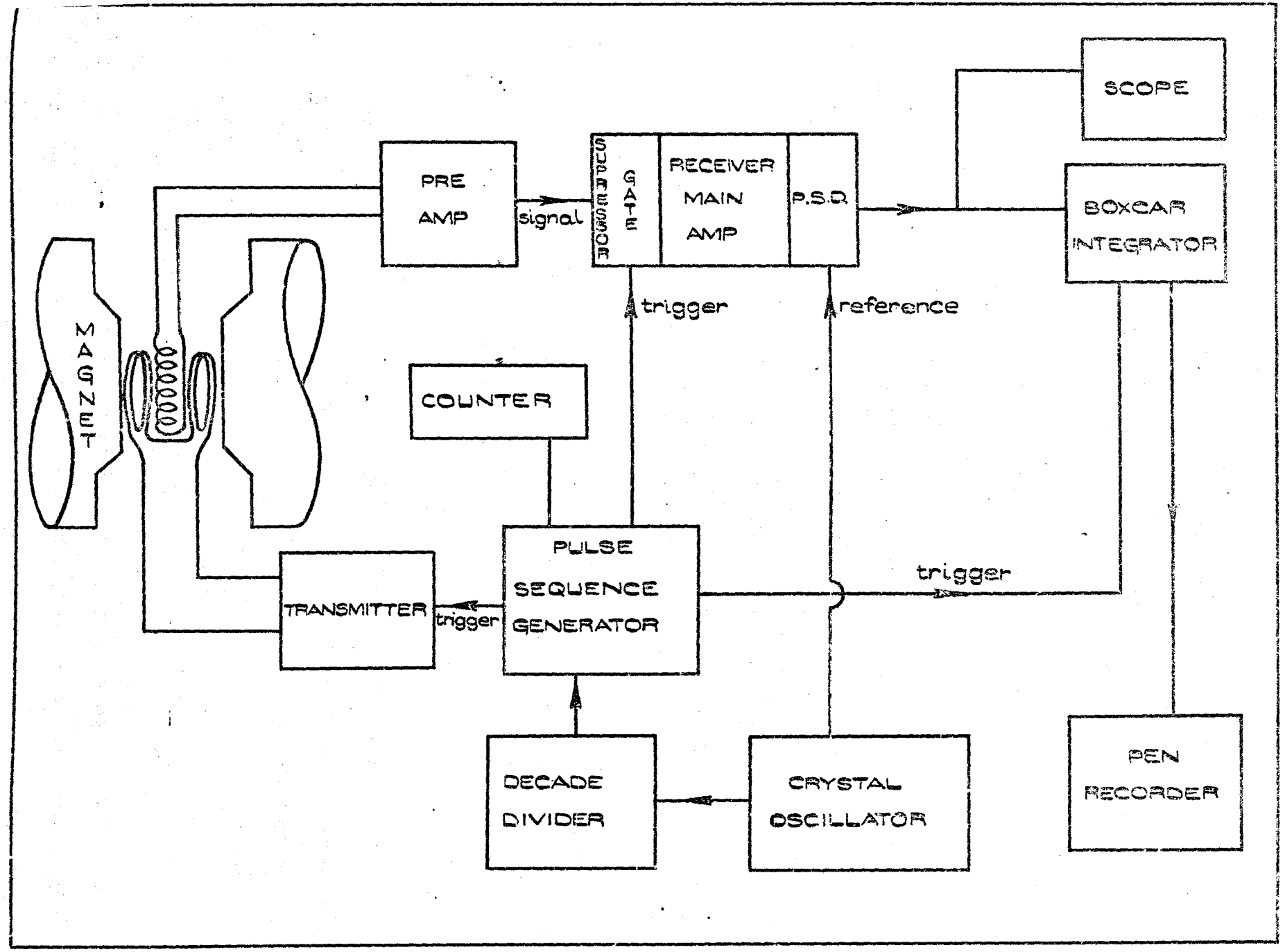

FIGURE 2.03.

BLOCK DIAGRAM OF PULSED N.M.R. APPARATUS.

integrator which has gate widths varying from 1 μs - 100 ms. The Boxcar output is finally fed to a pen recorder.

Measurements were made of the rate of decay, T_1, of the longitudinal magnetisation using the usual $180^\circ - \tau - 90^\circ$ sequence. The amplitude of the signal at a point immediately following the 90° pulse is proportional to M_τ, the longitudinal magnetisation existing at that time, and by setting the Boxcar gate to sample immediately after the 90° pulse, its output will be proportional to M_τ. Initially correct phasing is required and for this adjustment the Boxcar gate is made wide enough to encompass the whole of the free induction decay. The Boxcar output, as a function of magnetic field, is the Fourier transform of the free induction decay. The field is then swept and the exact position of resonance selected. The gate-width is then reduced and with the Boxcar output fed to an X - T recorder, the value of M_0 is determined by switching the field on and off resonance. On reducing the pulse separation τ by stages, the corresponding values of M_τ can be determined.

The spin-lattice relaxation time, T_1, is related to the longitudinal magnetisation at a time τ through:

$$M_\tau = M_0\{1-A\exp(-\tau/T_1)\}$$

where A is a constant, in theory equal to 2 but in practice usually lower than this. A graph of log $(M_0 - M_\tau)$ against τ is plotted and T_1 determined from the slope. This was done using a least squares computer programme supplied by Dr. E. M. Dickson.

2.4 Susceptibility Apparatus

The magnetic susceptibilities of the samples were measured using the Curie technique in which the sample of volume $\approx 0.1 cm^3$ is placed on one arm of a sensitive microbalance in an inhomogeneous magnetic field. The

force (y-direction) acting on a small sample between the pole faces of a magnet (x-direction) is

$$F_y = m\chi_x Y,$$

where χ is the mass susceptibility of a specimen of mass m and $Y \equiv H_x(\frac{\partial H_x}{\partial Y})$. The force on a sample of accurately known susceptibility was first measured so that Y was determined and subsequently used in the measurement of an unknown specimen. The specimen is suspended in a non-uniform magnetic field and F_y will therefore depend critically on the exact location of the sample. In measurements of this type[5] an effort is made to make Y as constant as possible over the sample so as to obtain good data reproductibility. In the present apparatus the pole pieces were of such a shape that Y went through a positive maximum followed by a negative maximum and if these positions are noted when traversing the magnet over the specimen the problem of accurate sample positioning is removed. A Sartorius microbalance with a sensitivity of 1μg was used to measure the force on the specimen which weighed approximately 1 gram.

In making a measurement, the magnet is jacked up to a position such that the specimen is below the Y maximum. Allowing a small amount of hydraulic fluid to escape from the jack holding the magnet, the magnet traverses slowly down over the specimen and at the same time the changing force on the specimen is followed on the microbalance. At the position of maximum force, maximum Y, the reading is voted. The magnet is then traversed quickly until it approaches the region of minimum Y whence it is slowed down and the minimum force on the sample noted. Thus the factor $(Y_{max} - Y_{min})$ is used in calculating the susceptibility and this was determined by making similar measurements on samples of Ge, Ag, and Sn whose susceptibilities are accurately known. A subsidiary experiment was performed in which the force

on the sample holder, a quartz bucket, was found at temperatures corresponding to those at which specimen observations were made. All measurements were made at a pressure of 400 torr of argon, this pressure being sufficient to inhibit preferential evaporation of a lower melting point alloy component. Pressures greater than 400 torr gave rise to convection currents which caused the balance reading to fluctuate, this effect becoming violent at the higher temperatures. The furnace used attained temperatures of 1400 K and consisted of a nichrome coil matched to the power supply, wound directly on to a silica tube which fitted the lower arm of the microbalance. Layers of Fibrefrax covered the heater coil, giving sufficient insulation for the attainment of higher temperatures, but allowed clearance for the magnet pole faces to pass over it whilst a measurement was being made. A chromel-alumel thermocouple indicated the temperature on the inside of the furnace tube and was located just 4 mm to the side of the sample.

2.5 Sample Preparation

Introduction Observation of NMR in pure metals requires ideally that the diameter of the particles be less than the radio-frequency skin depth. For most metals at normal frequencies and temperatures this involves diameters between 10 and 100 μm.

Measurements in alloys require further that every particle in the sample is of the nominal composition of the alloy, deviations from either of these conditions may result in distortion of the resonance spectrum. To date, powders have been produced mainly by one of two methods. The first is that in which the two constituents are melted together forming an ingot, which is then filed or ground and finally sieved[6]. Alternatively the metal can be melted under a silicone oil and then agitated to produce a dispersion of liquid droplets. After solidifying, the oil is washed off with organic

solvents and the metal particles again sieved. The first and most common method cited is subject to the following difficulties.

(i) The metallurgical phase diagram corresponding to a particular binary alloy system may be such that large scale phase separation may take place when the alloy is cast. If this occurs, particles produced by filing would be of different compositions and obviously further heat treatment of the particles would not change this. NMR measurements of the ^{119}Sn nucleus in a nominally $AuSn_2$ alloy, prepared by such a method, produced two distinct lines in its resonance spectrum corresponding to the ^{119}Sn nuclei finding themselves in two different environments probably due to phase separation on cooling[7].

(ii) The particles produced are irregular in shape and hence pack together rather badly in contrast to the packing of spherical particles. NMR measurements of the ^{119}Sn nucleus were made in 3 pure tin samples, the metal having been powdered by: a) filing; b) grinding on a wheel and c) dispersion from the liquid. In all cases the particles were insulated from each other by mixing in an equal volume of fused silica powder. The signal intensities obtained from the filed and ground specimens were a factor of approximately 3 less then those from the spherically shaped particles produced by dispersion. Fig. 2.05 contrasts powders produced by a) filing and b) dispersion from the liquid. The largest particles in b) have diameters of the order 50 μm.

(iii) Filing and grinding always introduce impurities into the resulting powder, this being particularly serious when iron files are used. Most or nearly all of the ferromagnetic impurities can be removed with a magnet, though the possibility of even one or two remaining is an undesirable feature.

The difficulties cited above may be overcome if the alloys are

prepared by dispersion in oil, this method producing spherical and homogeneous powder particles. However it is limited to alloys with melting points lower than about 600 K because of the low flashpoint of silicone oils available. Two methods of overcoming the above difficulties by using a spraying technique will now be described[8].

Spraying from the solid In this technique, the samples were fed in the form of a solid rod 3/16" in diameter into a metal spraying pistol. A Mk - 45 pistol available from Metallisation Ltd., Dudley, Worcs., was used which runs on oxypropane or oxyacetylene fuel together with compressed air for dispersing the molten metal into droplets. Metals with melting points up to 2800 K may be sprayed, though to date Rh, which melts at 2239 K, is the highest melting point metal yet sprayed. The initial form of the alloy was an ingot approximately 20 mm in length and 10 mm in diameter, which is cast by melting the alloy constituents in a silica tube, the melt being kept well above the alloy liquidus to ensure complete mixing. Alloys which are malleable in the solid may be reduced to the required 3/16" diameter accepted by the gun, by cold swaging. Those systems, however, in which certain compositions correspond to brittle phases or a mixture of phases, had to be cast in the form of a rod. As the rod is taken into the pistol, it emerges from the outlet nozzle, is melted by the oxypropane flame and dispersed into a spray by the compressed air. The metal is quenched in water which is contained in a glass vessel. The powder is washed to the bottom of the vessel, removed, cleaned with acetone and sieved. The actual spraying process is rapid, the speed at which the metal is fed into the gun depending on its melting point. For zinc a rate of 6m per min. produced a powder of which approximately 90% passed through a 50 μm sieve. Such a

high yield, however, required some initial adjustments of the speed with which the wire was fed into the pistol. Particles produced by this method are shown in fig. 2.05 and may be compared with those produced by filing. However, as in the filing methods, composition variations in the rod resulted in a spread of composition in the powders which limited this method to pure metals and alloy compositions malleable enough to be swaged as this process helps to improve homogeneity within the rod by creating a large number of vacancies which assist the diffusion process.

Spraying from the liquid The experimental arrangement for this technique is shown in fig. 2.04 . An alloy ingot, cast in the same way as described previously, is broken up into small pieces of size 4 mm or less. These pieces are then inserted into the lower half of the silica vessel which may be split at the ground glass joint. At the base where the alloy is contained is a ground glass valve capable of holding a vacuum of 0.2 torr which may be raised to allow the molten metal to run down into the tapered section of the vessel which is terminated by a fine jet of diameter 2 mm. The pumping stem on the upper half of the vessel allows it to be evacuated, while the brass top-cap contains an O-ring clamping device which holds the ground glass valve in the closed position. The tip of the jet is located immediately beneath a copper nozzle through which nitrogen gas escapes at a pressure of 20 lb in^{-2}, which disperses the molten metal. The sprayed metal is collected and sieved as in the previous method. The mode of operation is as follows. The alloy, being in small pieces, lodges between the valve and walls of the tube and rests in the lower half of the silica tube. With the two halves of the vessel clamped at the ground glass joint, the whole is evacuated and flushed with argon. A slight over-pressure of argon is then introduced to prevent preferential evaporation of either component when the alloy is molten. The vessel is then heated with

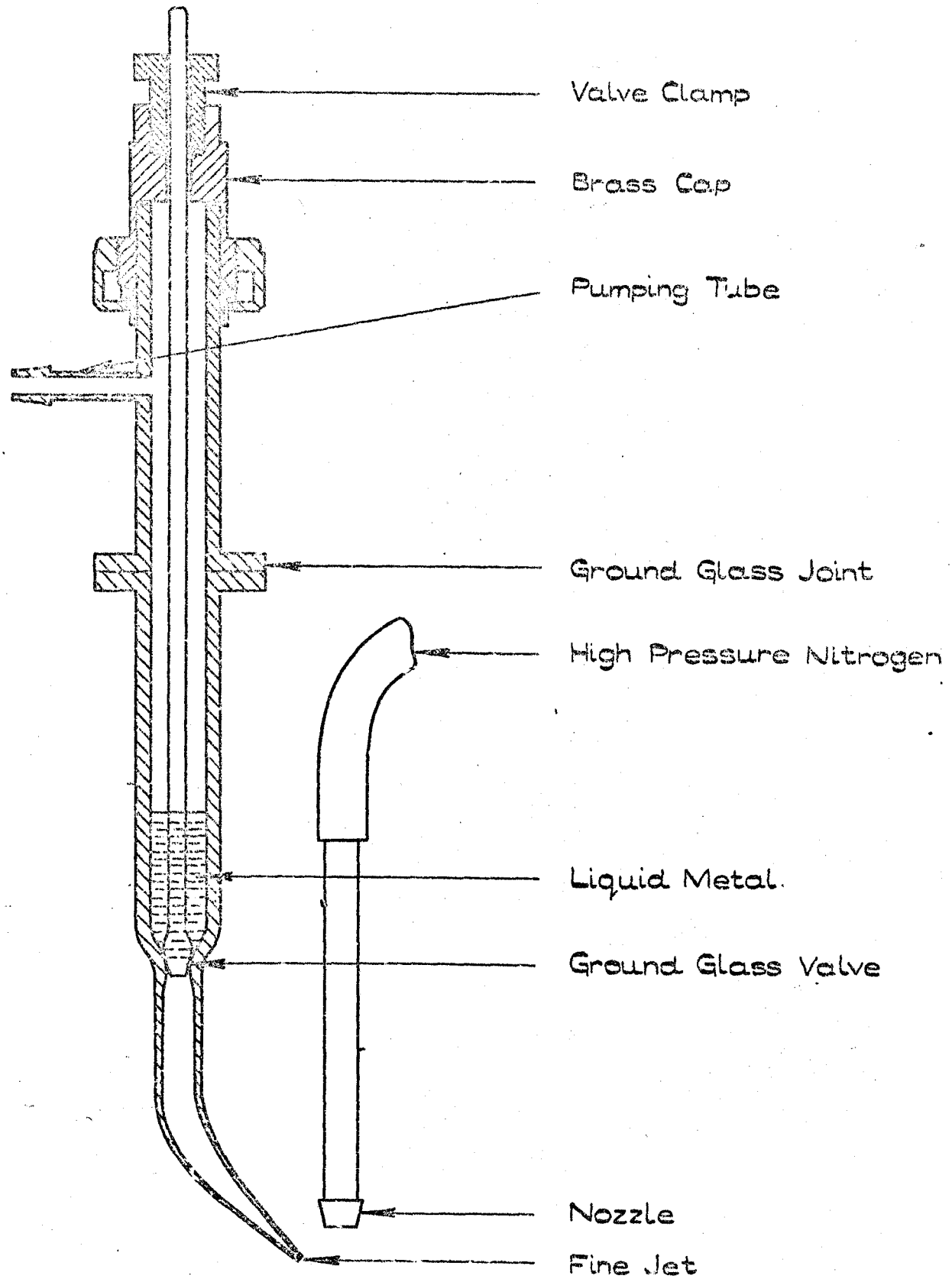

FIGURE 2.04.

SILICA SPRAYING TUBE.

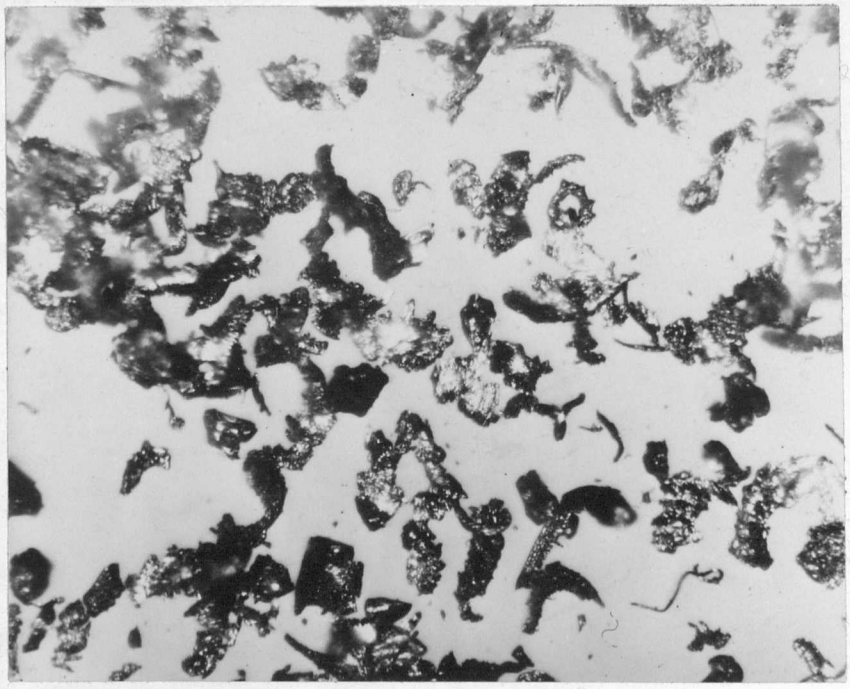

a) powder produced by filing

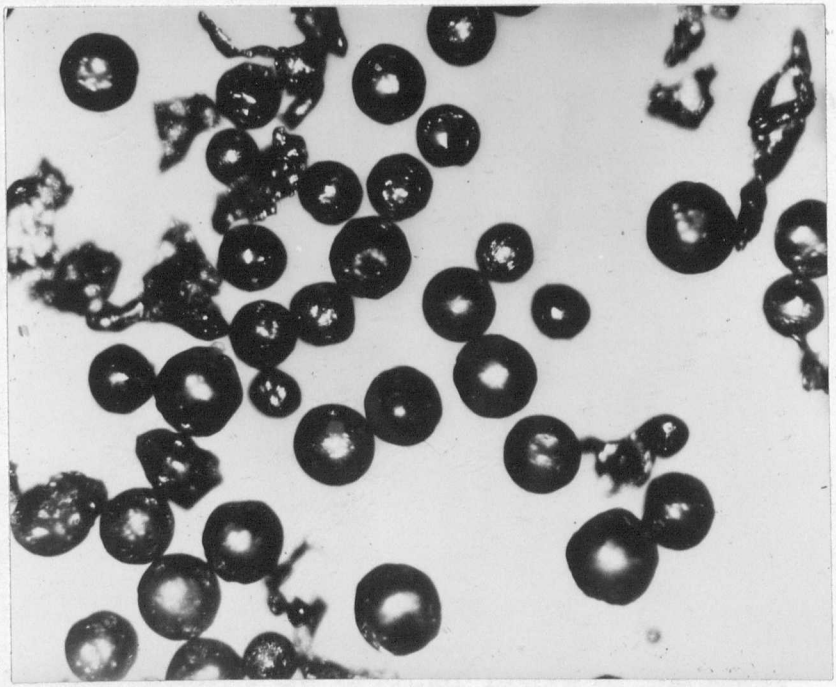

b) powder produced by dispersion from the liquid.

FIGURE 2.05

COMPARISON OF POWDERS PRODUCED BY FILING AND LIQUID DISPERSION.

The largest particles in b) have diameters of the order of 50μm.

an oxypropane torch until the alloy melts, the tapered section and jet being kept at the same temperature as the alloy. A further overpressure of 8 cm Hg is created in the vessel and simultaneously with the valve being withdrawn to let through the liquid metal, the nitrogen jet is turned on. The overpressure of argon forces the liquid metal out in a fine jet and is dispersed by nitrogen gas, heat continuing to be applied, particularly to the orifice through which the metal escapes which tends to be cooled by the blast of nitrogen. The particles quench in the water jacket and collect in the bottom of the dewar. The process is interrupted if a) oxide blocks the orifice or b) the metal solidifies due to insufficient heat being applied. The actual spraying process takes one or two minutes. The yield of particles is somewhat less than in the previous technique with only about one third of the powder passing through a 50 μm sieve. Hopefully the yield from this technique could be improved by a suitable combination of size of orifice, metal flow rate and strength of the nitrogen blast. Alloys with melting points up to 1100 K were prepared in this way, this limit being set by the softening point of the silica. No possibility of particle inhomogeneity exists as the alloy is liquid right up to the point where the droplets are formed, and subsequent measurements on alloys prepared this way confirmed this. Powder density measurements showed that these powders, as those sprayed from the solid, were approximately three times as dense as the filed or ground specimens. Powders obtained by both spraying methods showed slight signs of oxidation, though for nearly all of the alloys prepared the powders retained the original lustre of the metal. This, however, does not affect the NMR measurements since even if a resonance is detected in the oxide, its position will be different from that in the metal because of the metallic Knight shift.

Summary The two methods described have, within the limitations stated, produced powders simply and rapidly over a wide range of alloys.

The advantages these methods have over those previously used are threefold. Firstly, the particles are spherical and pack together with a density of a factor 3 better than filed or ground samples; thus yielding a subsequent increase in the NMR signal. Secondly, sources of contaminations and impurities are removed and finally composition variations between particles are eliminated.

Table 2.01 summarizes the methods by which all the alloys measured were prepared. Those alloys prepared by crushing in a pestle and mortar correspond to particular phases or intermetallic compounds in that particular alloy system. All of the alloys were made from 5N pure materials obtained from Koch-Light Laboratories, Bucks.

A check on sample composition was provided by a quantitative analysis for both constituents, made by Johnson and Matthey Ltd. on Ag-55% In and Cu-75% In. The results are shown below.

Nominal	Analysis
45% Ag-55% In	44.89% Ag-54.90% In
25% Cu-75% In	24.10% Cu-75.82% In

TABLE 2.01

Alloy	Method of Preparation
All copper-tin and silver-tin alloys	sprayed from the solid
AuSn	crushed in a pestle and mortar
$AuSn_4$, $AuSn_2$, Au-29% Sn, Au-25%Sn, Au-21% Sn.	sprayed from the liquid
Ag-90% In, Ag-80% In, $AgIn_2$, Ag_3In, Ag-55% In, Ag-40% In, Ag-30% In, Ag-17% In	sprayed from the liquid
Ag_2In, Ag-40% In	crushed in a pestle and mortar
Cu-90% In, Cu-75% In, Cu-60% In, Cu-45% In, Cu-62.5% In, Cu-20% In	sprayed from the liquid
Cu-30% In, Cu-37.5% In	crushed in a pestle and mortar
Au-90% In, Au-80% In, Au-40% In, Au-20% In	sprayed from the liquid
$AuIn_2$, AuIn, Au-30% In.	crushed in pestle and mortar.

REFERENCES

(1) Andrew E. R., Nuclear Magnetic Resonance (C.U.P. 1958).

(2) Schreiber D. S., Rev. Sci. Instr., 35, (1964), 1582.

(3) Styles, G. A., PhD. Thesis, Leeds, (1964).

(4) Clarke W. G., Rev. Sci. Instr., 35, (1964), 316.

(5) Collings E. W., Phys.kondens.Materie, 8, (1969), 284.

(6) Rowland T. J., Phys.Rev., 125, (1962), 459.

(7) Hansen M., Constitution of Binary Alloys, McGraw Hill (1958), 233.

(8) Heighway, J., Host I. P., Styles G.A., J.Phys. (E), 3, (1970), 391.

CHAPTER THREE

EXPERIMENTAL RESULTS

3.1 Knight Shifts and Line Widths

The Knight shift, K, in a metal is defined as the shift of the resonance field from that of the same isotope in a non-conducting reference material at the same frequency. It may be written:

$$K = \frac{(H/\nu)_r - (H/\nu)_m}{(H/\nu)_m} \qquad 3\cdot1$$

where $(H/\nu)_r$ is the field to frequency ratio at the resonance position for the reference compound and $(H/\nu)_m$ is that for the metal. Due to chemical shifts, however, $(H/\nu)_r$ will differ depending on which reference compound is chosen. The present investigation was concerned only with relative changes in K and for all metals and alloys measured, K was calculated from 3·1 using a $(H/\nu)_r$ value taken from the Varian chart.[1] When a comparison of a solvent Knight shift with different solutes is made, the relative shift $\delta K/K$ is plotted with respect to the pure solvent K value; $\delta K/K$ being calculated from:

$$\frac{\delta K}{K} = \frac{K_a - K_m}{K_m} = \frac{\{(H/\nu)_r - (H/\nu)_a\}.\ (H/\nu)_m}{\{(H/\nu)_r - (H/\nu)_m\}.\ (H/\nu)_a} - 1$$

where the subscript 'a' devotes the alloy and 'm' the pure solvent.

The linewidths, ΔH are the separations, of the peaks of the absorption derivatives and they have been corrected for amplitude modulation broadening using the treatment of Smith[2] which is appropriate for the Lorentzian lineshapes observed in all the liquid metals and alloys. For all K and Δ values plotted and tabulated, the result is the mean of at least three

readings with increasing field sweep and three with decreasing field sweep.

Tin and the Noble-metal-tin alloys Tin has three naturally occurring isotopes of interest ^{115}Sn, ^{117}Sn and ^{119}Sn being 0.35, 7.7 and 8.7 abundant respectively. All have spin ½ and measurements of K and ΔH were made only on ^{119}Sn where these are listed in appendix 1 and displayed graphically in figures 3.1, 3.2, 3.3, 3.4, 3.10 and 3.11. The only measurement in the solid was made on the intermetallic compound AuSn. The crystal strucutre of AuSn is hexagonal close packed and as a result there are isotropic and anisotropic contributions to the Knight shift which result in asymmetric resonance lines in the polycrystalline sample used. As this work is concerned only with the properties of liquid metals, in which $K_{ax}(^{119}Sn) = 0$, only the isotropic value $K(^{119}Sn)$ for solid AuSn is recorded and is obtained using the method of Borsa and Barnes[3]. Since the line is asymmetric in the solid, line widths are given for the liquid only. The variation of $K(^{119}Sn)$ as a function of temperature in the liquid specimens of Sn, Au-80%Sn, Au-66%Sn, Au-50%Sn, and Au-29%Sn is linear for all specimens within the experimental error and the temperature coefficients are given in table 3.1. The value of $K(^{119}Sn)$ in pure tin compared favourably with previous measurements[4]. Measurements were made in the supercooled regions of Au-50%Sn and Au-29%Sn, these alloys supercooling by 50 K and 60 K respectively. Because of the anomalous behaviour of $K(^{119}Sn)$ in the supercooled region of Au-29%Sn (see figure 3.2), a second alloy was prepared by spraying from the liquid; measurements of $K(^{119}Sn)$ agreed within experimental error with those taken initially. Due to the limitations of the gas-cooled furnace values of $K(^{119}Sn)$ at a single temperature only were made on Au-25%Sn and Au-21%Sn.

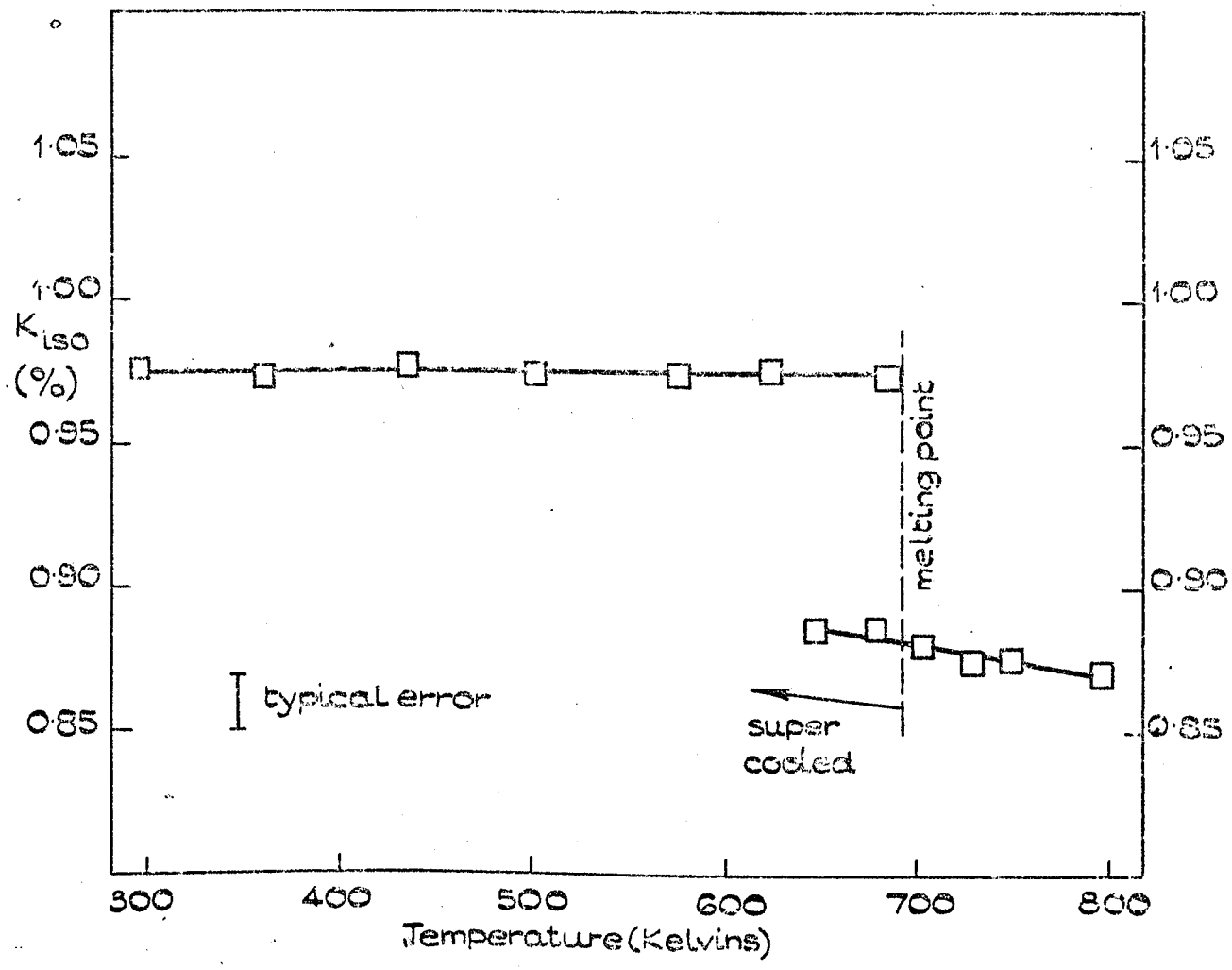

FIGURE 3.1.

VARIATION OF THE ^{119}Sn ISOTROPIC KNIGHT SHIFT IN PER CENT WITH TEMPERATURE IN THE INTERMETALLIC COMPOUND AuSn.

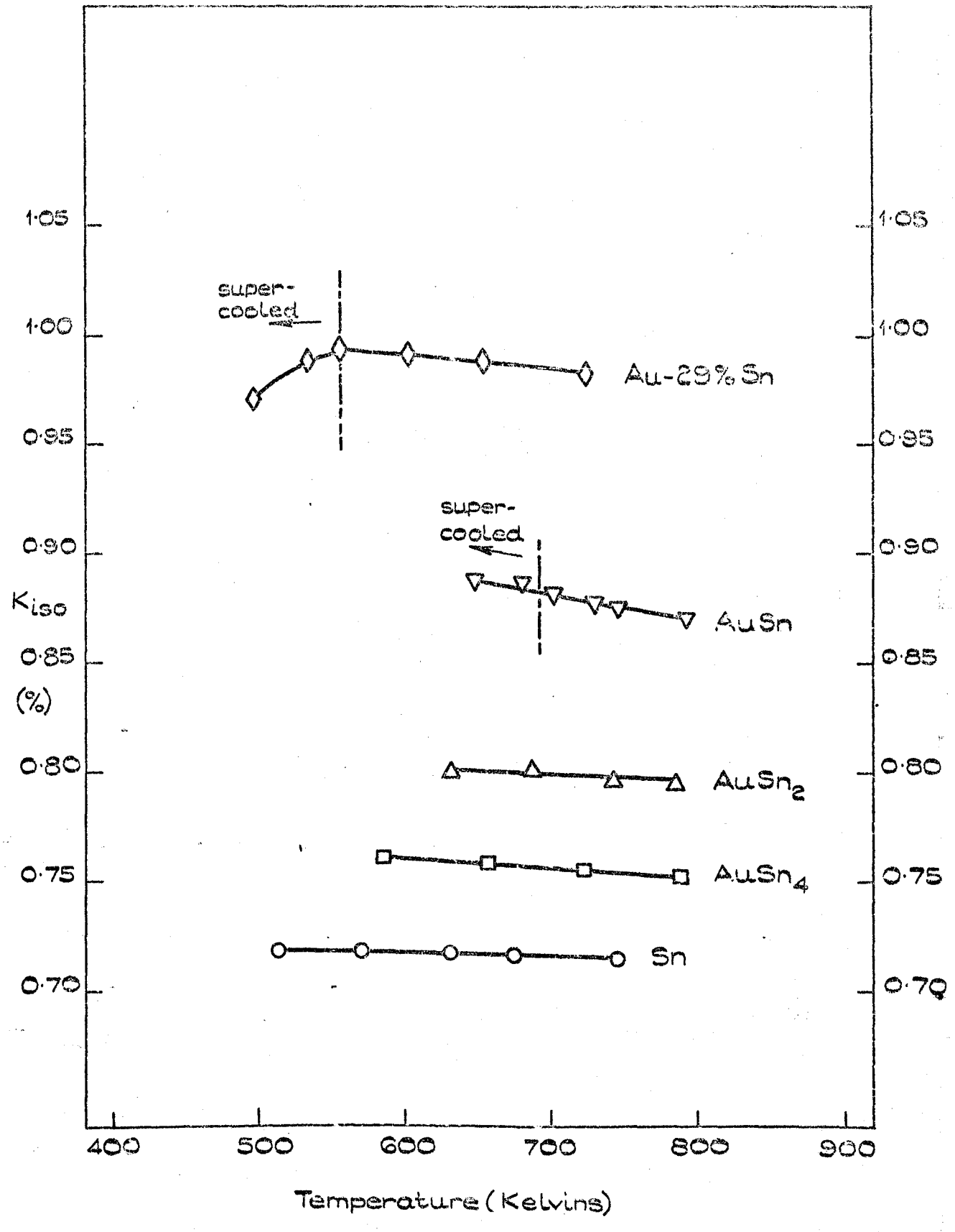

FIGURE 3.2.

VARIATION OF ^{119}Sn ISOTROPIC KNIGHT SHIFT IN PER CENT WITH TEMPERATURE IN LIQUID TIN AND SOME LIQUID GOLD-TIN ALLOYS.

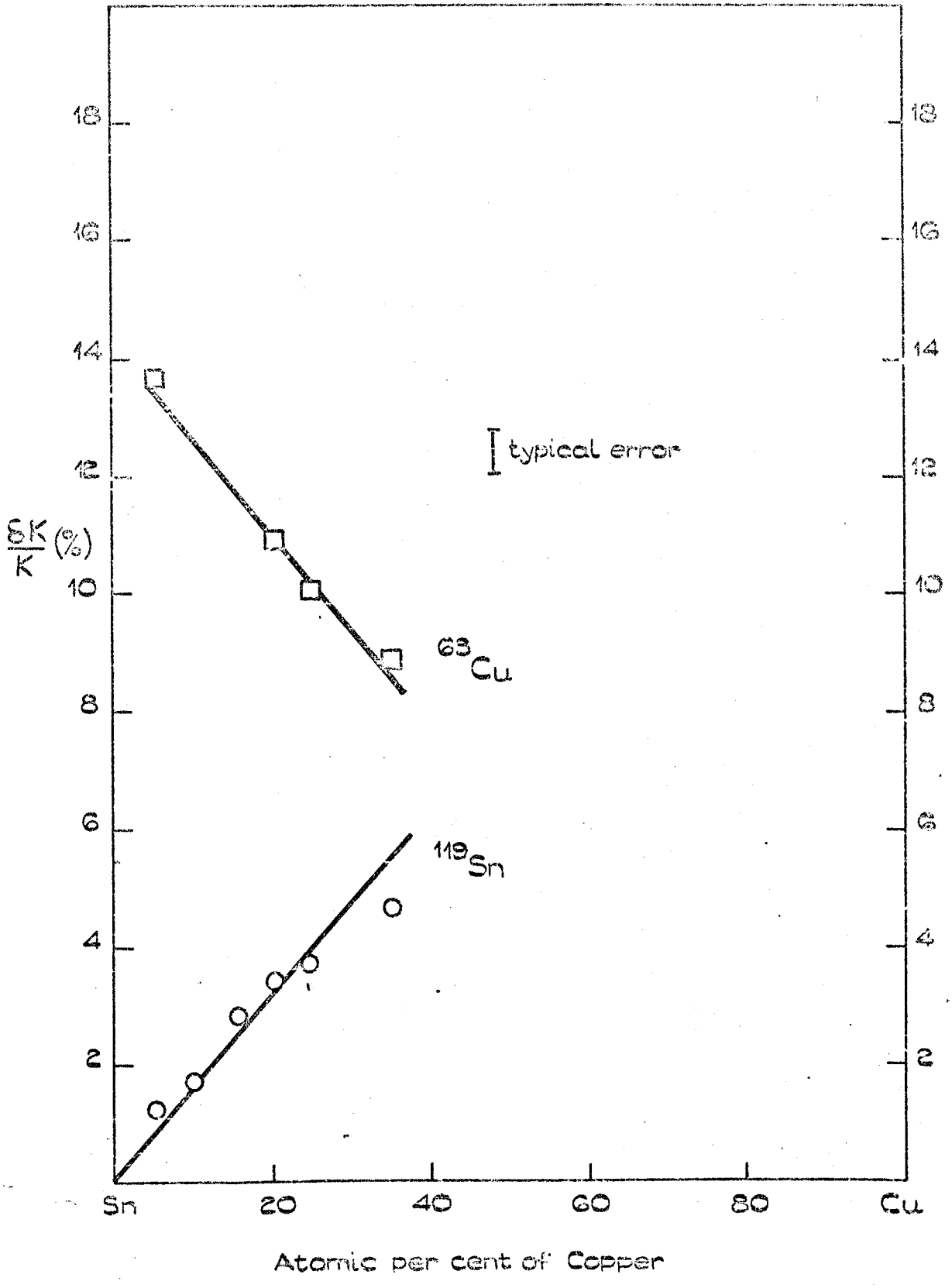

FIGURE 3.3.

FRACTIONAL CHANGE OF THE ^{119}Sn ISOTROPIC AND ^{63}Cu KNIGHT SHIFTS IN SOME LIQUID COPPER-TIN ALLOYS AT 830K.

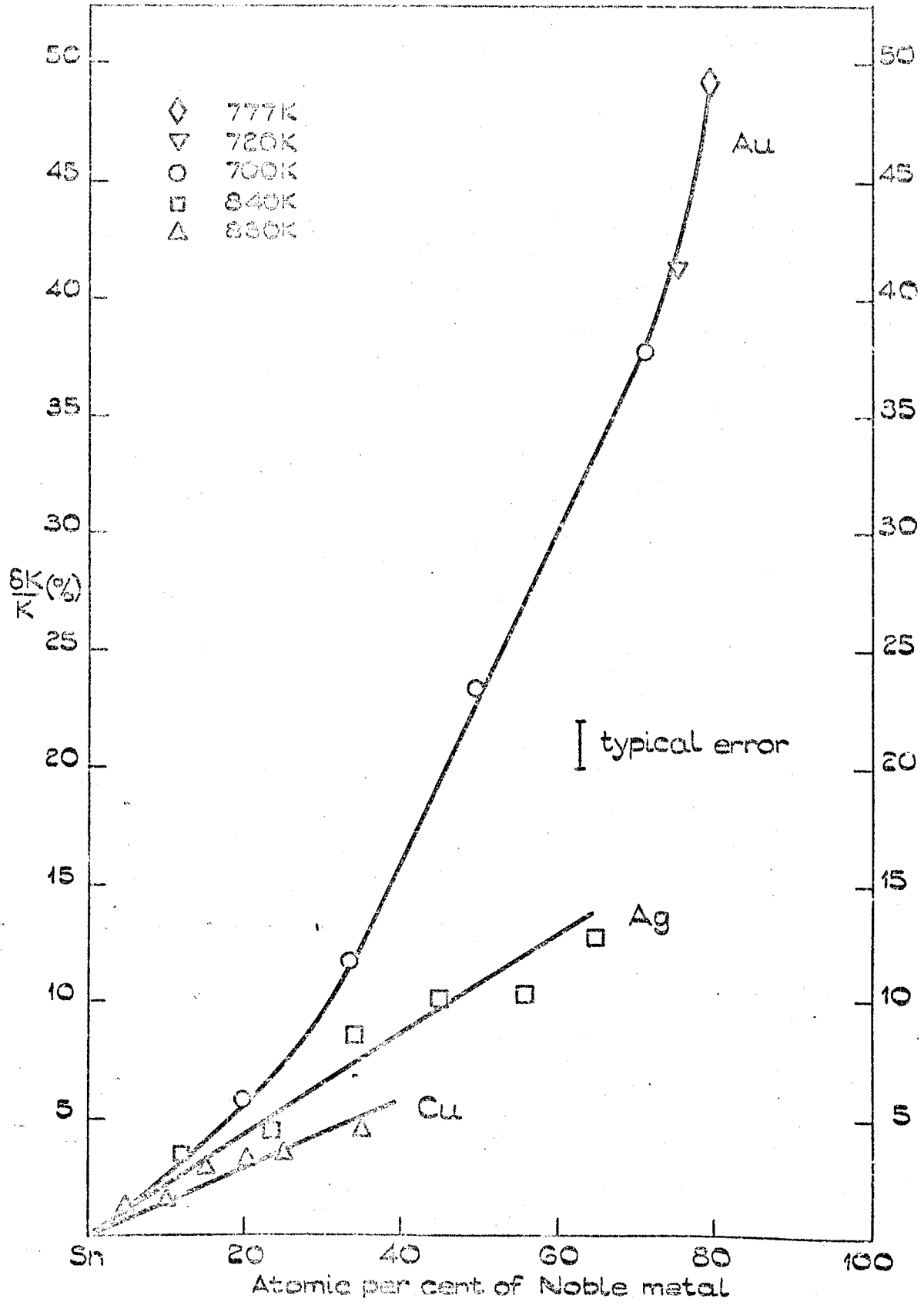

FIGURE 3.4.

FRACTIONAL CHANGE OF THE ^{119}Sn ISOTROPIC KNIGHT SHIFT WITH CONCENTRATION IN THE LIQUID NOBLE METAL-TIN SYSTEMS.

Table 3.1

Temperature coefficients of $K(^{119}Sn)$ in liquid tin and some liquid gold-tin alloys

Specimen	$(1/K)(dK/dT)$, K^{-1}
Sn	$1.80\ (\pm 0.04) \times 10^{-5}$
Au-80%Sn	$5.24\ (\pm 0.06) \times 10^{-5}$
Au-66%Sn	$4.08\ (\pm 0.05) \times 10^{-5}$
Au-50%Sn	$1.45\ (\pm 0.04) \times 10^{-4}$
Au-29%Sn	$5.33\ (\pm 0.05) \times 10^{-5}$

Liquid state measurements of $K(^{119}Sn)$ and $-\Delta H(^{119}Sn)$ were made in the copper and silver-tin systems and of $K(^{63}Cu)$ and $\Delta H(^{63}Cu)$ in the copper-tin alloys. The signals from the silver and copper-tin alloys were generally poorer than those obtained from the gold-tin alloys because of the way in which they were prepared. As shown in table 2.01 these alloys were sprayed from the solid. Some of them showed considerable signs of oxidation while others, namely Cu-90% Sn and Cu-85% Sn, gave distorted ^{63}Cu resonance lines, indicating spread in particle composition in the liquid. This was not evident in the ^{119}Sn resonance lines due to the weaker signal strength; hence the points representing $K(^{119}Sn)$ in these two alloys must be considered with caution. The readings for $K(^{63}Cu)$ in these two alloys are thus omitted from graph 3.3. $K(^{119}Sn)$ for the silver and copper-tin alloys is plotted as a function of noble-metal concentration and for both systems the variation is linear, up to the concentration measured.

Indium and the Noble metal-indium alloys. Indium has two naturally occurring isotopes ^{113}In and ^{115}In, which are 4.2 and 95.8% abundant respectively. Both have spins of 9/2 and measurements of K and ΔH were made only on ^{115}In in the liquid. These data are tabulated in appendix 1 and plotted graphically in figures 3.5, 3.6, 3.7, 3.9. and 3.12. The value of $K(^{115}In)$ in pure liquid indium is in reasonable agreement with that of Styles[5]. $K(^{63}Cu)$ and ΔH (^{63}Cu) was measured in the copper-indium system and these data are tabulated in appendix 1 and shown graphically in figures 3.8 and 3.13. Figure 3.9.shows that for all three systems $K(^{115}In)$ passes through a maximum value between 40 and 60% of noble metal concentration.

3.2 Relaxation Rates and Times

Measurements of the ^{115}In relaxation rate, $R_1(^{115}In)$ were made in all of the copper-indium alloys and in a selected few of the silver-indium and gold-indium alloys. $R_1(^{63}Cu)$ was also measured in three copper-indium alloys. The values obtained for $R_1(^{115}In)$ in pure indium are in good agreement with those of Warren and Clark[6]. These data are tabulated in appendix 1 and shown graphically in figures 3.14, .3.15, 3.16 and 3.17. In all cases the R_1 measurements were made on the same specimens for which Knight shift data was obtained.

3.3 Magnetic Susceptibility

In every case each point for the alloys measured is the mean of at least three measurements, the error bar indicating the spread of the readings. The magnetic susceptibilities χ of Sn, Au-80% Sn, Au-66% Sn, Au-50% Sn, Au-29% Sn and Au-21% Sn as a function of temperature in the liquid state are given in figure 3.18 and tabulated in appendix 1. The

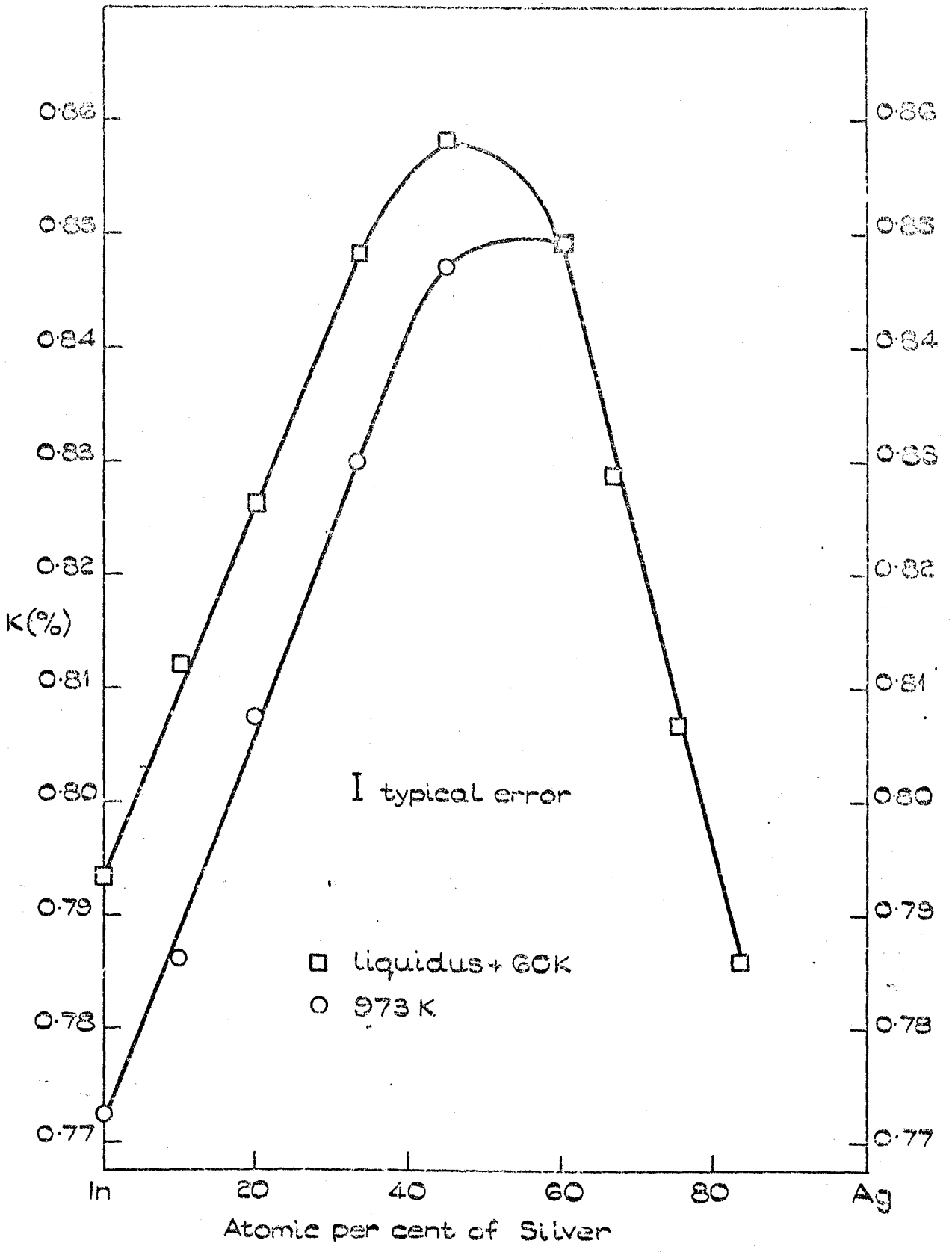

FIGURE 3.5.

VARIATION OF THE ^{115}In KNIGHT SHIFT WITH CONCENTRATION IN THE LIQUID SILVER-INDIUM SYSTEM.

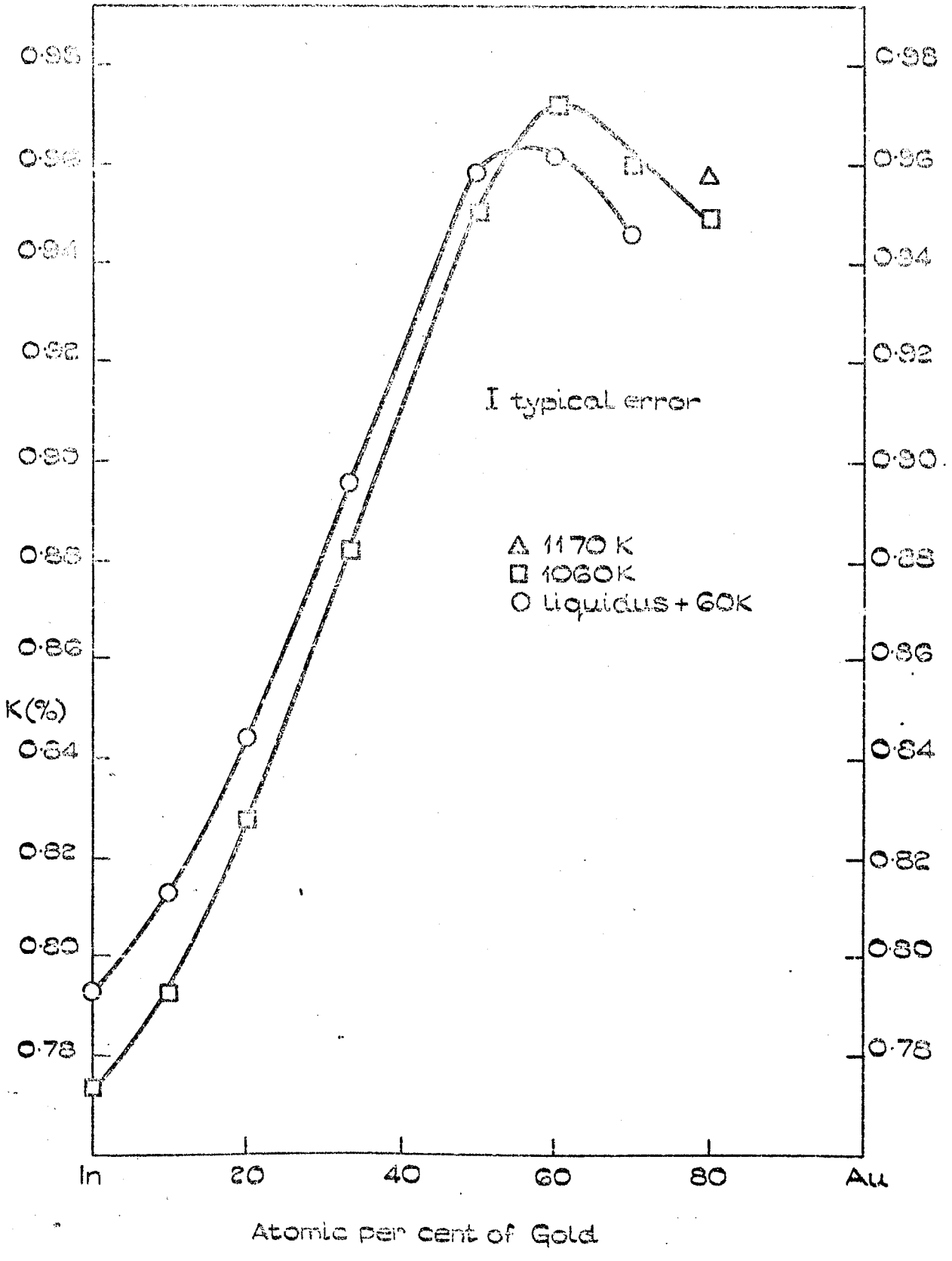

FIGURE 3.6.

VARIATION OF THE ^{115}In KNIGHT SHIFT WITH CONCENTRATION IN THE LIQUID GOLD-INDIUM SYSTEM.

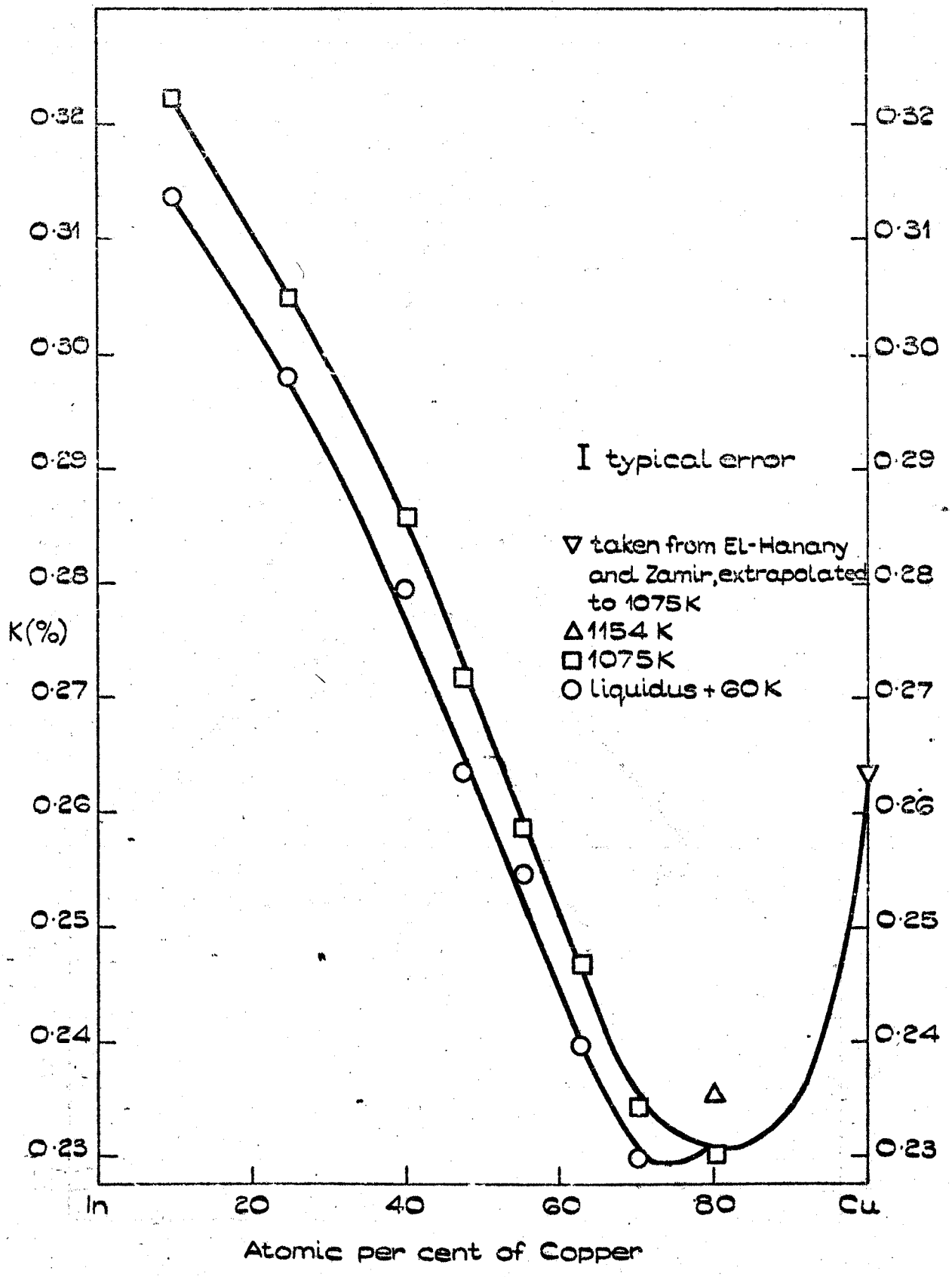

FIGURE 3.8.

VARIATION OF THE ^{63}Cu KNIGHT SHIFT WITH CONCENTRATION IN THE LIQUID COPPER-INDIUM SYSTEM.

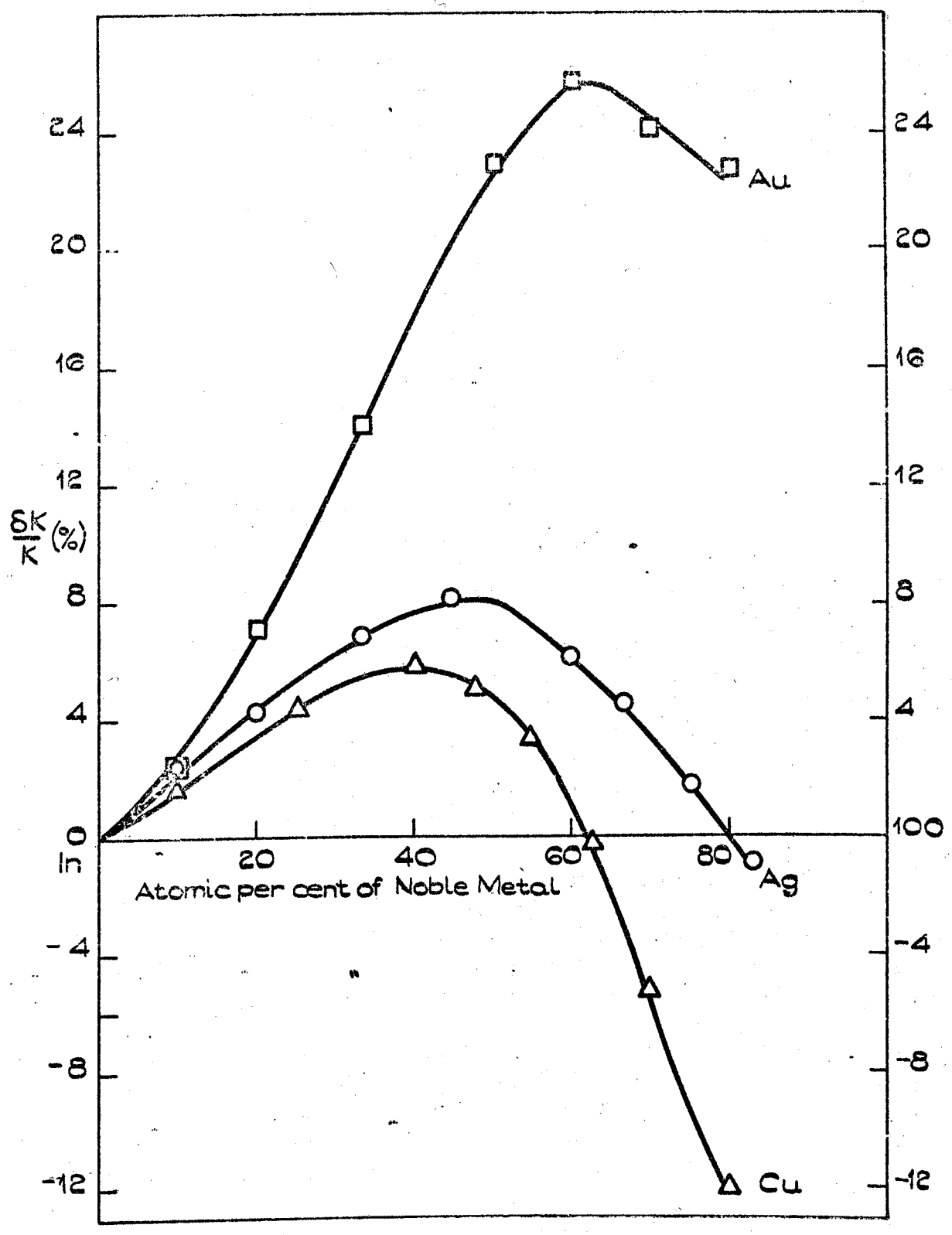

FIGURE 3.9.

FRACTIONAL CHANGE OF THE ^{115}In KNIGHT SHIFT WITH CONCENTRATION THE LIQU'D NOBLE METAL-INDIUM SYSTEMS AT 1100K.

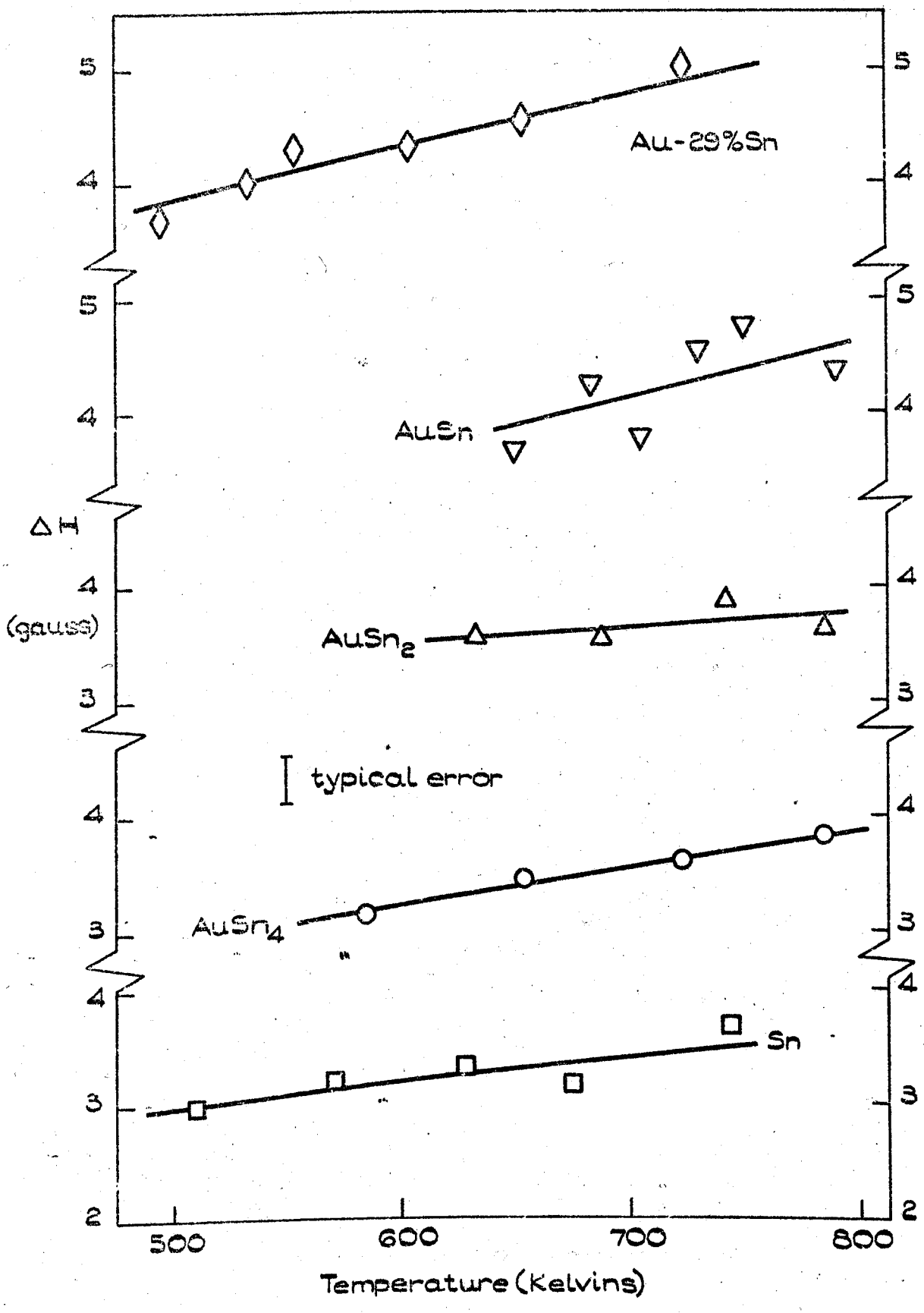

FIGURE 3.10.

^{119}Sn LINE WIDTHS IN LIQUID TIN AND SOME LIQUID GOLD-TIN ALLOYS.

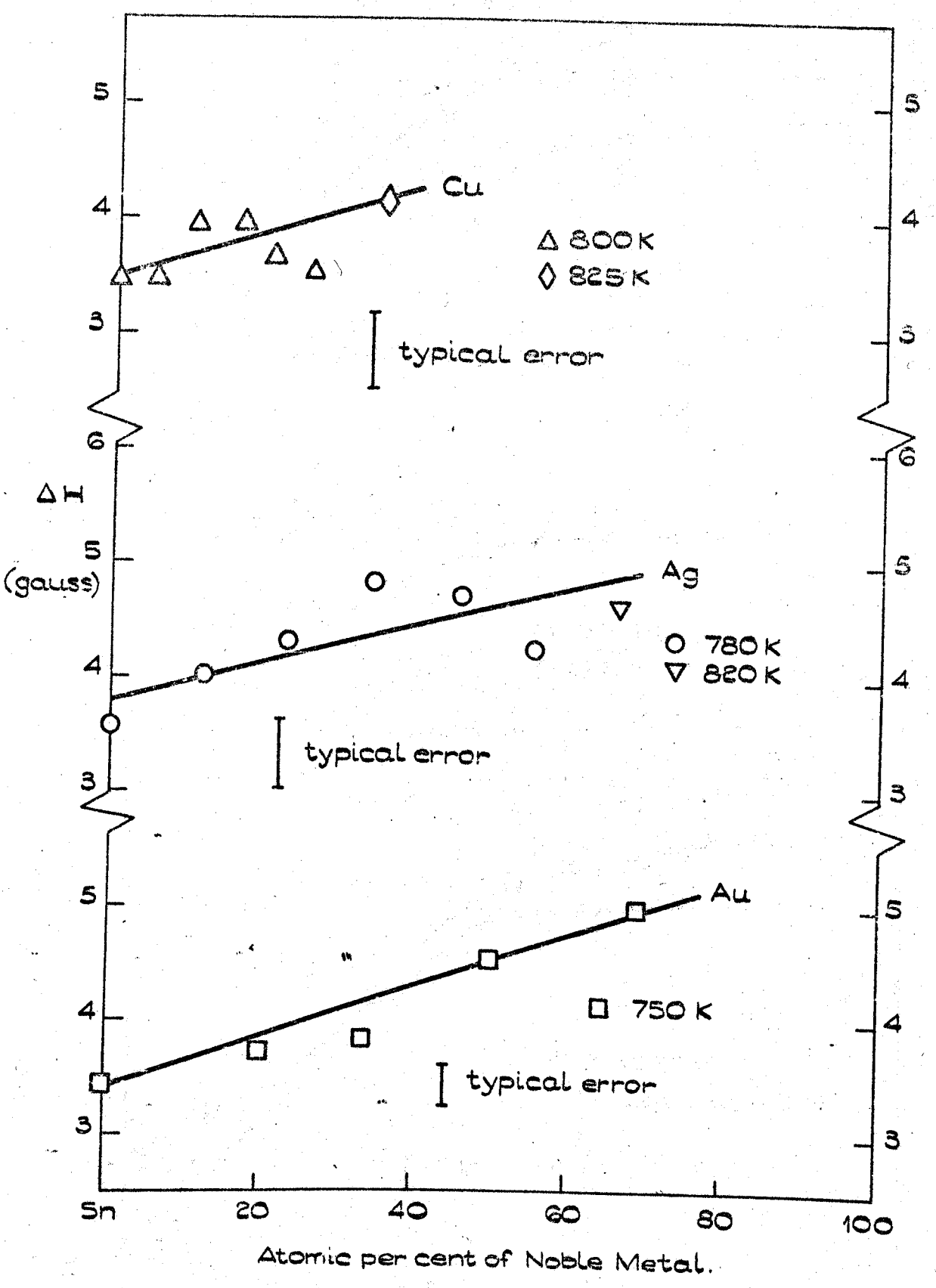

FIGURE 3.11.

^{119}Sn LINE WIDTHS IN SOME LIQUID NOBLE METAL - TIN ALLOYS.

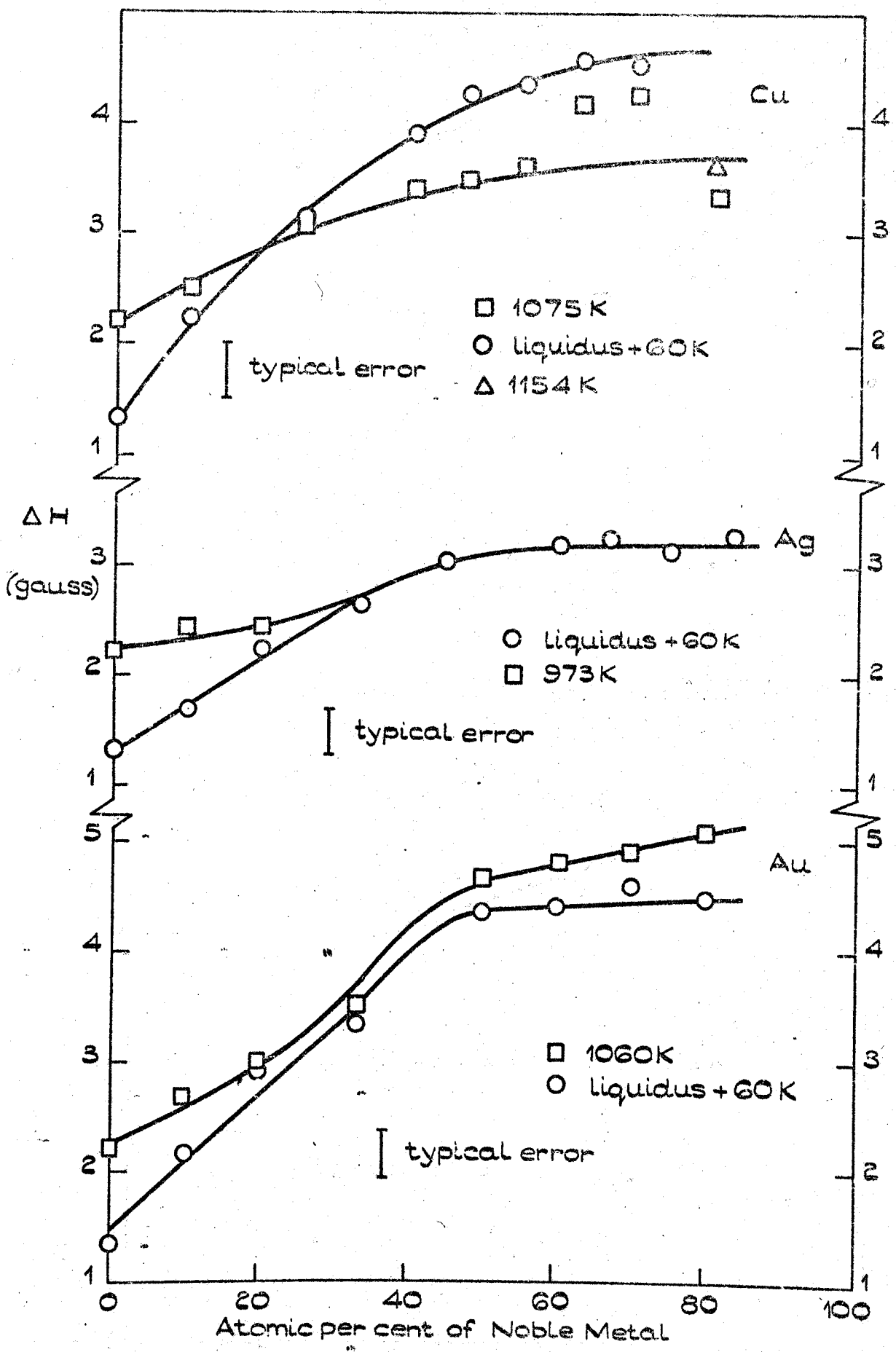

FIGURE 3.12.

^{115}In LINE WIDTHS IN SOME LIQUID NOBLE METAL - INDIUM ALLOYS.

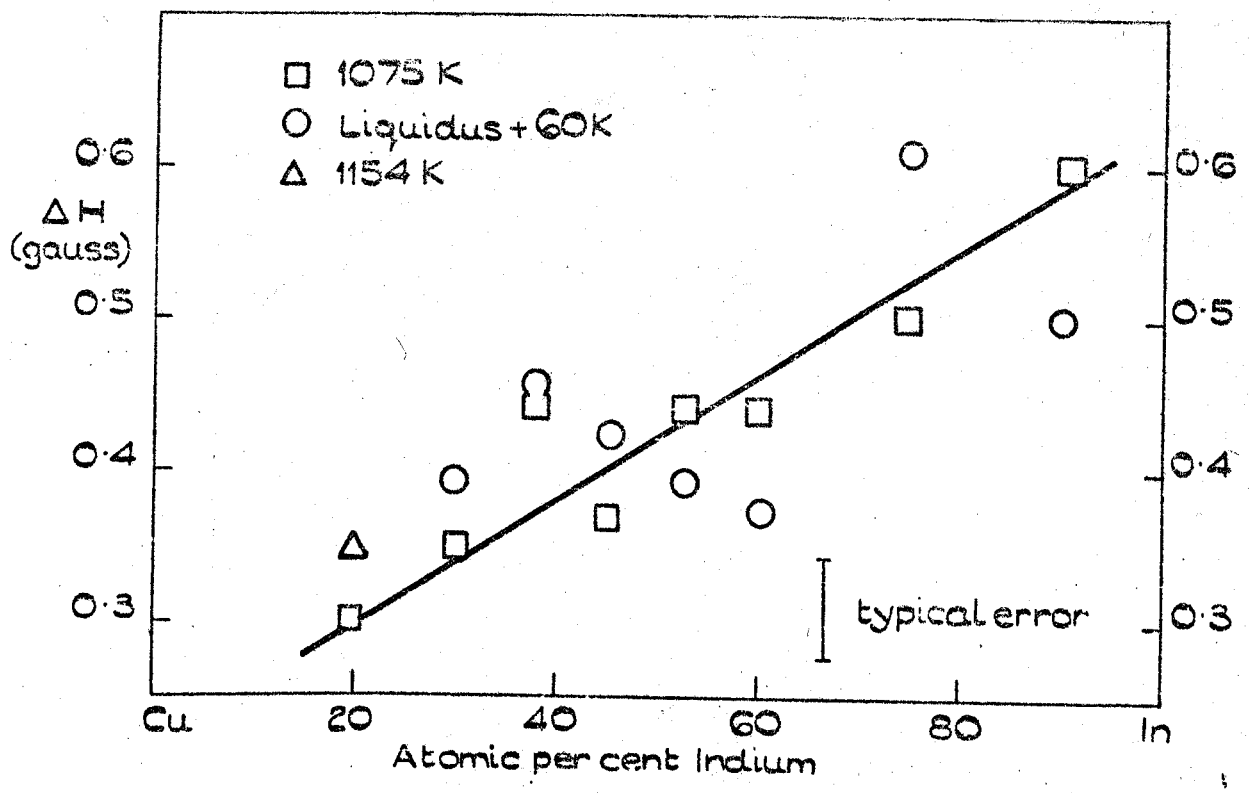

FIGURE 3.13.

^{63}Cu LINE WIDTHS IN SOME LIQUID COPPER-INDIUM ALLOYS.

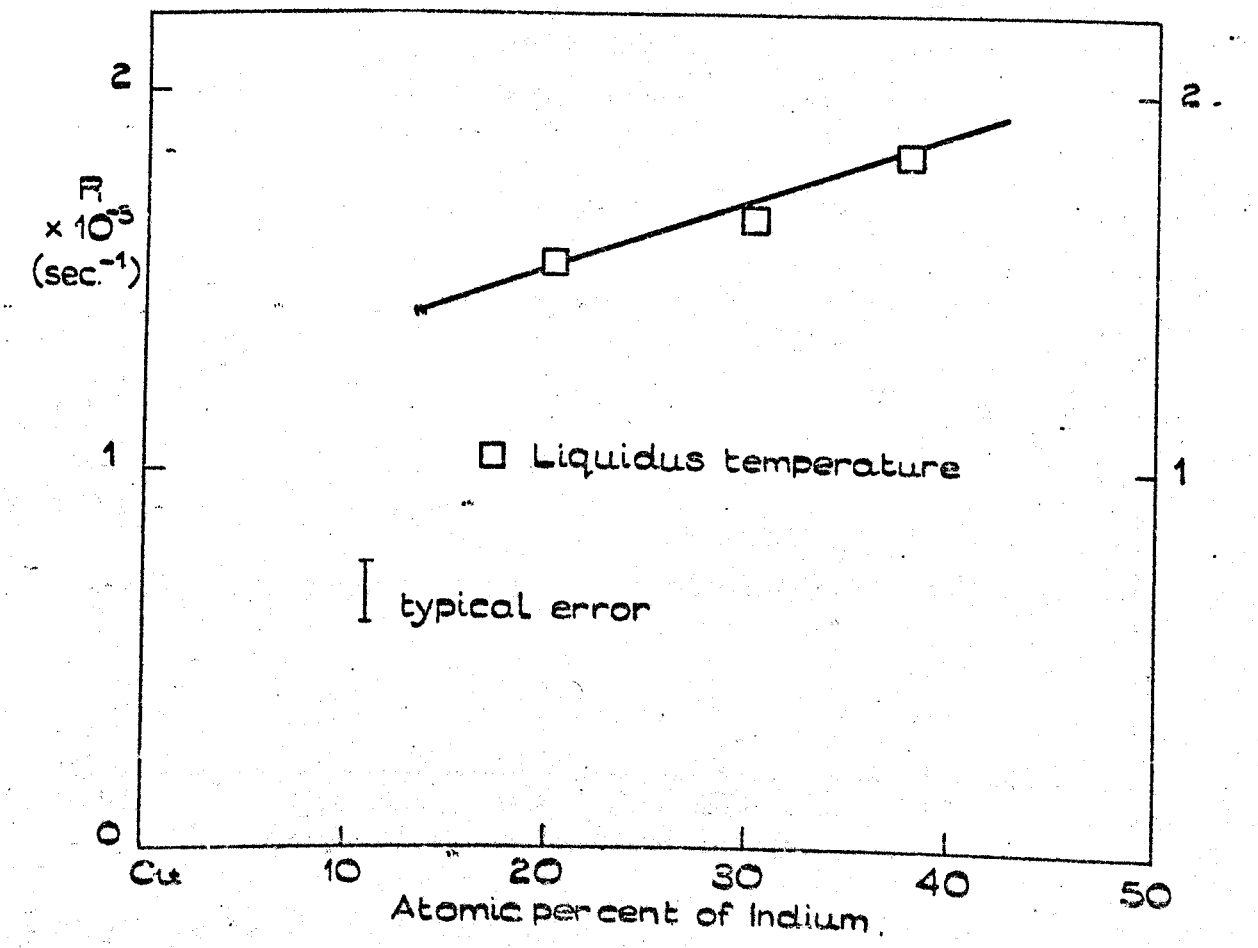

FIGURE 3.14.

^{63}Cu RELAXATION RATES IN SOME LIQUID COPPER - INDIUM ALLOYS.

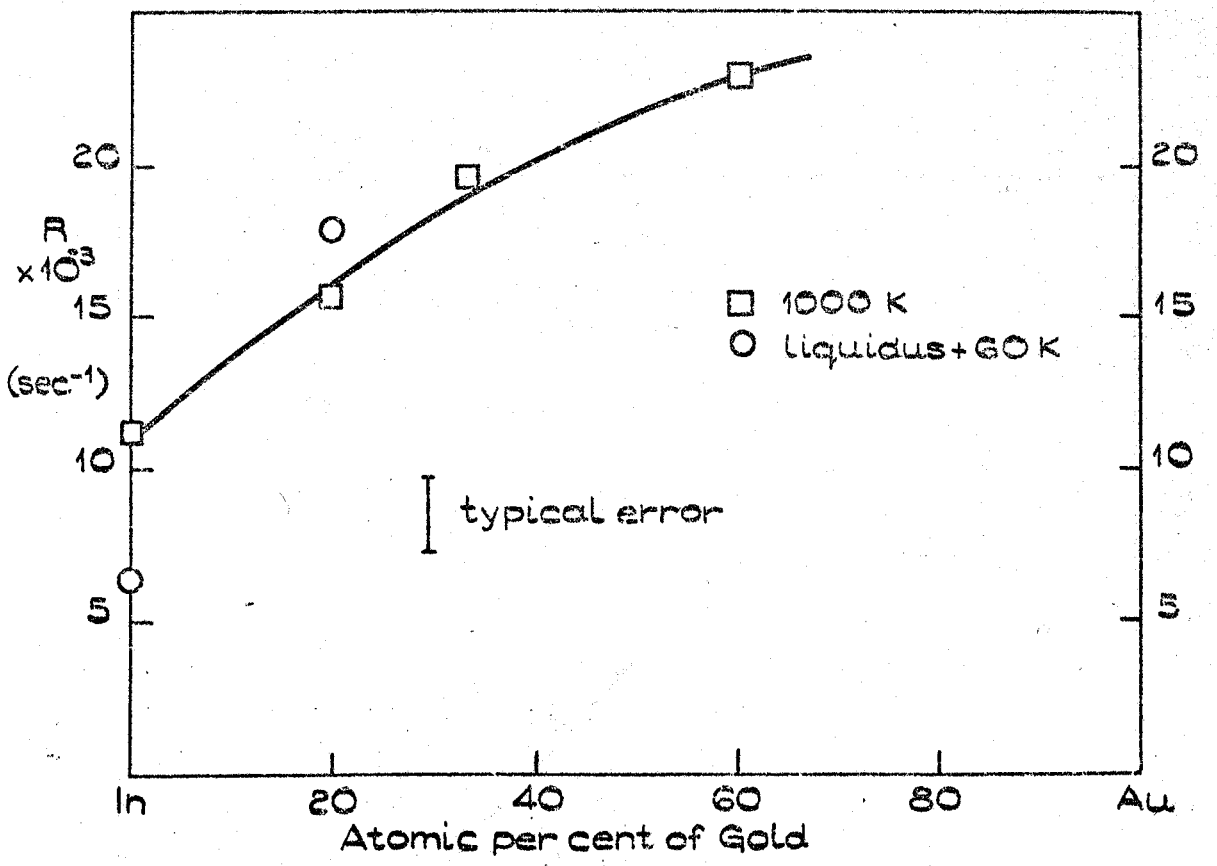

FIGURE 3.15. ^{115}In RELAXATION RATES IN SOME LIQUID GOLD-INDIUM ALLOYS.

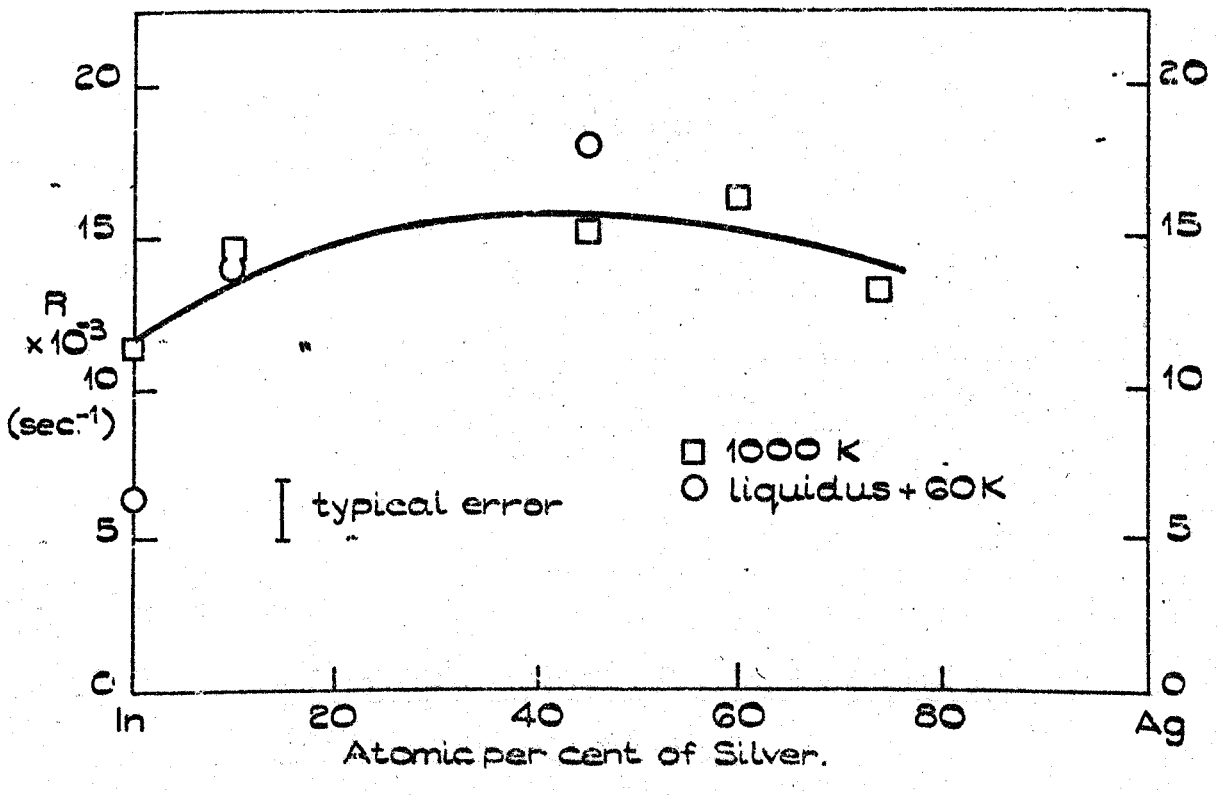

FIGURE 3.16. ^{115}In RELAXATION RATES IN SOME LIQUID SILVER-INDIUM ALLOYS.

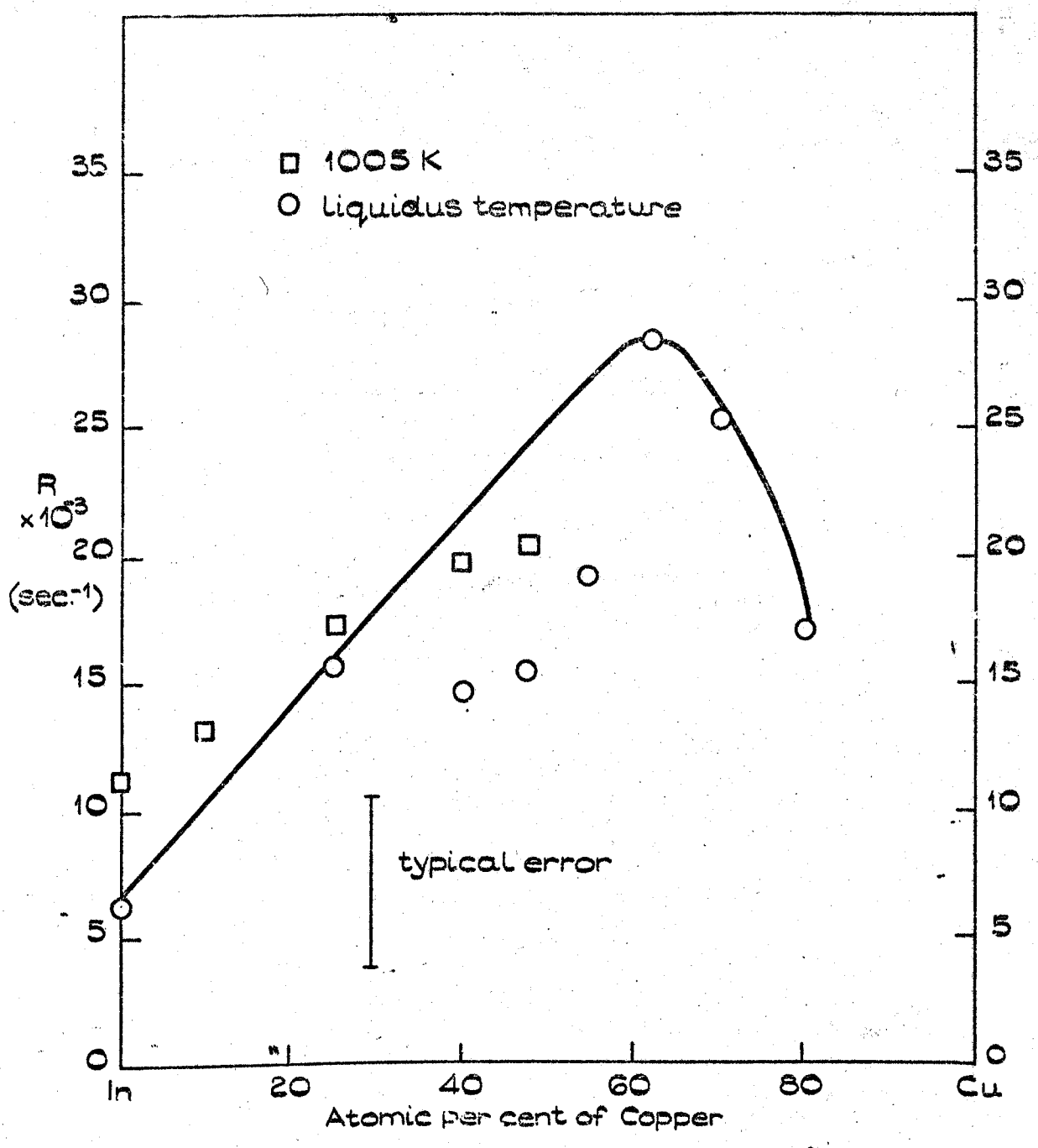

FIGURE 3.17.

^{115}In RELAXATION RATES IN SOME LIQUID COPPER-INDIUM ALLOYS.

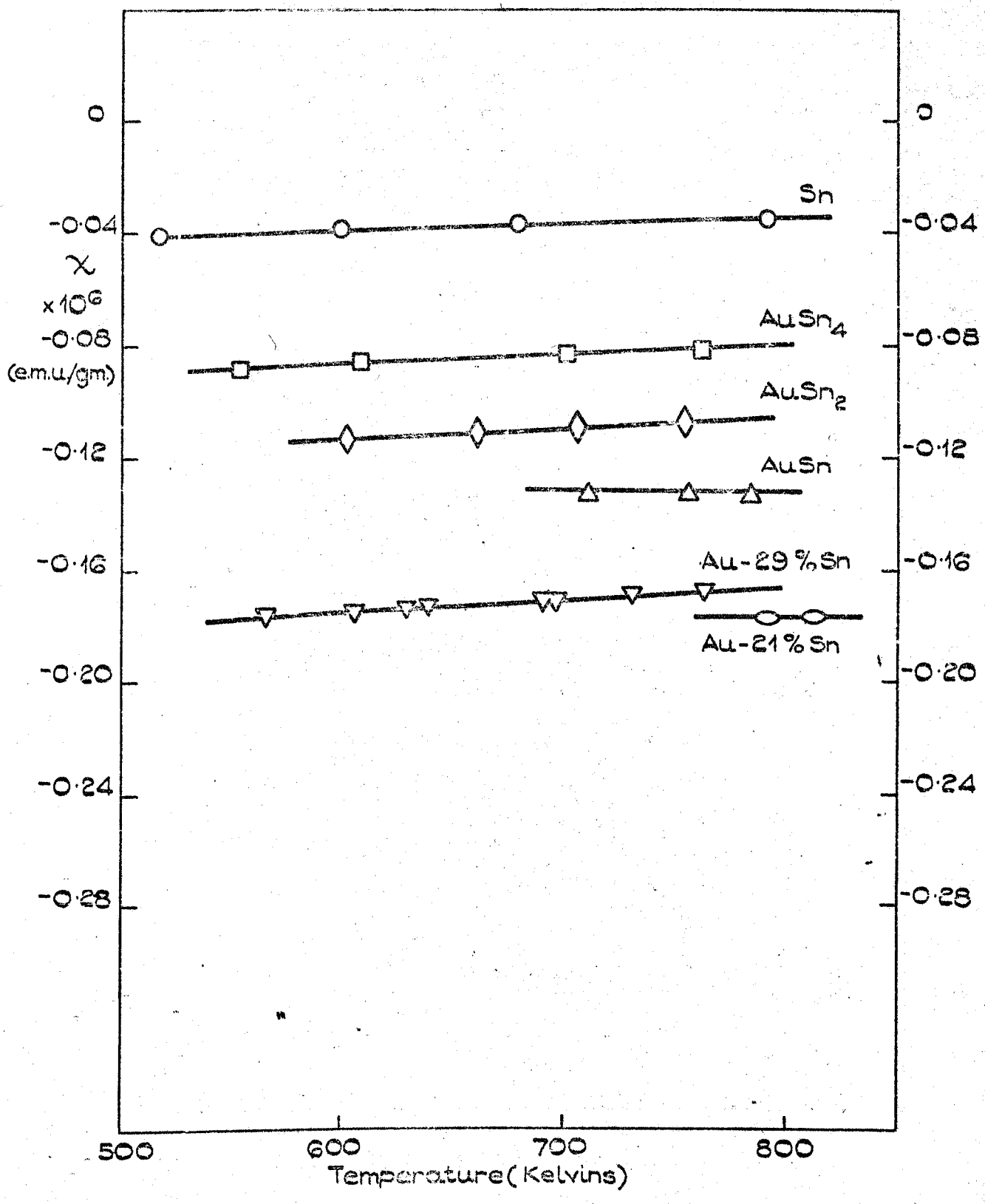

FIGURE 3.18.

MAGNETIC SUSCEPTIBILITIES OF SOME LIQUID GOLD-TIN ALLOYS.

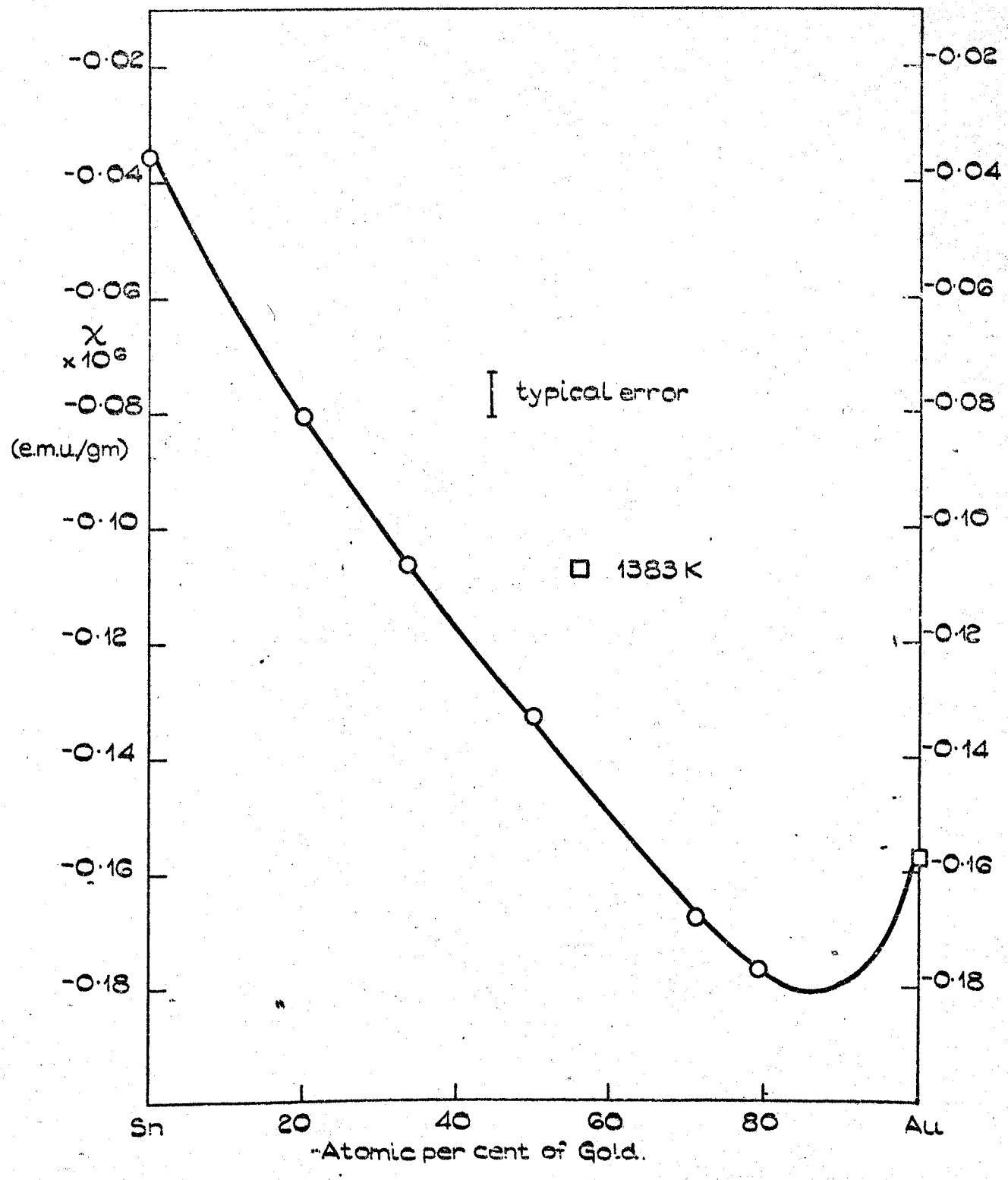

FIGURE 3.19.

VARIATION OF THE MAGNETIC SUSCEPTIBILITY WITH CONCENTRATION IN THE LIQUID GOLD-TIN SYSTEM AT 775K.

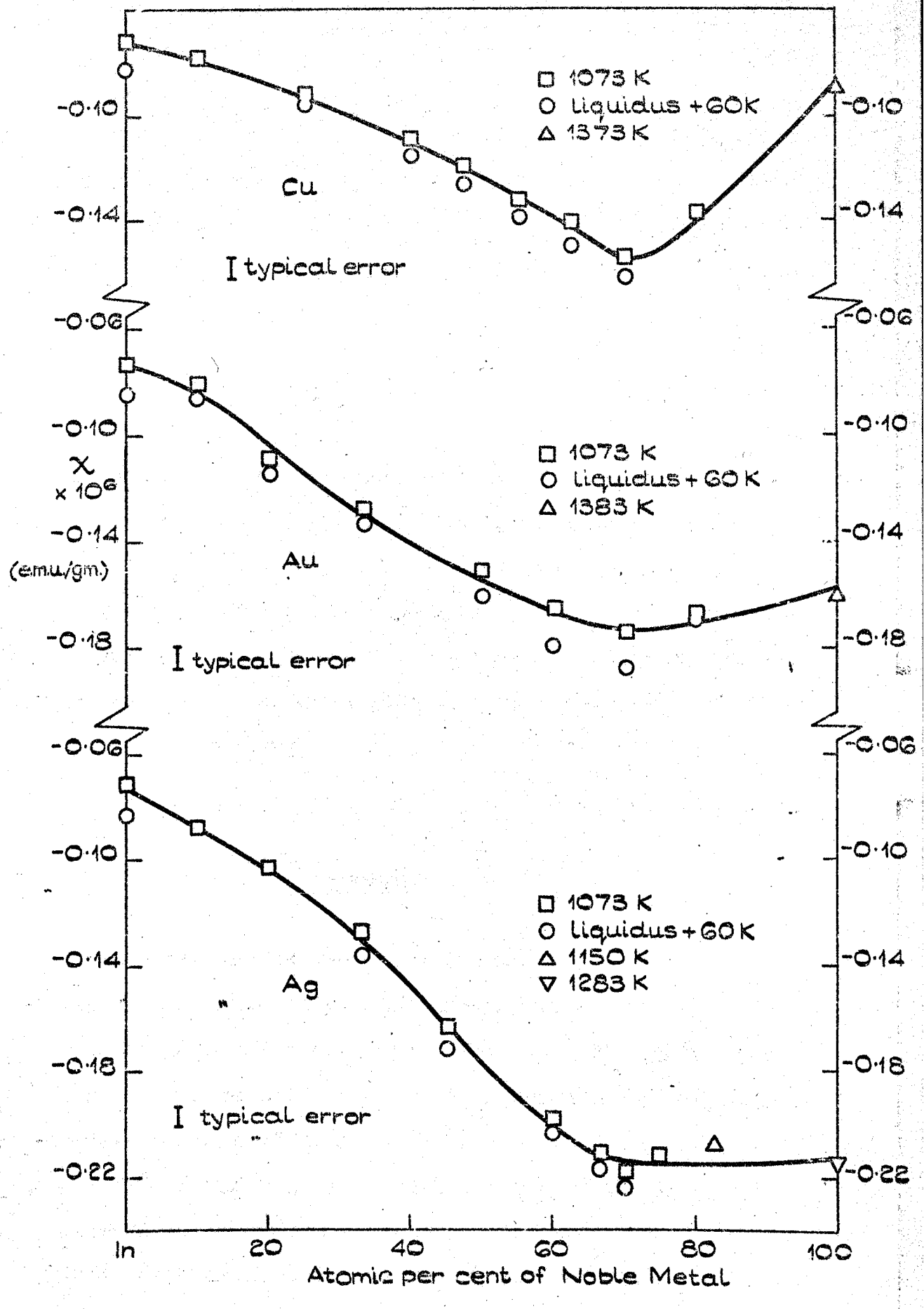

FIGURE 3.20.

VARIATION OF MAGNETIC SUSCEPTIBILITY WITH CONCENTRATION IN THE LIQUID NOBLE METAL - INDIUM SYSTEMS.

results obtained for Sn and Au-50% Sn are in good agreement with previous measurements[7,8]. All changes of χ with temperature were linear for tin and its alloys with gold. The specimens Sn, Au-80% Sn, Au-66% Sn and Au-29% Sn all showed the same temperature coefficient in the liquid, the value being

$$\frac{1}{\chi}\frac{d\chi}{dT} = 4.43(\pm 0.06) \times 10^{-4} K^{-1}.$$

Over the temperature range measured the alloys Au-50% Sn and Au-21% Sn showed no change within the experimental error. Figure 3.19 shows the variation of χ as a function of concentration in the gold-tin system. The results for the variation of χ across the noble metal-indium systems are shown in figure 3.20 and tabulated in appendix 1. The temperatures at which measurements were taken are approximately those for which Knight-shift measurements were made.

REFERENCES

(1) Varian Associates, NMR Table, 5th Edition.

(2) Smith, G. W., J.App. Phys., 35, (1964), 1218.

(3) Borsa F. and Barnes R. G., J. Phys. Chem, Sol., 25, (1964), 1305.

(4) Knight W. D., Berger A. G. and Heine V., Ann.Phys., 8, (1959), 173.

(5) Styles, G. A., Ph.D. Thesis, Leeds (1964).

(6) Warren W. W. and Clark W. G., Phys.Rev. 177, (1969), 600.

(7) Urbain G. and Übelacker E., Adv. Phys., 16, (1967) 429.

(8) Jan J. P., Pearson W. B., Kjekshus A. and Woods S. B., Can. J. Phys., 41, (1963), 2252.

CHAPTER FOUR

EVIDENCE FOR SHORT RANGE ORDER IN LIQUID ALLOYS

4.1 Introduction

The atomic distributions in a liquid metal are governed principally by the ion-ion repulsion. If this interaction is idealised by representing the ions as hard spheres, then the Percus-Yevick integral equation for the pair distribution function may be rigorously solved and the structure factor I(K) determined. This will depend only on the effective packing density of the liquid. Using the hard sphere model Ashcroft and Lekner[1] have obtained an analytic expression for I(K) which fairly successfully reproduces the experimental I(K) for a number of liquid metals. Ashcroft and Langreth[2] have subsequently shown that this model may be extended to describe the atomic distributions in liquid binary alloys. However a large body of experimental data exists which may not be accounted for by the hard sphere model but rather is interpreted in terms of the existence of non-random short range ordering of atoms in the liquid state[3,4]. Though the interpretation has been qualitative, nevertheless a model for clustering has emerged which can account for some of the experimental data. It is suggested that dissimilar atoms come together in a binary alloy to form a cluster, these coexisting with a random distribution of the remaining atoms. In the majority of cases, the alloy composition at which this clustering occurs corresponds to an intermetallic compound in the solid; though, as will be shown presently, this is not always the case. The evidence strongly indicates that if any ordering is present, it is progressively destroyed by the increased thermal motion as the temperature is increased above the liquidus.

The alloy systems for which the existence of this structure is most strongly indicated are the noble metal-tin systems. There is however still some disagreement between various authors as to whether ordering takes place at all and if so at what compositions. The present measurements were undertaken in the hope of resolving these differences of of interpretation. The following section examines previous experimental data for these systems and the models of clustering which have emerged from them. The final section discusses the present results in the light of these models.

4.2 Previous Experimental Data

4.2.1 X-ray and Neutron Diffraction Of all the evidence for ordering, that provided by X-ray and neutron diffraction is probably the most direct. Both yield the coherent scattered intensity per atom which may be related to the structure factor (or total interference function) I(K). A liquid binary alloy however is fully characterised by the three partial structure factors $I_{ij}(K)$, the total I(K) being a weighted sum of the $I_{ij}(K)$. Fourier transformations of I(K) and $I_{ij}(K)$ yield the total and partial distribution functions g(r) and $g_{ij}(r)$ respectively, from which are determined the number of atoms in the first co-ordination shell and the interatomic separations A-A, B-B and A-B in a liquid binary alloy of constituents A and B. However, errors may be introduced in making this transformation, in particular early truncation of the integral may introduce 'ripples' on the g(r) curve. This effect is shown in figure 5.5 in the following chapter, where a fuller discussion is given. If the hard sphere model is to describe adequately the atomic distributions in an alloy, then the $I_{ij}(K)$ and $g_{ij}(r)$ must have maxima which lie in between those of the pure elements, and the A-B separation is the weighted mean of A-A and B-B.

Those systems for which the hard sphere model is inadequate usually exhibit a smaller A-B separation than expected and when the $I_{ij}(K)$ are summed, give a double-headed maximum in I(K) at certain concentrations.

Au-Sn

The phase diagram for the Au-Sn system is shown in figure 4.1; it contains one intermetallic compound at the AuSn composition. Hendus[6] first obtained X-ray diffraction data for this system and observed a double peak in I(K) at the AuSn composition. His deduced atomic separation values however conflict with more recent measurements. Waghorne, Rivlin and Williams[7] examined five alloys containing 18,25,29.4,40 and 50 at % Sn; the first two alloys give a single diffraction peak while for the last three it is double. They interpreted their data by postulating that 'units' of Au_3Sn coexist at all concentrations with a random distribution of the remaining tin or gold atoms. Kaplow, Strong and Averbach[8] on the other hand, though obtaining very similar I(K) curves to Waghorne etal. explained their data in terms of an AuSn cluster, corresponding to a 'memory' in the liquid of the AuSn intermetallic compound which persits up to the liquidus. Recently Wagner, Halder and North[9] have re-examined the data of Kaplow et al. in terms of the partial interference and atomic distribution functions. The $g_{Au-Au}(r)$ and $g_{Sn-Sn}(r)$ yielded interatomic separations which agreed with those of the pure elements, i.e. 2.84Å and 3.16Å for Au and Sn respectively. $g_{Au-Sn}(r)$ however yielded an Au-Sn separation of 2.88Å, which is very close to the value of 2.86Å found in solid AuSn. This behaviour is not in accordance with the hard sphere model. These authors therefore confirm the conclusion of Kaplow etal. that clusters form at the AuSn composition, on the basis that the Au-Sn separation in the liquid state is almost identical to that in the solid compound.

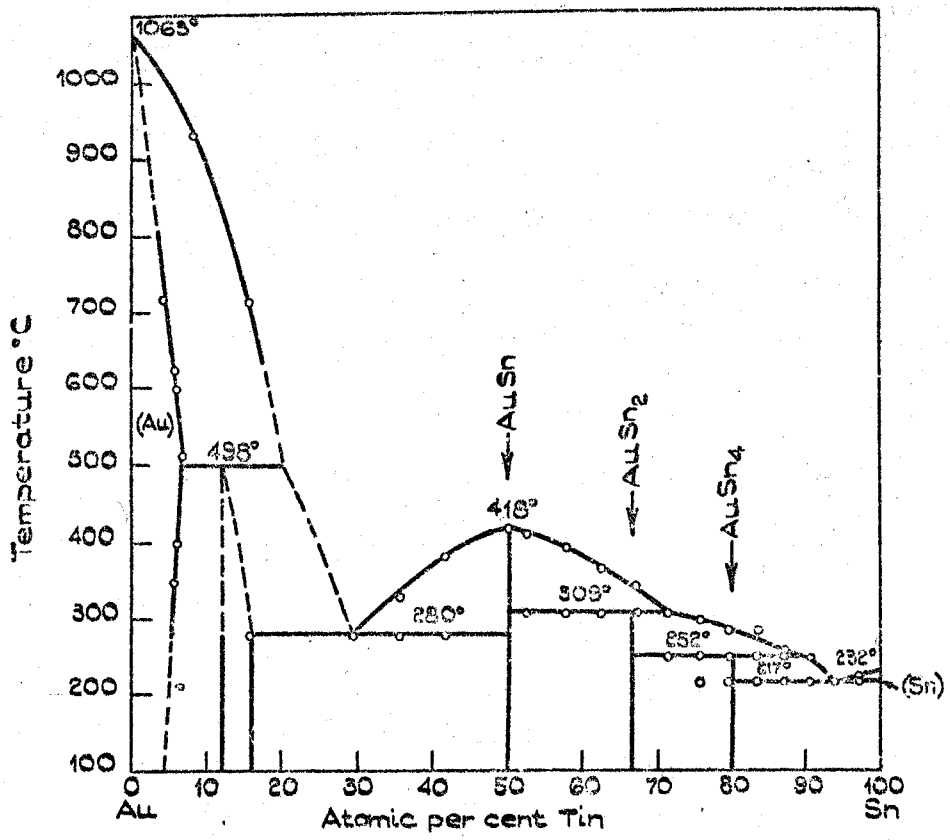

FIGURE 4.1.

THE GOLD-TIN PHASE DIAGRAM (ff. HANSEN).

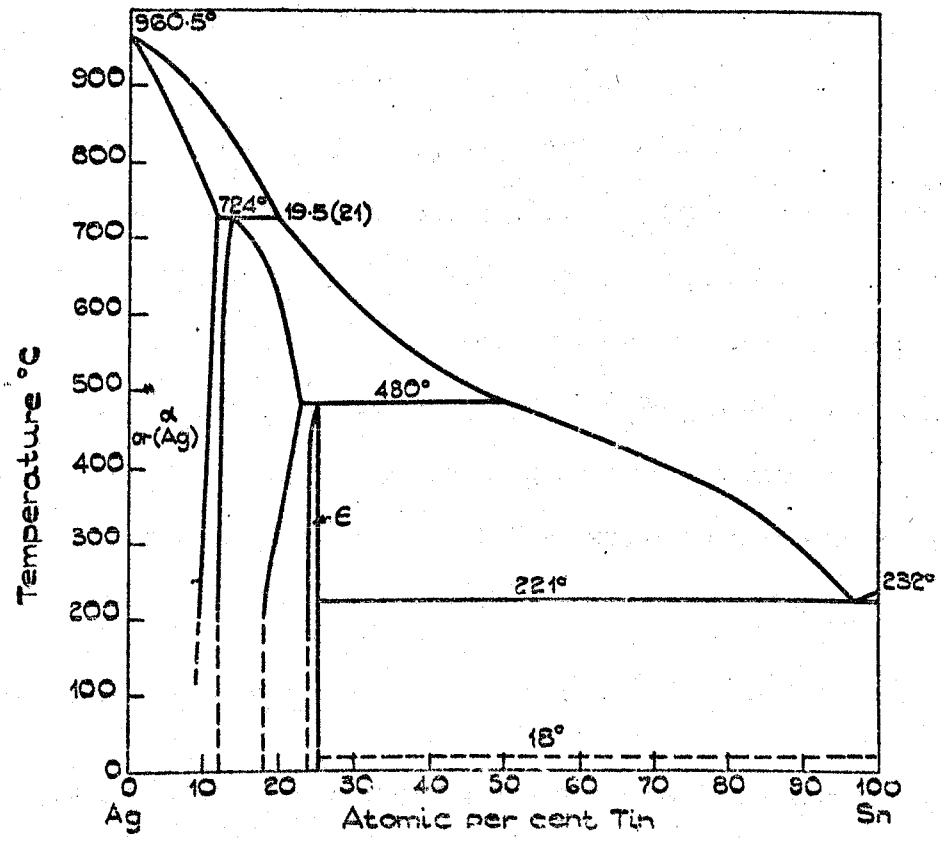

FIGURE 4.2.

THE SILVER-TIN PHASE DIAGRAM (ff. HANSEN).

Ag-Sn and Cu-Sn

The phase diagrams for these systems are shown in figures 4.2 and 4.3[5]. Recent X-ray diffraction measurements have been made on the Ag-Sn system over a wide range of concentrations by Halder and Wagner[10]. Their results, interpreted in terms of $I_{ij}(K)$ and $g_{ij}(r)$, may be completely explained in terms of the hard-sphere model and it is concluded that this system is a simple mixture of Ag and Sn. Enderby, North and Egelstaff[11] obtained the partial structure factors for the Cu-Sn system using neutron scattering from the liquid alloy Cu_6Sn_5. The hard sphere model, though predicting the Cu-Cu and Sn-Sn separations, breaks down for the Cu-Sn separation due to the non-additivity of the hard sphere diameters and they conclude that the system is not a simple mixture of the two elements. X-ray diffraction measurements across the whole Cu-Sn system by North and Wagner[12], have yielded partial structure factors in reasonable agreement with those obtained by Enderby etal. Distinct splitting of the first peak in I(K) was observed in the Cu-55 at.% Sn alloy, with the 45 and 78% Sn alloys giving broad, asymmetric first peaks. Though $I_{Sn-Sn}(K)$ very closely resembled that obtained for the pure element, $I_{Cu-Cu}(K)$ did not coincide with its pure Cu counterpart. As with the neutron scattering data, the Cu-Sn separation did not agree with the predictions of the hard-sphere model but closely resembled that existing in the Cu_3Sn phase in the solid. In agreement with Enderby etal., they conclude that this alloy is not a simple mixture, and further that this could be explained by Cu_3Sn groupings existing in the liquid state.

Au-In, Ag-In and Cu-In

The phase diagrams for these systems are shown in figures 4.4, 4.5 and 4.6[5]. The only measurements for these systems are the X-ray diffraction data of Waghorne, Rivlin and Williams[7] on Au-In. Double headed maxima

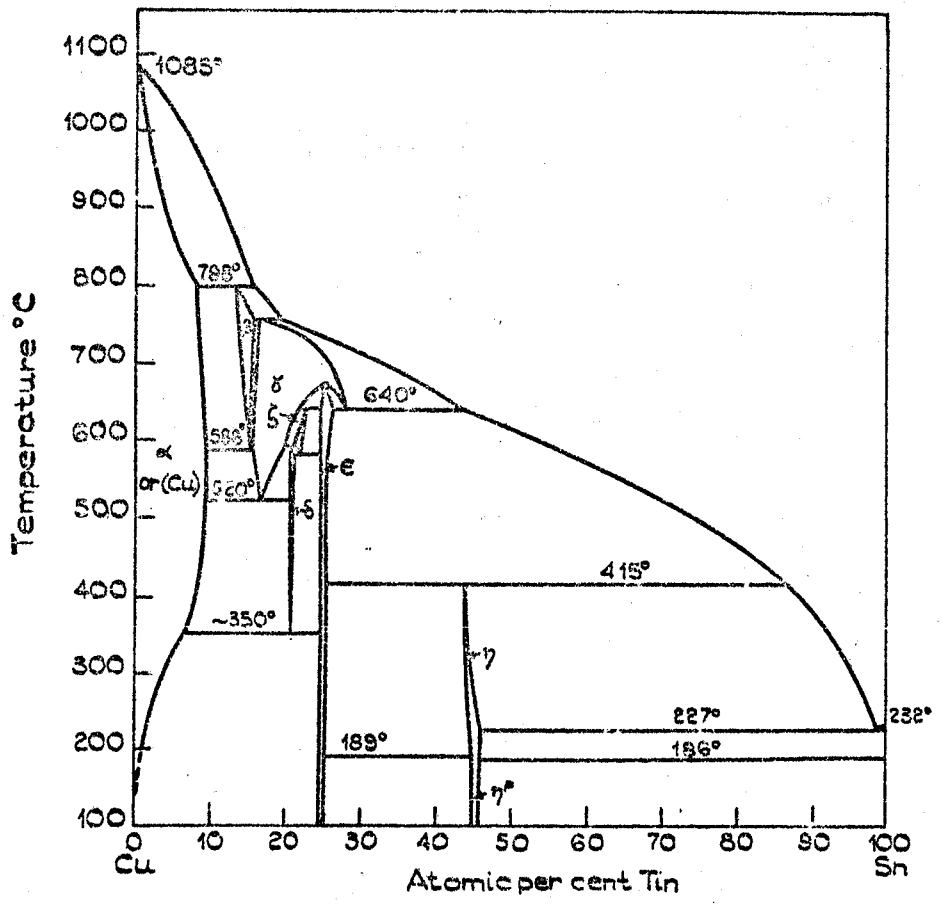

FIGURE 4.3

THE COPPER-TIN PHASE DIAGRAM (ff. HANSEN).

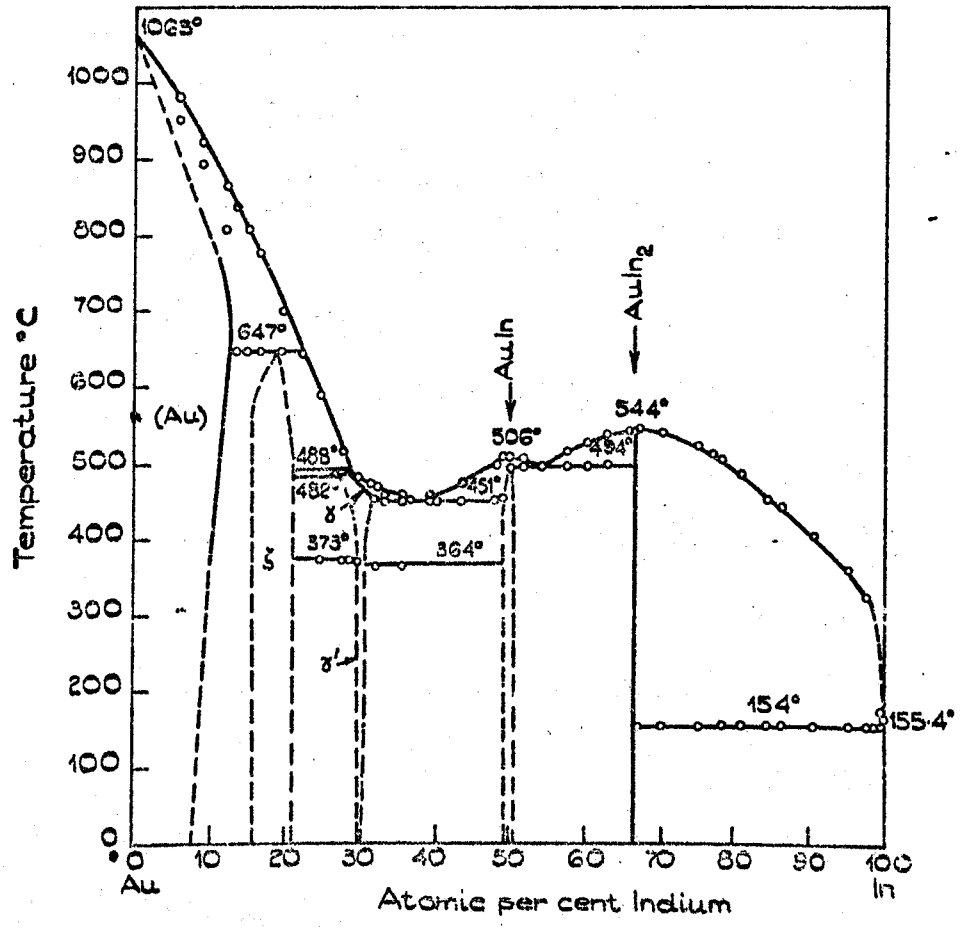

FIGURE 4.4.

THE GOLD-INDIUM PHASE DIAGRAM (ff. HANSEN).

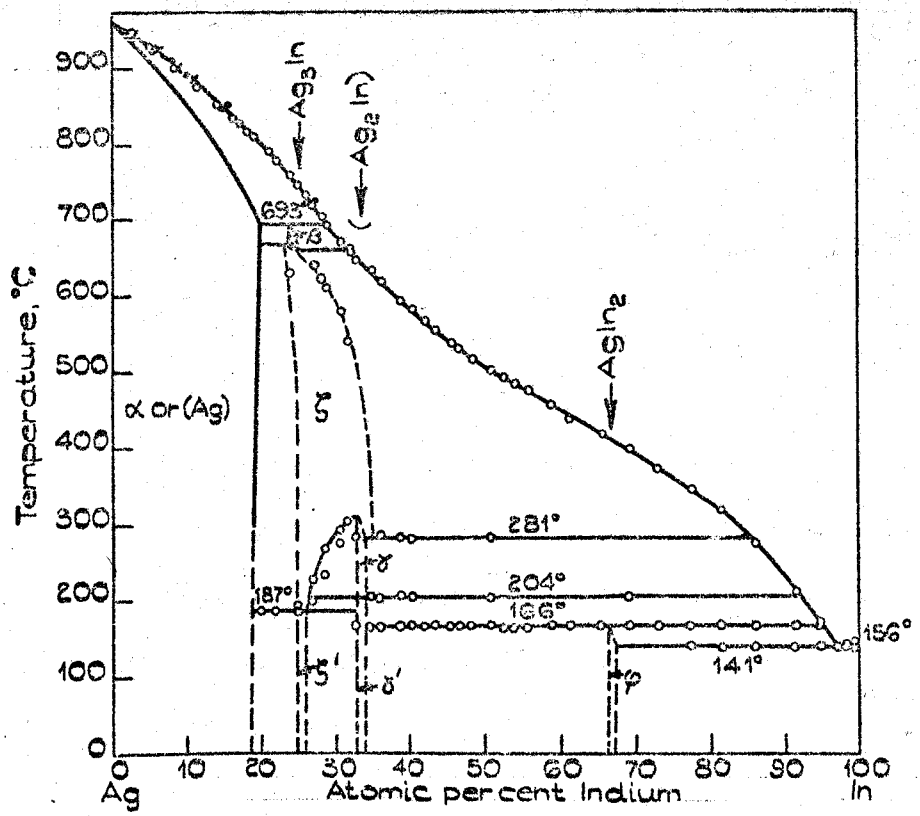

FIGURE 4.5. THE SILVER-INDIUM PHASE DIAGRAM (ff. HANSEN).

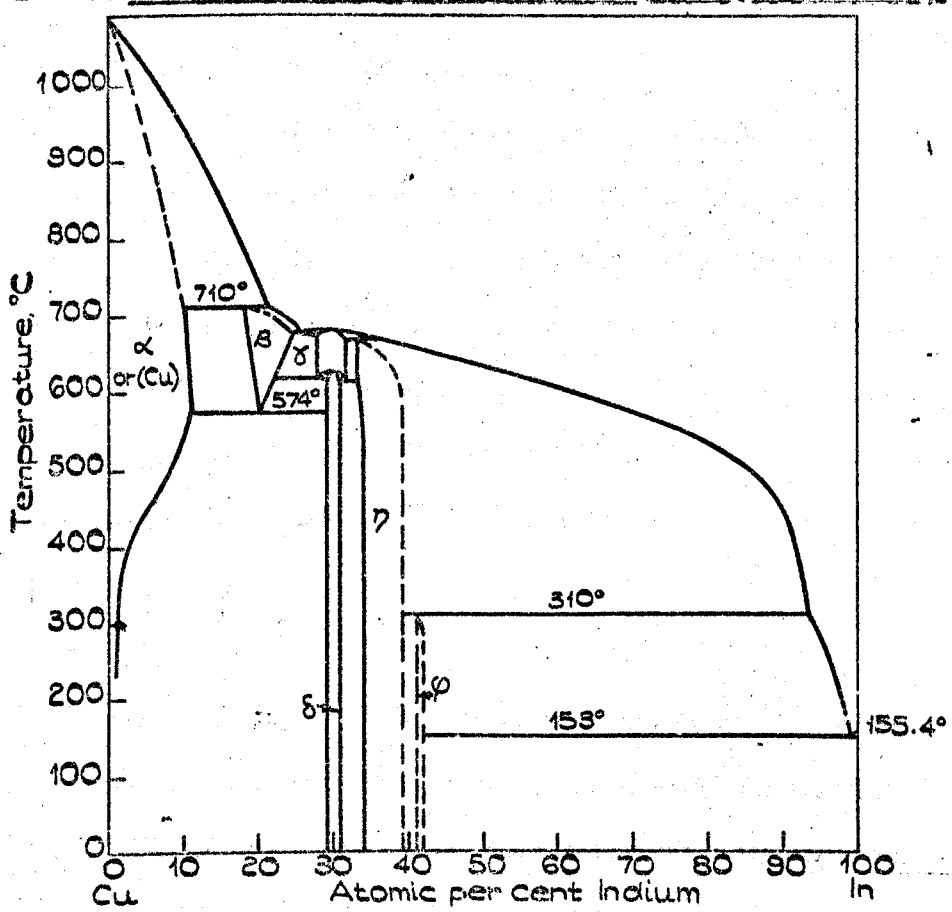

FIGURE 4.6. THE COPPER-INDIUM PHASE DIAGRAM (ff. HANSEN).

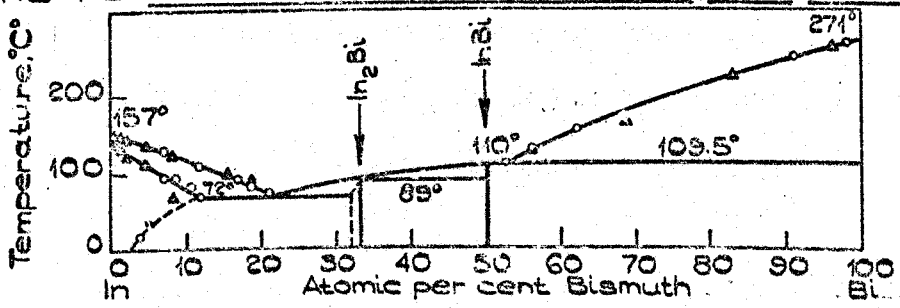

FIGURE 4.7. THE INDIUM-BISMUTH PHASE DIAGRAM (ff. HANSEN).

in the first peaks of I(K) were observed at the two intermetallic compound compositions AuIn and $AuIn_2$, suggesting that this system is not a simple two-component mixture.

4.2.2 Electron Transport Properties The Faber-Ziman[13] theory, which requires for an alloy the three partial structure factors and two atom pseudopotentials, has reproduced much, though not all, of the available resistivity and thermopower data for pure metals and alloys. The accuracy of the predictions is generally taken as an indication of the reliability of the $I_{ij}(K)$ values used in the calculations. These properties may therefore be taken as a reasonable test of the model used to derive the $I_{ij}(K)$. However, as Enderby[11] has pointed out, the fact that good agreement is obtained in, particularly, a noble-metal alloy system, without involving an energy dependent pseudopotential requires explanation; the possibility that errors in the Born approximation are cancelled out by errors due to this neglect must be born in mind. At the present time the only theory for the Hall effect in liquid metals is a free electron one. It does indicate however how free electron like the liquid is; specifically it yields the number of electrons per atom participating in this transport process.

Au-Sn, Ag-Sn and Cu-Sn

The electrical resistivity data of Davies and Leach[14] across the Au-Sn system, exhibits a maximum at approximately the Au_3Sn composition. Their data, including the maximum, are reasonably reproduced by application of the Faber-Ziman theory which incorporates the partial structure factors of Wagner etal.[9]. This may be taken as supporting the AuSn cluster hypothesis, only if one accepts the interpretation of Wagner etal. of their $I_{ij}(K)$. In a similar way, the resistivity data of Roll and Motz[15]

for the Ag-Sn system is well reproduced by Halder and Wagner[10], using their $I_{ij}(K)$ measurements. Enderby and Howe [15] have measured the absolute thermoelectric power across the liquid Cu-Sn system. Using the partial structure factors of Enderby etal. they successfully reproduce their data by applying the Faber-Ziman theory. The calculation is also performed using $I_{ij}(K)$ derived from a hard-sphere model, and show that this clearly fails to reproduce the experimental measurements. The resistivity data of Roll and Motz for this system is successfully fitted to theory by North and Wagner using their $I_{ij}(K)$ values; which are in reasonable agreement with those of Enderby etal. The Hall effect in some liquid Cu-Sn alloys, from Sn up to Cu-60 at .% Sn, has been measured by Enderby, Hasan and Simmons[17]. Their results deviate from free-electron predictions, in which it was assumed that Sn contributed 4 and Cu 1 electrons per atom to the conduction band. However, they interpret their results by suggesting that bound states form at the expense of the Sn electrons due to Sn behaving as a divalent metal dissolved in small amounts in Cu.A modified free-electron theory reproduces their data by assuming that the effective valency of Cu is always unity while that for Sn varies linearly from two at the Cu-rich end to four at the Sn-rich end.

Clearly the reproducibility of the resistivity and thermopower data using the Faber-Ziman theory is sensitive to the partial structure factors used and thus the model from which these are derived. Where the theory successfully reproduces the experimental transport property data, support is given to the particular model of the liquid structure used in the calculations.

Au-In, Ag-In and Cu-In

The Hall coefficients for the Au-In and Ag-In systems have been measured by Busch and Güntherodt[18]. Their results are in agreement with a

free-electron model, which assumes a contribution of 1 and 3 electrons per atom from the noble-metal element and indium respectively. Electrical resistivity data for these systems, by the same authors, was fitted reasonably well by Faber-Ziman theory using a hard-sphere I(K).

4.2.3 Thermodynamic Properties The quantities of interest in liquid alloy systems are the excess free energy, excess entropy and excess enthalpy of mixing, ΔG^{ex}, ΔS^{ex} and ΔH^{ex} respectively. In a miscible liquid alloy ΔG^{ex} is always negative, whereas ΔS^{ex} and ΔH^{ex} may be either positive or negative depending on the bonding between unlike and like atoms. These excess quantities measure the deviation of a particular alloy system from an ideal solution and their signs give information regarding bond energies. If the pair bond energies between atoms are E_{ii}, E_{jj} and E_{ij} then positive values of ΔH^{ex} are associated with $E_{ij} < \frac{1}{2}(E_{ii}+E_{jj})$ or a preference for like-atom pair bonding. For negative values of ΔH^{ex} then $E_{ij} < \frac{1}{2}(E_{ii}+E_{jj})$, which indicates a preference for unlike pair bonding. Most of the information regarding the nature of bonding in alloys comes from the quantity ΔH^{ex}. If a particular alloy system shows a preference for unlike pair bonding, then ΔH^{ex} will be negative across the concentration range with a maximum at the 50%-50% concentration where the maximum number of unlike pair bonds may be formed. The shape of the ΔH^{ex} curve is parabolic if the pair-bonding is independent of concentration, however if an asymmetry in the ΔH^{ex} curve is found this will indicate that the pair-bonding is not independent of concentration. In fact an asymmetry in ΔH^{ex} may be caused either by a concentration dependent pair-bonding or a more complicated bonding in which three or more atoms take part.

This information however is only qualitative as attempts to quantify the relationship between the E_{ij}'s and the measured thermodynamic properties have met with little success in liquid alloys due to the lack of information of the interatomic bond in metals.

Au-Sn, Ag-Sn and Cu-Sn

All of the measurements on the Au-Sn system show that there is a preference for unlike atomic bonding. The results of Kleppa[19] revealed that at the Au_3Sn composition there was either a strengthening of the pair-bonding or a favourable configuration of 1 tin and 3 gold atoms was occurring. The calorimetric measurements of Jena and Leach[20] confirmed the data of Kleppa and showed that at Au_3Sn strong unlike pair-bonding was taking place. Detailed measurements of ΔH^{ex} around the Au-50% Sn composition, 47→51 at.% Sn, have been made by Masse, Orr and Hultgren[21]. Their results show ideal behaviour, no anomalies occurring in the range covered thus giving no support to the hypothesis that atomic associations in the equiatomic alloy resemble those in solid AuSn. Measurements of ΔH^{ex} for the Ag-Sn and Cu-Sn systems[4] show negative values across the concentration range with an indication that the pair-bonding is at its strongest at Ag-20% Sn and Cu-22% Sn.

To summarise, the data indicate that in all three systems pair-bonding between dissimilar atoms is occurring across the whole concentration range but is strongest around the 25% Sn composition.

Au-In, Ag-In and Cu-In

Of the sparse data available for these systems, that of Alcock etal.[22] of ΔH^{ex} and ΔS^{ex} for the liquid Ag-In system shows only slight deviations from ideal behaviour, no marked effects occurring at any composition.

4.2.4 NMR Knight shift and Magnetic susceptibility It has long been known that the Knight shift K is sensitive to the local atomic and electronic character in a metal or alloy. This is clearly evident in the work of Drain[23] who found marked changes in $K(^{113}Cd)$ and $K(^{109}Ag)$ as a function of concentration in the solid Ag-Cd system. His observed variations were not

explained in terms of a simple change in electron/atom ratio and therefore similar behaviour in K in liquid alloys could be expected when ordering occurs.

The evidence provided by magnetic susceptibility is less direct. The total electronic susceptibility χ_e obtained from measurements of the total susceptibility, would be expected to show a minimum at the particular alloy composition at which covalent bonding is occurring due to the pairing of electrons in the bonds. However before observation of this minimum in χ_e is taken directly as evidence for bonding, the approximations made in the determination of χ_e must be very closely examined. This is particularly important for the noble metals and their alloys and will be discussed in detail in the following chapter.

In-Bi

A recent paper by Styles[24] has interpreted $K(^{115}In)$, $K(^{209}Bi)$ and $\Delta H(^{115}In)$ and $\Delta H(^{209}Bi)$ in the liquid In-Bi system in terms of the persistence of InBi and In_2Bi groupings in the liquid state. The phase diagram, shown in figure 4.7[5], is divided into three ranges; c(Bi)>50%, $33\frac{1}{3}\%<c(Bi)\leq 50\%$ and $c(Bi)<33\frac{1}{3}\%$. In the first region there is a mixture of InBi and Bi, in the second a mixture of In_2Bi and InBi and in the third a mixture of In_2Bi and In. In the first region, as the concentration c is decreased, the relative amounts of InBi and Bi vary, starting with pure Bi at c=100% and finishing with pure InBi at c=50%. Hence in this region, the ^{115}In nuclei are always in an InBi environment and $K(^{115}In)$ is the same at all concentrations. The ^{209}Bi nuclei however are in either an InBi or pure Bi environment and as such will exhibit different Knight shifts. However, since the correlation time of the interdiffusion of the Bi atoms is very short compared with the reciprocal (10^{-4}s) of the difference between the two resonance frequencies in the two environments, the two resonances collapse into one. $K(^{209}Bi)$ thus varies as the relative amounts of InBi and Bi change with composition. Similar

behaviour occurs in the third region, but now the ^{209}Bi nuclei always find themselves on In_2Bi environment and $K(^{209}Bi)$ is constant, whereas $K(^{115}In)$ varies with concentration. In the intermediate region there is a mixture of the two compounds, so that both shifts change with concentration. All of the above features are observed in the experimental results. If the collapse of the resonances from nuclei in any two coexisting environments is not complete, but is sufficiently so for the residual separation to be small compared with the line width due to other sources (e.g. Korringa broadening), then the overall width should pass through a maximum when there are equal numbers of nuclei in the two environments. The maximum observed in the ^{209}Bi line width at about 60% Bi was consistent with this model. As expected, at higher temperatures the variations with composition of both K and ΔH become smoother. The behaviour of K and ΔH in the systems under study will be considered in the following section in the light of the observations and interpretations given in the In-Bi system.

4.3 Present Results

Au-Sn

We consider first the model which suggests that Au_3Sn units form in the liquid state. If this were the case, then as the gold content is increased, $K(^{119}Sn)$ should change up to the Au_3Sn concentration, after which it should flatten out since all the Sn atoms are in an Au_3Sn environment. Figure 3.4 shows that $K(^{119}Sn)$ is still increasing rapidly beyond the Au_3Sn composition, which lends no support to the Au_3Sn cluster model. Also to be expected from this model is a maximum in $\Delta H(^{119}Sn)$ at approximately Au-40% Sn; figure 3.11 shows that this feature does not occur.

The most recent work of Wagner et al.[9] points to the existence of AuSn groupings in the liquid and this model will now be considered. If these do persist into the liquid $K(^{119}Sn)$ would not be expected to change very much

in Au-50% Sn as it goes through the liquidus but, as the 'units' begin to break up with increasing temperature, the Knight shift should exhibit a more marked temperature dependence than normally seen in the liquid state. In fact the observed change in $K(^{119}Sn)$ on melting is approximately 10% of itself, which is more than is usually observed for liquid metals. Again beyond the AuSn composition, one would expect a flattening out of $K(^{119}Sn)$; figures 3.1 and 3.4 shows that these features are not observed within the experimental error. However figure 3.2 shows that the temperature dependence of $K(^{119}Sn)$ in liquid AuSn in probably greater than for any of the other gold-tin alloys. This can be caused by the temperature variation of density and atomic volume being greatest in this alloy (see chapter five, section 5.5) and it is a more likely explanation than the break-up of AuSn clusters which is expected to produce a more dramatic varation than observed.

Figure 5.1 shows that a minimum occurs in χ_e at approximately 80% of Au, on the assumption that χ_e varies linearly between the pure metal values. As was recently mentioned, this may be taken as evidence for covalent bonding within the approximations made for the determination of χ_e.

Ag-Sn and Cu-Sn

The composition range covered by the NMR measurements in these systems is somewhat less than that for Au-Sn; as seen in figures 3.3, 3.4 and 3.11, linear variations in $K(^{119}Sn)$, $K(^{63}Cu)$ and $\Delta H(^{119}Sn)$ were observed. Thus no evidence for structure was found in these two systems up to the concentrations measured. The previous data for these systems consistently indicates that while Ag-Sn is a simple mixture of Ag and Sn, the Cu-Sn system is far from random. It is hoped shortly to measure the susceptibilities and thus χ_e for these systems across the concentration range to see whether any difference exists in their behaviour.

Au-In, Ag-In and Cu-In

The Au-In system has, in common with the In-Bi system, two intermetallic compounds at $AuIn_2$ and AuIn shown in figure 4.4. If these persist as groupings into the liquid state, then $K(^{115}In)$ should exhibit similar behaviour to $K(^{115}In)$ in the In-Bi system, as should $\Delta H(^{115}In)$. Figures 3.6 and 3.12 reveal none of this expected behaviour. However, figure 3.9 shows that the common feature in the behaviour of $K(^{115}In)$ in these systems is a distinct maximum between 40 and 60 at .% of noble metal. No way is seen of explaining this maximum in terms of the above model of clustering.

Figures 5.2 and 5.3 show the behaviour of χ_e in these systems. Their common feature is that χ_e shows a marked increase between 60 and 80 at .% of noble metal, in contrast with the behaviour of $K(^{115}In)$ which, for all three systems, passes through a maximum. Although the rapid decrease of χ_e on adding indium to the noble metal could be taken as evidence of the formation of groupings like Cu_3Sn due to covalent bonding, the Knight shift evidence just discussed is clearly inconsistent with this picture. It is emphasized that the interpretation of the χ_e data is very tentative in view of the possible invalid assumptions made when determining it from measured susceptibilities (see chapter five, section 5.2).

Linewidths A large part of ΔH is expected to come from the rapid spin-lattice relaxation produced by the interaction of the nuclei with the conduction electrons. A calculation of the relaxation rates, R_1, of ^{115}In, ^{119}Sn and ^{63}Cu from the observed Knight shifts using the Korringa relation was made for both the noble metal-tin and noble metal-indium systems. These were compared with R_1 values calculated from measured line widths, as shown in figures 6.1, 6.2, 6.3, 6.4 and 6.8.

In the noble metal-tin systems, the relaxation rates calculated from

the Knight shifts, agree quite closely with those obtained from the line width, for the ^{119}Sn nucleus. However, for ^{63}Cu in the copper-tin and copper-indium systems and for ^{115}In in the noble metal-indium systems, the two values show marked differences. As will be more fully discussed in chapter six, it is believed that the discrepancy is chiefly due to an additional quadrupolar relaxation process (the ^{63}Cu and ^{115}In nuclei possess electric quadrupole moments while ^{119}Sn does not), which is often observed in liquid metals and alloys and is not necessarily associated with ordering.

Summary The X-ray and neutron diffraction data, and to a less extent the thermodynamic data, strongly suggest that short range ordering occurs in the liquid Au-Sn and Cu-Sn systems. The Ag-Sn system on the other hand is probably a simple mixture of Ag and Sn.

The susceptibility measurements tentatively confirm the existence of groupings at Au_3Sn and suggest that similar bonding is occurring in the noble metal-indium alloys at the same composition. However the NMR measurements, which for the In-Bi system have conclusively shown the existence of groupings in the liquid, give no evidence at all that ordering is taking place at any composition in any of the alloys.

Consequently the quantitative interpretation of the Knight-shift data, which follows in the next chapter, is based on the assumption that the alloys are random mixtures of the two constituents.

REFERENCES

(1) Ashcroft N. W. and Lekner J., Phys. Rev., 145, (1966), 83.

(2) Ashcroft N. W. and Langreth J., Phys. Rev., 156, (1967), 685.

(3) Wilson J. R., Metall. Revs., 10, (1965), 381.

(4) Mott B. W., UKAEA report AERE - R5565, (1967).

(5) Hansen M., Constitution of Binary Alloys, McGraw Hill (1958).

(6) Hendus H., Zeit. Naturforsch., 2, (1947), 505.

(7) Waghorne R. M., Rivlin V. G. and Williams G. I., Adv. Phys., 16, (1966), 215.

(8) Kaplow R., Strong S. L. and Averbach B. L., MIT Report OSR-7954, (1965).

(9) Wagner C. N. J., Halder N. C. and North D. M., Zeit. Naturforsch., 24a, (1969), 432.

(10) Halder N. C. and Wagner C. N. J., J. Chem. Phys., 47, (1967), 4385.

(11) Enderby J. E., North D. M. and Egelstaff P. A., Adv. Phys., 16, (1966), 171.

(12) North D. M. and Wagner C. N. J. (to be published in Phys. Chem. Liquids).

(13) Faber T. E. and Ziman J. M., Phil. Mag., 11, (1965), 153.

(14) Davies, H. A. and Llewelyn Leach J. S., Phil. Mag., 19, (1969), 1271.

(15) Roll A. and Motz H., Z. Metallk., 48, (1957), 435.

(16) Enderby J. E. and Howe R. A., Phil. Mag., 18, (1968), 923.

(17) Enderby J. E., Hasan S. B.and Simmons C. J., Adv. Phys., 16, (1967), 667.

(18) Busch G. and Guntherodt H. J., Phys. Kond.Mat., 6, (1967), 325.

(19) Kleppa O. J., J. Amer. Chem. Soc., 72, (1950), 3346.

(20) Jena A. K. and Leach J. S. L., Acta Met., 14, (1966), 1595.

(21) Masse J. D. G., Orr R. L. and Hultgren R., Trans. Metall. Soc., 236, (1966), 1202.

(22) Alcock C. B., Sridhar R. and Svedberg R. C., Acta Met., 17, (1969), 839.

(23) Drain L. E., Phil. Mag., 4, (1959), 484.

(24) Styles G. A., Adv. Phys., 16, (1966), 275.

CHAPTER FIVE

CALCULATION OF KNIGHT SHIFTS IN LIQUID ALLOYS

5.1 Introduction

As shown previously the Knight shift K_s may be written

$$K_s = \frac{8\pi}{3} \chi_p \Omega P_F . \qquad 5.01$$

This chapter is wholly concerned with the calculation of both χ_p and ΩP_F for the liquid noble metal-tin and noble metal-indium systems. The best way of obtaining χ_p for a metal is by direct measurement using conduction electron spin resonance (CESR), but this has been possible for only a very few metals. Recently however Dupree and Seymour[1] have shown that reasonably consistent values of χ_p may be obtained from measurements of the total susceptibility χ_{tot}. Section 5.2 discusses in detail the extraction of χ_p from χ_{tot} for the alloys of concern here. Recent calculations of Mahanti and Das[31] have yielded exchange core polarisation contributions to the Knight shift for the alkali metals. Unfortunately such calculations do not exist for any of the systems considered here and they are beyond the scope of this thesis. The P_F term in equation 5.01 to be calculated is hence due solely to the direct contact interaction which dominates the magnitude of the observed shifts. Most of the theoretical effort in the calculation of P_F has been towards a determination of its change on alloying or with temperature. To determined the former effect, two distinct approaches have been used. The first is applicable to low impurity concentrations and involves a partial wave analysis of the impurity screening using phase shifts obtained from the model potential representing the impurity.

Two potentials have been used, a square well and a more realistic screened free atom potential recently proposed by Asik et al.[2]. Sections 5.3 and 5.4 are concerned with the calculation of the coefficients describing the liquid atomic distributions and the phase shifts. In the second approach the extension of the Faber[3] theory outlined by Perdew and Wilkins[4] is used, in which the solute and solvent ion-core potentials are replaced by a weaker pseudopotential. Their calculation is valid across the complete range of alloy concentration. Section 5.5 contains an extension of their work to polyvalent alloy systems, in particular those of Sn and In alloyed with the noble metals.

The calculations use free electron parameters throughout and assume that the direct contact hyperfine interaction is dominant for these alloys and that the variation of K arises from a change of either or both the factors χ_p and ΩP_F. The fractional change of shift may then be written

$$\frac{\delta K}{K} = \frac{\delta \chi_P}{\chi_P} + \delta\left(\frac{\Omega P_F}{\Omega P_F}\right). \qquad 5.02$$

The effect of a change in χ_p and its determination is now considered.

5.2 Discussion of the Magnetic Susceptibility data

5.2.1 Basic Theory of Susceptibility in Metals. The total magnetic susceptibility in a metal may be expressed by

$$\chi_{tot} = \chi_e + \chi_c$$

where χ_c is the ion core susceptibility and χ_e the total electronic contribution. There have been a number of determinations of χ_c and these are discussed by Dupree and Seymour[1] who conclude that the values given by Angus[5] yield the

most consistent values of χ_e. The calculation involves a summation over the ion-core wave functions, which are taken as simple Slater[6] analytic wave functions, these being a good approximation at large distances from the nucleus where the main contribution to the core susceptibility arises. The conduction electron susceptibility may be written

$$\chi_e = \chi_p + \chi_d, \qquad 5.03$$

where χ_d is the Landau diamagnetic term. For free non-interacting electrons

$$\chi_{po} = \frac{\mu_B^2 N(E_F)}{V} = 3\left(\frac{\pi}{3}\right)^{\frac{2}{3}}\left(\frac{N}{V}\right)^{\frac{1}{3}}\frac{\mu_B^2 m}{\pi^2\hbar^2} \qquad 5.04$$

and

$$\chi_{do} = -\frac{1}{3}\chi_{po}$$

where μ_B is the Bohr magneton, $N(E_F)$ the density of states at the Fermi level and V the volume of the sample containing N electrons. However allowance must be made in metals for (1) the presence of ions, (2) electron-electron interactions, (3) electron-phonon interactions and (4) the effect of electron scattering involving spin reversal. The last two effects have been shown to be small and are not considered further.

The influence of the ions via their potential may be taken into consideration by using the effective mass approximation. Assuming a spherical Fermi surface in a liquid metal or alloy, m* is the same for all electrons at E_F. The Pauli susceptibility then becomes $\chi_p = \chi_{po}\,(m^*/m)$ and the Landau term $\chi_d = \chi_{do}\,(m/m^*)$. There have been a number of estimates of the effect of electron-electron interactions on χ_p. The most recent by Dupree and Geldart[7], which assumes $m^*/m = 1$, has yielded the best theoretical fit to the experimental χ_p values deduced by the method described in this section. A recent calculation by Kanazawa and Matsudawa[8] of the effects of electron-

electron interactions on χ_d, predicts an enhancement given by

$$\frac{\chi_d}{\chi_{do}} = 1 + \frac{\alpha r_s}{6\pi}\{\ln r_s + 4 + \ln(\frac{\alpha}{2\pi})\}, \qquad 5.05$$

where r_s is defined by $\frac{4\pi r^3}{3}_s = \frac{V}{N}$ and $\alpha = (\frac{4}{9\pi})^{\frac{1}{3}}$.

For the metals considered here the enhancement amounts to some 15 → 25%.

5.2.2 Analysis and Discussion of Experimental Data. χ_{tot} values in mass units for the Au-Sn and noble metal-indium systems at various temperatures are tabulated in appendix I. The values obtained for pure In and Sn are in good agreement with previous data[9,10]; however those for the noble metals disagree (by as much as 40% for Au, though only a single previous measurement for Au exists in the literature). It will be shown that the values obtained for Ag and Cu yield χ_p's which are not unreasonable and though the value for Au is rather high, there seems no reason to doubt the measurements on Au rather than any of the other metals.

Tabulated below in column 3 is χ_e for all the metals and alloys. The core susceptibilities from Angus have been subtracted from χ_{tot}, on the assumption that the ionic contribution to χ_{tot} is simply made up of the sum of χ_c times the number density for each alloy component. Because of the uncertainty in the absolute magnitude of χ_c, it is probably adequate to assume that it is independent of its electronic environment, which will obviously be changing across the concentration range. To obtain the values of χ_e given in the table in volume units from the measured susceptibilities in mass units, it is necessary to know the density as a function of concentration in these systems. Apart from the pure metal densities, the only alloy density measurements in these systems are of four Au-Sn alloys at 1073 K by Williams[11]; these results only deviate by approximately 4% from values given by a linear interpolation between the pure metal densities. Such an

interpolation was used for the noble metal-indium alloys and this approximation is allowed for in the error bars in figures 5.2 and 5.3, assuming that the deviation from linearity is not greater than 4%. The variation of χ_e in these systems is shown in figures 5.1, 5.2 and 5.3. For the Au-Sn and Au-In systems, the increase in χ_e is linear until about the 70 at .% Au concentration, after which χ_e increases rapidly up to the Au value. Both the Ag-In and Cu-In systems exhibit a minimum in χ_e between 60 and 80 at .% of the noble metal.Values for χ_p may be extracted from these χ_e values by using equation 5.04 and 5.05 to estimate χ_d. As no measurements of χ_{tot} were made on the Cu-Sn or Ag-Sn systems, the χ_p values given below are deduced from a linear interpolation between the pure metal values. Tables 5.1 and 5.2 contain the susceptibilities and initial slope of χ_p with concentration respectively for the noble metal-tin and noble metal-indium systems.

Table 5.1

Electronic magnetic susceptibilities in the noble metal-indium and gold-tin systems

System	Temp. K	χ_e (expt.) c.g.s. vol.x 10^6	χ_{po} (theory) c.g.s. vol.x 10^6	χ_d (theory) c.g.s. vol.x 10^6	χ_p (expt.) c.g.s. vol.x 10^6	m*/m
Au	1383	2.39	0.83	-0.34	2.73	2.04
Au-20%In	1133	1.82	0.921	-0.37	2.19	
	1033	1.81			2.18	
Au-30%In	1073	1.51	0.96	-0.38	1.89	
	823	1.31			1.69	
Au-40%In	1073	1.43	0.98	-0.39	1.82	
	773	1.24			1.63	

Table 5.1 (continued

System	Temp. K	χ_e (expt.) c.g.s. vol.x 10^6	χ_{po} (theory) c.g.s. vol.x 10^6	χ_d (theory) c.g.s. vol.x 10^6	χ_p (expt.) c.g.s. vol.x 10^6	m*/m
Au-50%In	1073	1.41	1.00	-0.40	1.81	
	833	1.32			1.72	
Au-66%In	1073	1.34	1.03	-0.40	1.75	
	877	1.31			1.72	
Au-80%In	1073	1.26	1.04	-0.41	1.67	
	816	1.25			1.66	
Au-90%In	1073	1.20	1.04	-0.41	1.61	
	731	1.21			1.62	
In	1073	1.13	1.06	-0.41	1.54	1.03
	486	1.05			1.46	
Ag-90%In	1073	1.17	1.03	-0.41	1.57	
Ag-80%In	1073	1.20	1.02	-0.40	1.61	
Ag-66%In	1073	1.20	1.00	-0.39	1.60	
	733	1.18			1.57	
Ag-55%In	1073	1.14	0.97	-0.39	1.53	
	798	1.09			1.48	
Ag-40%In	1073	1.09	0.95	-0.38	1.47	
	893	1.04			1.42	
Ag-33%In	1073	1.10	0.93	-0.37	1.47	
	991	1.05			1.43	
Ag-30%In	1073	1.09	0.93	-0.37	1.46	
	990	1.05			1.42	

Table 5.1 continued

System	Temp.	χ_e (expt.) c.g.s. vol.x 10^6	χ_{po} (theory) c.g.s. vol.x 10^6	χ_d (theory) c.g.s. vol.x 10^6	χ_p (expt.) c.g.s. vol.x 10^6	m*/m
Ag-25%In	1073	1.22	0.91	-0.37	1.58	
Ag-17%In	1150	1.39	0.89	-0.36	1.75	
Ag	1283	1.62	0.82	-0.33	1.94	1.51
Cu	1373	1.77	0.95	-0.38	2.15	1.50
Cu-20%In	1073	1.22	0.99	-0.39	1.61	
Cu-30%In	1073	1.02	1.01	-0.40	1.41	
	993	0.95			1.35	
Cu-37.5%In	1073	1.05	1.02	-0.40	1.45	
	992	1.00			1.40	
Cu-45%In	1073	1.08	1.03	-0.40	1.48	
	962	1.02			1.42	
Cu-52.5%In	1073	1.12	1.03	-0.40	1.52	
	950	1.08			1.48	
Cu-60%In	1073	1.14	1.04	-0.40	1.54	
	923	1.11			1.51	
Cu-75%In	1073	1.16	1.04	-0.41	1.56	
	873	1.16			1.56	
Cu-90%In	1073	1.15	1.05	-0.41	1.56	

Table 5.1 continued

System	Temp. K	χ_e (expt.) c.g.s. vol.x 10^6	χ_{po} (theory) c.g.s. vol.x 10^6	χ_d (theory) c.g.s. vol.x 10^6	χ_p (expt.) c.g.s. vol.x 10^6	m*/m
Sn	773	1.11	1.14	-0.44	1.55	1.01
Au-80%Sn	773	1.21	1.14	-0.44	1.65	
Au-66%Sn	773	1.29	1.12	-0.43	1.72	
Au-50%Sn	773	1.38	1.08	-0.42	1.80	
Au-29%Sn	773	1.42	1.00	-0.40	1.82	
Au-25%Sn	773	1.48	0.98	-0.39	1.87	
Au-21%Sn	773	1.50	0.96	-0.38	1.88	

Interpolated Pauli spin susceptibilities for the copper-tin and silver-tin systems

Alloy	Interpolated χ_p, c.g.s. vol.x 10^6	Alloy	Interpolated χ_p, c.g.s. vol.x 10^6
Cu-95%Sn	1.58	Ag-88%Sn	1.60
Cu-90%Sn	1.61	Ag-77%Sn	1.64
Cu-85%Sn	1.64	Ag-66%Sn	1.68
Cu-80%Sn	1.67	Ag-55%Sn	1.73
Cu-75%Sn	1.70	Ag-45%Sn	1.77
Cu-70%Sn	1.73	Ag-35%Sn	1.80
Cu-65%Sn	1.76		

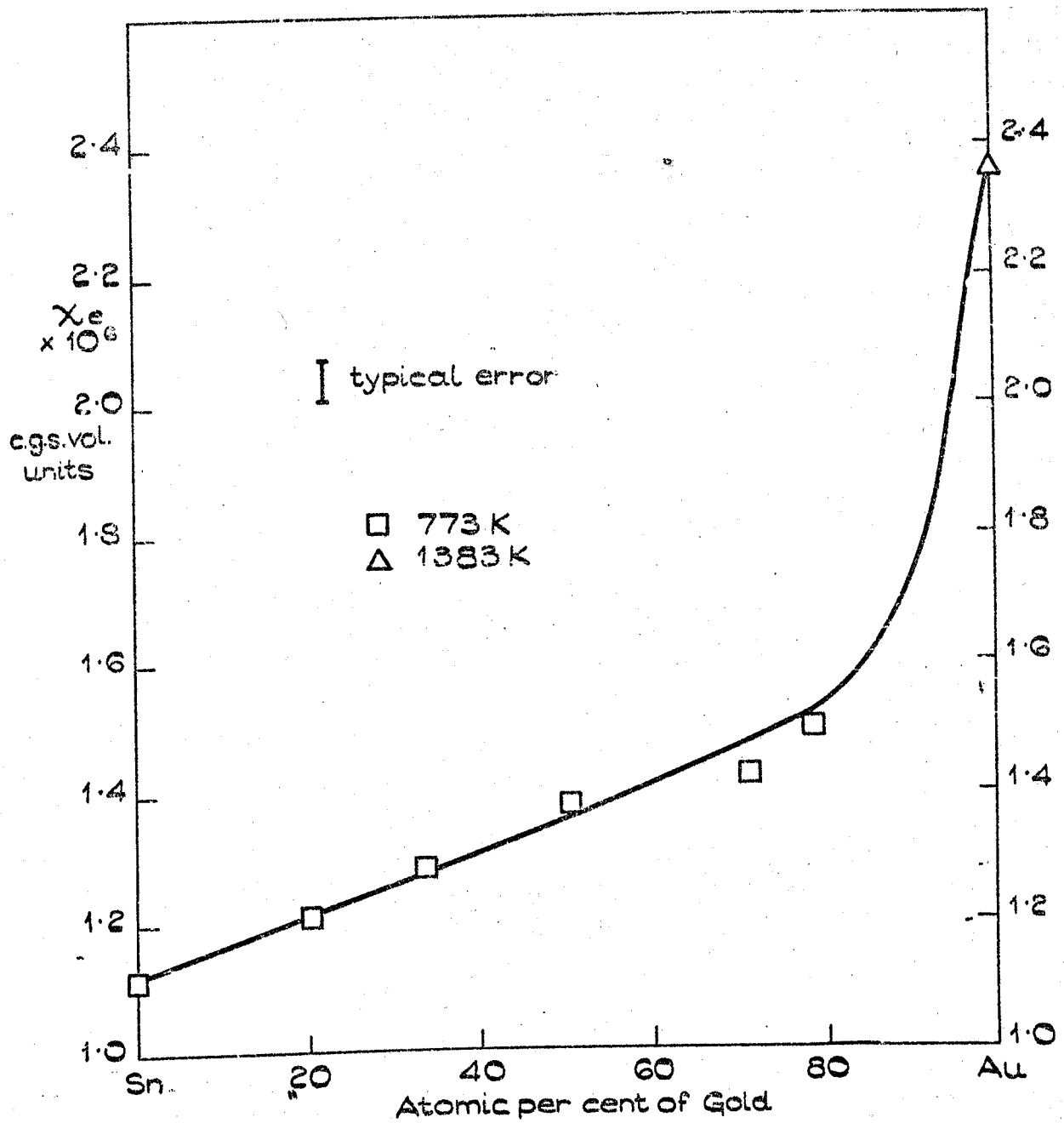

FIGURE 5.1.

VARIATION OF THE TOTAL ELECTRONIC SUSCEPTIBILITY WITH CONCENTRATION IN THE LIQUID GOLD-TIN SYSTEM.

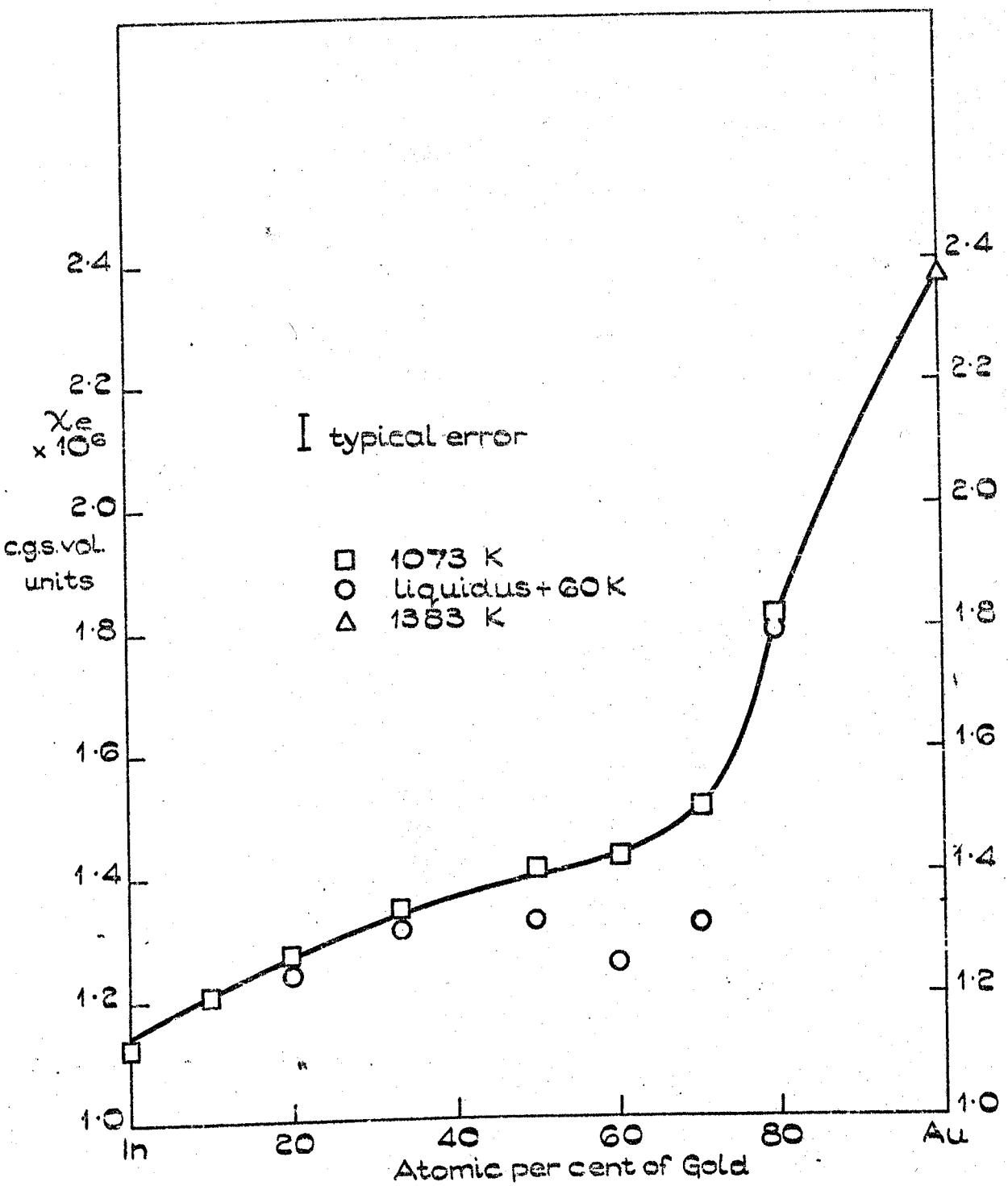

FIGURE 5.2.

VARIATION OF THE TOTAL ELECTRONIC SUSCEPTIBILITY WITH CONCENTRATION IN THE LIQUID GOLD-INDIUM SYSTEM.

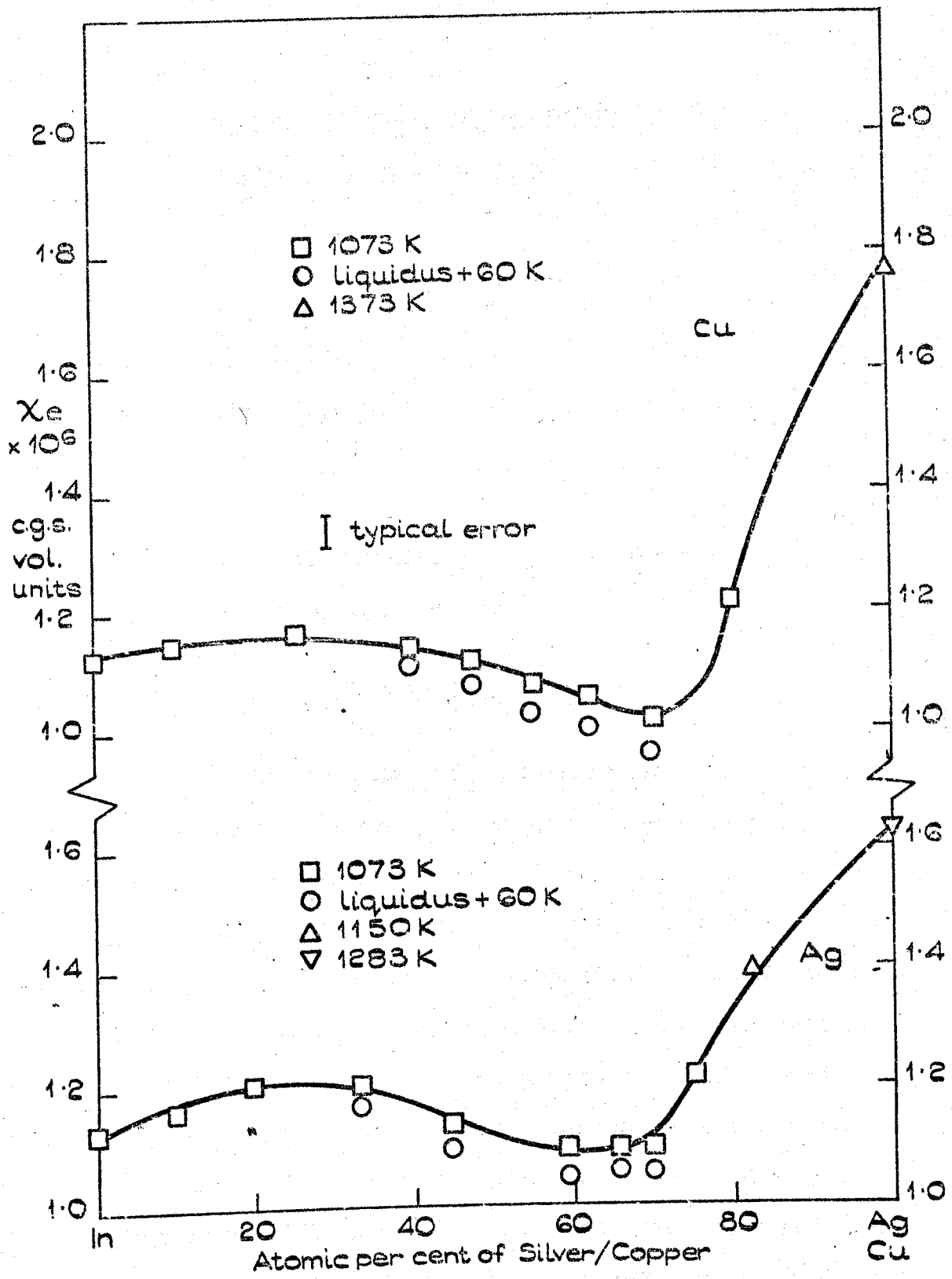

FIGURE 5.3.

VARIATION OF THE TOTAL ELECTRONIC SUSCEPTIBILITY WITH CONCENTRATION IN THE LIQUID COPPER-INDIUM AND SILVER-INDIUM SYSTEMS.

Table 5.2

Initial slopes of spin susceptibility calculated from χ_p(expt.) given in table 5.1

solvent solute	In Au	In Ag	In Cu	Sn Au	Sn Ag	Sn Cu	Cu In	Cu Sn
$\frac{1}{c}\cdot\frac{\delta\chi_p}{\chi_p}$	0.45	0.19	0.13	0.32	0.25	0.39	-0.28	-0.28

An indication of the reliability of these χ_p values for the pure metals may be made in the following way. By writing

$$\chi_e = \chi_p \left(\frac{m^*}{m}\right) + \chi_d \left(\frac{m}{m^*}\right) \qquad 5.06$$

the effects of both the ion potential, through m*, and electron-electron interactions are included, χ_p and χ_d being the enhanced values. By taking the χ_e and χ_d values calculated as described, and a χ_p value taken from Dupree and Geldart (in which they assume $m^*/m = 1$), a value for m^*/m may be obtained which satisfies equation 5.06. For liquid In and Sn, m^*/m has a value almost exactly equal to 1 while Cu and Ag require m^*/m to be 1.5. Values of $m^*/m>1$ have been obtained both experimentally and theoretically for some of the monovalent metals. A recent APW band structure calculation by Rudge[12] for solid Li gave $m^*/m = 1.6$, the small change of χ_{tot} on melting indicates presumably that this value is not greatly changed in the liquid. El-Hanany and Zamir's[13] recent paper yields a value of $m^*/m = 1.3$ for Cu at room temperature, which decreases to 1.1 at the melting point. For Au, m^*/m needs to be 2.04 in order that equation 5.06 be satisfied, which seems an unreasonably large value.

El-Hanany and Zamir have deduced from their analysis of K and the spin-lattice relaxation time, T_1 data that the Fermi electrons of Cu

have approximately 18% of d-character in the liquid and conclude that s-d hybridization considerably influences the electronic structure and properties of Cu, both in the solid and liquid. This effect has been ignored by assuming that χ_c is independent of its environment and its neglect will surely cause the final values of χ_p to be in error. A calculation of the s-d hybridization contribution in the noble metals and their alloys is beyond the scope of this thesis, though its magnitude and influence will be discussed more fully in section 5.5.

It has been shown that the assumptions made when extracting χ_p from χ_{tot} become increasingly poor as one approaches the pure noble metal concentration, where m*/m must become unreasonably large to obtain agreement between χ_p(expt.) and χ_p(theory). The reason for this is thought to be due to the existence of strong s-d hybridization and an expected strong spin-orbit coupling, neither of which have been taken into account. However the values of χ_p for pure In and Sn are in good agreement with those of Dupree and Geldart which lends support to this method of obtaining χ_p for the simple metals. The χ_p values given in table 5.1 are the best available for the Knight-shift calculations, with the exception of the Cu-Sn and Ag-Sn data where a linear interpolation has been used. To what extent the Knight shift behaviour is accounted for by the χ_p term will be discussed in section 5.5 where the ΩP_F term is evaluated in these alloys.

5.3 Calculation of the change in the Knight shift using partial wave analysis

5.3.1 Electron Density oscillations Friedel et al. have shown that the introduction of an impurity atom into a pure solvent, causes a distortion of the conduction electron wave functions in such a way that they screen out the excess charge on the impurity. The resultant oscillations in the electron density about the impurity, calculated using a partial-

wave analysis of the impurity scattering, extend to large distances in the solvent and affect P_F at the solvent nuclei. In order to calculate the oscillating charge density, and hence the change in K, some representation of the impurity potential must be made. Until recently the presence of the impurity was simulated using a potential square well or barrier. Calculations for some alkali-alkali alloys gave fair agreement with experiment. However Styles[15] used this model for polyvalent solvents and solutes, and was unable to account for his experimental data. Recently Meyer[16] et al. have used a more realistic model, in which the impurity is represented by a screened free atom potential. Their calculations are limited to mono-valent solvents and solutes, but give better agreement with experiment than the square well model. Asik, Ball and Slichter[2] have used an almost identical model to Meyer et al., and when applied to the alkali alloys[33] obtained good agreement for the change of K. In this section the theory from which the change in P_F is determined will be outlined. This will then be calculated at ^{119}Sn and ^{115}In alloyed with the noble metals and for ^{63}Cu alloyed with In and Sn, using both model potentials, the more realistic model potential being derived from Asik et al.

5.3.2 Square Well Model Potential Friedel's model of an impurity atom in an alloy was that of a spherically symmetric square potential well or barrier which scattered the conduction electrons.

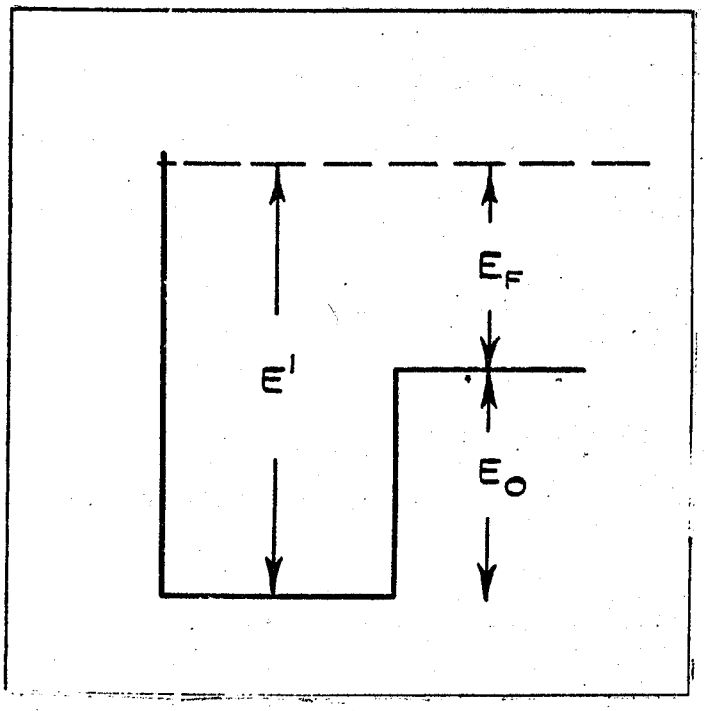

In the figure below the impurity potential is given by $E_o = \frac{h^2k^2}{2m}$ and E_F is the Fermi energy and E' is the energy from the bottom of the potential well to the Fermi level. The Schrodinger equation is solved both inside and outside the potential well, which has a radius equal in value to that of the solute ion it is representing. Because of the simple form of the potential the equation may be solved analytically, the solutions for the incident and scattered electron wave functions being expressed in terms of partial waves. From these solutions the phase shifts of the l^{th} partial waves γ_ℓ are determined by matching the electron wave functions at the potential boundary. The depth of the potential well is varied until the γ_ℓ's satisfy the Friedel sum rule

$$Z' = \frac{2}{\pi} \Sigma_\ell (2\ell + 1)\gamma_\ell(k_F), \qquad 5.07$$

where Z' is the effective charge on the impurity, modified by volume dilatation. Using the method of Blatt[17], the effective charge on the impurity is given by $Z' = Z_1 - Z_o \frac{\Omega_1}{\Omega_o}$ where Z is the charge and Ω the

atomic volume; the suffices 1 and 0 referring to the solute and solvent respectively and where it is assumed that the solute ions retain their pure metal volumes when in solution. The actual values of the atomic volumes are given in table 5.8, section 5.5.

Having obtained the phase shifts for such a potential, the following applies for any model. The relative variation of the electronic charge density may be expressed as a function of $\underline{r}$ from the solute, in terms of the phase shifts by

$$\frac{\Delta\rho(\underline{r})}{\rho(\underline{r})} = \Sigma\ (2\ell+1)\left(\{n^2_\ell(k_F r)-j^2_\ell(k_F r)\}\sin^2\gamma_\ell - j_\ell(k_F r)n_\ell(k_F r)\sin 2\gamma_\ell\right), \qquad 5.08.$$

where n_ℓ and j_ℓ are spherical Bessel and Neumann functions respectively. The change in K at a solvent nucleus situated at $\underline{r} = \underline{R}_j$ is then given by

$$\frac{\Delta K_j}{K} = \frac{\Delta\rho(R_j)}{\rho}$$

which represents a spectrum of resonance values. To obtain the average shift for all the solvent nuclei, an integration over all $\underline{R}$ must be made so that

$$\frac{\Delta K}{K} = c\int \Delta\rho(\underline{R})/\rho \; g(r).d^3\underline{r} \qquad 5.09$$

In fact the change in the solute P_F value may be found in a similar way but they have not been calculated here. There are three assumptions implicit in equation 5.09. These are (i) that the alloy is perfectly disordered (ii) that multiple scattering of the Fermi surface electrons may be neglected and (iii) that the excess electron densities at any point are additive, which is a valid assumption for low impurity concentrations. Combining equations 5.08 and 5.09 the expression for the fractional change in K is finally given by

$$\Gamma \equiv \frac{1}{K}\frac{d\bar{K}}{dc} = \Sigma_\ell\{\alpha_\ell \sin^2\gamma_\ell + \beta_\ell \sin^2\gamma_\ell\} \qquad 5.10$$

with α_ℓ and β_ℓ given by

$$\alpha_\ell = (2\ell + 1)\int\rho'(\underline{r})\{n^2{}_\ell(k_F r) - j^2{}_\ell(k_F r)\}d^3\underline{r} \qquad 5.11$$

and

$$\beta_\ell = -(2\ell + 1)\int_0^\infty \rho'(\underline{r}).n_\ell(k_F r)j_\ell(k_F r).d^3\underline{r}. \qquad 5.12$$

where $\rho'(r) = g(r).\ 4\pi r^2\rho_o$.

The coefficients α_ℓ and β_ℓ are independent of the model scattering potential; they describe the atomic distributions in the liquid metal.

5.3.3 Screened Free atom model potential This model potential is compatible with Ziman's[18] pseudo-atom concept of an atom in a metal; which is treated as an 'ion + screening charge'. Though the present treatment is a single centre scattering calculation, this representation contains an element of self-consistency not present in the previous model in that the screening part is built into the potential. Asik et al. first determined spin-dependent phase shifts for electrons scattered by such a potential. The calculation was simply modified to calculate spin-independent phase shifts, the effect of spin-orbit coupling being neglected. It has been shown that this is unimportant except when the Knight shift itself is small. The form of the model potential is shown schematically below. The self-consistent atomic potentials of Herman and Skillman are used together with a variable parameter A which essentially provides the screening shell at a distance $r = R_T$. At large r, a real potential would

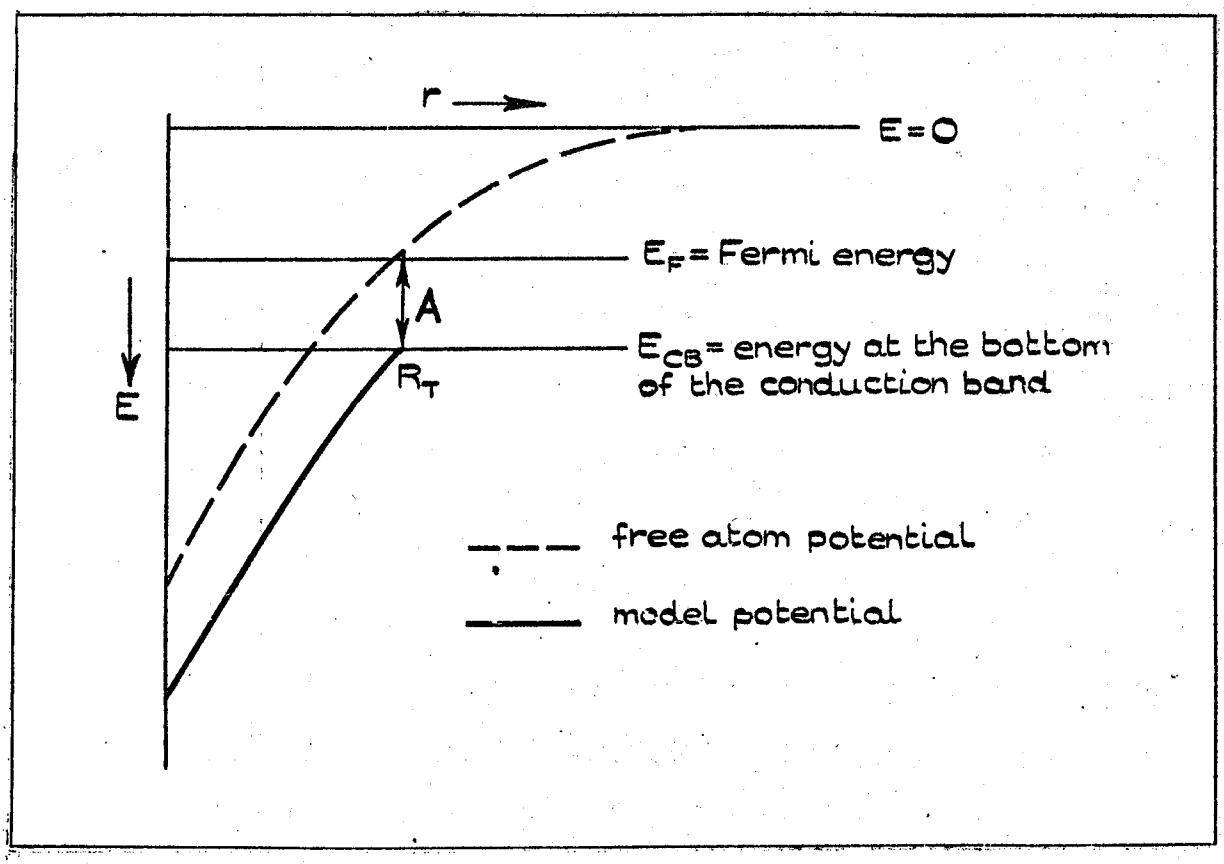

smoothly meet E_{CB}, whereas the free atom potential reduces to $1/r$ dependence. The model potential meets E_{CB} at R_T; at which point it is terminated. To determine the incident and scattered electron wave-functions, the Schrödinger equation must again be solved. However, because of the form of the potential this cannot be done analytically, except in the region where $r>R_T$. From r=o up to R_T, the Schrödinger radial equation is solved numerically using the Numerov method[19]. The radial equation for $r>R_T$ is

$$\frac{d^2P_\ell(r)}{dr^2} = h(r).P_\ell(r)$$

$$\text{where } h(r) = -\left\{E_F + W(r) - \frac{\ell(\ell+1)}{r^2}\right\}$$

W(r) is the model potential and $P_\ell(r)$ is the wave function. The Numerov method requires two starting values of $P_\ell(r)$. To a good approximation for small r, $P_\ell(r) = r^\ell$. The Schrödinger equation is then solved for $\ell = 0$, 1 and 2, the phase shifts for higher values being negligibly small. As before, matching the electron wave functions at the potential boundary yields the phase shifts. The parameter A is varied until the Friedel sum

rule is satisfied.

Tables 5.3 and 5.4 contain the phase shifts calculated from the screened free atom model potential, with and without dilatation. Table 5.5. lists the phase shifts obtained using the square well potential, where dilatation effects have been included. The slight discrepancy between the Z' values in tables 5.3 and 5.5 for the same system is because two different methods were used to calculate the atomic volumes.

Table 5.3

Asik, Ball and Slichter (ABS) phase shifts from the Screened free atom potential with dilatation effects

Solute in Solvent		Au In	Ag In	Cu In	Au Sn	Ag Sn	Cu Sn	In Cu	Sn Cu
Z'		-1.083	-1.130	-0.337	-1.653	-1.713	-0.703	0.756	1.651
ABS	γ_o	-.5783	-.5518	-.2138	-.7984	-.7270	-.3909	.2637	.5992
DIL	$\tilde{\gamma}_1$	-.0660	-.1121	.0573	-.1757	-.1830	-.0001	.3148	.6332
γ_ℓ	γ_2	-.1808	-.1737	-.0929	-.2569	-.2873	-.1419	-.0181	.0081
Actual Z'		-1.070	-1.118	-.322	-1.662	-1.727	-. 701	. 712	1.617
R_T(a.u.)		2.65	2.19	2.25	2.46	2.04	2.07	2.84	2.90

Table 5.4

Asik, Ball and Slichter (ABS) phase shifts from the screened free atom potential without dilatation effects

Solute in Solvent		Au In	Ag In	Cu In	Au Sn	Ag Sn	Cu Sn	In Cu	Sn Cu
Z'		-2	-2	-2	-3	-3	-3	2	3
ABS NO DIL γ_ℓ	γ_o	-1.2681	-.7167	-.4685	-1.4612	-.8488	-.5469	.6254	.8365
	γ_1	-.6470	-.1711	-.0408	-1.1090	-.2325	-.0642	.8305	1.1990
	γ_2	.0097	-.3792	-.5955	.0100	-.6401	-.6586	.0182	.0504
Actual Z'		- 2.012	-1.990	-2.272	-3.017	-3.022	-2.567	2.042	2.983
R_T(a.u.)		1.42	2.00	1.98	1.35	1.90	1.93	3.34	3.32

Table 5.5

Friedel square well phase shifts with dilatation effects

Solute in Solvent		Au In	Ag In	Cu In	Au Sn	Ag Sn	Cu Sn	In Cu	Sn Cu
Z'		-1.062	-1.090	-0.386	-1.618	-1.537	-0.759	0.835	1.726
γ_ℓ	γ_o	-.7781	-.7963	-.3273	-1.0391	-1.0193	-.5888	0.5669	0.9292
	γ_1	-.2310	-.2372	-.0781	-.3489	-.3426	-.1616	0.2117	0.5155
	γ_2	-.0354	-.0366	-.0083	-.0659	-.0641	-.0216	0.0204	0.0438

5.4 Calculation of the Blandin-Daniel coefficients, α_ℓ and β_ℓ.

5.4.1 Evaluation of I(K) and g(r). The remaining factors required for the evaluation of equation 5.10 are the coefficients α_ℓ and β_ℓ. As experimental I(K) or g(r) values were not available for all of the solvents, use was made of the hard-sphere structure factors of Ashcroft and Lekner[20].

The total structure factor is given by Ashcroft and Lekner as

$$I(K\sigma) = \{1-\rho_o c(K\sigma)\} \qquad 5.13$$

where ρ_o is the number density of ions, σ the hard sphere diameter and $c(K\sigma)$ the direct correlation function in momentum space. $c(K\sigma)$ is given by

$$c(K\sigma) = -4\pi\sigma^3 \int s^2 \frac{\sin sK\sigma}{sK\sigma} (\alpha + \beta s + \gamma s^2) ds, \qquad 5.14$$

where α, β and γ are functions of a packing density parameter η, defined as the fraction of the total fluid volume occupied by hard spheres. These quanities are defined as

$$\eta = (\pi/6)\rho_o\sigma^3, \quad \alpha = (1 + 2\eta)^2/(1-\eta)^4,$$

$$\beta = -6\eta(1 + \eta/2)^2/(1-\eta)^4, \quad \gamma = (1/2)\eta(1 + 2\eta)^2/(1 - \eta)^4.$$

The values of σ and η used in the present calculations were obtained from Ashcroft and Lekner. Integration of equation 5.14 is immediate and gives

$$c(K\sigma) = \left(\frac{-4\pi\sigma^3}{K\sigma}\right) \{\cos(K\sigma)\{\frac{(2\beta + 12\gamma)}{(K\sigma)^3} - \frac{(\alpha + \beta + \gamma)}{K\sigma} - \frac{24\gamma}{(K\sigma)^5}\}$$

$$+ \sin(K\sigma)\{\frac{(\alpha + 2\beta + 4\gamma)}{(K\sigma)^2} - \frac{24\gamma}{(K\sigma)^4}\} - \frac{2\beta}{(K\sigma)^3} + \frac{24\gamma}{(K\sigma)^5}\} \qquad 5.15$$

whence I(K) is given by equation 5.13 in terms of elementary functions. The radial distribution function is defined by

$$g(r) = 1 + \frac{1}{2\pi^2 \rho_o r} \int_0^\infty \{I(K) - 1\} \, K \sin Kr \, dK. \qquad 5.16$$

Equation 5.16 cannot be evaluated analytically and therefore a numerical integration procedure was adopted to evaluate g(r). Clearly the numerical integration must be truncated at some stage, though not too early because the information contained in I(K) at large K gives g(r) at small r. The effects of an early truncation are shown in figure 5.5, where 'structure' is introduced into the first peak of g(r) and 'ripples' occur before the first peak, at small r. A straight-forward Simpsons rule type of numerical integration of equation 5.16 with a fixed interval in K, cannot be simply carried out because at large r the term sin Kr oscillates rapidly with K. This problem was overcome in the following way. A change of variable was made such that

$$K = \frac{\pi x}{r} + \frac{(2n+1)\pi}{r}, \text{ thus } dK = dx.\frac{\pi}{r} \text{ and } \sin Kr = \sin(x+1)\pi$$

The integral then becomes

$$I = \sum_{n=0}^{N} \int_{x=-1}^{x=+1} \{I\{(x + 2n + 1)\pi/r\} - 1\} \frac{(x + 2n + 1)\pi}{r} \sin(x+1)\pi \, dx \, \left(\frac{\pi}{r}\right)$$

where the upper limit of K is determined by the value of N. For example when n = o, K is integrated between the following limits

$$x = -1, \quad K = \frac{-\pi}{r} + \frac{\pi}{r} = o,$$

$$x = +1, \quad K = \frac{\pi}{r} + \frac{\pi}{r} = \frac{2\pi}{r}.$$

For n = 1, K varies from $\frac{2\pi}{r} \rightarrow \frac{4\pi}{r}$; as n increases each time by unity, so K

increases by $\frac{2\pi}{r}$. However, as r increases, so $\frac{2\pi}{r}$ decreases, but the integration range remains at $\frac{2\pi}{r}$. Thus the integration is performed each time for a cycle of the oscillating function and the accuracy does not decrease on increasing r. The integration over $\frac{2\pi}{r}$, or x varying from -1→ +1, may be simply and accurately performed using a Gaussian integration technique, for which:

$$\int_{-1}^{+1} f(x)dx \simeq \sum_{i=1}^{n} \Omega_i f(x_i) \qquad 5.13$$

where the abscissae and the weighting factors, Ω_i, are given in Abramowitz and Stegun[21]. By using both a 16 and 32-point fit to evaluate the integral in equation 5.13, no discernible difference in the g(r) values was obtained. Subsequently a 32-point fit was used. However g(r) was considerably affected if the upper K limit, or N value, was too low; as seen in figure 5.5. A value of N = 30 was finally used, no improvement ensuing if a higher value was taken. As shown in figure 5.4 for N = 30, g(r) is a smoothly varying function of r, approaching 1 for r>≃15 x 10^{-8}cm. The data for N = 8, in figure 5.5, is for Na at 573K and for N = 30 is Sn at 573K. A listing of the Alg ol 60 computer program which calculated g(r) is given in appendix 11.

5.4.2 Evaluation of α_ℓ and β_ℓ. The g(r) values calculated as above are substituted into equations 5.11 and 5.12, and an integration out to large r gives α_ℓ and $-\beta_\ell$. Two requirements are necessary before acceptable values for the coefficients are obtained; the calculation being performed initially for Na in order that a comparison with Thornton and Youngs'[22] values can be made. The first is that in order to make the integral converge, an exponential damping factor exp(-δr) must multiply the integrand. The integral was repeated for several values of δ and the coefficients

obtained plotted as a function of δ; the plots were all approximately linear. Extrapolation of $\delta \to o$, gave the final values of the coefficients for $\ell = o, 1, 2$ and 3. The second requirement is that the integration must be taken out at least 100σ for each value of δ as earlier truncation caused the values to change. As may be seen in figure 5.4 $g(r) \simeq 1$ at $r = 15 \times 10^{-8}$cm and therefore, the integration was performed exactly up to $r = 20 \times 10^{-8}$cm, after which it was assumed that $g(r) \equiv 1$. The α_ℓ's and β_ℓ's for Na, In, Sn and Cu are tabulated below and for Na are compared with those obtained by Thornton and Young.

Table 5.6

Blandin-Daniel coefficients α_ℓ and β_ℓ

Solvent	α_o	α_1	α_2	α_3	β_o	β_1	β_2	β_3
In	-0.23	0.60	0.04	-3.21	-0.04	0.27	-0.87	0.56
Sn	-0.06	-0.02	0.80	1.79	-0.07	0.26	-0.33	-0.47
Cu	0.63	-1.38	-1.78	4.40	0.07	-0.70	1.58	3.74
Na	0.69	-1.59	-1.95	5.53	0.073	-0.81	1.93	4.04
Na*	0.68	-1.62	-1.86	5.63	0.04	-0.70	1.84	4.25

* Value from Thornton and Young[22].

Table 5.6 shows that the present values of α_ℓ and β_ℓ for Na compare favourably with those of Thornton and Young. The rough calculations of Flynn et al.[23] for Cu and Al are in reasonable agreement with the present values for Cu and In respectively.

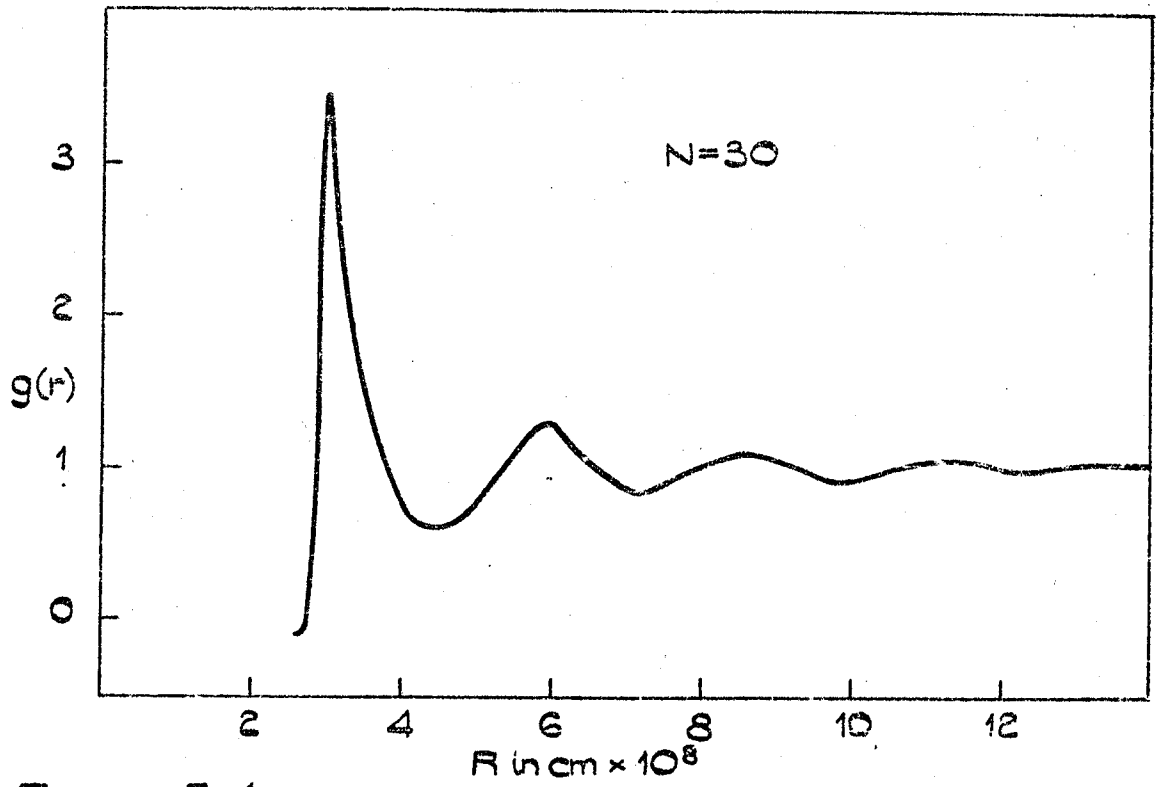

FIGURE 5.4.

RADIAL DISTRIBUTION FUNCTION FOR Sn AT 573K. USING A HARD SPHERE I(K).

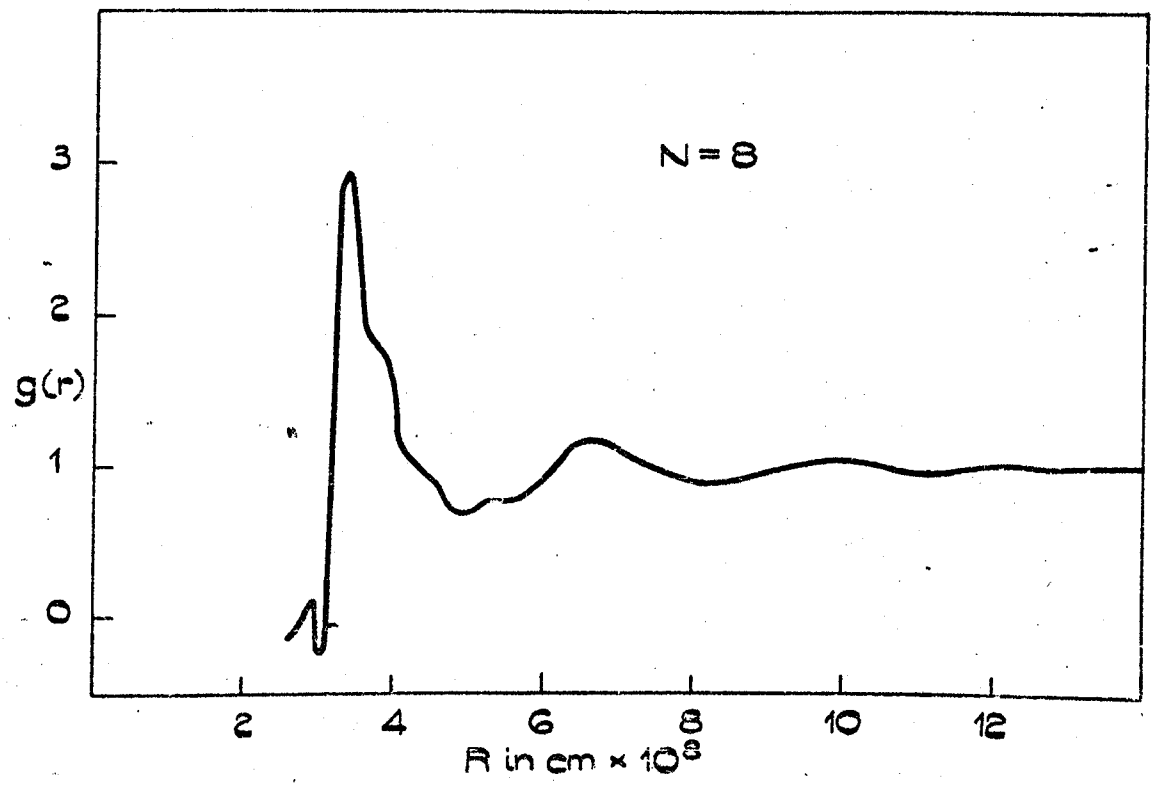

FIGURE 5.5.

RADIAL DISTRIBUTION FUNCTION FOR Na AT 573K, SHOWING EFFECT OF EARLY TRUNCATION OF I(K) INTEGRAL.

5.4.3 Results and Discussion Combining the phase shifts γ_ℓ and the coefficients α_ℓ and β_ℓ, the initial slopes of the Knight shift as a function of concentration may be calculated for In and Sn alloyed with the noble metals and for Cu alloyed with In and Sn. The results are tabulated below.

Table 5.7

Comparison of Γ_{expt} with values calculated using two model potentials

Solvent	Solute	Γ_{expt}	Γ (square well potential)	Γ (screened atom potential-with dilatation)	Γ (screened atom potential-without dilatation)
^{115}In	Au	.283	-.109	.239	-.248
	Ag	.222	-.112	.213	.466
	Cu	.114	-.026	.198	.780
^{119}Sn	Au	.281	-.092	.168	-.269
	Ag	.150	-.089	.197	-.109
	Cu	.133	-.016	.151	-.006
^{63}Cu	In	-.478	-.031	-.523	-1.109
	Sn	.137	-.372	-.859	-1.101

Considering first the results for ^{115}In and ^{119}Sn, table 5.7 above shows that the experimental values of Γ are in reasonable agreement with the theoretical

values obtained using phase shifts calculated from the screened free atom potential with dilatation effects included. In the noble metal-indium systems the variation in magnitude is reproduced, which is largest for Au-In and smallest for Cu-In. In view of the approximations made, exact agreement is not to be expected; in particular the effects of dilatation are considerable and the assumption that the solute ions retain their pure metal volumes when in solution is probably unsatisfactory. Also no account has been taken of the possible variation of χ_p. However values of $\frac{1}{\chi_p} \cdot \frac{d\chi_p}{dc}$ given in table 5.2 shows that in some cases the agreement of $\Gamma_{ABS-DIL}$ with Γ_{expt} is improved and sometimes worsened. Contrasting with this good agreement are the poor results obtained using the square well model potential which gives values of Γ of the wrong sign.

The results obtained for ^{63}Cu in Cu-In and Cu-Sn are less encouraging, though the screened atom potential phase shifts do lead to good agreement with Γ_{expt} in Cu-In, where dilatation effects are included. In fact Γ_{expt} for Cu-Sn is obtained by extrapolating the results from low to high Cu concentrations. It is possible that this extrapolation may not be valid. None of the calculated Γ values predict the correct sign for Cu-Sn. A frequent and valid criticism of the phase shift approach is that its application is not justified to systems in which k_F changes strongly on alloying, since this method assumes that k_F remains constant. Table 5.8 shows that the maximum change in k_F for In and Sn is approximately 3% when alloyed with 10% of noble metal. Hopefully this will not cause the phase shift approach to be grossly in error. Recently[13] it has been shown that the Cu Fermi surface electrons have 18% d-character in the liquid due to the close proximity of the filled 3-d band to the conduction band. This s-d hybridization has not been taken into account in any of the models used.

to calculate the Γ's. The following section discusses this effect in more detail.

Thornton and Young[22] have suggested an alternative method of accounting for the screening by taking the γ_ℓ's as a difference between the phase shifts which screen out the solute and solvent ions respectively. However it is not clear from their work how dilatation effects may be included. Table 5.7 clearly shows the importance of these effects by the marked difference from $\Gamma_{expt.}$ of the Γ values obtained from the screened atom potential which neglects dilatation.

These calculations plainly show that the screened free atom model potential of the scattering ion leads to a much better prediction of the experimental data than the square well potential. The reasonable agreement obtained from the screened free atom potential indicates that the principles of the calculation are correct, at least for ^{115}In and ^{119}Sn. A further test of this model would be to calculate the change in the solute P_F values and also to calculate both solvent and solute P_F's for existing Knight shift data with polyvalent solvents and solutes. It is envisaged that these calculations will be undertaken in the near future.

5.5 Pseudopotential theory calculation of the Knight shift in alloys

5.5.1 The Pseudowavefunction Approach It has been shown by Faber[3] that an alternative to the phase shift approach for calculating ΩP_F in an alloy lies in the use of pseudopotential theory. The wave function of a Fermi surface electron at the nucleus as a function of concentration is found in terms of a pseudowavefunction which is formed by a first order perturbation of an electron plane wave by the weak local

pseudopotentials of the solvent and solute ions. The true wavefunction is obtained by orthogonalising the pseudowavefunction to the ionic core states and then renormalising. ΩP_F is finally calculated by evaluating the square of the true wavefunction at the nucleus and averaging over ionic positions. Unlike the phase shift approach, the pseudopotential theory is applicable across the complete range of concentration.

Recently Perdew and Wilkins[4] (henceforth PW) have extended the Faber theory by removing the assumption that the conduction electron plane wave is constant over the ion core so that the calculation is exact to 1st order. The calculations of PW were limited to the alkali-alkali alloys due to the non-availability of suitable analytic core wavefunctions for other metals.

This section contains an extension of the PW theory to polyvalent systems, in particular the liquid noble metal-tin and noble metal-indium systems. The PW theory is first set out in detail as this clarifies the work which follows and because it is not available elsewhere. However emphasis is given to the evaluation and computation of the PW expressions, which follow the theory.

5.5.2 The Theory of Perdew and Wilkins. The following notation contains a mixture of conventional and Dirac representation of wavefunctions. This is used, in the present context, because it combines clarity with conciseness.

In the pseudopotential formalism, a conduction electron wavefunction is written

$$\psi(\underline{r}) = C\{\phi(\underline{r}) - \sum_{i,\alpha} \langle\alpha|\phi\rangle \phi_\alpha(\underline{r}-\underline{R}_i)\}, \qquad 5.14$$

where $\phi(\underline{r})$ is the pseudowavefunction, ψ_α a core function and the sum is to be taken over all core states and all ions. The constant C normalises $\phi(\underline{r})$ in the volume of the specimen V and is simply determined by taking

$$\langle\psi|\psi\rangle = 1 = C^2 \{\phi^*(\underline{r})\phi(\underline{r}) - \sum_{\alpha,i}|\langle\alpha|\phi\rangle|^2 - \sum_{\alpha',j}|\langle\alpha'|\phi\rangle|^2\}.$$

The sums over i and j may be replaced by $\frac{c_A}{\Omega_{AB}}$ and $\frac{c_B}{\Omega_{AB}}$ respectively, where c_A and c_B are the concentrations of i and j type ions and Ω_{AB} is the ionic volume. The expression for C then becomes

$$C^{-2} = \{\phi^*(\underline{r})\phi(\underline{r}) - \frac{c_A}{\Omega_{AB}}\sum_{\alpha}|\langle\alpha|\phi\rangle|^2 - \frac{c_B}{\Omega_{AB}}\sum_{\alpha'}|\langle\alpha'|\phi\rangle|^2\}.$$

Taking the square modulus of $\psi(\underline{r})$ we obtain

$$|\psi(\underline{r})|^2 = C^2\{\phi^*(\underline{r})\phi(\underline{r}) - 2Re\sum_{i,\alpha}\langle\alpha|\phi\rangle\phi^*(\underline{r})\psi_\alpha(\underline{r}-\underline{R}_i) +$$

$$\sum_{i,j}\sum_{\alpha,\alpha'}\langle\alpha|\phi\rangle\langle\alpha|\phi\rangle^*\psi_\alpha(\underline{r}-\underline{R}_i)\psi_{\alpha'}(\underline{r}-\underline{R}_j)\}.$$

To zero order in the pseudopotential the pseudowavefunction may be written as a plane wave, $\phi(\underline{r}) = e^{i\underline{k}.\underline{r}}$; evaluating the wavefunction at a particular site $\underline{R}_s$ then gives

$$|\psi(\underline{R}_s)|^2 = C^2\{1 - 2Re\sum_{i,\alpha}\langle\alpha|k\rangle e^{-i\underline{k}.\underline{R}_s}\psi_\alpha(\underline{R}_s-\underline{R}_i)$$

$$+ \sum_{i,j}\sum_{\alpha,\alpha'}\langle\alpha|k\rangle\langle\alpha'|k\rangle\psi_\alpha(\underline{R}_s-\underline{R}_i)\psi^*_{\alpha'}(\underline{R}_s-\underline{R}_j)\}. \qquad 5.15$$

The overlap integral $\langle\alpha|k\rangle = \int\psi_\alpha^*(\underline{r}-\underline{R}_i)e^{i\underline{k}.\underline{r}}d\underline{r}$

$= e^{i\underline{k}.\underline{R}_i}\int\psi_\alpha^*(\underline{r}-\underline{R}_i)e^{i\underline{k}.(\underline{r}-\underline{R}_i)}d(\underline{r}-\underline{R}_i) = e^{i\underline{k}.\underline{R}_i}\langle\alpha^A|k\rangle$ and is the same for all ions in pure metal.

When these integrals are substituted into equation 5.15 the summations give non-zero terms only for i = j = s and the exponentials cancel with their complex conjugates. Equation 5.15 thus reduces to

$$|\psi(\underline{R}_s)|^2 = C^2\{1 - 2\mathrm{Re}\sum_{\alpha}\langle\alpha^A|k\rangle\psi_\alpha(0) + \sum_{\alpha,\alpha'}\langle\alpha^A|k\rangle\langle\alpha'^A|k\rangle\psi_\alpha(0)\psi_{\alpha'}^*(0)\}\ . \qquad 5.16$$

Since α^A only enters for s-states $\langle\alpha^A|\ k\rangle$ and $\psi_\alpha\ (0)$ are both real. Thus finally

$$|\psi(\underline{R}_s)|^2 = C^2\{1 - \sum_{\alpha}\langle\alpha^A|k\rangle\psi_\alpha(0)\ \}^2 \equiv C^2\ \gamma_A^{\ 2}(k). \qquad 5.17$$

Extending the theory to 1st order in the pseudopotential the pseudowave-funtion may be written

$$\phi_k(\underline{r}) = e^{i\underline{k}\cdot\underline{r}} + \sum_{k'}\frac{\langle k'|U|k\rangle}{E_{\underline{k}} - E_{\underline{k}'}}\ e^{i\underline{k}'\cdot\underline{r}}, \qquad 5.18$$

$\phi_k(\underline{r})$ being normalised to unit volume. Replacing the summation over k' by an integration and introducing $\underline{q} = \underline{k}' - \underline{k}$, equation 5.18 becomes

$$\phi_k(\underline{r}) = e^{i\underline{k}\cdot\underline{r}} + \frac{1}{(2\pi)^3}\int d\underline{q}\frac{\langle k+q|U|k\rangle}{E_{\underline{k}} - E_{\underline{k}+\underline{q}}}e^{i(\underline{k}+\underline{q})\cdot\underline{r}} = e^{i\underline{k}\cdot\underline{r}} + \int d\underline{q}.f(\underline{q})e^{i(\underline{k}+\underline{q})\cdot\underline{r}} \qquad 5.19$$

where $f(\underline{q}) = \dfrac{\langle k + q|U|k\rangle}{E_{\underline{k}} - E_{\underline{k}+\underline{q}}}$ and k may be taken as the Fermi wave vector since only Fermi surface electrons are involved in the Knight shift. Substituting 5.19 into 5.14 we have

$$\psi(\underline{r}) = C\{e^{i\underline{k}\cdot\underline{r}} + \int d\underline{q}f(\underline{q})e^{i(\underline{k}+\underline{q})\cdot\underline{r}} - \sum_{i,\alpha}\langle\alpha|k\rangle\psi_\alpha(\underline{r} - \underline{R}_i)$$

$$- \sum_{i,\alpha}\langle\alpha|\int f(\underline{q})e^{i(\underline{k}+\underline{q})\cdot\underline{r}}d\underline{q}\rangle\psi_\alpha(\underline{r} - \underline{R}_i)\}. \qquad 5.20$$

For an A-type atom at $\underline{R}_s$ and taking the square modulus of equation 5.20

$$|\psi_A(\underline{R}_s)|^2 = C^2|\{e^{i\underline{k}.\underline{R}_s} - \sum_\alpha e^{i\underline{k}.\underline{R}_s}\langle\alpha^A|\underline{k}\rangle\psi_\alpha(0) + \int d\underline{q} f(\underline{q}) e^{i(\underline{k}+\underline{q}).\underline{R}_s}$$

$$- \sum_{i,\alpha} \langle\alpha|\int f(\underline{q}) e^{i(\underline{k}+\underline{q}).\underline{r}} d\underline{q}\rangle\psi_\alpha(\underline{R}_s - \underline{R}_i)\}|^2$$

$$= C^2|\{e^{i\underline{k}.\underline{R}_s} - \sum_\alpha e^{i\underline{k}.\underline{R}_s}\langle\alpha^A|\underline{k}\rangle\psi_\alpha(0) + \int d\underline{q}\{f(\underline{q}) e^{i(\underline{k}+\underline{q}).\underline{R}_s}$$

$$- \sum_{i,\alpha} \langle\alpha|f(\underline{q}) e^{i(\underline{k}+\underline{q}).\underline{r}}\rangle\psi_\alpha(\underline{R}_s - \underline{R}_i)\}\}|^2.$$

As before, we may write

$$\langle\alpha|f(\underline{q}) e^{i(\underline{k}+\underline{q}).\underline{r}}\rangle = f(\underline{q}) e^{i(\underline{k}+\underline{q}).\underline{R}_i}\langle\alpha^A|\underline{k}+\underline{q}\rangle \quad \text{and therefore}$$

$$|\psi_A(\underline{R}_s)|^2 = C^2|\{ e^{i\underline{k}.\underline{R}_s} - \sum_\alpha e^{i\underline{k}.\underline{R}_s}\langle\alpha^A|k\rangle\psi_\alpha(0) +$$

$$\int d\underline{q}\, f(\underline{q}) e^{i(\underline{k}+\underline{q}).\underline{R}_s} \{1 - \sum_\alpha \langle\alpha^A|\underline{k}+\underline{q}\rangle\psi_\alpha(0)\}\}|^2$$

$$= C^2|\{e^{i\underline{k}.\underline{R}_s}\gamma_A(k) + \int f(\underline{q}) d\underline{q} e^{i(\underline{k}+\underline{q}).\underline{R}_s}\gamma_A(\underline{k}+\underline{q})\}|^2. \qquad 5.21$$

Expanding the square modulus and neglecting 2nd order terms containing expressions in $\{f(q)\}^2$, we then obtain

$$|\psi_A(\underline{R}_s)|^2 = C^2\{\gamma^2_A(k) + 2\gamma_A(k)\ \mathrm{Re}\int f(\underline{q}) e^{i\underline{q}.\underline{R}_s}\gamma_A(\underline{k}+\underline{q})\ d\underline{q}\}$$

$$\text{now } \int f(\underline{q}) e^{i\underline{q}.\underline{R}_s}\gamma_A(\underline{k}+\underline{q})\ d\underline{q} = \frac{1}{(2\pi)^3} \int d\underline{q} e^{i\underline{q}.\underline{R}_s} \frac{\langle\underline{k}+\underline{q}|U|\underline{k}\rangle\gamma_A(\underline{k}+\underline{q})}{E_{\underline{k}} - E_{\underline{k}+\underline{q}}},$$

however $U(\underline{r})$ may be taken as the sum of the individual ionic potentials, $U(\underline{r}) = \sum_i u_i(\underline{r} - \underline{R}_i)$ and hence $\langle\underline{k}+\underline{q}|U|\underline{k}\rangle = \int d\underline{r} e^{-i(\underline{k}+\underline{q}).\underline{r}} \sum_i u_i(\underline{r} - \underline{R}_i) e^{i\underline{k}.\underline{r}}$,

$$= \sum_i e^{-i\underline{q}.\underline{R}_i} \int d(\underline{r} - \underline{R}i) u_i(\underline{r} - \underline{R}_i) e^{-i\underline{q}.(\underline{r} - \underline{R}_i)},$$

$$= \sum_i e^{i\underline{q}.\underline{R}_i} u_i(q).$$

Thus $\int f(\underline{q}) e^{i\underline{q}.\underline{R}_s} \gamma_A(\underline{k}+\underline{q})d\underline{q} = \frac{1}{(2\pi)^3} \int e^{\underline{eq}.\underline{R}_s} \sum_i \frac{i\underline{q}.\underline{R}_i}{E_{\underline{k}} - E_{\underline{k}+\underline{q}}} u_i(q)\gamma_A(\underline{k}+\underline{q})\, d\underline{q}.$

It is necessary now to take the time average of $|\psi_A(\underline{R}_s)|^2$ over the ionic positions, which may be written

$$\langle|\psi_A(\underline{R}_s)|^2\rangle = \frac{1}{N_A} \overline{\sum_S^A |\psi_A(\underline{R}_s)|^2},$$

where N_A is the number of A-type ions and the summation is taken over the A ions at the R_s sites.

Hence $\langle|\psi_A(\underline{R}_s)|^2\rangle = C^2|\gamma_A(k)|^2 +$

$$\frac{C^2}{N_A} 2\gamma_A(k) \overline{\sum_S^A \frac{1}{(2\pi)^3} \mathrm{Re}\int d\underline{q} e^{i\underline{q}.\underline{R}_s} \sum_i \frac{e^{-i\underline{q}.\underline{R}_i} u_i(q)\gamma_A(\underline{k}+\underline{q})}{E_{\underline{k}} - E_{\underline{k}+\underline{q}}}}$$

$$= C^2|\gamma_A(k)|^2 + \frac{2C^2\gamma_A(k)}{(2\pi)^3} \int \frac{1}{N_A} \overline{\sum_S^A \sum_i e^{i\underline{q}(\underline{R}_s - \underline{R}_i)} \frac{u_i(q)\gamma_A(\underline{k}+\underline{q})}{E_{\underline{k}} - E_{\underline{k}+\underline{q}}}}\, d\underline{q}.$$

Now $\frac{1}{N_A} \overline{\sum_S^A \sum_i e^{i\underline{q}.(\underline{R}_s - \underline{R}_i)} u_i(q)} = \frac{1}{N_A}\{ N_A u_A + \sum_S^A \sum_i d^{i\underline{q}.(\underline{R}_s - \underline{R}_i)} u_A$

$$+ \sum_S^A \sum_i e^{i\underline{q}.(\underline{R}_s - \underline{R}_i)} u_B \} = u_A + \frac{Nc_A c_A}{N_A}\{I(q) - 1\}u_A + \frac{Nc_A c_B}{N_A}\{I(q) - 1\} u_B$$

$$= u_A + c_A\{I(q) - 1\} u_A + c_B\{I(q) - 1\} u_B,$$

where it has been assumed that the partial structure factors $I_{ii}(q) = I_{ij}(q) = I_{jj}(q) = I(q)$ are normalised such that all partial $g(r) \to 1$ as $r \to \infty$, and q is used instead of K to avoid confusion with k. Finally we obtain

$$\langle|\psi_A(\underline{R}_s)|^2\rangle_F = C^2|\gamma_A(k)|^2\{1 + \frac{2}{(2\pi)^3\gamma_A(k)}\int\frac{u_A(q)\gamma_A(\underline{k}+\underline{q})\,d\underline{q}}{E_{\underline{k}} + E_{\underline{k}+\underline{q}}}$$

$$+ \int\frac{\gamma_A(\underline{k}+\underline{q})}{E_{\underline{k}} + E_{\underline{k}+\underline{q}}}\{I(q) - 1\}\{c_A u_A(q) + c_B u_B(q)\}\,d\underline{q}\}\,. \qquad 5.22$$

Using equation 5.17, 5.22 may be written

$$\langle|\psi_A(\underline{R}_s)|^2\rangle_F = \frac{|\psi_A^{1 - OPW}(\underline{R}_s)|^2\{1 + \Sigma_A(k) + \Delta_{AB}(k,c_B)\}}{1 + \delta\frac{(C^2)}{C^2}} = \Omega P_F, \qquad 5.23$$

$$\text{where } \Sigma_A(k) = \frac{2}{(2\pi)^3\gamma_A(k)}\int\frac{u_A(q)\ \gamma_A(\underline{k}+\underline{q})\ d\underline{q}}{E_{\underline{k}} + E_{\underline{k}+\underline{q}}}\,, \qquad 5.24$$

$$\text{and } \Delta_{AB}(k,c_B) = \frac{2}{(2\pi)^3\gamma_A(k)}\int\frac{\gamma_A(\underline{k}+\underline{q})\{I(q) - 1\}\{c_A u_A(q) + c_B u_B(q)\}\,dq}{E_{\underline{k}} + E_{\underline{k}+\underline{q}}}. \qquad 5.25$$

The factor appearing in the denominator on the r.h.s. of equation 5.23 is a small, first order renormalisation correction which will be ignored as PW have shown it to be small. The first term on the r.h.s. of equation 5.23 is the contact density for a single orthogonalised plane wave (OPW). The self-term, $\Sigma_A(k)$ has been neglected in former alloy Knight shift calculations. It measures the effect or influence of the ion pseudopotential at $\underline{R}_A$ on its own Knight shift. The distinct term, $\Delta_{AB}(k,c_B)$ is a general expression of the Faber theory and if $\gamma_A(\underline{k})$ is substituted for $\gamma_A(\underline{k}+\underline{q})$, his formula results. $\Delta_{AB}(k,c_B)$ is a measure of the influence of the ions other than at R_A in the alloy. The following section contains a complete breakdown and full statement of all the terms in equation 5.23.

5.5.3 Details of the Calculation PW evaluated the terms in equation 5.23 for the alkali-alkali alloys, performing the angular and

radial integrations explicitly using analytic core wave functions. These however are not available for any of the elements of concern here, except Cu. As a first approximation the calculation was performed using simple Slater[6] analytic core functions. However the value of $|\Psi_A^{1\text{-OPW}}(\underline{R}_s)|^2$ for Na using these functions bore no resemblance to the value obtained by PW. The present calculations have therefore been performed using the numerical core functions tabulated for all elements by Herman and Skillman. Use of these numerical core functions requires a different method of calculation from that used by PW in that all integrations over core functions must be performed numerically. In fact the total core function is written as a product of a radial part and angular part. As will now be shown, the angular integrals are performed explicitly, leaving a numercial integration over the radial part.

Overlap Integrals The full core function may be written $\Psi_\alpha = R_{n\ell}(r) \cdot Y_{\ell m}(\theta,\phi)$, where $R_{n\ell}(r) = P_{n\ell}(r)/r$ and the $Y_{\ell m}$'s are normalised spherical harmonics. Herman and Skillman tabulate the radial part $P_{n\ell}(r)$. In performing the integrations it is convenient to express the plane wave in terms of spherical harmonics, that is

$$e^{i\underline{k}\cdot\underline{r}} = 4\pi \sum_{\ell,m} i^\ell j_\ell(kr)\, Y^*_{\ell m}(\hat{k})\, Y_{\ell m}(\hat{r}),$$

thus $\langle\alpha|k\rangle = \int R^*_{n\ell}(r)\, Y_{\ell m}(\theta,\phi)\, 4\pi \sum_{\ell',m'} i^{\ell'} j_{\ell'}(kr) Y_{\ell'm'}(\hat{k}) Y_{\ell'm'}(\hat{r})\, d^3\underline{r}$

$$= 4\pi i^{\ell'} Y^*_{\ell'm'}(\hat{k}) \int R^*_{n\ell}(r) Y^*_{\ell m}(\theta,\phi) \sum_{\ell',m'} j_{\ell'}(kr) Y_{\ell'm'}(\theta,\phi)\, d^3\underline{r}\,.$$

The above integral may be split into angular and radial parts, the angular part only giving non-zero terms for $\ell' = \ell$ and $m' = m$. Since the $Y_{\ell m}$'s are normalised, the angular part becomes

$$\int_{\theta=0}^{\pi} \int_{\phi=0}^{2\pi} Y^*_{\ell m}\, Y_{\ell m} \sin\theta\, d\theta d\phi = \frac{1}{4\pi} \cdot 4\pi = 1.$$

Thus $\langle\alpha|k\rangle = 4\pi i^{\ell} Y^{*}_{\ell m}(\hat{k}) \int_0^{\infty} R^{*}_{n\ell}(r) j_{\ell}(kr) r^2 dr,$

i.e. $\langle\alpha|k\rangle = i^{\ell} Y^{*}_{\ell m}(\hat{k})\, B_{n\ell}(k)$,

where $B_{n\ell}(k) = \int_0^{\infty} R_{n\ell}(r)\, 4\pi r^2 j_{\ell}(kr)\, dr = \int_0^{\infty} P_{n\ell}(r) 4\pi r j_{\ell}(kr)\, dr.$ 5.26

Orthogonalisation Factors

$$\text{Now } \gamma_A(k) = 1 - \sum_{\alpha} \langle\alpha^{A}|k\rangle \psi_{\alpha}(0),$$

using the overlap integral result just derived gives

$$\gamma_A(k) = 1 - \sum_{n} R_{n\ell}(0)\, Y_{\ell m}(\theta,\phi)\, i^{\ell} Y^{*}_{\ell m}(\hat{k}) B_{n\ell}(k).$$

Now since only s-states contribute $\ell = m = 0$ and we have

$$\gamma_A(k) = 1 - \sum_{n} R_{no}(0) Y_{oo}(\theta,\phi)\, i^{o} Y^{*}_{oo}(\hat{k}) B_{no}(k)$$

i.e. $$\gamma_A(k) = 1 - \frac{1}{4\pi} \sum_{n} R_{no}(0) B_{no}(k).$$

First order corrections The $\Sigma_A(k)$ and $\Delta_{AB}(k,c_B)$ terms may be expressed as the product of an angular and radial integral. The angular integral, which appears in the same form in the self and distinct terms, is written

$$\Gamma(k,q) = \frac{1}{\gamma_A(k)} \frac{1}{2\pi} \frac{\hbar^2 q^2}{2m} P\int d\hat{q}\, \frac{\gamma_A(\underline{k}+\underline{q})}{E_{\underline{k}} + E_{\underline{k}} + \underline{q}},$$

where $d\hat{q}$ signifies an angular integral. Changing the variable so that $y = -\hat{k}.\hat{q} = -\cos\theta$, the above integral, which has a pole at $y = q/2k$, may be evaluated in a straightforward way to give

$$\Gamma(k,q) = \frac{1}{\gamma_A(k)} \{ \frac{q}{2k} \ln\left|\frac{1-q/2k}{1+q/2k}\right| - \frac{1}{4\pi n} \sum^{A} R^{A}_{no}(0) C^{A}_{o}(n,k,q) \},$$

where the sum is taken over the A-type ions and $C_o(n,k,q)$ is given by

$$C_o(n,k,q) = P\int_{-1}^{+1} dy \; \frac{B_{no}\{(k^2 + q^2 - 2Kqy)^{\frac{1}{2}}\}}{\frac{2k}{q}\, y - 1}.$$

If $u_A(q)$ and $u_B(q)$ are expressed in units of $\frac{2}{3} E_F$, then the self and distinct terms may be simply expressed by

$$\Sigma_A(k) = \frac{2}{\Omega'_{AB}} \int_0^\infty u_A(x)\; \Gamma(k,q)\; dx$$

and $$\Delta_{AB}(k,c_B) = \frac{2}{\Omega'_{AB}} \int_o^\infty \{c_A u_A(x) + c_B u_B(x)\}\; \{I(q) - 1\}\; \Gamma(k,q)\; dx,$$

where $x = q/2k$ and Ω'_{AB} is the average volume per electron in the alloy.

Normalisation factors The single OPW normalisation factor involves only

$$\frac{1}{\Omega_{AB}} \sum_\alpha |\langle\alpha|k\rangle|^2 = \frac{1}{\Omega_{AB}} \sum_{n,\ell,m} |i^\ell Y^*_{\ell m}(\hat{k}) B_{n\ell}(k)|^2 = \frac{1}{\Omega_{AB}} \sum_{n,\ell,} \frac{(2\ell+1)}{4\pi} B^2_{n\ell}(k).$$

The full normalisation term is then given by

$$C^{-2} = 1 - \frac{c_A}{\Omega_{AB}} \sum_{n,\ell} \frac{(2\ell+1)}{4\pi} B_{n\ell}{}^2(k) - \frac{c_B}{\Omega_{AB}} \sum_{n,\ell} \frac{(2\ell+1)}{4\pi} B_{n\ell}{}^2(k),$$

where Ω_{AB} is the average volume per ion in the alloy.

The following section describes the actual input parameters used to calculate ΩP_F.

5.5.4 Description of the input parameters Free electron values of the Fermi wave vector k_F are used throughout and are calculated using current liquid metal density values given at the melting point. For the alloys it is assumed that k_F and the density are linear between the pure metal values. The volumes Ω'_{AB} and Ω_{AB} are calculated from the alloy k_F and density values.

Structure factor Due to the non-availability of experimental I(q) data for these alloys, the hard-sphere model structure factors of Ashcroft and Lekner[2] were used, as fully described in section 5.4. However, in the present calculations on alloys, the packing density η was taken as 0.45 at all concentrations and an average hard sphere diameter used, given by

$$\bar{\sigma} = \frac{(18\pi\eta z)^{\frac{1}{3}}}{k_F},$$

where the valency Z and k_F are the current alloy values.

Pseudopotential The local electron-ion pseudopotential of Ashcroft[24] was used and is defined by

$$V(x) = \frac{-\lambda^2 \cos sx}{x^2 + \lambda^2 f(x)}, \qquad 5.27$$

where $x = q/2k_F, \lambda^2 = \frac{1}{\pi a_o k_F}$, $s = 2k_F R_{core}$ and the Lindhard function $f(x) = \frac{1}{2} + \frac{1 - x^2}{4x} \ln\left|\frac{1 + x}{1 - x}\right|$. The quantity s determines the location of the first node of the potential and values of R_{core} are listed for a number of elements by Ashcroft. V(x) is measured in units of $\frac{2}{3} E_F$.

Wave functions As previously mentioned numerical core wave functions of Herman and Skillman were used. The values of the s-state function at r = o, $R_{ns}(o)$, were obtained by extrapolating the Herman and Skillman values to r = o. The calculation was done in atomic units and tabulated

below is the input data for the elements Sn, In, Au, Ag and Cu in these units.

TABLE 5.8

Input parameters used in the first-order pseudopotential calculation of ΩP_F.

element	K_F	ionic volume Ω	R_{core}	$R_{1s}(o)$	$R_{2s}(o)$	$R_{3s}(o)$	$R_{4s}(o)$	$R_{5s}(o)$
Sn	0.837	202	1.297	696	227	98	45	-
In	0.772	193	1.323	679	219	97	43	-
Au	0.605	134	0.813	1380	465	220	110	49
Ag	0.600	137	1.040	639	207	91	41	-
Cu	0.701	86	0.813	304	94	36	-	-

5.5.5 Results and Discussion A full explanation and listing of the computer programme is given in appendices IV, V and VI. The programme was tested by running the calculation for Na as the A-element in pure Na and a NaRb alloy and comparing the results with those obtained by PW. Table 5.9 which follows compares the present and PW values.

Table 5.9

Comparison of PW and present calculations, for Na as the A-element.

	Na		0.6Na-0.4Rb	
	Present results	PW results	Present results	PW results
$\lvert\Psi_A^{1\text{-OPW}}(\underline{R}_s)\rvert^2$	165	151	186	175
$1 + \Sigma_A(k)$	1.04	0.99	1.35	1.32
$\Delta_{AB}(k, c_B)$	-0.31	-0.29	-0.34	-0.34
ΩP_F	121	102	188	162

In view of the different core functions used the close agreement between the present results and those of PW is very satisfactory and the results are presented for the noble metal-tin and noble metal-indium systems with some confidence. ΩP_F and other parameters are given for ^{115}In, ^{119}Sn and ^{63}Cu in these systems in tables 5.10, 5.11 and 5.12 respectively.

Table 5.10

Computed pseudopotential Knight shift parameters for ^{115}In in the noble metal--indium systems

System	C_B, at.% of noble metal	$\frac{\gamma_A^2(k)}{N_k(C_B)}$	$1 + \Sigma_A(k)$	$\Delta_{AB}(k,C_B)$	$1 + \Sigma + \Delta$	ΩP_F
In - Cu	0	508.5	0.831	0.035	0.866	440.5
	10	517.9	0.841	0.018	0.859	444.9
	20	527.4	0.848	0.005	0.854	450.2
	30	537.3	0.857	-0.007	0.850	456.7
	40	547.6	0.863	-0.011	0.852	466.4
	50	558.5	0.871	-0.011	0.871	480.6
	60	570.2	0.875	0.001	0.876	499.6
	70	583.1	0.877	0.017	0.894	521.3
	80	597.8	0.881	0.016	0.897	536.2
	90	614.9	0.882	-0.019	0.864	531.0
In - Ag	0	508.5	0.831	0.035	0.866	440.5
	10	535.1	0.858	0.013	0.871	465.9
	20	559.7	0.877	0.003	0.880	492.6
	30	582.8	0.848	0.041	0.889	518.2
	40	605.0	0.930	-0.020	0.910	550.4
	50	626.4	0.965	-0.035	0.930	582.8
	60	647.5	0.992	-0.036	0.956	619.1
	70	668.4	1.022	-0.042	0.980	655.0
	80	689.6	1.044	-0.059	0.985	679.3
	90	711.3	1.061	-0.104	0.957	680.6
In - Au	0	508.5	0.831	0.035	0.866	440.5
	10	537.5	0.857	0.013	0.870	467.8
	20	565.3	0.875	0.005	0.880	497.5
	30	592.4	0.874	0.021	0.895	530.3
	40	619.3	0.921	-0.001	0.920	569.9
	50	646.3	0.958	-0.002	0.956	617.9
	60	673.9	0.984	0.017	1.001	674.4
	70	702.6	1.012	0.030	1.042	732.4
	80	732.8	1.037	0.018	1.055	772.9
	90	765.3	1.052	-0.042	1.010	772.8

Table 5.11

Computed pseudopotential Knight shift parameters for ^{119}Sn in the noble metal-tin systems

System	C_B at.% of noble metal	$\frac{\gamma^2_A(k)}{N_k(C_B)}$	$1 + \Sigma_A(k)$	$\Delta_{AB}(k,C_B)$	$1 + \Sigma + \Delta$	ΩP_F
Sn - Cu	0	492.1	0.781	0.061	0.842	414.5
	10	509.1	0.784	0.055	0.839	427.3
	20	525.6	0.766	0.072	0.838	440.4
	30	541.9	0.804	0.029	0.833	451.3
	40	558.1	0.819	0.013	0.832	464.3
	50	574.6	0.835	0.002	0.837	481.0
	60	591.8	0.847	0.002	0.849	502.7
	70	610.3	0.862	0.010	0.872	532.1
	80	630.8	0.869	0.025	0.895	564.3
	90	654.4	0.874	-0.006	0.869	568.4
Sn - Ag	0	492.1	0.781	0.061	0.842	414.5
	10	530.2	0.788	0.061	0.848	449.7
	20	563.6	0.833	0.027	0.860	484.9
	30	593.7	0.864	0.012	0.876	520.2
	40	621.6	0.871	0.020	0.891	554.0
	50	648.1	0.928	-0.008	0.919	595.9
	60	673.7	0.970	-0.021	0.949	639.3
	70	698.9	1.006	-0.023	0.983	687.0
	80	724.3	1.040	-0.030	1.010	731.4
	90	750.4	1.064	-0.081	0.983	738.0
Sn - Au	0	492.1	0.781	0.061	0.842	414.5
	10	532.3	0.784	0.061	0.845	450.0
	20	568.7	0.831	0.023	0.854	485.8
	30	602.9	0.862	0.007	0.869	523.9
	40	635.7	0.877	0.011	0.888	564.3
	50	667.9	0.918	0.001	0.919	614.1
	60	700.5	0.962	0.003	0.965	676.3
	70	734.0	0.997	0.028	1.025	752.3
	80	769.3	1.031	0.048	1.079	830.1
	90	807.2	1.054	-0.004	1.050	847.5

Table 5.12

Computed pseudopotential Knight shift parameters for ^{63}Cu in the copper-tin and copper-indium systems

System	C_B, at.% of noble metal	$\frac{\gamma^2_A(k)}{N_k(C_B)}$	$1 + \Sigma_A(k)$	$\Delta_{AB}(k, C_B)$	$1 + \Sigma + \Delta$	ΩP_F
Cu - Sn	0	467.1	1.480	-0.140	1.340	625.9
	10	448.8	1.497	-0.045	1.453	652.0
	20	433.9	1.484	-0.006	1.478	641.3
	30	421.2	1.465	-0.017	1.449	610.2
	40	409.9	1.438	-0.022	1.416	580.5
	50	399.5	1.409	-0.020	1.389	555.0
	60	389.7	1.376	-0.009	1.367	532.6
	70	380.1	1.337	0.008	1.344	511.0
	80	370.7	1.257	0.044	1.301	482.1
	90	361.2	1.276	0.035	1.311	473.5
Cu - In	0	467.1	1.480	-0.140	1.340	625.9
	10	453.0	1.503	-0.083	1.420	643.2
	20	441.6	1.496	-0.039	1.456	643.2
	30	432.0	1.486	-0.032	1.454	628.3
	40	423.7	1.475	-0.041	1.434	607.5
	50	416.3	1.465	-0.049	1.416	589.2
	60	409.5	1.448	-0.047	1.401	573.6
	70	403.2	1.432	-0.041	1.392	561.1
	80	397.2	1.412	-0.027	1.385	550.1
	90	391.5	1.393	-0.013	1.380	540.3

Before discussing the alloy results it is instructive at this stage to point out the discrepancy in the pure metal values of $\gamma^2_A(k)/C^2$ between the present results and those recently obtained by Heighway and Seymour[25]. The values of $\gamma^2_A(k)/C^2$ obtained by them for In, Sn, Cu and Na are 646.3, 576.2, 467.3 and 178.9 respectively. Tables 5.9, 5.10, 5.11 and 5.12 show that their values are considerably higher for In and Sn than the present values. The

reason for this difference lies in two factors, the first and most important are the values of $R_{no}(o)$ used by Heighway and Seymour. In their calculation these were obtained at the smallest r value listed in Herman and Skillman instead of extrapolating $R_{no}(r)$ to r = o. Clearly these values will be in error and this could be as much as 10% for some elements. The second factor is that instead of expressing the plane wave in spherical harmonics, it was written

$$e^{i\underline{k}.\underline{r}} = 1 + i\underline{k}.\underline{r} - \frac{(\underline{k}.\underline{r})^2}{2}.$$

In their calculation only terms up to k^2 were included. It may be simply shown that neglect of these higher terms is justified. However marked discrepancies were found in some values of the overlap integral $B_{n\ell}(k)$, equation 5.26, between the present results and those of Heighway and Seymour. The reason for this is not known at present but a detailed comparison of the two calculations ought to reveal the cause of the discrepancy. Calculations of $\gamma^2_A(k)/C^2$ for a range of pure metals will be undertaken shortly using PW theory allowing a more extensive comparison with Heighway and Seymour's values.

The pseudopotential theory predictions of ΩP_F for ^{115}In and ^{119}Sn as a function of noble metal concentration are plotted in figures 5.6 and 5.7 respectively. In the noble metal-indium systems, comparison with the experimental K variation in figure 3.9 shows that the theory always predicts a larger effect than is observed, though for Cu - In the results are in agreement up to ≈40%Cu. For Ag - In and Au - In the theoretical predictions are too large by factors of 3 and 2 respectively. However, all of the other features of the experimental results are reproduced by the theory. The observed $K(^{115}In)$ always increases with increasing noble metal concentration, the magnitude being greatest for Au - In and smallest for Cu - In. The theory produces just this behaviour. However

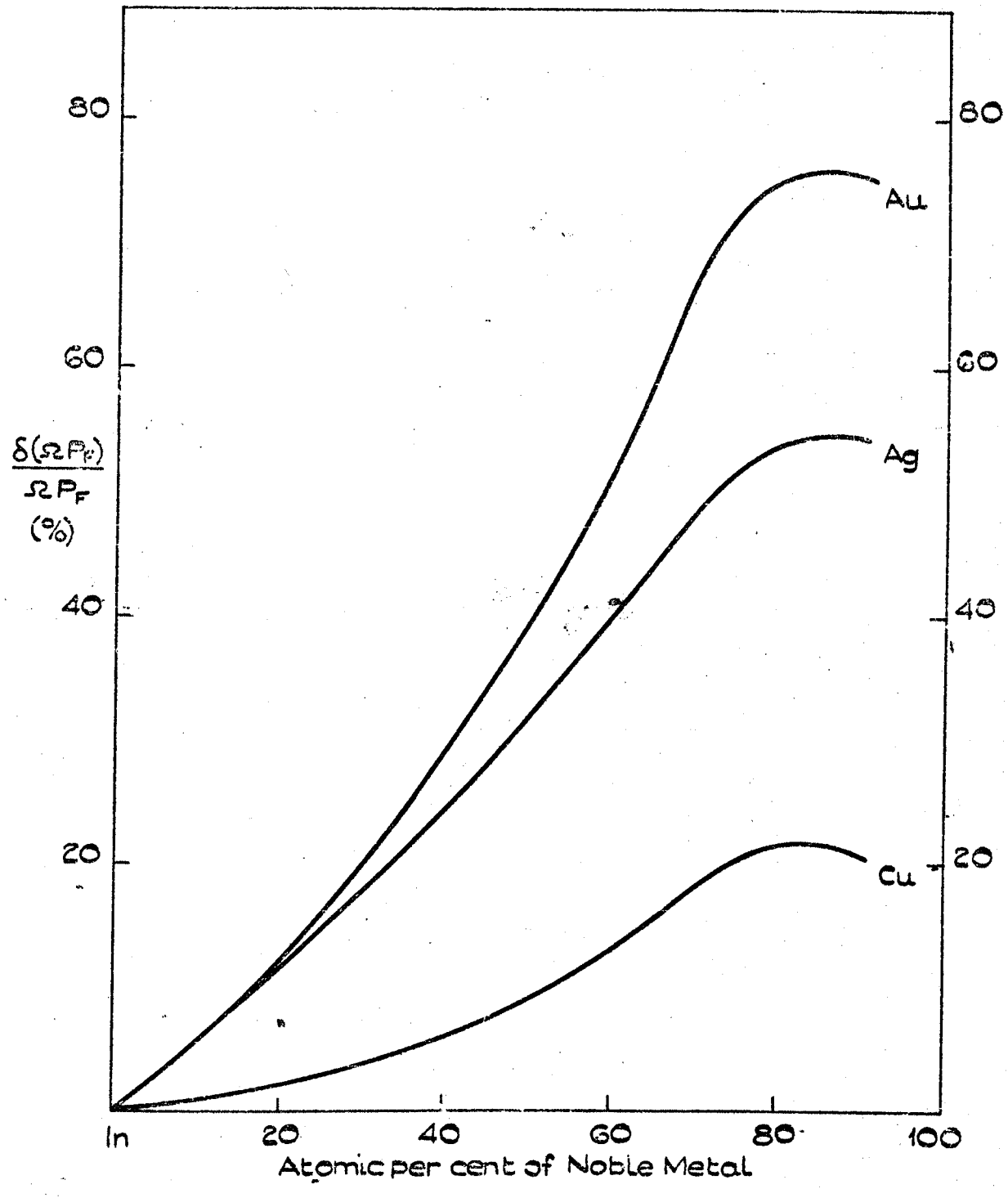

FIGURE 5.6.

PSEUDOPOTENTIAL THEORY RESULTS FOR $\delta(\Omega P_F)/\Omega P_F$ AT ^{115}In AS A FUNCTION OF NOBLE-METAL CONCENTRATION.

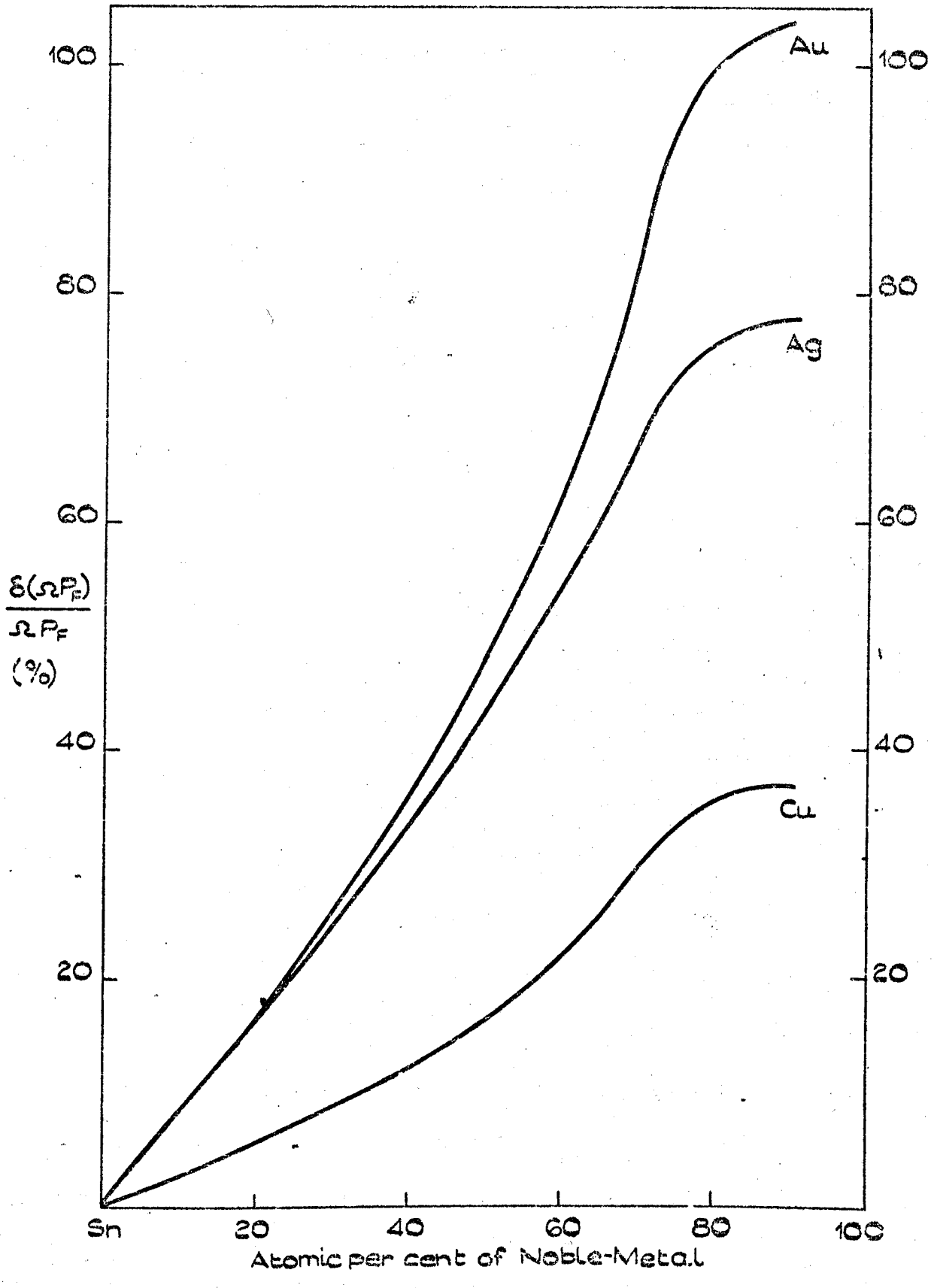

FIGURE 5.7

PSEUDOPOTENTIAL THEORY RESULTS FOR $\delta(\Omega P_F)/\Omega P_F$ AT ^{119}Sn AS A FUNCTION OF NOBLE-METAL CONCENTRATION

the other prominant feature in the observed $K(^{115}In)$ is the turnover between 40 and 60% of noble metal concentration. This behaviour is predicted by the theory, though always at a higher concentration of noble metal and is not so marked especially for the Ag - In and Cu - In systems.

Comparison of the observed and predicted results for $K(^{119}Sn)$, figures 3.4 and 5.7, show that the theory gives results which are approximately three times too large for all three systems. However the other features are reproduced, in that $K(^{119}Sn)$ increases with concentration of noble metal and the magnitude of the variation is largest for Au - Sn and smallest for Cu - Sn. Also the upward curve in the observed results for Au - Sn is predicted by the theory. As in the noble metal-indium systems, the theory predicts a turn over in $K(^{119}Sn)$ at high noble metal concentrations. It would be of interest to extend the measurements in these systems to higher noble metal concentrations to see if $K(^{119}Sn)$ does in fact flatten out as predicted. At the highest concentration measured Au-21%Sn, $K(^{119}Sn)$ is in fact still increasing rapidly.

For $K(^{63}Cu)$ in both the Cu - In and Cu - Sn systems the predicted variation is in the opposite direction to that observed experimentally; compare figures 3.3 and 3.8 with figure 5.8

A number of approximations have been made in the theory which could cause both the predicted variations and absolute values of K to be in error. Inspection of tables 5.10, 5.11 and 5.12 shows that the major contribution to the variation of ΩP_F comes from $\gamma^2_A(k)/C^2$. Now $\gamma^2_A(k)$ changes with composition via the variation of k_F while C^2 depends on the average ionic volume Ω_{AB}. Both k_F and Ω_{AB} have been calculated on the assumption that the alloy densities vary linearly between the pure metal

values. However since the OPW factor is so sensitive to the values of k_F and Ω_{AB} used, this assumption is probably not adequate. Unfortunately density measurements in these alloys are not yet available.

In this connection it is appropriate to consider the change in K with temperature in the liquid. Figure 3.2 shows the variation of K(^{119}Sn) in some liquid Au - Sn alloys, while figures 3.5, 3.6 and 3.7 show how the temperature coefficient of K(^{115}In) change sign beyond the turn over. In order to try and predict this behaviour the above calculations must be performed at different temperatures. A variation in ΩP_F would be expected to result from the variation of k_F and Ω with temperature. Again in order to calculate the k_F and Ω variations densities measured as a function of temperature are required. It is hoped to make density measurements in these and other systems in the near future.

Another approximation lies in the use of a local pseudopotential to represent the solvent and solute ions whereas a non-local pseudopotential ought to be used. PW show that this is not too serious for simple metals since the high q Fourier components of $u_A(q)$ and $u_B(q)$ are suppressed in the integrations over q in the present calculation. If the values of ΩP_F are combined with χ_P values given in table 5.1, for pure In and Sn, the K value obtained agrees fairly well with that observed experimentally. This agreement however is not reproduced for Cu where an excessively large value of ΩF_F is obtained. As previously mentioned this is probably due to the neglect of the strong s-d hybridization which will require a non-local pseudopotential representation if agreement with experiment is to be forthcoming. This problem has been fully discussed by Harrison[26] who proposes a non-local pseudopotential for the transition and noble metals, though it is not easy to see how these could be incorporated into the calculation. He does obtain however a total form factor for Cu, made up of a screened hybridization form factor and pseudopotential form factor. Moriarty[27]

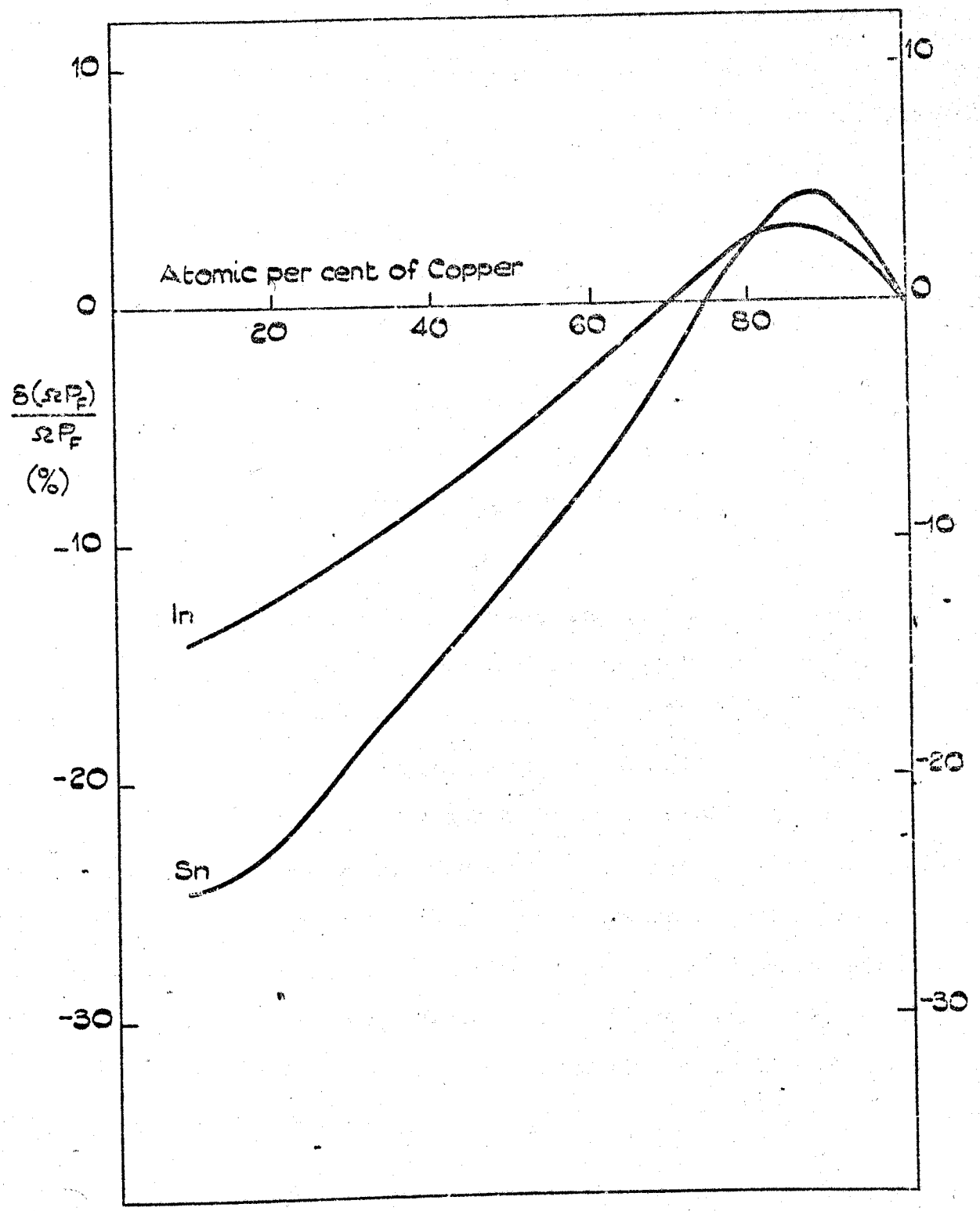

FIGURE 5.8.
PSEUDOPOTENTIAL THEORY RESULTS FOR $\delta(\Omega P_F)/\Omega P_F$ AT ^{63}Cu AS A FUNCTION OF Cu CONCENTRATION IN THE COPPER-INDIUM AND COPPER-TIN SYSTEMS.

has recently extended Harrison's work and calculated form factors for the noble metals at both solid and liquid densities. His calculation includes the full non-local character of the ordinary pseudopotential terms and additional hybridization terms without approximation. However because a Knight shift calculation requires all the matrix elements of a potential and not just those between Fermi surface states, a single form factor cannot adequately take account of the non-locality.

Perdew (private communication) has suggested a simple form of an energy dependent pseudopotential by using a concentration dependent value of the Ashcroft core radius given by $R_c = R_c^o \{1 - \alpha \frac{(k^2_F - k^{o2}_F)}{k^{o2}_F}\}$, where R^o_c and k^o_F refer to the pure liquid metal and α is an additional parameter characteristic of the pure metal. The value of R_c at an appropriate concentration and for a particular nucleus would then be used in Ashcrofts local pseudopotential expression and P_F calculated as already described. Recently Jena et al.[28] have successfully calculated the Knight shift in Cd as a function of temperature using a non-local pseudopotential and it is envisaged that such potentials will be used in predicting alloy Knight shifts in the near future. Also in a very recent paper El-Hanany and Zamir have accounted fairly well for the variation and magnitude of ΩP_F in solid and liquid Cu by a semi-quantitative consideration of the s-d hybridization and its volume dependence.

Another possible source of error is that the core functions of Herman and Skillman used in this calculation do not take into account relativistic effects, which are probably important for the heavier elements. However it is thought that the effects are probably small for In, Sn and Cu which do not lie particularly high in the periodic table.

The assumption that the partial structure factors $I_{ij}(K)$ in the alloy are identical is certainly not correct. This could be rectified without too much difficulty by incorporating the $I_{ij}(K)$ of Ashcroft and Langreth[29] into the calculation. However PW have found that for the alkali-alkali alloys, the use of partial structure factors only changed their results by ≈3%. Until they have been used for the present alloys, it is not clear by how much the present results would be changed.

It has been assumed throughout this work that the change and magnitude of ΩP_F has been due only to the direct hyperfine s-contact interaction. As mentioned earlier there will be other contributions due to orbital effects and core polarisation terms which may make a positive or negative contribution to the Knight shift. For example Mahanti and Das[30] have calculated that the core polarisation contribution is +18%, +23% and +26% of K_S in Cs, Rb and Na respectively. However Dickson[31] has estimated that the K_{other} contribution to K_s for ^{119}Sn is probably only a few per cent while Rossini and Knight estimate that for ^{115}In this is $-0.1\ K_s$. The discrepancy between the observed and present calculations of Knight shifts justifies the neglect of these small, additional terms.

Summary The initial changes in $K(^{115}In)$ and $K(^{119}Sn)$ due to alloying with the noble metals have been quantitatively reproduced using a partial wave analysis of the electron scattering from a screened free atom potential to calculate ΩP_F. The variation of $K(^{115}In)$ and $K(^{119}Sn)$ across the range of concentration has been semi-quantitatively reproduced using a pseudopotential calculation of ΩP_F. The agreement obtained by both methods indicates that the calculations in principle are correct and that the approximations made are not grossly in error. The spin susceptibility data listed in tables 5.1 and 5.2 show that χ_p increases on alloying In or

or Sn with a noble metal. Combining ΩP_F values with these χ_p's gives a total Knight shift for ^{115}In and ^{119}Sn which is generally larger than that observed. The theoretical estimates of ΩP_F for $K(^{63}Cu)$ in the Cu - In and Cu - Sn systems are less encouraging in that in all but one case they fail to predict the correct sign. The reason for this failure is thought to be due to the strong s-d hybridization which has not been taken into account. That this will affect $K(^{63}Cu)$ more seriously than $K(^{119}Sn)$ or $K(^{115}In)$ is evident from the absolute values obtained for K, which are good for In and Sn but poor for Cu. In order to improve the theoretical estimates for $K(^{63}Cu)$, as well as for $K(^{115}In)$ and $K(^{119}Sn)$ in these alloys, a treatment which takes account of the hybridization must be made. As a first step towards accounting for these effects the simple energy dependent pseudopotential suggested by Perdew should be used together with partial structure factors for these alloys. Other improvements will come when density measurements have been made on these alloys which will give more reliable k_F values and atomic volumes. These modifications may be fairly easily incorporated into the present pseudopotential calculation and it is envisaged that they will be carried out in the near future. Finally relativistic core functions and reliable χ_p values are required. However it is extremely unlikely that the χ_p values will become available from CESR and therefore the assumptions made when extracting χ_p from the total susceptibility must be carefully examined, especially for the noble metals and their alloys.

REFERENCES

(1) Dupree R. and Seymour E. F. W., Phys. Kondens. Materie, 12, (1970), 97.

(2) Asik J. R., Ball M. A. and Slichter C. P., Phys. Rev., 181, (1969), 645; Ibid; Phys. Rev., 181, (1969), 662.

(3) Faber T. E., Adv. Phys., 16, (1967), 637.

(4) Perdew J. P. and Wilkins J. W., Sol.State Comms., 8, (1970), 2041.

(5) Angus W. R., Proc. Roy. Soc., A 136, (1932), 569.

(6) Slater J. C., Quantum Theory of Atomic Structure Vol. 1, McGraw Hill, (1960).

(7) Dupree R. and Geldart D. J. W., Sol. State Comms., 9, (1971), 145.

(8) Kanazawa H. and Matsudawa N., Prog. Theoret. Phys., 23, (1960), 433.

(9) Güntherodt H. J., Menth A., and Tieche Y, Phys. Kondens. Materie, 5, (1966), 392.

(10) Urbain G. and Ubelacker E., Adv. Phys., 16, (1967), 429.

(11) Williams G. I., Fulmer Research Inst. Report R.129/8, (1962).

(12) Rudge W. E., Phys. Rev., 181, (1969), 1024.

(13) El-Hanany U. and Zamir D., to be published.

(14) Blandin A., Daniel E. and Friedel J., Phil. Mag., 4, (1959), 180.
Blandin A. and Daniel E., J. Phys. Chem. Sol., 10, (1959), 126.

(15) Styles G. A., Ph.D. Thesis, Leeds University, (1964).

(16) Meyer A., Nestor C. W. and Young W. H., Adv. Phys., 16, (1967), 581.; Ibid, Proc. Phys. Soc., 92, (1967), 446.

(17) Blatt F. J., Phys. Rev., 108, (1957), 285.

(18) Ziman J., Adv. Phys., 13, (1964), 89.

(19) Hartree D. R., Numerical Analysis, Oxford Press, (1958).

(20) Ashcroft N. W. and Lekner J., Phys. Rev., 145, (1966), 83.

(21) Abramowitz M. and Stegun I. A., Handbook of Mathematical Functions, Dover Publications, (1964).

(22) Thornton D. E. and Young W. H., J. Phys. C., 1, (1968), 1097.

(23) Odle R. L. and Flynn C. P., Phil. Mag., 13, (1966), 699.

(24) Ashcroft N. W., J. Phys. C., I, (1968), 232.

(25) Heighway, J. and Seymour E. F. W., Phys. Kond. Materie, 13, (1971).

(26) Harrison W. A., Phys. Rev., 181, (1969), 1036.

(27) Moriarty J. A., Phys. Rev. B., 1, (1970), 1363.

(28) Jena P., Das T. P., Gaspari G. D. and Halder N. C., Phys. Rev. B., 3, (1971), 2158.

(29) Ashcroft N. W. and Langreth, Phys. Rev., 156, (1967), 685.

(30) Mahanti S. D. and Das T. P., Phys. Rev. B, 3, (1971), 1599.

(31) Dickson, E. M., Phys. Rev., 184, (1969), 294.

(32) Rossini F. and Knight W. D., Phys. Rev., 178, (1969) 641.

(33) Devine R. A. B. and Dupree R., Phil. Mag., 23, (1971), 29.

CHAPTER SIX

RELAXATION IN LIQUID METALS AND ALLOYS

6.1 Introduction

In nearly all liquid metals and alloys the dominant contribution to the relaxation rate R_1 arises from the magnetic hyperfine interaction. However there are two other magnetic contributions which arise due to orbital and core polarisation effects. Obata[1] has shown that the relaxation rate due to the orbital motion of the p-electrons is given approximately by

$$R_{1orb} \simeq \frac{4\pi}{\hbar} (\gamma_e \gamma_n \hbar^2) kT.N_o(E_F) \langle 1/r^3 \rangle . \qquad 6.1$$

In fact this contribution turns out to be small for all elements and may therefore be neglected. The relaxation rate due to exchange core polarisation is given by[2]

$$R_{1cp} = \frac{4\pi kT}{3\hbar} \{\frac{\gamma_n}{\gamma_e}\}^2 \; K^2_{cp} . \qquad 6.2$$

The largest estimate of K_{cp} in any metal is $K_{cp} \simeq |0.25K_s|$ which gives $R_{1cp} \simeq 0.02\ R_{1s}$, which is smaller than a typical error in relaxation time measurements. Similarly it has been shown that the dipole-dipole, pseudo-exchange and pseudo-dipolar contributions to R_1 are very small[3].

The relaxation rate due to the magnetic hyperfine interaction is given by

$$R_{1M} = \frac{4\pi k}{\hbar} \{\frac{\gamma_n}{\gamma_e}\}^2 \; K_s^2 TK(\alpha) . \qquad 6.3$$

Calculations of the electron-electron correction factor $K(\alpha)$ have varied

with the choice of $V(q)$ the electron-electron interaction potential. Narath and Weaver[4] obtained $K(\alpha)$ as a function of α by assuming a spherical Fermi surface and $V(q)$ is a constant, i.e. V. is a δ-function in real space. More recently Shaw and Warren[5] have used a more realistic momentum dependent $V(q)$ and obtained $K(\alpha)$ for the alkali metals. Rossini and Knight[3] have found that for In, Ga, Sb and Rb a value of $K(\alpha) = 0.75$ gives a good fit with experimental R_{1M} data and suggest that this value may generally apply for all liquid metals. However El Hanany and Zamir[6] have recently found that for liquid Cu at its melting point a value of $K(\alpha) = 0.64$ more adequately describes their results. Equation 6.3 reasonably describes the observed relaxation rates in a number of liquid metals and alloys and in particular $R_1(^{119}Sn)$ for the noble metal-tin systems considered here. However there exists a large body of experimental relaxation rate data, in particular that for the noble metal-indium alloys, which is not accounted for solely by R_{1M}. Almost invariably these systems have nuclei with $I>\frac{1}{2}$ and it is now well established that dynamic electric quadrupole interactions contribute to the observed relaxation rates and in some cases dominate the competing magnetic process. The quadrupolar relaxation R_{1Q} is brought about by the coupling of the nuclear quadrupole moment with the time dependent electric field gradients which exist in a liquid metal. The sources of the electric field gradients are two-fold, the most important is the thermal modulation of the screened ionic charge around the nucleus by diffusional motion while the second is due to the direct nuclear interaction with the conduction electron charge. Attempts have recently been made to calculate the R_{1Q} contribution in liquid metals and alloys and have had some measure of success. A discussion of these calculations is deferred until sections 6.3 and 6.4.

The relaxation rate data for the noble metal-tin and indium

systems are considered to arise only from R_{1M} and R_{1Q}, all other contributions being negligibly small.

6.2 Discussion of Experimental data

6.2.1 Noble metal-tin systems Since ^{119}Sn has a spin of ½ there will be no quadrupolar contribution to $R_1(^{119}Sn)$, which should be completely described by $R_{1M}(^{119}Sn)$. No pulse measurements of relaxation time were made and the rates were therefore calculated from the Lorentzian line widths $\Delta\nu$ using the relation

$$\Delta\nu = \frac{1}{\sqrt{3}\pi} \cdot \frac{1}{T_2}, \qquad 6.4$$

where it was assumed that $T_1 = T_2$ in the pure liquid metals and alloys. $R_1(^{119}Sn)$ in pure liquid Sn measured in this way agreed within experimental error with the direct measurements of Dickson[7]. Figure 3.10 shows that $\Delta H(^{119}Sn)$ and thus $R_1(^{119}Sn)$ increases as a function of temperature in all the gold-tin alloys. This temperature dependence follows from equation 6.3 and is due to an increasing number of electrons about the Fermi level contributing to the relaxation process. Figure 6.1 shows the variation of $R_1(^{119}Sn)$ as a function of concentration in the noble metal-tin alloys and $R_{1M}(^{119}Sn)$ calculated from the measured Knight shifts using equation 6.3. In plotting $R_{1M}(^{119}Sn)$ it was assumed that $K(\alpha) = 1.0$ and $K_{other} = 0$. Dickson found that for Sn a value of $K(\alpha) = 0.80$ was required to fit $R_{1M}(^{119}Sn)$ to $R_1(^{119}Sn)$ as measured, with $K_{other} = 0$. Agreement within experimental error is obtained between $R_1(^{119}Sn)$ and $R_{1M}(^{119}Sn)$ showing that the relaxation is probably entirely magnetic in origin and thus $R_{1Q}(^{119}Sn) = 0$.

6.2.2 Noble metal-indium systems Pulse measurements of $R_1(^{115}In)$ were made across the Cu - In system and in a selected number of Ag - In and Au - In alloys. These are shown in figures 3.15, 3.16 and 3.17. $R_1(^{115}In)$ measurements from the line widths obtained for all the noble metal

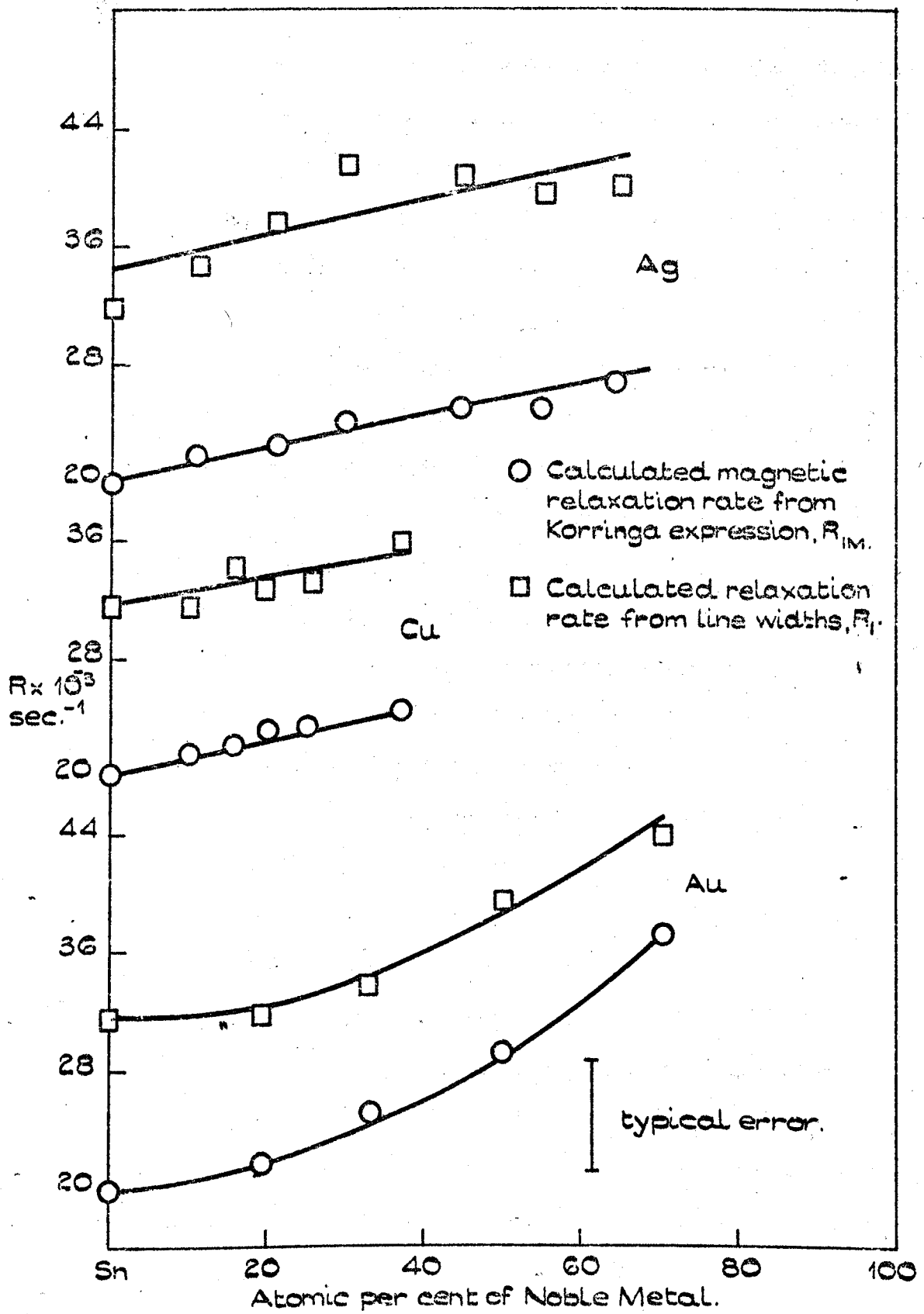

FIGURE 6.1.

^{119}Sn RELAXATION RATES IN THE LIQUID NOBLE METAL-TIN SYSTEMS.

indium alloys agreed within experimental error with those obtained from the present pulsed measurements and also those of Rossini.[8] However the errors on the pulse $R_1(^{115}In)$ measurements were much greater than those obtained from the line widths and consequently the $R_1(^{115}In)$ data plotted are obtained from the line widths. Figures 6.2, 6.3, 6.4 and 6.5, 6.6, 6.7 show $R_1(^{115}In)$ plotted across the concentration range in gold-indium, silver-indium and copper-indium at two temperatures, together with the magnetic hyperfine contribution, $R_{1M}(^{115}In)$. The latter was obtained by assuming that $K(\alpha) = 0.75$ for ^{115}In across the complete range of concentration for all three systems. This may be in error, particularly for the Cu - In system where $K(\alpha)$ has been found to be 0.64 for pure liquid Cu at its melting point. However Warren and Wernick[9] found that $K(\alpha) = 0.78$ for liquid Au - 66%In which suggests that the present assumption is a reasonable one. Rossini and Knight[3] have shown that for ^{115}In in pure liquid indium, $K_{other} = -0.1K_s$ and in the present treatment it has been assumed that this is the case across the whole range of concentration. Since ^{115}In has $I = {}^9/_2$ there exists the possibility that there is a quadrupolar contribution to $R_1(^{115}In)$ in these systems. Figures 6.2, 6.3, 6.4, 6.5, 6.6 and 6.7 all show that $R_1(^{115}In)$ cannot be accounted for by $R_{1M}(^{115}In)$ alone and that $R_{1Q}(^{115}In)$ must contribute importantly to the relaxation. Subtraction of $R_{1M}(^{115}In)$ from $R_1(^{115}In)$ gives $R_{1Q}(^{115}In)$, the quadrupolar contribution to the relaxation. In considering contributions to the relaxation it would be advantageous to be able to separate experimentally the observed relaxation rate uniquely into its magnetic and quadrupolar parts. Unfortunately this is possible only for elements with two measurable magnetic isotopes such as Ga or Sb. Warren and Clark[10] have done this for Sb and InSb and give a detailed description of the method.

Figures 6.2, 6.4 and 6.6 show that at a temperature 60K above the

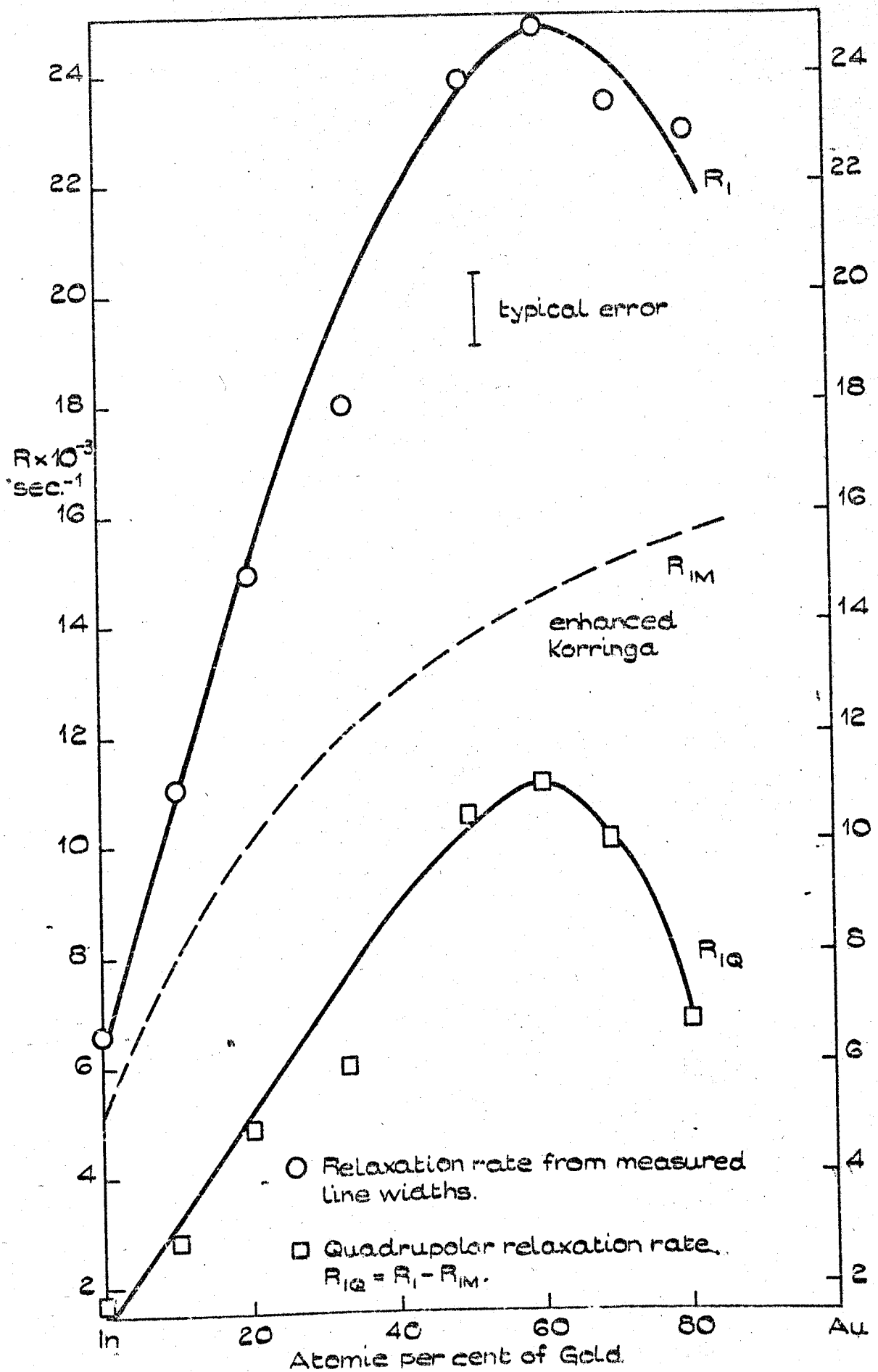

FIGURE 6.2. ^{115}In RELAXATION RATES IN THE LIQUID GOLD-INDIUM SYSTEM AT LIQUIDUS TEMPERATURE + 60K.

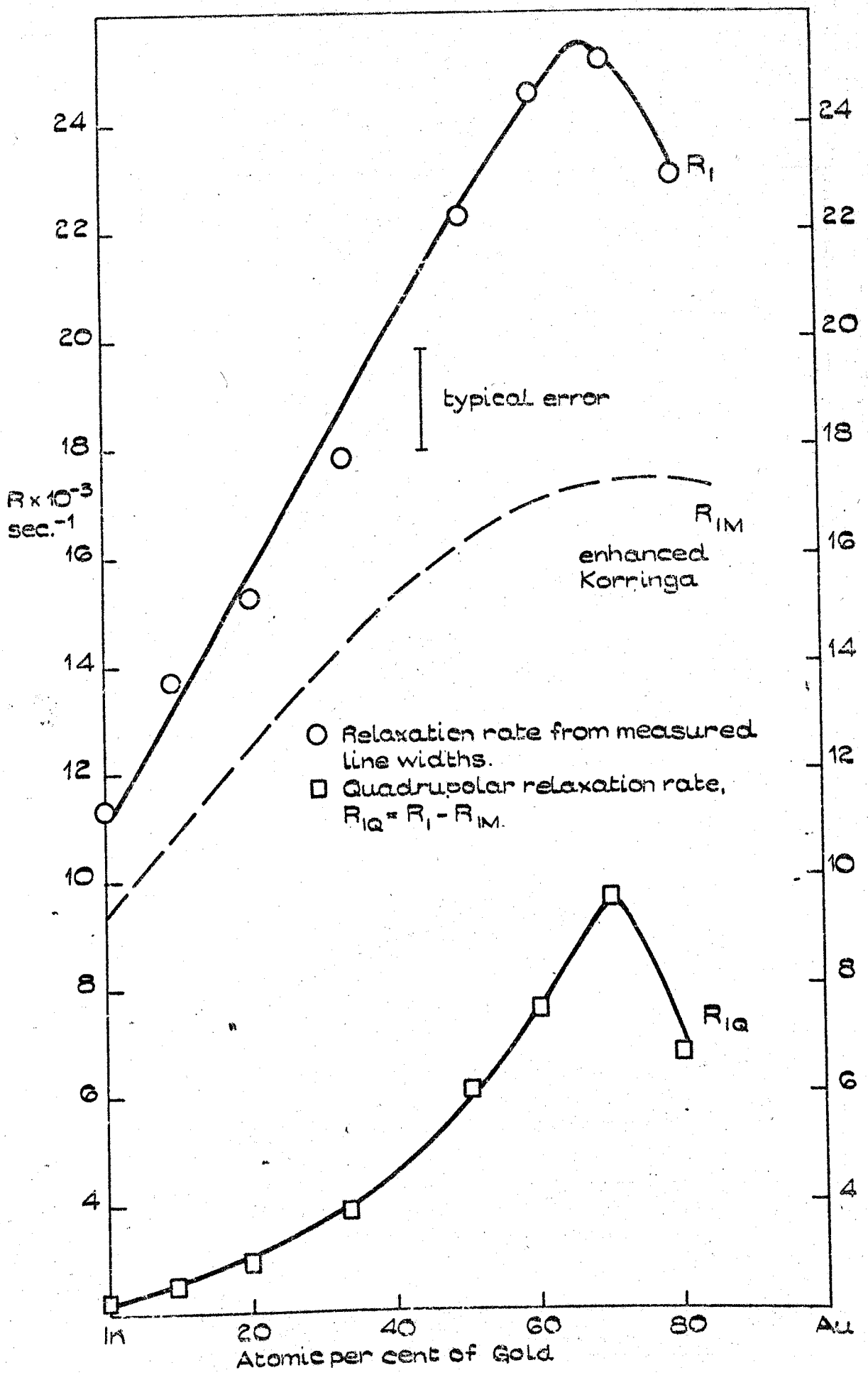

FIGURE 6.3.

^{115}In RELAXATION RATES IN THE LIQUID GOLD-INDIUM SYSTEM AT 1060 K.

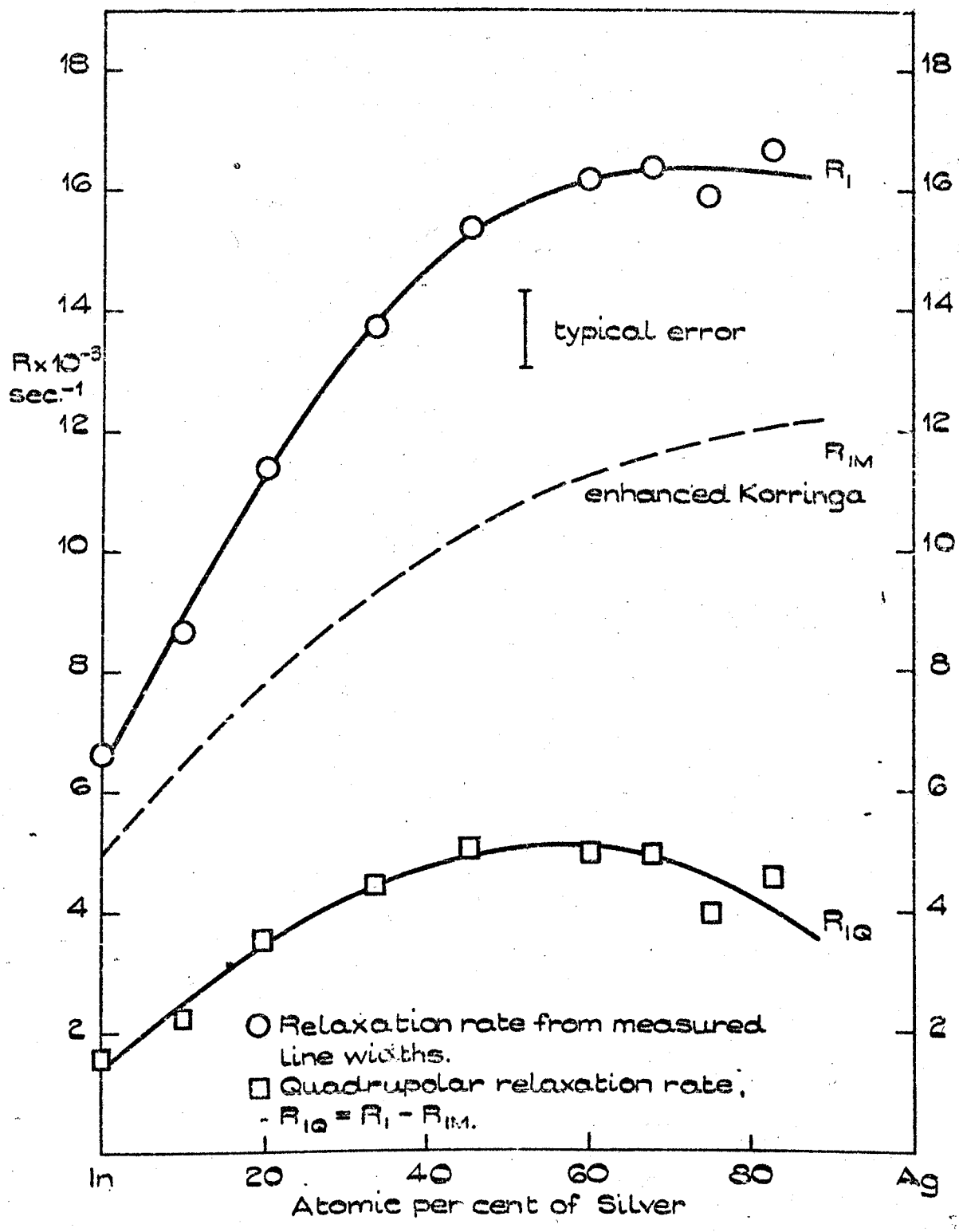

FIGURE 6.4.

^{115}In RELAXATION RATES IN THE LIQUID SILVER-INDIUM SYSTEM AT LIQUIDUS TEMPERATURE + 60K.

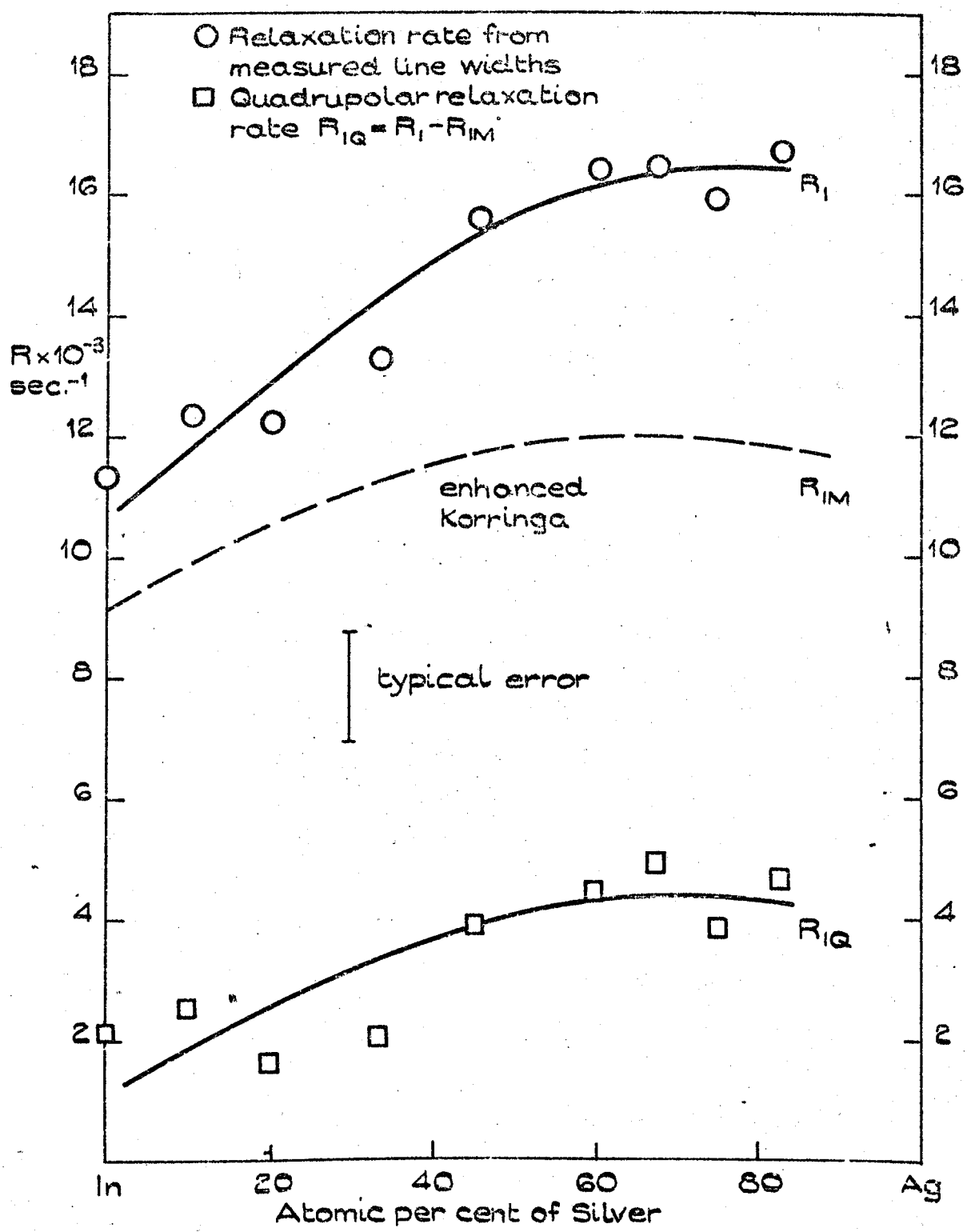

FIGURE 6.5.

^{115}In RELAXATION RATES IN THE LIQUID SILVER INDIUM SYSTEM AT 985K.

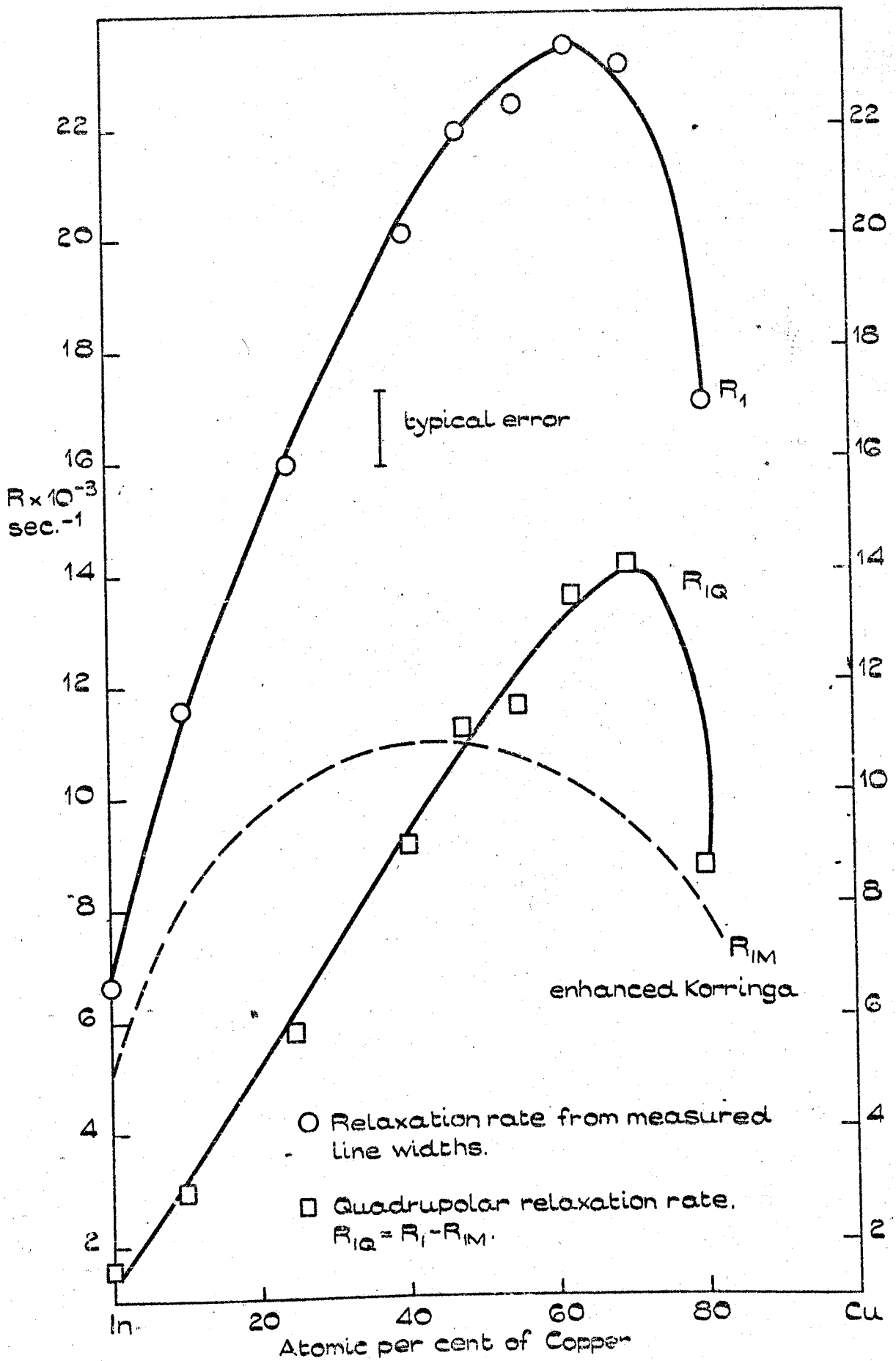

FIGURE 6.6.

^{115}In RELAXATION RATES IN THE LIQUID COPPER-INDIUM SYSTEM AT LIQUIDUS TEMPERATURE + 60K.

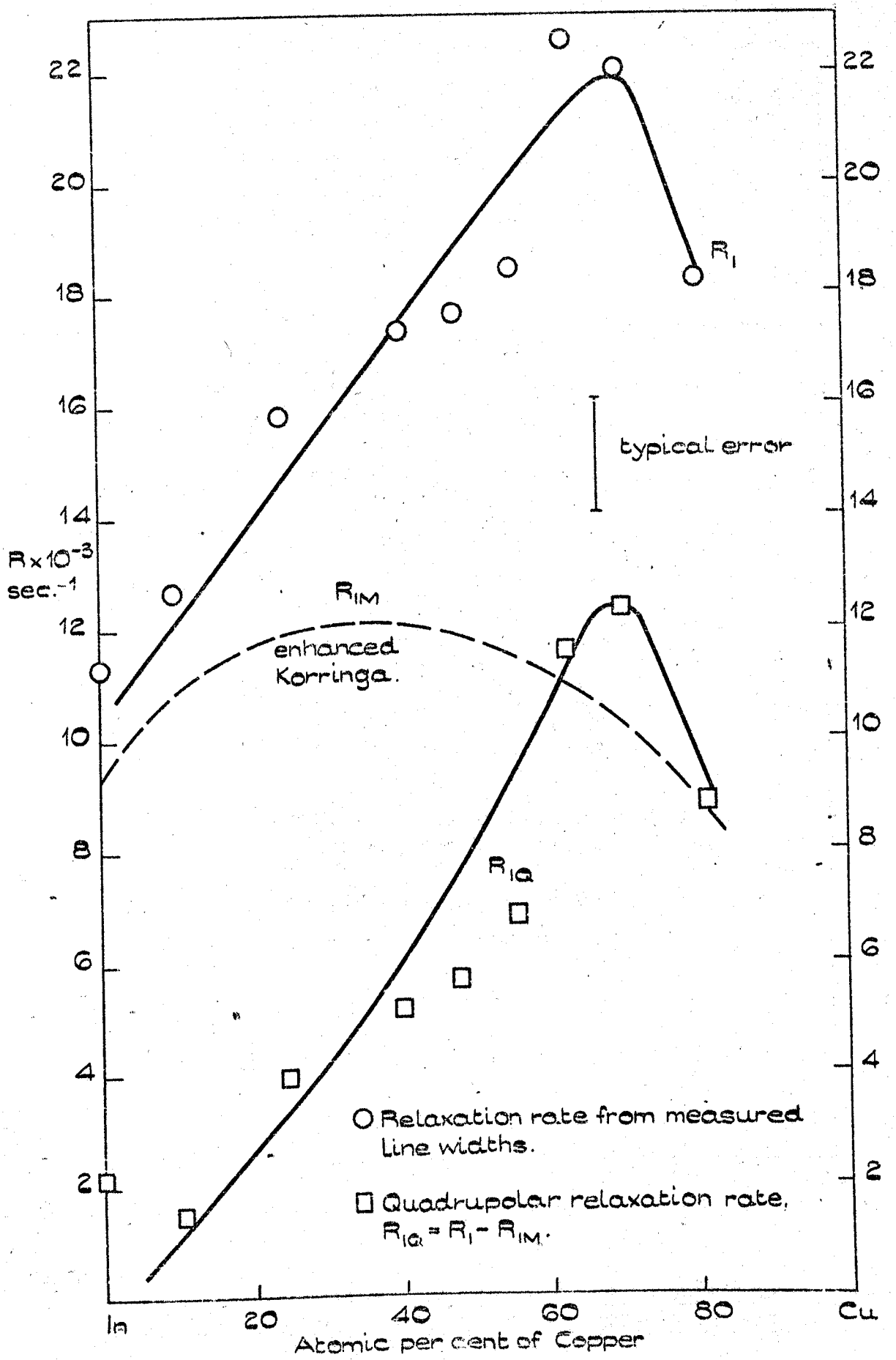

FIGURE 6.7.

^{115}In RELAXATION RATES IN THE LIQUID COPPER-INDIUM SYSTEM AT 1075 K.

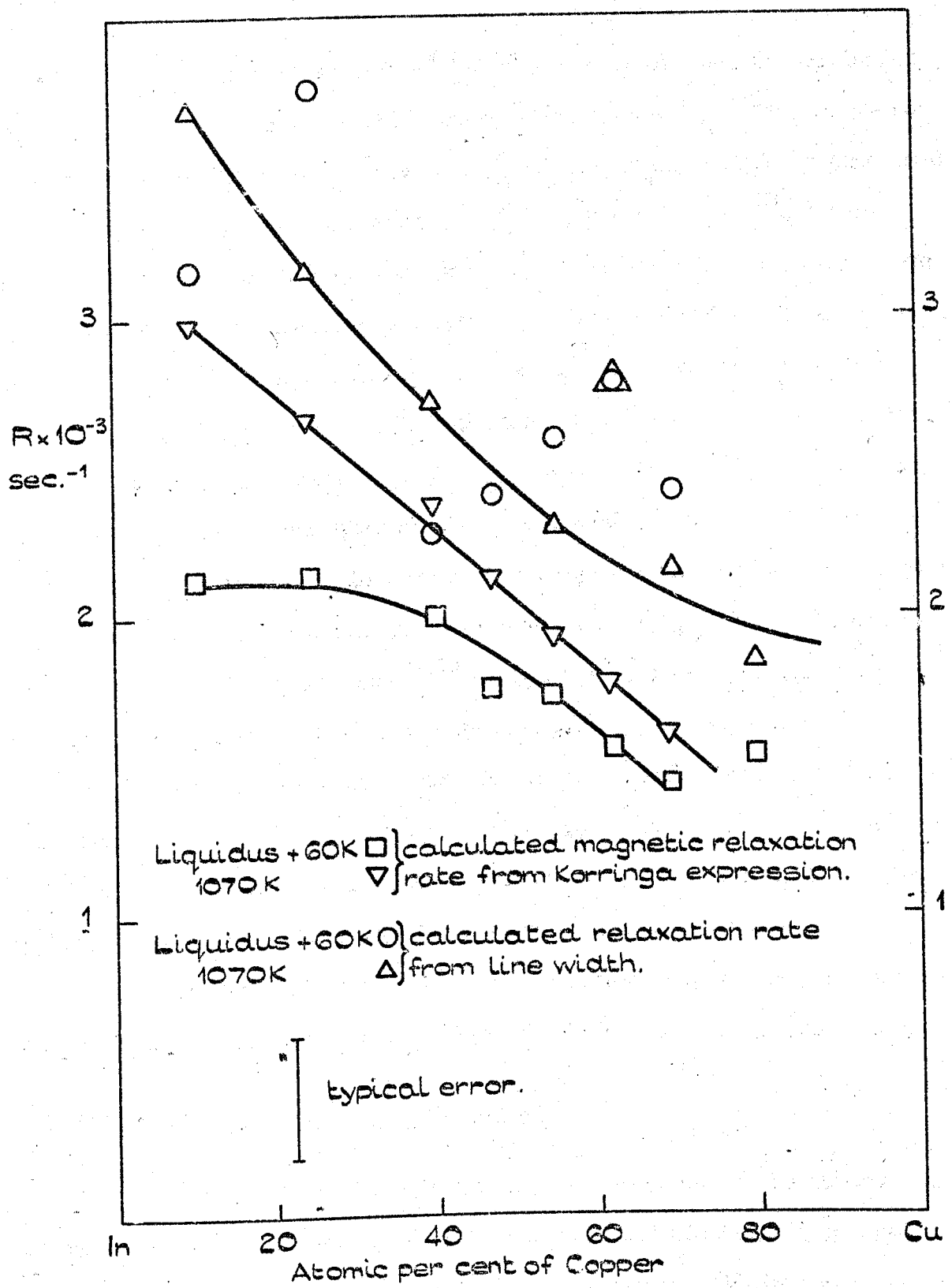

FIGURE 6.8.
^{63}Cu RELAXATION RATES IN THE LIQUID COPPER-INDIUM SYSTEM AT LIQUIDUS TEMPERATURE + 60K AND 1070K.

liquidus $R_{1M}(^{115}In)$ dominates in all of the gold-indium and silver-indium alloys, though in a few of the copper-indium alloys $R_{1Q}(^{115}In)$ dominates the relaxation. The dramatic drop in $R_1(^{115}In)$ at Cu - 20%In is confirmed both by direct pulse measurements and line width data. $R_1(^{63}Cu)$ was measured using pulsed NMR in only three Cu - rich Cu - In alloys and these rates agreed within experimental error with those calculated from the line widths. However the experimental error on $R_1(^{63}Cu)$ was considerable as figure 6.8 shows, where $R_{1M}(^{63}Cu)$ plotted as a function of concentration has been obtained by assuming that $K_{other} = 0$ and $K(\alpha) = 1.0$. While the former assumption is adequate, El Hanany and Zamir[6] have shown that the latter certainly is not. In view of the large errors involved this factor is not incorporated into the present estimation of $R_{1M}(^{63}Cu)$. El Hanany and Zamir also find from their $K(^{63}Cu)$ and $R_1(^{63}Cu)$ data in pure Cu that the only siginficant relaxation mechanism present is the magnetic hyperfine one, even though a quadrupolar contribution is possible since for ^{63}Cu $I = \frac{3}{2}$. The present data confirm this but on alloying Cu with In, $R_1(^{63}Cu)$ and $R_{1M}(^{63}Cu)$ diverge at high In concentrations suggesting that $R_{1Q}(^{63}Cu)$ begins to become important. In view of the errors incurred in the $R_1(^{63}Cu)$ measurements however these will not be considered further and the discussion which follows is devoted to $R_{1Q}(^{115}In)$ in the noble metal-indium alloys.

6.3 Quadrupolar relaxation in pure metals

The two factors which determine the magnitude of the quadrupolar interaction are the nuclear quadrupole moment Q and electric field gradient q. The electric field gradient at nuclei in solid and liquid metals arises from external charges of either other ions or electrons, the most important contribution arising from the electrons near to the nucleus concerned. The difficulty in calculating the field gradients arises because of the uncertainty

in representing the effect of the ions by a realistic screened potential. Also the field gradient is modified by the distortion of the core electrons due to these charges. This effect is taken into account by multiplying q by $(1 - \gamma_\infty)$, where γ_∞ is the Sternheimer anti-shielding factor. The factor $(1 - \gamma_\infty)$ may be as large as 100 for the heavier elements, though its determination is not straight forward however and only rough estimates of its magnitude have been made[11,12]. The most important source of the time dependent electric field gradients responsible for quadrupolar relaxation in liquid metals is the thermal modulation of the ionic charge distributions around the nucleus by vibrational, rotational and diffusional motion. In solid metals the lattice vibrations provide the dominant contribution to the electric field gradient modulation, and for $T>\theta_{Debye}$ it is found that $R_{1Q} \alpha T^2$. This has recently been verified by Warren and Wernick[9] for the alloys $AuGa_2$ and $AuIn_2$, who show that the self diffusion and defect diffusion provide negligible contributions to R_{1Q} in the solid. They point out that in the liquid this vibrational contribution to R_{1Q}, which has previously been ignored could well be significant. and estimate that it constitutes approximately 20% of $R_{1Q}(^{115}In)$ in liquid $AuIn_2$.

In a liquid metal the correlation time for thermal motion is typically $\tau_c < 10^{-11}$ sec, so that at a Larmour frequency of $\nu_o \simeq 10^7$HZ one is in the extreme narrowing limit where $\omega_o\tau \ll 1$. Under these conditions the quadrupolar relaxation rate has been shown to be[13]

$$R_{1Q} = \frac{3}{80} \frac{2I + 3}{I^2(2I-1)} \cdot \left\{ \frac{eQq}{\hbar} \right\} J(0), \qquad 6.5$$

where $J(\omega)$ is the Fourier transform of the reduced correlation function $G(t)$ which is given by

$$G(t) = \frac{\overline{F(t)\ F^*(t + \tau)}}{\overline{|F(t)|^2}}. \qquad 6.6$$

If $G(\tau) = \exp(-\tau/\tau_c)$, then $J(\omega) = \frac{2\tau_c}{1 + \omega^2\tau_c^2}$ and in the extreme narrowing limit $J(\omega_o) = J(0) \simeq 2\tau_c$. The quadrupolar relaxation then becomes

$$R_{1Q} = \frac{3}{40} \cdot \frac{2I + 3}{I^2(2I - 1)} \left\{\frac{eQq}{\hbar}\right\}^2 \tau_c . \qquad 6.7$$

Using equation 6.7 Rossini et al.[14] calculated R_{1Q} in liquid indium by considering the electric field gradient to be made up of an ionic part and a part due to the effect of the ions on the conduction electrons. They approximated the structure of liquid indium to be body centred cubic and calculated the r.m.s. electric field gradient produced by deviations of the ions at the lattice points from the equilibrium values. They found that the electric field gradient had its largest contribution from the effect of ionic motion on the p-conduction electrons which were assumed to bond covalently. The correlation time τ_c was deduced from the expression involving the r.m.s. jump distance, $\langle r^2 \rangle_{av}$ and the diffusion constant, $D = \langle r^2 \rangle_{av} / 6\tau_c$. Reasonable agreement with experiment was obtained using a jump distance obtained from the pair distribution function.

The calculation of Borsa and Rigamonti[15] assumed that the efg's were produced solely by the diffusing ionic charges and neglected contributions from the conduction electrons which Rossini et al. found to be so important. They represented the ion as an effective point charge Ze by a screened potential of the form $V(\underline{r}) = \frac{Ze}{r} \exp(-\alpha_s r)$ where the screening constant α_s is found from $\alpha_s^2 = 4\pi e^2 N(E_F)$. Taking the effect of the ions on the core electrons into account using the Sternheimer anti-shielding factor and using equation 6.4 with 6.5, Borsa and Rigamonti arrived at an expression for the quadrupolar relaxation rate, given by

$$R_{1Q} = \frac{\pi}{90} \frac{2I + 3}{I^2(2I-1)} \frac{e^4Q^2}{\hbar^2} \frac{NZ^2(1 - \gamma_\infty)^2 f(\alpha_s d)}{Dd}, \qquad 6.8$$

where d is the closest distance of approach, N is the ion number density and $f(\alpha_s d) = \exp(-2\alpha_s d)\{9 + \frac{37}{4}\alpha_s d + \frac{7}{2}(\alpha_s d)^2 + \frac{1}{2}(\alpha_s d)^3\}$. Using the above expressions, Borsa and Rigamonti obtained reasonable agreement with experimental R_{1Q} values in a number of liquid metals using current values of D, d and γ_∞.

Though the treatment of Rossini et al. and Borsa and Rigamonti consider that the efg's arise from different sources, both treatments give reasonable agreement with experiment which reflects the inherent uncertainty in both calculations.

Sholl's[16] calculation of R_{1Q} is more fundamental. He includes long range screening effects of the conduction electrons using an ionic potential of the form $V(\underline{r}) = \frac{A.\cos 2k_F r\ (1 - \gamma_\infty)}{(2k_F r)^3}$. 6.9

The factor $A(1 - \gamma_\infty)$ was determined from experimental measurements of the static quadrupole interaction in the corresponding solid metal. Sholl's expression for R_{1Q} is

$$R_{1Q} = \frac{2I + 3}{I^2(2I - 1)} \left\{\frac{A(1 - \gamma_\infty)eQ}{\hbar}\right\}^2 \frac{\pi\rho(I_1 + 2\pi\rho I_2)}{75D}, \qquad 6.10$$

where $I_1 = \int_0^\infty f(r)G(r)dr$ and

$$I_2 = \int_0^\infty f(r)g(r)r^2dr \int_{-0}^{\infty} G(r')dr' \int_{-1}^{+1} \{g(r) - 1\}\ P_2(z)dz, \qquad 6.11$$

with $f(r) = (2k_F)^2\ \frac{7(2k_F r)^2\sin(2k_F r) + \{15 - (2k_F r)^2\}\cos(2k_F r)}{(2k_F r)^5}$

and $G(r) = \frac{g^{\frac{1}{2}}(r)}{r}\{\int_0^{r_o} f(r)g^{\frac{1}{2}}(r)r^4dr + r_o^5 \int_{r_o}^{\infty} \frac{f(r)}{r} g^{\frac{1}{2}}(r)dr\}$,

g(r) is the familiar pair distribution function. In practice I_1 and I_2

are difficult to evaluate. Sholl obtains good agreement for R_{1Q} in liquid In only if the I_2 term is neglected.

The common feature of all three treatments outlined above is that the temperature dependence of R_{1Q} comes in through D and ρ, though in Sholls' expression a slight dependence comes from I_1 and I_2. The Sholl model has more in common with that of Rossini et al. in that the most significant part of the electric field gradient arises from the thermal modulation of the p-conduction electron charge in the vicinity of the nucleus. A further mechanism which may produce quadrupolar relaxation is the interaction between the nuclear quadrupole moment and the electric field gradient of the Fermi surface electrons. This contribution was found by Mitchell[17] to be approximately the same magnitude as that from orbital and core polarisation effects and is therefore fairly small.

The R_{1Q} data as a function of temperature in liquid metals is usually interpreted in terms of the temperature dependence of the diffusion coefficient D(T), such that $R_{1Q} \alpha \frac{1}{D(T)}$; equations 6.6 and 6.7 reduce to such a dependence. Usually an Arrhenius form is assumed such that $D = D_o \exp(-Q/KT)$ where $Q \simeq 3RT_m$. Heighway[11] recently obtained $R_{1Q}(^{209}Bi)$ as a function of temperature in pure liquid Bi. Assuming $R_{1Q}(^{209}Bi) \alpha \frac{1}{D(T)}$ he reasonably explained the temperature dependence of his data, though his experimental error was so large that this explanation could not be taken as conclusive. However the $R_{1Q}(^{115}In)$ values in pure liquid indium of Rossini and Knight (which agree with the present data) shows that the simple relationship of $R_{1Q} \alpha \frac{1}{D(T)}$ is not obeyed, as this in fact predicts a more rapid decrease in R_{1Q} than is actually observed. Warren and Wernick have suggested that a further contribution to $R_{1Q}(^{115}In)$ comes from the vibrational ionic motions and that these must be included if R_{1Q} as a function of temperature is to be adequately described.

6.4 Quadrupolar relaxation in alloys

As for the pure metals, the variation of R_{1Q} with temperature in a liquid alloy may be investigated by assuming that $R_{1Q}(T) \alpha \frac{1}{\bar{D}(T)}$ and Heighway has obtained good agreement with experimental $R_{1Q}(^{209}Bi)$ in the liquid alloys In - 50% Bi and Pb - 60%Bi assuming such a dependence. $R_{1Q}(^{115}In)$ was obtained only at two temperatures in the noble metal-indium systems and this prevented an investigation of an $R_{1Q}(^{115}In) \alpha \frac{1}{\bar{D}(T)}$ dependence. However the value of $R_{1Q}(^{115}In)$ was found to decrease at higher temperatures in all three systems as a comparison of figures 6.3, 6.5 and 6.7 with 6.2, 6.4 and 6.6 shows.

The calculation of the actual magnitude of R_{1Q} as a function of concentration in liquid alloys is difficult. The observed features of the R_{1Q} behaviour in many liquid binary alloy systems is that the magnitude of R_{1Q} increases on alloying and the value passes through a maximum around the middle of the concentration range. Figures 6.2, 6.4 and 6.6 show $R_{1Q}(^{115}In)$ as a function of concentration in the liquid gold-indium, silver-indium and copper-indium systems respectively. All three systems show $R_{1Q}(^{115}In)$ increasing as indium is alloyed with the noble metal and that $R_{1Q}(^{115}In)$ passes through a maximum value between 50 and 70% of concentration of noble metal. The magnitude of the increase in $R_{1Q}(^{115}In)$ is greatest for Cu - In and least for Ag - In. Warren and Wernick[9] have suggested that R_{1Q} increases on alloying due to the onset of molecular association which would lead to an increase in τ_c and, as equation 6.7 shows, an increase in R_{1Q}. If atomic associations were occuring at a particular concentration in a liquid alloy system then τ_c would be at its maximum value at this concentration and therefore so would R_{1Q}. Although the noble metal-indium systems do contain compounds in the solid (see figures 4.4, 4.5 and 4.6)

the maximum values of $R_{1Q}(^{115}In)$ observed here do not coincide with these compounds. Further, as discussed in chapter four, the Knight shift data do not point to the existence of groupings in the liquid state and $K(^{115}In)$ in these systems has been fairly well reproduced theoretically by assuming the alloys to be random mixtures of the two components. An explanation of $R_{1Q}(^{115}In)$ in these systems will therefore be sought in the light of the two existing calculations of R_{1Q} in liquid alloys where both treatments in fact predict a maximum in R_{1Q} across the range of concentration.

Heighway[11] has assumed that the only effect of alloying was to modify the electric field gradient by ionic diffusion. By postulating the liquid alloy to be face centred cubic with twelve nearest neighbours, he calculated the extra electric field gradient at a host nucleus due to increasing numbers of impurities with valence Z' where the host ion has valence Z. His expression for the quadrupolar relaxation rate is

$$R_{1Q} = \frac{3}{40}\,\frac{2I+3}{I^2(2I-1)}\,\frac{e^4Q^2}{\hbar^2}(1-\gamma_\infty)^2\left\{\sum_{i=0}^{12} P_i\overline{q^2}_i\right\}\tau_c', \qquad 6.12$$

where P_i is the probability that there are i impurity ions in a nearest neighbour position, q_i is the extra electric field gradient due to the added solute ions and the sum is taken over the nearest neighbour positions. Heighway only evaluated the summation inside the brackets and found that the predicted curve for R_{1Q} was approximately parabolic in shape and passed through a maximum at 50% of impurity concentration. Figures 6.2, 6.4 and 6.6 show that Heighway's model does not predict either the shape or the position of the maxima in $R_{1Q}(^{115}In)$ observed in the noble metal-indium alloys.

Both the model of Heighway and Sholl, which is to be discussed shortly, have assumed that R_{1Q} arises solely from the diffusional motion

of the ions. Warren and Clark[10] have recently measured $R_{1Q}(^{115}In)$, $R_{1Q}(^{121}Sb)$ and $R_{1Q}(^{123}Sb)$ in the liquid alloy In - 50%Sb and found that contributions to the electric field gradient from the Fermi surface electrons are important. Their measurements of $R_{1Q}(^{115}In)$ and $R_{1Q}(^{121}Sb)$ as a function of temperature in the liquid were markedly different. Since Q and $(1 - \gamma_\infty)$ are nearly equal for In and Sb the effect of the diffusing ions should have comparable magnitude for both species. They concluded that the contribution to the electric field gradient from the Fermi surface p-electrons were important and that In - 50%Sb retains a memory of its compound which exists in the solid.

A more rigorous and fundamental approach to the problem has been taken by Sholl (private communication) who has extended his theory for pure metals in a straight forward way to calculate R_{1Q} in alloys. His theory gives a final expression for the quadrupolar relaxation rate as

$$R_{1Q} = \{\frac{c}{D_A} I_1 + c^2 \frac{I_2}{D_A} + \frac{1-c}{D_B} \alpha^2 I_1 + \frac{(1-c)^2}{D_B} \alpha^2 I_2 + c(1-c)\, \alpha I_2 (\frac{1}{D_A} + \frac{1}{D_B})\}. \quad 6.13$$

In the above expression c is the impurity concentration and D_A and D_B are the diffusion constants for type A and B ions respectively. Unfortunately there is very little experimental data on alloy diffusion constants, which in some systems have been found to change by a factor of 2 across the concentration range. I_1 and I_2 are similar to the integrals defined in equation 6.11 but are modified for a particular alloy system. In particular this requires triplet correlation functions, one of which is $g_{AAA}(r_o, r_2)$ which is the probability of finding A type ions at r_o and r_2 given an ion A at the origin. In practice these are very difficult to determine though they may be obtained in a less accurate form using the superposition approximation where they are written as the product of 3 two-body correlation

functions. The term α is defined by $q_B = \alpha q_A$, where q_A and q_B are the electric-field gradients at the A and B nuclei respectively. Due to the present difficulty in obtaining I_1 and I_2 and the indeterminacy of q_A and q_B, only an empirical fit of equation 6.13 with the experimental data is possible at present. However D. S. Moore (private communication) has found that the magnitude and position across the concentration range of the maximum in R_{1Q} observed experimentally may be fitted to the Sholl theory by varying the parameters α and I_1/I_2 in a consistent way. His work, which is still in the preliminary stage, reveals that α shows no systematic variation with either atomic number or valence ratio of the two alloy elements. The present data of $R_{1Q}(^{115}In)$ in the noble metal-indium alloys bear out his findings where α needs to be largest for Cu - In and smallest for Ag - In in order that the theory predict the maximum and minimum magnitudes of $R_{1Q}(^{115}In)$ in the Cu - In and Ag - In systems respectively. The calculations are at an early stage and await a full evaluation of I_1 and I_2 together with calculations of q_A and q_B and experimental diffusion coefficients before meaningful comparison of the theory and experiment is possible.

Summary

The experimental relaxation rate data for ^{119}Sn in all of the noble metal-tin alloys are accounted for by the magnetic hyperfine contributions $R_{1M}(^{119}Sn)$, where it is assumed that the electron-electron enhancement $K(\alpha) = 1.0$ and $K_{other} = 0$. The total relaxation rate in the noble metal-indium alloys could only be accounted for with a magnetic contribution to the relaxation $R_{1M}(^{115}In)$ and a quadrupolar contribution $R_{1Q}(^{115}In)$. Reasonable values of $R_{1Q}(^{115}In)$ in these systems were obtained by subtracting from $R_1(^{115}In)$ the magnetic term $R_{1M}(^{115}In)$, where it was assumed that $K(\alpha) = 0.75$ and $K_{other} = 0.1K_s$ across the concentration range. $R_{1Q}(^{115}In)$

increased on alloying In with a noble metal giving a maximum between 50 and 70 at .% of noble metal concentration. The simple model of Heighway was unable to predict with any accuracy either the position or the magnitude of the variation in $R_{1Q}(^{115}In)$. Although atomic association in the liquid could result in a maximum in $R_{1Q}(^{115}In)$, the Knight shift evidence for these systems does not support this view. The Sholl theory, though it has not been applied specifically to these alloys is able to predict both the position and magnitude of $R_{1Q}(^{115}In)$, however the theory is at present only applicable on a semi-quantitative basis.

Clearly there is a need for improvement in the calculation of R_{1Q} in both pure liquid metals and alloys and in particular to include vibrational effects as well as Fermi surface electron contributions, both of which seem to contribute importantly to quadrupolar relaxation rates.

References

(1) Obata Y., J. Phys. Soc. Japan, 18, (1963), 1020.

(2) Yafet Y. and Jaccarino V., Phys. Rev., 133, (1964), A1630.

(3) Rossini F. A. and Knight W. D., Phys. Rev., 178, (1969), 641.

(4) Narath A. and Weaver H. T,, Phys. Rev., 175, (1968), 373.

(5) Shaw R. W. and Warren W. W., Phys. Rev. B, 3, (1971), 1562.

(6) El-Hanany and Zamir D., to be published.

(7) Dickson E. M., Phys. Rev., 184, (1969), 294.

(8) Rossini F. A., Ph.D. Thesis, University of California, Berkeley (1968).

(9) Warren W. W. and Wernick J. H. Phys. Rev. B, 4, (1971), 1401.

(10) Warren W. W. and Clark W. G., Phys. Rev., 177, (1969), 600.

(11) Heighway J., Ph.D. Thesis, University of Warwick, (1969). 736.

(12) Sternheimer R. M., Phys. Rev., 84, (1951), 244; Phys. Rev., 86, (1952), 316; Phys. Rev., 95, (1954).

(13) Abragam A., The Principles of Nuclear Magnetism; Clarendon Press, Oxford, (1961).

(14) Rossini F. A., Geissler E., Dickson E. M. and Knight W. D., Adv. Phys., 16, (1967), 287.

(15) Borsa F. and Rigamonti A., Nuovo Cimento, 488, (1967), 144.

(16) Sholl C. A., Proc. Phys. Soc., 91, (1967), 130.

(17) Mitchell, A. H., J. Chem. Phys., 26, (1957), 1714.

(18) Egelstaff P. A., Page D. I. and Heard C. R. T., Phys. Lett., 30A, (1969), 376.

CHAPTER SEVEN

THE CESIUM-OXYGEN SYSTEM

7.1 Introduction

The importance of the existence of oxygen in the corrosion processes of many metals used to contain alkali metals is fully recognised but the detailed role played by the oxygen is not understood. The present work was initiated in support of the investigation by Kendall[1] of the form in which oxygen exists in the liquid alkali metals. Kendall measured the Hall effect in a number of liquid cesium-oxygen alloys and successfully interpreted his data using a free electron model in which two electrons are removed from the conduction band for each oxygen ion added. He concluded therefore that oxygen in liquid cesium exists in the form of O^{--} ions. Knight shift (K) measurements offer the opportunity of distinguishing between the metal atoms forming a regular oxide in solution and those solvated as a charged species. In the first case K would be expected to remain unaltered from that of the pure metal of those nuclei not involved in oxide formation, while the oxide forming nuclei would show a zero shift. In the second case K for all nuclei would be shifted below that in the pure metal due to removal of electrons from the conduction band and the redistribution of electrons to screen the negative oxygen ions. Cesium was chosen because the solubility of oxygen in liquid cesium is much higher than in the other alkali metals and further ^{133}Cs exhibits a strong resonance signal due to its large isotopic abundance and magnetic moment.

7.2 Experimental results

Measurements have been made of $K(^{133}Cs)$ and $\Delta H(^{133}Cs)$ in pure liquid cesium metal, in liquid cesium containing approximately 12at.% oxygen and in solid Cs_2O. The metallic specimens were prepared by immersing

the molten samples under paraffin wax in a sealed ampoule and then shaking to produce a fine dispersion, the resulting droplets having diameters less than the r.f. skin depth. The measurements were made on a Varian spectrometer as described in Chapter 2. The results are given below in table 7.1. The line widths in both metallic specimens could be closely approximated by Lorentzian functions and that in Cs_2O by a Gaussian.

Table 7.1

^{133}Cs Knight shifts (K) and line widths (ΔH).

Specimen	$K(^{133}Cs)$ (%)	$\frac{1}{C}\frac{\delta K}{K}$	ΔH (gauss)	Temp. (K)
Cs	1.443(±0.022)	0	1.16(±0.05)	309±1
Cs - 12%O	1.303(±0.020)	-0.81	1.30(±0.05)	312±3
Cs_2O	0	-	4.4	293±1

One resonance only was observed in the Cs-12%O specimen and this showed a shift of about 90% of that in pure cesium. An extended search for a further resonance in this specimen at the position of that in Cs_2O produced no detectable signal. A comparison of the signal strength obtained under identical conditions in Cs_2O indicated that not more than 1 part in 40 of the cesium in the Cs-12%O specimen was in the form of Cs_2O. A similar search showed no resonance at the position of pure Cs in this sample.

7.3 Discussion

The fact that the ^{133}Cs nuclei in Cs-12%O give a single resonance with a shift slightly less than that in the pure metal is a clear indication

that the oxygen atoms go into cesium as dissolved ions and that there is no oxide formation. This change of shift is in fact quite comparable with that observed when the alkalis are alloyed with metallic solutes such as Hg, Tl or Pb[2]. The magnitude of the observed change in K offers the possibility of determining the degree of ionisation of the oxygen atoms and in particular of distinguishing between O^- and O^{--}. The Knight shift is proportional to the product of P_F and χ_p and the change in shift with solute concentration is given by equation 5.02. The spin susceptibility in the free electron approximation which should be adequate for a liquid alkali metal is given by $\chi_p \propto N^{\frac{1}{3}} \Omega^{-\frac{1}{3}}$, where electron-electron and electron-ion interactions have been neglected. The volume change on adding oxygen may be deduced from the density data obtained by Kendall and the change in N from the concentration and assumed charge of the oxygen ion. This yields values for $\frac{1}{c}\frac{\delta\chi}{\chi}$ of 0.0 for O^- (the effects of the changes in N and V fortuitously cancelling) and -0.47 for O^{--}. The possibility of a change in the enhancement of χ_p due to the electron-electron interaction[3] has been neglected since this is not thought to have a strong dependence on electron density. The product ΩP_F will change due to the electrostatic screening of the oxygen ions by the conduction electrons. In Chapter five it was shown that using a partial wave analysis of the impurity scattering the change in the solvent ΩP_F value per unit atomic concentration of solute ion is given by

$$\Gamma = \frac{1}{c}\cdot\frac{\delta(\Omega P_F)}{\Omega P_F} = \sum_{\ell}(\alpha_\ell \sin^2\gamma_\ell + \beta_\ell \sin 2\gamma_\ell). \qquad 7.1$$

As no experimental data for ion distributions are available for this system, the hard sphere structure factor of Ashcroft and Lekner for a pure liquid alkali metal is used and the values of α_ℓ and β_ℓ so obtained are listed in table 5.6 As before, two model potential representations of the solute are

used to find the phase shifts, γ_ℓ. Taking volume dilatation into account the Friedel sum z' values were -1.57 and -2.57 for O^- and O^{--} respectively. When using the square potential barrier the γ_ℓ's are usually determined by ascribing a width to the barrier and then adjusting the height until the Friedel sum rule is satisfied. In the absence of a specific value for the radius of an oxygen ion in cesium, the γ_ℓ's were first calculated by taking the O^{--} value of 1.4×10^{-10}m found by Tsai et al.[4] for solid Cs_2O. For this width however it was impossible to find a barrier height such that the γ_ℓ's satisfied the sum rule. Instead, therefore, three trial values were ascribed to the width of the barrier for which it was possible to choose heights which allowed the sum rule to be satisfied. The result was that for O^- and O^{--} separately the three sets of phase shifts for the different combinations of barrier height and width were identical and thus so long as the sum rule is satisfied the actual electron density distribution about the solute is independent of the barrier height and width separately. No such problem was encountered using the screened free atom model potential of Asik, Ball and Slichter[5], though as table 7.2 shows actual Friedel sums obtained were -1.43 and -2.72 compared with the effective valence differences of -1.57 and -2.57 for O^- and O^{--} respectively. Thus the sums are in error by approximately 10%, however this is probably not too serious in view of the uncertainties in the other parameters in the calculation, particularly the values of α_ℓ and β_ℓ. Table 7.2 lists the phase shifts obtained for O^- and O^{--} using both model potentials.

Table 7.2

Phase shifts for O^- and O^{--} using two model potentials

		Screened free atom potential		Square well potential	
System		O^- in Cs	O^{--} in Cs	O^- in Cs	O^{--} in Cs
Z'		-1.57	-2.57	-1.57	-2.57
Phase Shifts	γ_0	-.6015	-.6092	-1.2201	-1.5896
	γ_1	-.5473	-1.2230	-.3363	-.5852
	γ_2	.0001	.0001	-.0410	-.1200
Actual Z'		-1.43	-2.72		
R_T a.u.		1.73	1.76		

These values of γ_ℓ together with the coefficients α_ℓ and β_ℓ when inserted into equation 7.1 give the values of $\frac{1}{c}\cdot\frac{\delta(\Omega P_F)}{\Omega P_F}$ listed below in table 7.3.

Also given in the table are the contributions $\frac{1}{c}\cdot\frac{\delta\chi}{\chi}$ and the total theoretical change in Knight shift, $\frac{1}{c}\cdot\frac{\delta K}{K}$(theory).

Table 7.3

Changes in Knight shift parameters with solute concentration

Model	Z'	$\frac{1}{c}\frac{\delta\chi_P}{\chi_P}$	Square well $\frac{1}{c}\frac{\delta(\Omega P_F)}{\Omega P_F}$	screened atom $\frac{1}{c}\frac{\delta(\Omega P_F)}{\Omega P_F}$	Exptl. $\frac{1}{c}\frac{\delta K}{K}$	$\frac{1}{c}\frac{\delta K}{K}$ theory	
						square well	screened atom
O^-	-1.57	0	.741	.445	-.81	.741	.445
O^{--}	-2.57	-.47	.662	-.03		.192	-.50

As can be seen in the table the agreement between theory and experiment is very poor for the square potential barrier model no matter whether the oxygen is taken to be singly or doubly ionised. In view of the results discussed in Chapter five this is not surprising. However assuming doubly ionised oxygen atoms the screened free atom potential gives reasonable agreement between theory and experiment. Exact agreement is not expected in view of the approximate estimate of the χ_p changes and the uncertainties involved in the parameters used in the calculation of the γ_ℓ's. Also the coefficients α_ℓ and β_ℓ are probably inappropriate for the Cs - 12% oxygen specimen as they do not take into account the 17% change in the density over the pure metal.

7.4 Conclusion

Clearly the changes in χ_p alone cannot account for the observed change in K and screening of the charged oxygen ions by the conduction electrons must be considered to play an important role. This reinforces the

earlier statement that the oxygen atoms form a metallic solution with the cesium. Table 7.3 shows that reasonable agreement with experiment is obtained for the O^{--} model using the phase shifts calculated from the screened free atom potential. Indeed only this model gives a values of $\frac{l}{c}.\frac{\delta K}{K}$ of the same sign as that observed experimentally. Thus the present results in conjunction with the measurements of Kendall point to the existence of the oxygen atoms in the doubly ionised state and clearly establish that no oxygen exists in the Cs_2O molecular form.

References

(1) Kendall, P. W., J. Nuc. Mat., 35, (1970), 41.

(2) Kellington S. H. and Titman J. M., Phil. Mag., 15, (1967), 1045.

(3) Pines D., Solid State Physics, Vol. 1, eds. Seitz and Turnbull (Academic Press Inc., 1965), 367.

(4) Tsai K. R., Harris P. M. and Lassettre E. N., J. Phys. Chem., 60, (1956), 338.

(5) Asik, J. R., Ball M. A. and Slichter C. P., Phys. Rev., 181, (1969), 645; Ibid, Phys. Rev., 181, (1969), 662.

APPENDIX I

Table 1

The temperature dependence of the isotropic Knight shift K and line width ΔH of ^{119}Sn in tin and some gold-tin alloys

Specimen	Conditions	Temp. (K)	K(%)	ΔH(gauss)
Sn	liquid state, H_o = 8.6 kgauss	511	0.717 (±0.002)	2.97 (±0.10)
		571	0.716 (±0.001)	3.19 (±0.15)
		628	0.715 (±0.001)	3.28 (±0.20)
		675	0.715 (±0.002)	3.06 (±0.20)
		744	0.714 (±0.001)	3.66 (±0.20)
Au-80%Sn	liquid state H_o = 8.6 kgauss	585	0.760 (±0.001)	3.13 (±0.10)
		654	0.759 (±0.002)	3.44 (±0.15)
		723	0.757 (±0.002)	3.57 (±0.20)
		786	0.752 (±0.002)	3.82 (±0.20)
Au-66%Sn	liquid state H_o = 8.6 kgauss	632	0.801 (±0.001)	3.53 (±0.10)
		687	0.802 (±0.001)	3.52 (±0.10)
		741	0.798 (±0.001)	3.83 (±0.30)
		785	0.796 (±0.002)	3.53 (±0.10)
Au-29%Sn	liquid state, H_o = 8.5 kgauss	494	0.972 (±0.003)	3.66 (±0.40)
		533	0.988 (±0.002)	3.96 (±0.20)
		553	0.993 (±0.002)	4.31 (±0.35)
		603	0.990 (±0.003)	4.34 (±0.28)
		653	0.988 (±0.003)	4.52 (±0.22)
		723	0.984 (±0.004)	5.03 (±0.30)

Table 2

The temperature dependence of the isotropic Knight shift K and line width ΔH of ^{119}Sn in some gold-tin alloys

Specimen	Conditions	Temp. (K)	K(%)	ΔH (gauss)
Au-50%Sn	solid state, H_o = 8.6 kgauss	295	0.975 (±0.002	line assymetric in the solid, width not recorded
		362	0.972 (±0.003)	
		435	0.978 (±0.005)	
		502	0.975 (±0.003)	
		576	0.975 (±0.002)	
		625	0.976 (±0.001)	
		683	0.973 (±0.003)	
	liquid state, H_o = 8.6 kgauss	650	0.886 (±0.002)	3.66 (±0.40)
		683	0.886 (±0.001)	4.23 (±0.40)
		705	0.882 (±0.002)	3.76 (±0.20)
		729	0.876 (±0.003)	4.52 (±0.20)
		750	0.876 (±0.004)	4.73 (±0.30)
		790	0.871 (±0.003)	4.32 (±0.20)
Au-25%Sn Au-21%Sn	liquid state, H_o = 9.3 kgauss	720	1.010 (±0.007)	widths not recorded
		777	1.068 (±0.013)	

Table 3

The variation of the isotropic Knight shift K and line width Δ_H of ^{119}Sn in the liquid silver-tin and copper-tin systems

Specimen	Conditions	Temp. (K)	K %	ΔH(gauss)
Sn			0·704 (±0·002)	3·8 (±0·3)
Ag-88% Sn	liquid		0·729 (±0·004)	4·0 (±0·2)
Ag-77% Sn	state		0·735 (±0·002)	4·3 (±0·5)
Ag-66% Sn	H_o = 8.4	840	0·765 (±0·004)	4·8 (±0·5)
Ag-55% Sn	kgauss		0·775 (±0·004)	4·7 (±0·4)
Ag-45% Sn			0·777 (±0·006)	4·3 (±0·6)
Ag-35% Sn			0·794 (±0·004)	4·6 (±0·7)
Sn		830	0·714 (±0·003)	3·8 (±0·3)
Cu-95% Sn	liquid	755	0·722 (±0·002)	3·5 (±0·2)
Cu-95% Sn	state	830	0·723 (±0·004)	3·5 (±0·2)
Cu-90% Sn	H_o = 10.8	790	0·730 (±0·003)	3·6 (±0·3)
Cu-90% Sn	kgauss	830	0·726 (±0·002)	4·0 (±0·2)
Cu-85% Sn			0·735 (±0·003)	4·0 (±0·5)
Cu-80% Sn		830	0·738 (±0·002)	3·7 (±0·2)
Cu-75% Sn			0·740 (±0·003)	3·5 (±0·2)
Cu-65% Sn			0·747 (±0·005)	4·1 (±0·2)

Table 4

The variation of the Knight shift K of ^{63}Cu in the liquid copper-tin system

Specimen	Conditions	Temp. (K)	K(%)
Cu-95%Sn	liquid		0.282 (±0.003)
Cu-80%Sn	state,	830	0.275 (±0.001)
Cu-75%Sn	H_o = 10.8		0.274 (±0.002)
Cu-65%Sn	kgauss		0.270 (±0.002)

Table 5

The variation of the Knight shift K and line width ΔH of ^{115}In in the liquid silver-indium system

Specimen	Conditions	Temp. (K)	K %	ΔH (gauss)
In	liquid state	473	0·793 (±0·002)	1·30 (±0·08)
		513	0·793 (±0·002)	1·41 (±0·15)
		921	0·773 (±0·001)	2·22 (±0·12)
Ag-90% In	H_o = 11.0 kgauss	578	0·812 (±0·001)	1·69 (±0·06)
		939	0·786 (±0·002)	2·42 (±0·15)
Ag-80% In		673	0·826 (±0·002)	2·21 (±0·12)
		954	0·808 (±0·001)	2·40 (±0·15)
Ag-66% In		766	0·848 (±0·002)	2·67 (±0·20)
		971	0·830 (±0·001)	2·61 (±0·15)
Ag-55% In		831	0·858 (±0·001)	2·99 (±0·15)
		970	0·847 (±0·002)	3·05 (±0·30)
Ag-40% In		922	0·849 (±0·002)	3·16 (±0·12)
		985	0·849 (±0·001)	3·19 (±0·20)
Ag-33% In		988	0·829 (±0·003)	3·23 (±0·12)
Ag-25% In		1085	0·807 (±0·001)	3·11 (±0·15)
Ag-17% In		1153	0·786 (±0·001	3·28 (±0·16)

Table 6

The variation of the Knight shift K and line width $\Delta_{\frac{1}{2}}$ of ^{115}In in the liquid gold-indium system

Specimen	Conditions	Temp. (K)	K %	ΔH (gauss)
Au-90% In	liquid state, H_o = 12.0 kgauss	743	0·812 (±0·001)	2·16 (±0·10)
		1050	0·792 (±0·001)	2·69 (±0·16)
Au-80% In		838	0·843 (±0·001)	2·91 (±0·12)
		1057	0·828 (±0·001)	2·97 (±0·10)
Au-66% In	Solid state H_o = 12.0 kgauss	293	0·894 (±0·002)	2·67 (±0·10)
		416	0·902 (±0·001)	2·99 (±0·09)
		634	0·905 (±0·002)	3·51 (±0·25)
		784	0·901 (±0·001)	3·37 (±0·12)
		798	0·901 (±0·001)	3·59 (±0·15)
	liquid state H_o = 12.0 kgauss	838	0·898 (±0·001)	3·30 (±0·12)
		877	0·895 (±0·001)	3·49 (±0·15)
		966	0·889 (±0·001)	3·51 (±0·16)
		1060	0·882 (±0·001)	3·47 (±0·20)
Au-50% In	liquid state	860	0 958 (±0·002)	4·65 (±0·18)
		1056	0·950 (±0·002)	4·35 (±0·30)
Au-40% In	H_o = 12.0 kgauss	787	0·961 (±0·001)	4·40 (±0·18)
		876	0·970 (±0·002)	4·84 (±0·30)
		1061	0·972 (±0·002)	4·80 (±0·30)
Au-30% In	liquid state	843	0·946 (±0·002)	4·58 (±0·50)
		1004	0.959 (±0.004)	4.92 (±0.50)
Au-20% In	H_o = 12.0 kgauss	1065	0·949 (±0·002)	4·48 (±0·20)
		1170	0·958 (±0·003)	5·08 (±0·15)

Table 7

The variation of the Knight shift K and line width ΔH of ^{115}In in the liquid copper-indium system

Specimen	Conditions	Temp. (K)	K %	ΔH (gauss)
Cu-90% In	liquid state, H_o = 12.7 kgauss	790	0·801 (±0·001)	2·25 (±0·10)
		1070	0·786 (±0·001)	2·47 (±0·08)
Cu-75% In		894	0·816 (±0·001)	3·11 (±0·12)
		1071	0·807 (±0·001)	3·09 (±0·15)
Cu-60% In		958	0·822 (±0·001)	3·90 (±0·12)
		1072	0·818 (±0·001)	3·37 (±0·17)
Cu-52·5% In		962	0·814 (±0·001)	4·29 (±0·20)
		1072	0·813 (±0·001)	3·45 (±0·30)
Cu-45% In		1000	0·798 (±0·002)	4·35 (±0·40)
		1073	0·799 (±0·001)	3·59 (±0·10)
Cu-37·5% In		1008	0·764 (±0·002)	4·58 (±0·30)
		1082	0·771 (±0·001)	4·38 (±0·30)
Cu-30% In		1012	0·723 (±0·002)	4·51 (±0·40)
		1080	0·732 (±0·003)	4·32 (±0·40)
Cu-20% In		1075	0·679 (±0·002)	3·32 (±0·40)
		1154	0·691 (±0·002)	3·57 (±0·50)

Table 8

The variation of the Knight shift K and line width ΔH of ^{63}Cu in the liquid copper-indium system

Specimen	Conditions	Temp. (K)	K %	ΔH (gauss)
Cu-90% In	liquid state, H_o = 10.5 kgauss	793	0.314 (±0·001)	0·50 (±0·03)
		1070	0.322 (±0·001)	0·60 (±0·03)
Cu-75% In		895	0·298 (±0·001)	0·61 (±0·05)
		1070	0.305 (±0·002)	0·50 (±0·03)
Cu-60% In		962	0·279 (±0·001)	0·37 (±0·04)
		1072	0·286 (±0·001)	0·44 (±0·10)
Cu-52·5% In		962	0·263 (±0·001)	0·39 (±0·06)
		1072	0·272 (±0·001)	0·44 (±0·03)
Cu-45% In		1000	0.255 (±0·002)	0·42 (±0·07)
		1073	0·259 (±0·001)	0·37 (±0·04)
Cu-37·5% In		1008	0·240 (±0·001)	0·45 (±0·03)
		1082	0·247 (±0·001)	0·45 (±0·03)
Cu-30% In		1012	0·230 (±0.001)	0·39 (±0·03)
		1080	0.234 (±0·001)	0·35 (±0·03)
Cu-20% In		1075	0.230 (±0·001)	0·30 (±0·03)
		1154	0·235 (±0·001)	0·35 (±0·03)

Table 9

^{63}Cu and ^{115}In relaxation rates R_1 in some liquid copper-indium alloys

Specimen	Nucleus	Conditions	Temp. (K)	$R_1 \times 10^{-3}$ (sec.$^{-1}$)
In	^{115} In	liquid	500	6·15 (±0·80)
			1008	11.41 (±2·5)
Cu-90% In	^{115} In	state	1006	13·1 (±1·0)
Cu-75% In	^{115} In	H_o = 9.6	835	15·4 (±0·4)
		kgauss	1003	17·1 (±2·0)
Cu-60% In	^{115} In		875	14·5 (±2·0)
			1005	19·6 (±1·8)
Cu-52·5 % In	^{115} In		900	15·3 (±0·7)
			1000	20·3 (±2·0)
Cu-45% In	^{115} In		923	19·1 (±1·0)
Cu-37·5% In	^{115} In		943	28·5 (±5·5)
	^{63} Cu		943	1·85 (±0·20)
Cu-30% In	^{115} In		960	25.2 (±2·0)
	^{63} Cu		960	1·66 (±0·10)
Cu-20% In	^{115} In		1010	16·9 (±5·0)
	^{63} Cu		1010	1·55 (±0·20)

Table 10

^{115}In relaxation rates R_1 in some liquid silver-indium and liquid gold-indium alloys

Specimen	Nucleus	Conditions	Temp. (K)	$R_1 \times 10^{-3}$ (sec.$^{-1}$)
Ag-90% In	^{115}In	liquid	597	14·0 (±0·7)
			937	14·6 (±0·4)
Ag-55% In		state,	790	17·9 (±0·7)
			991	15·0 (±0·2)
Ag-40% In		H_o = 9.6	1007	16·3 (±0·3)
Ag-25% In		kgauss	1010	13·1 (±0·4)
Au-80% In			797	17·8 (±1·0)
			984	15·5 (±0·6)
Au-66% In		solid	346	6·72 (±0·20)
		state,	595	10·16 (±0·35)
		H_o = 9.6 kgauss	781	13·1 (±0·4)
		liquid	880	20·8 (±0·9)
		state,	1009	19·7 (±0·7)
Au-40% In		H_o = 9.6 kgauss	1008	22·9 (±0·5)

Table 11

The variation of the magnetic susceptibility, χ, with concentration in some liquid noble metal-indium alloys

Specimen	Temp. (K)	$\chi \times 10^6$ (emu.gm^{-1})	Specimen	Temp. (K)	$\chi \times 10^6$ (emu.gm^{-1})
Ag	1283	-0·217 (±0·004)	Au-50%In	1073	-0·152 (±0·003)
Ag-17%In	1150	-0·208 (±0·003)		833	-0·161 (±0·004)
Ag-25%In	1073	-0·213 (±0·002)	Au-66%In	1073	-0·129 (±0·005)
Ag-30%In	1073	-0·218 (±0·003)		877	-0·133 (±0·002)
	990	-0·223 (±0·004)	Au-80%In	1073	-0·109 (±0·003)
Ag-33%In	1073	-0·211 (±0·002)		816	-0·114 (±0·003)
	991	-0·216 (±0·003)	Au-90%In	1073	-0·091 (±0·002)
Ag-40%In	1073	-0·198 (±0·003)		731	-0·096 (±0·004)
	893	-0·204 (±0·002)	Cu	1373	-0·088 (±0·006)
Ag-55%In	1073	-0·164 (±0·004)	Cu-20%In	1073	-0·137 (±0·006)
	798	-0·172 (±0·006)	Cu-30%In	1073	-0·154 (±0·003)
Ag-66%In	1073	-0·129 (±0·002)		993	-0·162 (±0·004)
	733	-0·136 (±0·004)	Cu-37·5%	1073	-0·142 (±0·004)
Ag-80%In	1073	-0·104 (±0·005)	In	992	-0·150 (±0·003)
Ag-90%In	1073	-0·088 (±0·004)	Cu-45%In	1073	-0·132 (±0·002)
In	1073	-0·071 (±0·003)		962	-0·140 (±0·005)
	488	-0·083 (±0·002)	Cu-52.5%	1073	-0·120 (±0·002)
Au	1383	-0·159 (±0·003)	In	950	-0·126 (±0·003)
Au-20%In	1133	-0·167 (±0·004)	Cu-60%In	1073	-0·110 (±0·003)
	1033	-0.167 (±0.003)		923	-0·115 (±0·003)
Au-30%In	1073	-0·174 (±0·006)	Cu-75%In	1073	-0·093 (±0·004)
	823	-0.189 (±0.005)		873	-0·095 (±0·005)
Au-40%In	1073	-0·166 (±0·003)	Cu-90%In	1073	-0·079 (±0·003)
	773	-0·181 (±0·004)			

Table 12

The temperature dependence of the magnetic susceptibility χ in liquid tin and some gold-tin alloys

Specimen	Temp. (K)	$\chi \times 10^6$ (emu.gm^{-1})
Sn	514	-0.041 (±0.002)
	598	-0.039 (±0.002)
	681	-0.038 (±0.002)
	789	-0.036 (±0.002)
Au-50%Sn	712	-0.134 (±0.003)
	754	-0.133 (±0.004)
	783	-0.133 (±0.004)
Au-29%Sn	567	-0.177 (±0.003)
	605	-0.176 (±0.002)
	629	-0.175 (±0.002)
	638	-0.174 (±0.002)
	690	-0.171 (±0.003)
	694	-0.171 (±0.003)
	730	-0.170 (±0.002)
	767	-0.168 (±0.003)
Au-80%Sn	553	-0.088 (±0.003)
	612	-0.086 (±0.005)
	699	-0.084 (±0.004)
	759	-0.082 (±0.002)
Au-66%Sn	601	-0.113 (±0.006)
	659	-0.111 (±0.002)
	705	-0.109 (±0.002)
	754	-0.108 (±0.004)
Au-21%Sn	789	-0.178 (±0.004)
	811	-0.177 (±0.004)

APPENDIX 11

Calculation of the radial distribution function, g(r), which is subsequently used to evaluate the coefficients α_ℓ and β_ℓ.

The weighting factors, W (J), and abscissae, X (J), required in the Gaussian integration are taken from M.Abramowitz and I. A. Stegun, Handbook of Mathematical Functions, P.917. The other data is read in the following order: ETA = packing fraction, SIGMA = hard sphere diameter, NN = number density of ions/cm^3. The parameter ERROR is not used in the calculation. All parameters are in c.g.s. units.

N.B. All the Algol 60 programmes listed in the appendices were run on an Elliot 4130 computer at the University of Warwick.

```
&JOB;PH/R004/46;ARDF;


 &ALGOL;
LIBRARY
ALGOL


&LIST;
   1   RADIAL DISTRIBUTION FUNCTIONS IN LIQUID METALS;
   2   "BEGIN""REAL"ETA,SIGMA,NN,R,PR,K,ALPHA,BETA,GAM,I,ERROR,GR;
   3   "REAL""ARRAY"W{0:31},X{0:31};
   4   "INTEGER"J,Q,N;
   5   "REAL""PROCEDURE"A(K);"VALUE"K;"REAL"K;
   6   "BEGIN""REAL"C,X;X:=K*SIGMA;
   7         C:=(COS(X)*((2*BETA+12*GAM)/X↑3-(ALPHA+BETA+GAM)/X
   8         -24*GAM/X↑5)+SIN(X)*((ALPHA+2*BETA+4*GAM)/X↑2-24*GAM/X↑4)
   9         +24*GAM/X↑5-2*BETA/X↑3)*(-12,5664*SIGMA↑3/X);
  10         A:=1/(1-NN*C);
  11   "END";
  12   "PRINT"''S7'Q'S7'GR'L'';
  13   "FOR"J:=0"STEP"1"UNTIL"31"DO""READ"W{J},X{J};
  14   "READ"ETA,SIGMA,NN,ERROR;
  15   ALPHA:=((1+2*ETA)↑2)/(1-ETA)↑4;
  16   BETA:=(-6*ETA*((1+ETA/2↑2))/(1-ETA)↑4;
  17   GAM:=0,5*ETA*((1+2*ETA)↑2)/(1-ETA)↑4;
  18    "FOR"J:=0"STEP"1"UNTIL"31"DO"
  19   "BEGIN "W{J}:=W{J}*SIN((X{J}+1)*3.1416);
  20   "END";
  21   "FOR"Q:=1"STEP"1"UNTIL"240"DO"
  22   "BEGIN"R:=Q*1_10-9;I:=0;
  23         "FOR"N:=0"STEP"1"UNTIL"30"DO"
  24         "BEGIN""FOR"J:=0"STEP"1"UNTIL"31"DO"
  25               "BEGIN"K:=(X{J}+(2*N+1))*3,1416/R;
  26         I:=I+W{J}*(A(K)-1)*4*3,1416↑2*K/((2*3,1416)↑3*R↑2*NN);
  27               "END";
  28         "END";
  29   GR:=I+1:
  30   "PRINT"PREFIX(''S4''),''L'',DIGITS(3),Q,GR;
  31   "END";
  32   "END";
```

APPENDIX III

Calculation of the Blandin-Daniel coefficients, α_ℓ and β_ℓ, used in chapter 4.

The weighting factors, W(J), and Abscissae, X(J), required in the gaussian integration are taken from M.Abramowitz and I.A.Stegun, Handbook of Mathematical Functions, P.917. The other date is read in the following order: ETA = packing fraction, SIGMA = hard sphere diameter, NN = number of ions/cm^3, RADZERO = starting value of integration over r, usually just less than SIGMA, DELR = interval of R, KF = Fermi wave-vector. All parameters are in c.g.s. units.

```
&JOB;PH/R004/20;BDLM;
SWOP
BATCH

&ALGOL;
LIBRARY
ALGOL

&LIST;
    1   BLANDIN DANIEL COEFFICIENTS FOR LIQUID METALS;
    2   "BEGIN""REAL"ETA,SIGMA,NN,R,K,ALPHA,BETA,GAM,I,GR,RADZERO,DELR,KF,RO,B,
    3                DELTA;
    4         "REAL""ARRAY"W,X{0:31},JK,NK{0:3},FALPHA,FBETA{0:3,0:2500},SA1,
    5                      SA2,SB1,SB2,SC1,S1,S2,SUMAL,SUMBL{0:3};
    6         "INTEGER"J,Q,N,M;
    7         "REAL""PROCEDURE"A(K);"VALUE"K;"REAL"K;
    8         "BEGIN""REAL"C,X;X:=K*SIGMA:
    9                C:=(COS(X)*((2*BETA+12*GAM)/X↑3-(ALPHA+BETA+GAM)/X
   10                -24*GAM/X↑5)+SIN(X)*((ALPHA+2*BETA+4*GAM)/X↑2-24*GAM/X↑4)
   11                +24*GAM/X↑5-2*BETA/X↑3)*(-12,5664*SIGMA↑3/X):
   12                A:=1/(1-NN*C);
   13         "END":
   14         "PRINT"''S8'A,S'S10'B,S'L'';
   15         "FOR"J:=0"STEP"1"UNTIL"31"DO""READ"W{J},X{J};
   16         "READ"ETA,SIGMA,NN,RADZERO,DELR,KF:
   17         ALPHA:=((1+2*ETA)↑2(/(1-ETA)↑4;
   18         BETA:=(-6*ETA*((1+ETA/2)↑2))/(1-ETA)↑4:
   19         GAM:=0.5*ETA*((1+2*ETA)↑2)/(1-ETA)↑4:
   20         "FOR"J:=0"STEP"1"UNTIL"31"DO"
   21         "BEGIN"W{J}:=W{J}*SIN((X{J}+1)*3,1416):
   22         "END":
   23      "FOR"B:=7,22"DO"
   24          "BEGIN"DELTA:=B*1₁₀5:
   25          "PRINT"''L3'DELTA=':SCALED(5),DELTA,''L'':
   26          "FOR"Q:=0"STEP"1"UNTIL"200"DO"
   27          "BEGIN"R:=RADZERO+Q*DELR;I:=0;
   28                "FOR"N:=0"STEP"1"UNTIL"30"DO"
   29                "BEGIN""FOR"J:=0"STEP"1"UNTIL"31"DO"
   30                      "BEGIN"K:=(X{J}+(2*N+1))*3,1416/R;
   31                            I:=I+W{J}*(A(K)-1)*2*K:
   32                      "END";
   33                "END";
   34                "RO":=(4*3,1416*R↑2*NN+1)*EXP(-DELTA*R):
   35                JK{0}:=SIN(KF*R)/(KF*R):
   36                NK{0}:=-COS(KF*R)/KF*R):
   37                JK{1}:=JK{0}/(KF*R)+NK{0}:
   38                NK{1}:=NK{0}/(KF*R)-JK{0}:
   39                "FOR"M:=2"STEP"1"UNTIL"3"DO"
   40                "BEGIN"JK{M}:2(2*M-1)*JK{M-1}/(KF*R)-JK{M-2}:
   41                      NK{M}:2(2*M-1)*NK{M-1}/(KF*R)-NK{M-2}:
   42                "END":
   43                "FOR"M:20"STEP"1"UNTIL"3"DO"
   44                "BEGIN"FALPHA{M,Q}:=RO*(NK{M}↑2-JK{M}↑2):
   45                      FBETA{M.Q}:=RO*NK{M}*JK{M}:
```

```
46              "END";
47          "END":
48          "FOR"Q:=201"STEP"1"UNTIL"2500"DO"
49          "BEGIN"R:=RADZERO+Q*DELR;
50                  RO:=(4*3,1416*R↑2*NN)*EXP(-DELTA*R):
51                  JK{O}:=SIN(KF*R)/(KF*R):
52                  NK{O}:2-COS(KF*R)/(KF*R):
53                  JK{1}:=JK{O}/(KF*R)+NK{O}:
54                  NK{1}:=NK{O}/(KF*R)-JK{O}:
55                  "FOR"M:=2"STEP"1"UNTIL"3"DO"
56                  "BEGIN"JK{M}:=(2*M-1)*JK{M-1}/(KF*R)-JK{M-2}:
57                          NK{M}:=(2*M-1)*NK{M-1}/(KF*R)-NK{M-2}:
58                  "END";
59                  "FOR"M:=O"STEP"1"UNTIL"3"DO"
60                  "BEGIN"FALPHA{M,Q}:=RO*(NK{M}↑2-JK{M}↑2):
61                          FBETA{M.Q}:=RO*NK{M}*JK{M}:
62                  "END";
63          "END";
64          "COMMENT" AT THIS STAGE WE HAVE CALCULATED THE FUNCTION AT ALL
65                    VALUES OF R.WE NOW WISH TO SUM THESE FOR EACH M(=L)
66                    VALUE USING SIMPSONS RULE , HENCE OBTAINING THE
67                    BLANDIN DANIEL COEFFICIENTS:
68          "FOR"M:=O"STEP"1"UNTIL"3"DO"
69          "BEGIN"SA1{M}:=O;
70                  SA2{M}:=O;
71                  "FOR"Q:=1"STEP"2"UNTIL"2499"DO"
72                  "BEGIN"SA1{M}:=SA1{M}+FALPHA{M,Q}:
73                          SA2{M}:=SA2{M}+FBETA{M,Q}:
74                  "END";
75                  SB1{M}:=O;
76                  SB2{M}:=O;
77                  "FOR"Q:=2"STEP"2"UNTIL"2498"DO"
78                  "BEGIN"SB1{M}:=SB1{M}+FALPHA{M,Q}:
79                          SB2{M}:=SB2{M}+FBETA{M,Q}:
80                  SC1{M}:=FALPHA{M.O}+FALPHA{M,2500}:
81                  SC2{M}:=FBETA{M,O}+FBETA{M,2500}:
82                  "END";
83                   S1{M}:=4*SA1{M}+2*SB1{M}+SC1{M}:
84                   S2{M}:=4*SA2{M}+2*SB2{M}+SC2{M}:
85                   SUMAL{M }:=S1{M}*DELR/3*(2*M+1);
86                   SUMBL{M}:=S2{M}*DELR/3*(2*M+1);
87                   "PRINT"PREFIX(''S4''),''L'',SUMAL{M},SUMBL{M}:
88          "END";
89          "END";
90  "END";
```

APPENDIX IV

The following is a full parameter list of the Algol 60 programme used in the alloy Knight shift calculation. The programme listing follows in appendix V.

K - number used to set alloy concentration

K2 - k_F^2

R - r, in atomic units, the distance from the nucleus.

RZERO - r starting value of Simpsons rule integration before conversion to atomic units (taken directly from Herman and Skillman)

BL - overlap integral before it is equated to overlap integral procedure result.

F - Simpsons rule interval parameter.

B1, B2, B3, B4 - Intermediate sums in Simpsons rule, BLL procedure.

HCON - Simpsons rule interval in BLL procedure.

RZEROCON - starting value of Simpsons rule integration (in atomic units) in BLL procedure.

COD, CEV - Intermediate sums in CO procedure.

CIN - final sum of CO procedure.

X - $q/2k_F$

DELY - interval in y in Simpsons rule in CO procedure.

DELF - CO procedure parameter, starting value of interval in y.

DELYA, DELYB - starting values for interval in y, to be used in CO procedure.

Y - y, abscissa of y - integration in procedure CO

KF - k_F

Q - q

Q2 - q^2

K2Q - $2k_F q$

YB)
) Starting values for y in Simpsons rule in CO procedure.
YA)

YBR)
) - Ranges of integration for y in Simpsons rule in CO procedure.
YAR)

CZ)
) - first and last terms in Simpsons rule in CO procedure.
CN)

KFA - k_F for pure A element.

KFB - k_F for pure B element

OMEGAA)
) - ionic volumes of pure A and B elements.
OMEGAB)

RCA) - core radiiof Ashcroft pseudopotential for A and B elements.
)
RCB)

PI - 3·14159

WI - $1/\pi k_F$, term in Ashcroft potential

GAMMA - γ_A (k)

TERMA)
) - Normalisation terms for A and B elements.
TERMB)

PS) - Intermediate sums in Simpsons rule integration of self and
)
PD) distinct terms Σ and Δ.

H3 - Simpsons rule integration interval divided by 3 for use inΣ and Δintegration.

SIG - hard-sphere diameter

STR - $I(k\sigma) - 1$

FL - $\ell n \left|\frac{1 - q/2k_F}{1 + q/2k_F}\right|$

XFL - $q/2k_F \quad \ell n \left|\frac{1 - q/2k_F}{1 + q/2k_F}\right|$

CAPGAM - $\Gamma(k,q)$

RB)
) - intermediate sums used in evaluation of $\Gamma(k,q)$
RC)

VA)
) - Ashcroft potentials for A and B elements.
VB)

GS)
) - self and distinct term integrands in Simpsons rule.
GD)

PST)
) - final sums in Simpsons rule integration of Σ and Δ.
PDT)

DENS - γ_A^2 (k)/ N (C_B) {1 + Σ + Δ}.

PF - DENS/Ω

QRA - q X R^A core.

QRB - q X R^B core.

VAL - alloy valence.

N - principal quantum number of core state.

L - angular momentum quantum number of core state.

RAD - abscissa integer for core state.

M - running integer used in integration over q.

KINT - k - value integer.

RADZERO - integer representing starting r value in overlap interval.

C,I - integers used in BLL procedure.

A,B - integers used in CO procedure.

E - integer representing A or B element (E = 1 or 2)

NJ1, T - integers used in q - integration.

BLA {E,L,N,KINT} - overlap integral array, E specifies element, L - quantum number, N -n quantum.number, KINT - the k value.

J{L} - Bessel function array.

P{E,L,N,RAD} - core state wave function array.

CA{K}, CB{K} - concentrations of A and B elements.

OMEGAE{K} - volume per electron.

BETA {K} - N_k (C_B).

OPW {K} - γ_A^2 (k)/ N_K (C_B).

H{T} - Simpsons rule interval, q integration.

AJ{T} - starting q - values for Simpsons rule q integration.

PT{K}- $1 + \Sigma + \Delta$, for a given concentration.

OMEGAI{K} - average volume per ion at a given concentration.

XS{N} - R_{no} (O) for s-core functions.

PLK{N} - BLL for $K = k_F$, overlap integral.

CON{E} - conversion factor for Herman and Skillman wavefunctions.

NMAX{E} - maximum n - value for core functions.

LMAX{E} - maximum l - value for core functions.

NRAD {E,L,N} - number of wave function ordinates for given core state.

NWF{E} - number of core states for given element.

APPENDIX V

```
&JOB;PH/R004/94;

&ALGOL;
LIBRARY
ALGOL

&LIST;

&TIME;10;

    1   PERDEW AND WILKINS CALCULATION OF KNIGHT SHIFTS IN LIQUID ALLOYS;
    2   "COMMENT"CALCULATES PF IN LIQUID ALLOYS AT SPECIFIC CONCENTRATIONS,USES
    3   ASHCROFT AND LEKNER STRUCTURE FACTORS,ASHCROFTS LOCAL PSEUDOPOTENTIAL
    4   AND HERMAN AND SKILLMAN CORE WAVE FUNCTIONS;
    5   "BEGIN""REAL"K,R,RZERO,BL,F,B1,B2,B3,B4,HCON,RZEROCON,COD,CEV,CIN,X,
    6   DELY,DELF,Y,KF,K3,Q,Q2,K2Q,YB,YA,YBR,YAR,DELYB,DELYA,CZ,CN,KFA,KFB,
    7   OMEGAA,OMEGAB,RCA,RCB,PI,WI,GAMMA,TERMA,TERMB,PS,PD,H3,SIG,STR,FL,XFL,
    8   CAPGAM,RB,RC,VA,VB,GS,GD,PST,PDT,DENS,PF,QRA,QRB,VAL;
    9           "REAL""ARRAY"BLA{1:2,0:3,1:5,0:80},J{0:4},P{1:2,0:3,1:5,0:100},
   10           CA,CB,OMEGAE,BETA,OPW,H,AJ,NJ,PT,OMEGAI{1:11}, XS,BLK{1:6},
   11           CON{1:2};
   12           "INTEGER"N,L,RAD,M,KINT,RADZERO,I,C,A,B,E,NJ1,T;
   13           "INTEGER""ARRAY"NMAX 1:2 ,LMAX 1:2,1:5 ,NRAD 1:2,0:3,1:5 ,
   14                       NWF{1:2};
   15           "COMMENT"PROCEDURE CO EVALUATES Q DEPENDANT INTEGRAL REQUIRED IN
   16           SELF AND DISTINCT TERMS;
   17           "REAL""PROCEDURE"CO(N);
   18           "INTEGER"N;
   19           "BEGIN""REAL""PROCEDURE"CINT(YZERO,DELF,S):
   20                   "VALUE"YZERO,DELF,S;
   21                   "REAL"YZERO,DELF;
   22                   "INTEGER"S;
   23                   "BEGIN"CIN:=0;
   24                           "FOR"A:=1"STEP"1"UNTIL"7"DO"
   25                       "BEGIN"COD;=CEV:=0;
   26                               DELY:=DELF*(10↑A)/10;
   27                               "FOR"B:=1"STEP"2"UNTIL"9"DO"
   28                               "BEGIN"Y:=YZERO+S*DELY*B;
   29                               KINT:=ENTIER(10*SQRT(K2+Q2-K2Q*Y)):
   30                               COD:=COD+(BLA{1,0,N,KINT}-BLK{N})/(Y/X-1);
   31                               "END";
   32                               "FOR"B:=2"STEP"2"UNTIL"8"DO"
   33                               "BEGIN"Y:=YZERO+S*DELY*B:
   34                               KINT:=ENTIER(10*SQRT(K2+Q2-K2Q*Y)):
   35                               CEV:=CEV+(BLA{1,0,N,KINT}-BLK{N})/(Y/X-1):
   36                               "END";
   37                               KINT:=ENTIER(10*SQRT(K2+Q2-K2Q*YZERO)):
   38                               CZ:=(BLA{1,0,N,KINT}-BLK{N})/(YZERO/X-1);
   39                               YZERO:=YZERO+S*10*DELY;
   40                               KINT:=ENTIER(10*SQRT(K2+Q2-K2Q*YZERO));
```

```
                        CN:=(BLA{1,0,N,KINT}-BLK{N})/(YZERO/X-1);
                        CIN:=CIN+(DELY/3)*(CZ+CN)+(4*DELY/3)*COD
                              +(2*DELY/3)*CEV;
                "END";
                CINT:=CIN;
        "END"OF PROCEDURE CINT;
        K=:=KF*KF;
        Q2:=Q*Q;
        K2Q:=2*KF*Q;
        "IF"X>1"THEN"CO:=CINT(1,0,00000018,-1)"ELSE
        "BEGIN"YB:=X-0,0000002;
                YA:=X+0,0000002;
                YBR:=YB+1;
                YAR:=1-YA;
                DELYB:=0.00000009*YBR;
                DELYA:=0.00000009*YAR;
                "IF"YAR<0.0000002"THEN"CO:=CINT(YB,DELYB,-1)
                "ELSE"CO:=CINT(YA,DELYA,1)+CINT(YB,DELYB,-1);
        "END";
"END" OF PROCEDURE CO;
"COMMENT"PROCEDURE S CALCULATES STRUCTURE FACTOR USING CURRENT
ALLOY VALUES OF KF AND SIGMA, THE PACKING FRACTION ETA IS 0,45
THROUGHOUT;
"REAL""PROCEDURE"S(Z);
"REAL"Z;
"BEGIN""REAL"ZZ,ZZZ,R1,R2,R3,R4,R5;
        "IF"Z<0.5"THEN"S:=0,025"ELSE"
        "BEGIN"
        ZZ:=Z*Z;
        ZZZ:=Z*Z*Z;
        R1:=-13.5988O-213,0346/ZZ;
        R2:=-4.049587*Z+17,96189/Z-213.0346/ZZZ;
        R3:=88.55543/Z*213,0346/ZZZ;
        R4:=10,8/ZZZ;
        R5:=R4*(R1*SIN(Z)+R2*COS(Z)*R3);
        S:=1/(1+R5);
        "END";
"END"OF PROCEDURE S;
"COMMENT"PROCEDURE V CALCULATES THE PSEUDOPOTENTIAL USING THE
APPROPRIATE CORE RADIUS,IT IS TRUNCATED AT THE SECOND NODE;
"REAL""PROCEDURE"V(QR);
"REAL"QR;
"BEGIN""REAL"DENOM,X2;
      "IF"X<0.01"THEN"V:=-1,0"ELSE""IF"QR>4,71"THEN"V:=0.00
"ELSE""BEGIN"X2:=X*X;
                DENOM:=X2+WI*(0.5-0,25*(1-X2)*FL/X);
                V:=-WI*COS(QR)/DENOM;
      "END";
"END" OF PROCEDURE V;
"REAL""PROCEDURE"BINT(N,L,RAD,E);
"INTEGER"N,L,RAD,E;
"BEGIN""REAL"XKR;
        XKR:=KF*R;
        "IF"XKR<0.01"THEN"XKR:=0.01;
        J{0}:=SIN(XKR)/XKR;
        "IF"L>0"THEN"J{1}:=J{0}/XKR-COS(XKR)/XKR;
        "IF"L>1"THEN"J{2}:=3*J{1}/XKR-J{0};
        "IF"L>2"THEN"J{3}:=5*J{2}/XKR-J{1};
        "IF"L>3"THEN"J{4}:=7*J{3}/XKR-J{2};
        BINT:=4*3.14159*R*R*P{E,L,N,RAD}*J{L};
```

```
101             "END"OF PROCEDURE BINT;
102             "REAL""PROCEDURE"BLL(N,L,KF,E);
103             "REAL"KF;
104             "INTEGER"N,L,E;
105             "BEGIN"RZERO;=-0.05;
106                                     BL:=0;
107                                     "FOR"C:=1"STEP"1"UNTIL"(NRAD{E,L,N}-1)"DIV"
108                                             10"DO"
109                                     "BEGIN"F:=0.01*(2↑C)/2;
110                                             B1:=B2:=0;
111                                             RADZERO:=10*(C-1);
112                                             RZERO:=RZERO+5*F;
113                                                             HCON:=F*CON{E};
114                                             RZERCON:=RZERO*CON{E};
115                                             "FOR"I:=1"STEP"2"UNTIL"9"DO"
116                                             "BEGIN"RAD:=RADZERO+1:
117                                                     R:=RZEROCON+HCON*1;
118                                                     B1:=B1+BINT(N,L,RAD,E);
119                                             "END";
120                                             "FOR"I:=2"STEP"2"UNTIL"8"DO"
121                                             "BEGIN"RAD:=RADZERO+1;
122                                                     R:=RZEROCON+HCON*1;
123                                                     B2:=B2+BINT(N,L,RAD,E);
124                                             "END";
125                                             RAD:=RADZERO;
126                                             R:=RZEROCON;
127                                             B3:=BINT(N,L,RAD,E);
128                                             RAD:=RADZERO+10;
129                                             R:=RZEROCON+10*HCON;
130                                             B4:=BINT(N,L,RAD,E);
131                                             BL:=BL+(HCON/3)*(B3+B4)+4*(HCON/3)*B1
132                                                     +2*(HCON/3)*B2;
133                                     "END";
134                                     BLL:=BL;
135             "END" OF PROCEDURE BLL;
136             "FOR"E:=1,2"DO"
137             "BEGIN""READ"CON{E},NWF{E},NMAX{E};
138                     "FOR"N:=1"STEP"1"UNTIL"NMAX{E}"DO""READ"LMAX{E,N};
139                     "FOR"M:=1"STEP"1"UNTIL"NWF{E}"DO"
140                     "BEGIN""READ"N,L,NRAD{E,L,N};
141                             "FOR"RAD:=0"STEP"1"UNTIL"NRAD{E,L,N}-1"DO"
142                                     "READ"P{E,L,N,RAD};
143                             "FOR"KF:=0"STEP"0,1"UNTIL"8,0"DO"
144                             "BEGIN"KINT:=ENTIER(10*(KF+0,001));
145                                     BLA{E,L,N,KINT}:=BLL(N,L,KF,E);
146                             "END";
147                     "END";
148             "END";
149 "FOR"E:=1,2"DO"
150 "BEGIN""PRINT"E;
151         "FOR"N:=1"STEP"1"UNTIL"NMAX{E}"DO"
152         "BEGIN""PRINT"N;
153                 "FOR"L:=0"STEP"1"UNTIL"LMAX E,N "DO"
154                 "BEGIN""PRINT"L;
155                         "FOR"KINT:=0"STEP"1"UNTIL"80"DO"
156                         "PRINT"PREFIX(''S2''),SAMELINE,BLA{E,L,N,KINT};
157                 "END"
158         "END";
159 "END";"
160         "READ"KFA,KFB,OMEGAA,OMEGAB,RCA,RCB;
```

```
"PRINT"KFA,SAMELINE,KFB,OMEGAA,OMEGAB,RCA,RCB;
      "FOR"N:=1"STEP"1"UNTIL"NMAX{1}"DO""READ"XS{N};
"FOR"N:=1"STEP"1"UNTIL"NMAX{1}"DO""PRINT"XS{N};
      PI:=3.14159;
      "COMMENT"THE PROGRAMME NOW SETS UP CONCENTRATIONS FOR WHICH
      CALCULATIONS WILL BE PERFORMED.  THE FOLLOWING INSTRUCTION MUST BE
      CHANGED TO CHANGE THESE CONCENTRATIONS;
      "FOR"K:=1,5"DO"
      "BEGIN"CA{K}:=1-0.1*(K-1);
            CB{K}:=1-CA{K};
            OMEGAE{K}:=2*PI*PI*(CA{K}/KFA↑3+CB{K}/KFB↑3);
            OMEGA1{K}:2CA{K}*OMEGAA+CB{K}*OMEGAB;
            VAL:=(CA{K}*OMEGAA*KFA↑3+CB{K}* OMEGAB*KFB↑3)/(3*PI*PI);
            KF:=(3*PI*PI/OMEGAE{K})↑(1/3);
            W1:=0,31831/KF;
            KINT:=ENTIER(10*(KF+0.0001));
"PRINT"CA{K},SAMELINE,CB{K},OMEGAE{K},OMEGAI{K},KF,W1;
            GAMMA:=1;
            TERMA:=0;
            "FOR"N:=1"STEP"1"UNTIL"NMAX{1}"DO"
            "BEGIN"GAMMA:=GAMMA-(1/(4*PI))*XS{N}*BLL(N,0,KF,1);
                  BLK{N}:=BLL(N,0,KF,1);
            "FOR"L:=0"STEP"1"UNTIL"LMAX{1,N}"DO"
            TERMA:=TERMA+((2*L+1)/(4*PI))*BLL(N,L,KF,1)↑2;
            "END";
            "TERMB:=0;
            "FOR"N:=1"STEP"1"UNTIL"NMAX{2}"DO"
            "BEGIN""FOR"L:=0"STEP"1"UNTIL"LMAX{2,N}"DO"
            TERMB:=TERMB+((2*L+1)/(4*PI))*BLL(N,L,KF,2)↑2;
            "END";
            BETA{K}:=1-(CA{K}*TERMA+CB{K}*TERMB)/OMEGAI{K};
            OPW{K}:=GAMMA*GAMMA/BETA{K};
"PRINT"GAMMA,SAMELINE,TERMA,TERMB,BETA{K},OPW{K};
            PS:=1;PD:=0;
            H{1}:=H{10};=0.05;H{2}:=H{9}:=0.025;H{3}:=H{8}:=0.01;
            H{4}:=H{7}:=0.00475;H{5}:=H{6}:=0.00045;H{11}:=0.10;
            AJ{1}:=0.05;AJ{2}:=0.5;AJ{3}:=0.9;AJ{4}:=0.98;
            AJ{5}:=0.999;AJ{6}:=1.0001;AJ{7}:=1.001; AJ{8}:=1.02;
            AJ{9}:=1.40;AJ{10}:=2.50:AJ{11}:=3.40;
            NJ{1}:=9;NJ{2}:=16;NJ{3}:=8;NJ{4}:=NJ{7}:=4;
            NJ{5}:=NJ{6}:=2;NJ{8}:=28;NJ{9}-=44;NJ{10}:=18;NJ{11}:=26;
      "COMMENT"PROGRAMME NOW ENTERS Q LOOP,INTEGRATION MESH
            FINEST CLOSE TO SINGULARITY (Q=2*KF);
            "FOR"T:=1"STEP"1"UNTIL"11"DO"
            "BEGIN"NJ1:=NJ{T}+1;
                  H3:=H{T}/3;
                  "FOR"M:=1"STEP"1"UNTIL"NJ1"DO"
                  "BEGIN"X:=AJ{T}+(M-1)*H{T};
                        Q:=X*2*KF;
                        QRA:=Q*RCA;QRB:=Q*RCB;
                        "IF"QRA>5.2"AND"QRB>5.2"THEN""GOTO"CONTINUE;
                        SIG:=((25.447*VAL)↑(1/3))/KF;
                        STR:=S(Q*SIG)-1;
                        FL:=LN(ABS((1-X)/(1+X)));
                        XFL:=X*FL;
                        RB:=RC:=0;
                        "FOR"N:=1"STEP"1"UNTIL"NMAX{1}"DO"
                        "BEGIN"RB:=RB+XS{N}*BLK{N};
                              RC:=RC+XS{N}*CO(N);
                        "END";
```

```
221                 CAPGAM:=(XFL*(1-(1/(4*PI))*RB)-(1/(4*PI))*RC)/GAMMA;
222                                 VA:=V(QRA);VB;=V(QRB);
223                                 GS:=2*CAPGAM*VA;
224                                 GD:=2*CAPGAM*(CA{K}*STR*VA+CB{K}*STR*VB);
225                                 "COMMENT"INTEGRATION OF SELF AND DISTINCT
226                                 TERM INTEGRANDS OVER Q WILL NOW BE DONE
227                                 USING SIMPSONS RULE;
228                                 "IF"M=1"THEN""GOTO"FIRSTANDLAST;
229                                 "IF"M=NJ1"THEN""GOTO"FIRSTANDLAST;
230                                 "IF"M-ENTIER(M/2)*2=0"THEN""GOTO"EVEN"ELSE"
231                                 "GOTO"ODD;
232                 FIRSTANDLAST:   PS:=PS+H3*GS;
233                                 PD:=PD+H3*GD;PST:=PS;PDT:=PD;
234                                 "GOTO"EXIT;
235                         EVEN:   PS:=PS+4*H3*GS;
236                                 PD:=PD+4*H3*GD;
237                                 "GOTO"EXIT;
238                         ODD:    PS:=PS+2*H3*GS;
239                                 PD:=PD+2*H3*GD;
240                         EXIT:   PT{K}:=PST+PDT;
241         CONTINUE;               "END";
242                 "END";
243   "PRINT"PST,SAMELINE,PDT,PT{K};
244                 DENS:=OPW{K}*PT{K};
245                 PF:=DENS/OMEGAI{K};
246                 "PRINT"''L''S3'CA'S8'DENS'S11'PF';
247                 "PRINT"FREEPOINT(5),CA{K},PREFIX(''S4''),DENS,PF;
249   "END"OF PROGRAMME;
```

APPENDIX VI

The Pseudopotential calculation Computer programme

A listing of the programme is given in appendix V, the following briefly describes what the programme does. There are five procedures which are used frequently in the programme and they are listed in the order in which they occur.

Procedure BINT This evaluates the integrand $P_{n\ell}(r).4\pi r j_\ell(kr)$ used in determining $B_{n\ell}(k)$. In order to avoid divergence of the j_ℓ's for small arguments, if $kr<0.01$, it is set equal to 0.01.

Procedure BLL This evaluates the integral $B_{n\ell}(k)$ using the integrands found by procedure BINT, a Simpsons rule numerical integration being performed. In order to save computer time these overlap integrals are evaluated for a large number of k-values and stored as an array BLA. When the $B_{n\ell}$'s are required in further integrations, the array element nearest to the value of k actually required is selected and used. If a specific $B_{n\ell}$ is required that is not being used in an integration, then it is calculated exactly.

Procedure Co This calculates $C_o'(n,k,q)$ and uses the integrals $B_{n\ell}(k)$ calculated by procedure BLL.

Now $$C_o(n,k,q) = \int_{-1}^{+1} \frac{B_{no}\{(k^2 + q^2 - 2kqy)^{\frac{1}{2}}\}}{\frac{2k}{q}y - 1}$$

however the integrand has a singularity at $y = q/2k$ and to get round this difficulty $C_o(n,k,q)$ is written

$$C_o(n,k,q) = \int_{-1}^{+1} \frac{\{B_{no}\{(k^2 + q^2 - 2kqy)^{\frac{1}{2}}\} - B_{no}\{k\}\}dy}{\frac{2k}{q}y - 1} + \int_{-1}^{+1} \frac{B_{no}\{k\}dy}{\frac{2k}{q}y - 1}$$

The first integral no longer diverges so that we may write

$$C_o(n,k,q) = \frac{q}{2k} \ln\left|\frac{1 - q/2k}{1 + q/2k}\right| B_{no}\{k\} + \int_{-1}^{q/2k-\varepsilon} \frac{\{B_{no}\{(k^2 + q^2 - 2kqy)^{\frac{1}{2}}\} - B_{no}\{k\}\}}{\frac{2k}{q} y - 1}\, dy$$

$$+ \int_{q/2k+\varepsilon}^{1} \frac{\{B_{no}\{(k^2 + q^2 - 2kqy)^{\frac{1}{2}}\} - B_{no}\{k\}\}}{\frac{2k}{q} y - 1}\, dy, \text{ with } \varepsilon << 1.$$

Writing this equation in another way

$$C_o(n,k,q) = \frac{q}{2k} \ln\left|\frac{1 - q/2k}{1 + q/2k}\right| B_{no}\{k\} + C_o'(n,k,q)$$

Procedure CO evaluates $C_o'(n,k,q)$ using a Simpsons rule numerical integration and functions in three different ways depending on the value of q/2k.

If q/2k>1 then the singularity is outside the range of integration which is then performed 'downwards' from y = +1. The integration range is divided into 7, each range having 11 points. The interval is increased by a factor of 10 each time the range moves downward from y = +1, the starting interval being 0.0000018.

If 0.9999998<q/2k≤1 the singularity is effectively at y = +1 and the integration is again performed downwards from y = +1. The integration is started at q/2k - 0.0000002, the range is again divided into 7 and the interval increased by 10 as the next range is covered. The smallest interval is chosen so that the complete integration range is exactly covered.

All other values of q/2k, the integration is performed upwards from q/2k + 0.0000002 to y = +1 and downwards from q/2k - 0.0000002 to y = -1; the ranges and intervals being chosen as above. For clarity, the

integration procedure is shown diagrammatically in figure A1.

Procedure S(Z) This evaluates the Ashcroft-Lekner structure factor using an average hard sphere diameter for the alloy.

Procedure V(QR) This calculates Ashcrofts pseudopotential; setting $V = 0$ for $q \times R_{core} > 4.71$, i.e. it is truncated at the second node.

Main programme Following the procedure declarations, the programme enters a routine for the calculation and storage as an array of the the overlap integrals $B_{n\ell}(k)$. Each array element is identified by E = 1,2 - the element; N and L - the quantum numbers of the wave function involved and an integer KINT = ENTIER (10 * K); i.e. KINT = 35 corresponds to K = 3.5 a.u. The array elements (overlap integrals) are printed out by the routine which follows. In this routine the core functions are read in and stored as an array, as well as other information relating to the core functions. This is clearly seen from the programme and parameter listings given in the preceding appendices. The concentrations at which the calculation is to be performed are set up and the programme goes round the K-loop once for each concentration. The Q-loop is inside the K-loop and after the mesh in q is set up a Simpsons rule integration over q is performed. Finally the parameters required are printed. The entire calculation is performed in atomic units and for, say, the Sn-Ag system the programme took 28 minutes of computer time where the parameters for ^{119}Sn were calculated at 10 concentrations.

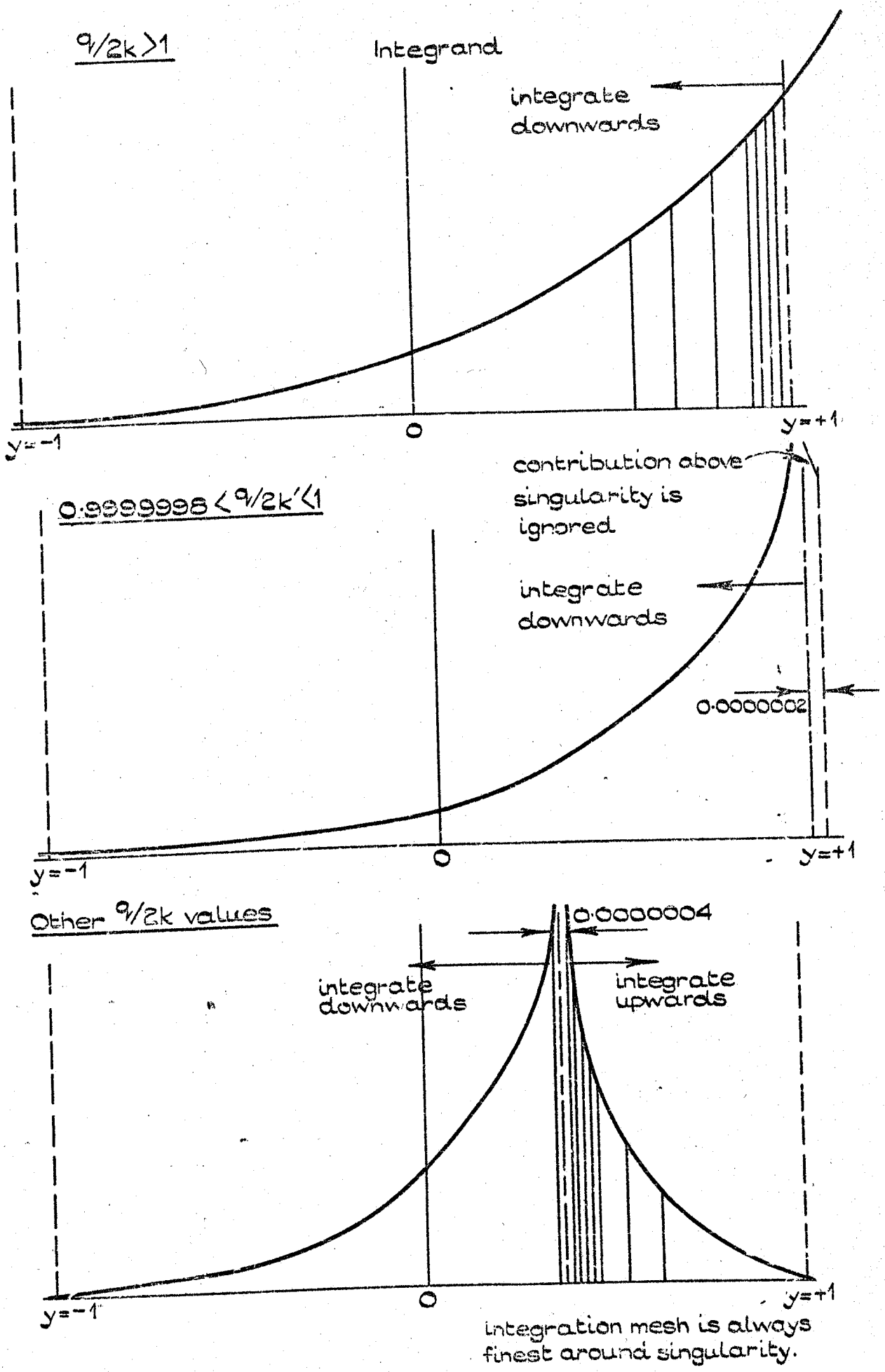

FIGURE A1.

DIAGRAMMATIC REPRESENTATION OF THE INTEGRATION PROCEDURE $C_0'(n,k,q)$.